



University of HUDDERSFIELD

University of Huddersfield Repository

Raharjo, Parno

An Investigation of Surface Vibration, Airbourne Sound and Acoustic Emission Characteristics of a Journal Bearing for Early Fault Detection and Diagnosis

Original Citation

Raharjo, Parno (2013) An Investigation of Surface Vibration, Airbourne Sound and Acoustic Emission Characteristics of a Journal Bearing for Early Fault Detection and Diagnosis. Doctoral thesis, University of Huddersfield.

This version is available at <http://eprints.hud.ac.uk/id/eprint/19034/>

The University Repository is a digital collection of the research output of the University, available on Open Access. Copyright and Moral Rights for the items on this site are retained by the individual author and/or other copyright owners. Users may access full items free of charge; copies of full text items generally can be reproduced, displayed or performed and given to third parties in any format or medium for personal research or study, educational or not-for-profit purposes without prior permission or charge, provided:

- The authors, title and full bibliographic details is credited in any copy;
- A hyperlink and/or URL is included for the original metadata page; and
- The content is not changed in any way.

For more information, including our policy and submission procedure, please contact the Repository Team at: E.mailbox@hud.ac.uk.

<http://eprints.hud.ac.uk/>

**AN INVESTIGATION OF SURFACE VIBRATION, AIRBORNE
SOUND AND ACOUSTIC EMISSION CHARACTERISTICS OF A
JOURNAL BEARING FOR EARLY FAULT DETECTION AND
DIAGNOSIS**

PARNO RAHARJO

A thesis submitted to the University of Huddersfield
in partial fulfillment of the requirements for
the degree of Doctor of Philosophy

The University of Huddersfield
May 2013

LIST OF CONTENTS

LIST OF CONTENTS	2
LIST OF FIGURES	8
LIST OF TABLES	14
LIST OF ABBREVIATIONS	15
LIST OF NOTATIONS	16
DECLARATION	21
DEDICATION	22
ACKNOWLEDGEMENTS	23
CHAPTER ONE	25
INTRODUCTION	25
1.1 Background	25
1.2 Motivation and Topic of Research	26
1.3 Research Aims and Objectives	29
1.4 Outline of Thesis	30
CHAPTER TWO	32
JOURNAL BEARINGS, FAILURE MODES AND MONITORING TECHNIQUES	32
2.1 Bearing types	32
2.2 Journal bearing	33
2.1.1 Solid bearings.....	33
2.1.2 Bushing	34
2.1.3 Thrust bearing	36
2.1.4 Tilting pad bearing.....	37
2.1.5 Self-aligning spherical journal bearing	37
2.2 Journal bearing lubrication	38

2.2.1 Lubricant selection.....	38
2.2.2 Lubricant supply methods.....	41
2.2.3 The lubrication regimes	42
2.3 Journal bearing failures	44
2.3.1 Scratching	45
2.3.2 Wiping.....	45
2.3.3 Wear.....	46
2.3.4 Fatigue.....	47
2.3.5 Eccentric bearing	47
2.4 Review of journal bearing monitoring techniques.....	48
2.4.1 Monitoring using the human senses.....	50
2.4.2 Lubrication analysis	50
2.4.3 Vibration analysis	51
2.4.4 Acoustic or airborne sound analysis	52
2.5 Analysis of surface vibration and airborne sound signals	56
2.5.1 Time-domain analysis of vibration signals	56
2.5.2 Frequency-domain analysis of vibration signal.	58
2.6 Summary.....	59
CHAPTER THREE	62
SURFACE VIBRATION, AIRBORNE SOUND AND ACOUSTIC EMISSION SOURCES IN A SELF-ALIGNING SPHERICAL JOURNAL BEARING	62
3.1 Introduction.....	62
3.2 Surface vibration sources.....	66
3.2.1 Vibration model	66
3.2.2 Responses due to external forces	68
3.2.3 Responses due to asperity contact.....	74
3.3 Airborne sound sources.....	75
3.3.1 Lubricant pressure fluctuation	75
3.3.3 Bearing roughness excitations	79
3.3.4 Component vibration	80
3.3.5 Fluid flow turbulence.....	81
3.4 Acoustic emission sources	81

3.4.1 Asperity contact excitation	81
3.4.2 Acoustic emission energy release	84
CHAPTER FOUR.....	91
EXPERIMENTAL FACILITIES.....	91
4.1 Introduction.....	91
4.2 Test rig construction and components	91
4.2.1 Testing bearings	92
4.2.2 AC driving motor.....	93
4.2.3 Hydraulic cylinder	94
4.2.4 Hard rubber coupling	96
4.2.5 DC Generator	96
4.3 Speed and torque controller.....	97
4.4 Data acquisition and measurement systems	98
4.4.1 Data acquisition system for vibration and airborne sound.....	98
4.4.2 Data acquisition system for AE	101
4.4.3 Load cell.....	103
4.4.4 Temperature sensor	104
4.4.5 Pressure sensor.....	104
4.4.6 Shaft encoder	105
4.5 Seeded faults.....	105
4.5.1 Water contaminated lubricant	105
4.5.2 Surface scratch.....	106
4.6 Experimental procedure.....	107
4.6.1 Radial load and speed variation.....	107
4.6.2 Lubricant viscosity variation.....	108
4.6.3 Lubricant deterioration due to water contaminant	108
4.6.4 Scratching surface deterioration	108
4.6.5 Summary of experiment procedure.....	109
CHAPTER FIVE	111
SURFACE VIBRATION, AIRBORNE SOUND AND ACOUSTIC EMISSION	
CHARACTERISTICS OF A SA35M SELF-ALIGNING SPHERICAL JOURNAL	
BEARING UNDER DIFFERENT OPERATION	111

5.1 Introduction.....	111
5.2 Repeatability of experimental results.....	113
5.2.1 Surface vibration.....	113
5.2.2 Airborne sound.....	116
5.2.3 Acoustic emission.....	119
5.3 Surface vibration characteristics.....	124
5.3.1 Time domain analysis.....	124
5.3.2 Frequency domain analysis.....	127
5.4 Airborne sound characteristics.....	130
5.4.1 Time domain analysis.....	130
5.4.2 Frequency domain analysis.....	132
5.5 Acoustic emission characteristics.....	134
5.5.1 Time domain analysis.....	135
5.5.2 Frequency domain analysis.....	137
5.6 Discussion of load and speed characteristics.....	140
5.6.1 Repeatability.....	140
5.6.2 Radial load characteristics.....	141
5.6.3 Speed characteristics.....	142
5.6.4 Frequency characteristics.....	142
5.7 Summary of load and speed characteristics.....	143
5.7.1 Repeatability experimental results.....	143
5.7.2 Surface vibration, airborne sound and acoustic emission characteristics.....	144
CHAPTER SIX.....	146
LUBRICANT QUALITY MONITORING.....	146
6.1 Introduction.....	146
6.2 Abnormal lubricating.....	148
6.2.1 Surface vibration analysis.....	148
6.2.2 Airborne sound characteristics.....	154
6.2.3 Acoustic Emission characteristics.....	159
6.2.3.2 Frequency domain analysis.....	164
6.3 Water contaminated lubricant monitoring.....	168

6.3.1 Surface vibration monitoring	168
6.3.2 Airborne sound characteristics.....	173
6.3.3 Acoustic emission characteristics	178
6.4 Discussion of abnormal viscosity and water contaminated lubricant monitoring....	186
6.4.1 Viscosity changing of lubricant	186
6.4.2 Water contaminant in lubricant.....	187
6.5 Summary of lubricant quality monitoring	189
6.5.1 The effect of changing viscosity on the surface vibration, airborne sound and acoustic emission responses.....	189
6.5.2. The effect of water contaminant concentration in the lubricant on surface vibration, airborne sound and acoustic emission responses.....	191
CHAPTER SEVEN.....	193
SURFACE SCRATCH MONITORING.....	193
7.1 Introduction.....	193
7.2 Test method	193
7.3 Surface vibration analysis	194
7.3.1 Time domain analysis	194
7.3.2 Frequency domain analysis.....	196
7.3 Airborne sound analysis.....	198
7.3.1 Time domain analysis	198
7.3.2 Frequency domain analysis.....	200
7.4 Acoustic emission analysis.....	202
7.4.1 Time domain analysis	202
7.4.2 Frequency domain analysis.....	204
7.5 Discussion of monitoring of scratched surface.....	207
7.6 Summary of surface scratched bearing monitoring	209
CHAPTER EIGHT.....	211
CONCLUSIONS AND SUGGESTIONS FOR FURTHER WORK.....	211
8.1 Conclusions.....	211
8.2 Review of Aims and Objectives	214

8.3 Contributions to knowledge	218
8.4 Suggestion for future work	218
8.5 List of Publications	219
REFERENCES	221
APPENDIX	229

LIST OF FIGURES

Figure 1. 1 Self-aligning spherical journal bearing	25
Figure 2. 1 Rolling bearing	32
Figure 2. 2 Journal bearing	33
Figure 2. 3 Solid journal bearing	34
Figure 2. 4 Simple bronze bushing	34
Figure 2. 5 Flanged bush.....	35
Figure 2. 6 Split flange bushing	35
Figure 2. 7 Schematic of split long flange bushing	36
Figure 2. 8 Pivot bearing.....	36
Figure 2. 9 Radial and thrust pad bearing	37
Figure 2. 10 Self-aligning spherical journal bearing	38
Figure 2. 11 Selection of lubricant viscosity	40
Figure 2. 12 Ring oil lubrication.....	41
Figure 2. 13 Oil collar lubrication.....	42
Figure 2. 14 The Stribeck curve.....	43
Figure 2. 15 Scratch marking on bearing surface	45
Figure 2. 16 Wiping damage.....	46
Figure 2. 17 Mechanical fatigue	47
Figure 2. 18 Wear pattern caused by a tapered journal.....	48
Figure 2. 19 Interaction contact between two surfaces in relative motion	49
Figure 2. 20 Deployment of monitoring techniques in the early wear regime	49
Figure 2. 21 AE signal types.....	54
Figure 2. 22 A burst AE signal and the characteristic parameters.....	55
Figure 3. 1 Self aligning spherical journal bearing components	62
Figure 3. 2 Vibro-acoustic responses generation process	63
Figure 3. 3 Surface vibration, airborne sound and AE generation.....	65
Figure 3. 4 Free body diagram of self-aligning spherical journal bearing.....	67
Figure 3. 5 Calculated time domain response due to unbalance	71
Figure 3. 6 Calculated spectrum response due to unbalance	72
Figure 3. 7 Frequency responses in different damping coefficients	73
Figure 3. 8 Frequency responses in different stiffness	74
Figure 3.9 A schematic of the self-aligning journal bearing under hydrodynamic lubrication	75
Figure 3. 10 Journal bearing acoustic transmission	76

Figure 3. 11 Bearing pressure level (dB) in three different viscosities	79
Figure 3. 12 Contact of rough and smooth surfaces	82
Figure 3. 13 Contact between shaft surface and journal bearing	86
Figure 3. 14 Energy release under three different load variation	89
Figure 3. 15 AE Energy release under three different speed variation	89
Figure 4. 1 Test rig construction	91
Figure 4. 2 Self-aligning journal bearing SA35M	92
Figure 4. 3 Self aligning spherical journal bearing assembly	93
Figure 4. 4 Hydraulic system schematic	95
Figure 4. 5 Siemens Micro Master Controller and data acquisition system	97
Figure 4. 6 Sinocera YE6232B	98
Figure 4. 7 PCI-2 AE System board	101
Figure 4. 8 AE signal measurement and data streaming system configuration	102
Figure 4. 9 Self-aligning spherical journal bearing, normal and with seeded scratch	106
Figure 5. 1 Instrumentation measurement installation	112
Figure 5. 2 SV signal of bearing under 10bar radial loads for three tests	113
Figure 5. 3 SV RMS value from raw signal of DE and NDE bearing under three loads and four speeds for three test runs	114
Figure 5. 4 SV spectra of DE and NDE bearing under 20 bar load and 100% maximum speed	115
Figure 5. 5 SV mean spectrum response value on bearing under different load and speeds for three test runs	116
Figure 5. 6 AS signal for DE and NDE bearings under 10bar radial loads at maximum speed for three test runs	117
Figure 5. 7 AS RMS values from raw time domain signals for DE and NDE bearings under three loads and four speeds for three test runs	117
Figure 5. 8 AS spectra for DE and NDE bearings under maximum load and at maximum speed for three tests runs	118
Figure 5. 9 AS mean spectra for DE and NDE bearing under different speeds and radial load	119
Figure 5. 10 AE time domain signal for DE and NDE bearing under three loads at maximum speed for three test runs	120
Figure 5. 11 AE RMS values for DE and NDE bearings in three loads at four speeds for three test runs	121
Figure 5. 12 AE spectra for DE and NDE bearings under three loads at 100% speeds for three test runs	122
Figure 5. 13 AE mean value for DE and NDE bearings in three loads at four speeds for three test runs	123

Figure 5. 14 SV signal for DE and NDE bearings for three radial loads at maximum speed	125
Figure 5. 15 Kurtosis values of raw SV time domain signal for both DE and NDE bearings.	126
Figure 5. 16 SV RMS value for time domain signal for both DE and NDE bearings for three radial loads and four speeds.....	127
Figure 5. 17 SV spectra for DE and NDE bearings under three radial loads at 25% maximum speed	128
Figure 5. 18 SV spectra for DE and NDE bearings under three radial loads at maximum speed	128
Figure 5. 19 SV mean value of spectrum (high frequency range 4 kHz to 7 kHz) for DE and NDE bearings under three radial loads at four speeds.....	129
Figure 5. 20 AS signals for DE and NDE bearings for maximum speed and three radial loads	130
Figure 5. 21 AS RMS value of raw signal for DE and NDE bearing for four speeds and three radial loads.....	131
Figure 5. 22 Kurtosis value of AS time domain raw signal in DE and NDE bearings for three radial loads and four speeds.....	132
Figure 5. 23 AS spectra for DE and NDE bearings under three radial loads at speed 25% maximum	133
Figure 5. 24 AS spectra for the DE and NDE bearings at maximum speed and three radial loads.....	133
Figure 5. 25 AS mean value of spectrum (7 kHz to 18 kHz) for DE and NDE bearings for three radial loads and four speeds.....	134
Figure 5. 26 AE signal for DE and NDE bearing for three radial loads at 50% maximum speed	135
Figure 5. 27 AE signal for DE and NDE bearing for three radial loads at maximum speed	135
Figure 5. 28 Kurtosis values of raw AE signal for both DE and NDE bearings for three radial loads and four speeds.....	136
Figure 5. 29 AE RMS value from raw signal for DE and NDE bearings for four different speeds and three radial loads.....	137
Figure 5. 30 AE spectra for DE and NDE bearing for radial load 20 bar at 100% maximum speed at frequency range 1-100kHz.....	138
Figure 5. 31 AE spectra for DE and NDE bearing for radial load 20 bar at maximum speed at frequency range 100-500kHz.....	138
Figure 5. 32 AE mean amplitude for low (20 kHz to 90 kHz) and high frequency (90 kHz to 320 kHz) ranges for the DE bearing for three loads and four speeds	139
Figure 5. 33 AE mean amplitude for low (20 kHz to 90 kHz) and high frequency (90 kHz to 320 kHz) ranges for the DE bearing for three loads and four speeds	139
Figure 6. 1 Bearing life with water contamination of lubricating oil	147

Figure 6. 2 SV signal on bearing for different lubricant viscosities at 100% speed and radial load of 10bar	149
Figure 6. 3 Kurtosis value of raw signal for three different loads, four speeds and three lubricant viscosities.....	150
Figure 6. 4 SV RMS value from raw signal in DE and NDE under different speed, radial loads and lubricant viscosity	151
Figure 6. 5 SV spectrum in DE and NDE bearing for three different lubricant viscosities at 50% maximum speed, radial load 20 bar	152
Figure 6. 6 SV spectrums in DE and NDE bearing for three different lubricants at maximum speed, radial load 20 bar	152
Figure 6. 7 SV mean value in DE and NDE bearing under different speed, radial loads and lubricant viscosity at high frequency	153
Figure 6. 8 AS signal in DE and NDE bearing under different lubricant viscosity at maximum speed with 10 bar radial load	154
Figure 6. 9 AS RMS value raw signal for DE and NDE bearings under three different loads, four speeds and three viscosities.....	155
Figure 6. 10 Kurtosis value of AS raw signal for DE and NDE bearings under three different loads, four speeds and three viscosities	156
Figure 6. 11 AS spectrum for DE and NDE bearings under 10 bar radial load, at 50% maximum speed for three different lubricant viscosities	157
Figure 6. 12 AS spectrum for NDE bearings under 10 bar radial load, at maximum speed for three different lubricant viscosities.....	157
Figure 6. 13 AS spectral mean value (3 kHz to 6 kHz) for DE and NDE bearings for four speeds and three loads with three different lubricants	158
Figure 6. 14 AE signal for DE and NDE bearings under three radial loads and three viscosities at 50% maximum speed	160
Figure 6. 15 AE signal for DE and NDE bearings under three radial loads and three viscosities at maximum speed.....	161
Figure 6. 16 AE RMS value from raw signal for DE bearing under three radial loads, four speeds and three lubricant viscosities	162
Figure 6. 17 AE RMS value from raw signal for NDE bearing under three radial loads, four speeds and three lubricant viscosities	163
Figure 6. 18 Kurtosis of AE signal from DE and NDE bearing under different radial loads, for four speeds and three lubricant viscosities	164
Figure 6. 19 AE spectrum for DE and NDE bearings for three radial loads, three lubricant viscosities at 100% maximum speed at frequency range 1-100kHz.....	165
Figure 6. 20 AE spectrum for DE and NDE bearings for three radial loads, three lubricant viscosities at maximum speed.....	166
Figure 6. 21 AE mean amplitude in frequency range 20 kHz to 90 kHz for NDE bearing for three radial loads, four speeds and three lubricant viscosities	167

Figure 6. 22 AE mean amplitude in frequency range 90 kHz to 320 kHz for NDE bearing for three radial loads, four speeds and three lubricant viscosities	168
Figure 6. 23 SV signal with three different levels of water contaminant at 100% speed under 10bar radial load	169
Figure 6. 24 SV RMS of raw signal for four speeds, three radial loads and three levels of contaminant.....	170
Figure 6. 25 Kurtosis for raw signal from DE and NDE bearings for four speeds, three radial loads and three levels of contaminant.....	170
Figure 6. 26 SV spectrum under different water contaminants at 50% speed.....	171
Figure 6. 27 SV spectrum under different contaminants at 100% speed.....	172
Figure 6. 28 SV mean spectrum 7 kHz to 9 kHz for radial load of 10 bar, maximum speed and three levels of water contaminant	173
Figure 6. 29 AS signal for three levels of water contaminant concentration, 10 bar radial load at maximum speed	174
Figure 6. 30 AS RMS from raw signal in different load, speed and water contaminant concentration.....	175
Figure 6. 31 Kurtosis value of in different load, speed and water contaminant concentration	175
Figure 6. 32 AS spectrum under 10bar radial load at 50% speed with different water contaminant concentration.....	176
Figure 6. 33 AS spectrum under 10bar radial load at 100% speed with different water contaminant concentration.....	177
Figure 6. 34 AS mean spectrum with different water contaminant concentration under 10bar radial load and 100% speed	178
Figure 6. 35 signal under different levels of water contamination and load at 50% speed .	179
Figure 6. 36 AE signal under different levels of water contamination, and load at 100% speed	180
Figure 6. 37 AE RMS from raw signal under speed, radial load and different water contaminant concentration.....	181
Figure 6. 38 AE RMS from raw signal for NDE bearings for three radial load, four speeds and three water contaminant concentrations.....	181
Figure 6. 39 AE spectrum under radial load and different water contaminant concentration at 100% speed.	182
Figure 6. 40 AE spectrum under radial load and different water contaminant concentration at 100% speed in frequency range 100kHz-500kHz.	183
Figure 6. 41 AE mean value in DE bearing under different speed, radial load and with water contamination at frequency range 20 kHz-90 kHz	184
Figure 6. 42 AE mean value in DE bearing under different speed, radial load and with water contamination at frequency range 90kHz-320kHz	185
Figure 6. 43 SV spectrum under 20 bar, 100% and in different viscosity.....	187
Figure 6. 44 Vibration spectrum under 20 bar, 100% and in different contaminant	189

Figure 7. 1 SV signals for a normal bearing and a scratched bearing under different radial load at 100% speed.	194
Figure 7. 2 RMS value from raw signal in different load, speed and bearing condition.....	195
Figure 7. 3 Kurtosis value on bearing in different load, speed and bearing condition	195
Figure 7. 4 SV spectrum under different load and condition at 100% of speed.....	196
Figure 7. 5 SV mean value in bearing under different load, speed and bearing condition at low frequency range.....	197
Figure 7. 6 SV mean value in bearing under different load, speed and bearing condition at high frequency range.....	198
Figure 7. 7 AS signal different bearing condition and radial load at speed 100%	199
Figure 7. 8 AS RMS value from raw signal in bearing under different speed, radial load and bearing condition	199
Figure 7. 9 Kurtosis value in bearing under different radial load, speed and bearing condition	200
Figure 7. 10 AS spectrum in bearing under different radial load and different condition...	201
Figure 7. 11 AS mean value in bearing under different load and different condition at low frequency band.....	201
Figure 7. 12 AS mean value in bearing under different load and different condition at high frequency band.....	202
Figure 7. 13 AE signal comparison for similar bearing condition under different load at 100% speed	203
Figure 7. 14 AE RMS value in bearing under different load and different condition	203
Figure 7. 15 AE spectrum in different bearing condition under different radial load at 100% speed	204
Figure 7. 16 AE spectrum in different bearing condition under different radial load at 100% speed	205
Figure 7. 17 AE mean value in different bearing condition under different radial load and speed at low frequency.....	206
Figure 7. 18 AE mean value in different bearing condition under different radial load and speed at high frequency	206
Figure 7. 19 Vibration spectrum under 20 bar radial load and 100% speed for scratched and healthy bearings	208

LIST OF TABLES

Table 2. 1 Viscosity selection for medium pressure.....	39
Table 2. 2 Viscosity selection in general	39
Tabel 3. 1 Journal bearing parameter data	70
Tabel 3. 2 Journal bearing operation parameter data.....	71
Tabel 3. 3 Geometrical journal bearing parameter	78
Tabel 3. 4 Journal bearing geometrical design parameter data.....	88
Table 4. 1 Self-aligning journal bearing SA35M housing dimensions.....	93
Table 4. 2 Test rig motor specification	94
Table 4. 3 Hydraulic ram specification.....	94
Table 4. 4 Hydraulic hand pump specification	95
Table 4. 5 Hydraulic pump tank specification	95
Table 4. 6 Specification for Fenner Coupling HRC130H.....	96
Table 4. 7 Technical specifications of the Sinocera	99
Table 4. 8 Specification of the Sinocera accelerometer model CA-YD-185TNC.....	100
Table 4. 9 Specifications of the Sinocera microphone model BAST YG 201	101
Table 4. 10 Specifications of the PCI-2 AE system specification	102
Table 4. 11 AE transducer specification	103
Table 4. 12 Sinocera load cell specification	103
Table 4. 13 Thermocouple specification.....	104
Table 4. 14 Pressure transmitter specification	104
Table 4. 15 Encoder specification.....	105
Table 4. 16 Experiment procedure for repeatability and viscosity variation	109
Table 4. 17 Water contaminant in oil and scratching surface bearing.....	110

LIST OF ABBREVIATIONS

AC	Alternating current	TBN	Total Base Number
AE	Acoustic emission	USB	Universal serial bus
ALE	Adaptive line enhancement	VA	Vibration analysis
AS	Airborne sound	TBN	Total Base Number
BPF	Blade pass frequency	VG	Viscosity grade
CF	Crest factor	WDA	Wear debris analysis
CM	Condition monitoring		
cps	Cycle per second		
cSt	Centistokes		
DAC	Data acquisition card		
DAS	Data acquisition system		
dB	Decibels		
DC	Direct current		
DE	Drive end		
EN	Entropy		
FF	Fundamental frequency		
FL	Frequency of electrical line		
HFRT	High frequency resonance technique		
HP	Horse power		
HRC	Hard rubber coupling		
Hz	Hertz		
ISO	International Standard for Organisation		
kHz	Kilohertz		
KT	Kurtosis		
kWatt	Kilowatt		
NDE	Non drive end		
OA	Oil analysis		
Pa	Pascal		
PDF	Probability density function		
PK	Peak		
RB	Rolling bearing		
RMS	Root mean square		
rpm	Revolution per minutes		
SASJB	Self-aligning spherical journal bearing		
SB	Sliding bearings		
SK	Skewness		
STFT	Short time Fourier transform		
SV	Surface vibration		
TAN	Total Acid Number		

LIST OF NOTATIONS

X_{RMS}	arithmetic mean or average of the square of the X value	dimensionless
X_i	value of variable X at instant i	dimensionless
X_{PK}	maximum absolute value of the waveform	dimensionless
$ X $	absolute value of X	dimensionless
\bar{X}	mean of data set	dimensionless
S	standard deviation of the distribution	dimensionless
N	number of set	dimensionless
$EN(X)$	Shannon entropy	dimensionless
$p(X_i)$	probability of variable X	dimensionless
$f(x)$	normal distribution of a continuous variable X_i	dimensionless
$S_x(\omega)$,	power spectrum	dimensionless
$x(t)$	time signal	dimensionless
$Cp_x(\tau)$,	power ceptrum	dimensionless
h	film thickness	M
η	viscosity dynamic	Pa.s
V	linear velocity	m/s
p	pressure distribution	Pa
c_r	radial clearance	m
ε	eccentricity ratio	dimensionless
θ	contact angle	rad
p_f	oil pressure fluctuation	Pa
p_r	pressure reflected	Pa
p_a	surrounding air pressure	Pa
Z_b	acoustic impedance of bearing	(kg/m ² s)
ρ_b	bearing density	Kg/m ³
C_b	sound speed in bearing	m/s
Z_a	acoustic impedance of the surrounding air	(kg/m ² s)
ρ_a	air density	Kg/m ³
c_a	sound speed in air	m/s
p	pressure on the projected area	Pa
p_m	mean pressure of the oil	Pa
p_{firms}	RMS pressure of oil	Pa
t	time interval	s
Lp	pressure level in fluid film	dB
p_{ref}	reference of sound pressure $2 \cdot 10^{-5}$ Pa	Pa
L_{pa}	sound level transmitted into air in a radial direction	dB
L_{pab}	average sound pressure transmitted into the air	dB
L_v	noise or airborne sound level	dB
R_{a2}	mean arithmetic surface roughness for second component	μm
Z_b	acoustic impedance of bearing	(kg/m ² s)
ρ_b	bearing density	Kg/m ³
C_b	sound speed in bearing	m/s

R_{a1}	mean arithmetic surface roughness for first component	μm
V_1	sliding speed for first component	m/s
V_2	sliding speed for second component	m/s
P_{ra}	radiated airborne sound power	dB
R_a	mean arithmetic surface roughness	micron
Ac	apparent contact area	m^2
λ_a	exponent of acoustic	dB/decade
P_{ra}	radiates sound power	Watt
c_s	speed of sound	m/s
A_v	vibrating area	m^2
η_{rad}	radiation efficiency	dimensionless
P_{rat}	radiates sound power	Watt
U	speed of sound	m/s
λ_u	constant due to speed of sound	dimensionless
R_{a1}	mean arithmetic surface roughness for first component	μm
V_1	sliding speed for first component	m/s
V_2	sliding speed for second component	m/s
P_{ra}	radiated airborne sound power	dB
R_a	mean arithmetic surface roughness	micron
Ac	apparent contact area	m^2
λ_a	exponent of acoustic	dB/decade
P_{ra}	radiates sound power	Watt
R_a	surface roughness (R_a)	m or μm
R_{a1}	height of the individual asperities, R_{a1}	m or μm
W_i	average load	N
W	applied radial load	N
n_a	asperity density	peak/ m^2
A_i	asperity area of contact	m^2
E_{ei}	stored of energy of elasticity	Nm
$d\delta$	deformation	m
E'	equivalent elasticity modulus of the two materials	Pa
ν_1	Poisson ratio for the first materials	dimensionless
ν_2	Poisson ratio for the second materials	dimensionless
E_e	stored energy of elasticity	Nm
E_1	modulus of elasticity for the first materials	N/m^2
E_2	modulus of elasticity for the second materials	N/m^2
E_{ei}	energy of elasticity	Nm
\dot{E}_e	releasing rate of the elastic energy	Nm/s
L	half-length	m
R'	equivalent radius of cylinder	m
R_1	shaft or journal radius	m
R_2	bearing bore radius	m
b	half width of the two cylinder contact	m

ABSTRACT

High power machinery such as steam turbines, large pumps and motors often use journal bearings as rotor supports. This type of bearing is simple, low cost and with high load carrying capacity. However, abnormal operating conditions in the journal bearings will degrade machine performance, increase operating cost and may cause unexpected sudden failure which is dangerous in both engineering and safety terms.

Bearing condition monitoring can detect faults at an early stage and prevent the occurrence of such failures which can be catastrophic.

Monitoring techniques that have been used for monitoring of journal bearing are lubricant analysis, vibration analysis, noise and acoustic emission analysis. Lubricant analysis has been used effectively for condition monitoring for a long time but cannot be implemented in real time.

Many researchers have studied the use of the vibration and sound signals and acoustic emissions generated by the hydrodynamic journal bearing for detecting and diagnosing faults. The studies give relatively little information regarding surface vibration and airborne sound characteristics for self-aligning spherical journal bearings, nor has comprehensive condition monitoring been implemented for a particular self-aligning spherical bearing journal.

Surface vibration, airborne sound analysis and acoustic emission monitoring can be used simultaneously to detect any signal emitted from the bearing at very wide frequency range. Sound vibration occurs in solid structure, liquid and gases transmitted to air surrounding create airborne sound.

This study has conducted a thorough review of theoretical and experimental studies. The research began with designing and building a test rig consisting of a drive system, radial loading system, torsion loading system, the bearing testing system itself and control, data acquisition and measurement instrumentation systems include encoder, pressure transducers, thermocouples, load cells, vibration transducer, acoustic and acoustic emission sensors.

Preliminary experiments were conducted to ensure all equipment and instrumentation worked well and also to test measurement repeatability. Preliminary experiment results showed that all the equipment either driving, loading, data acquisition and measurement system works well.

Experimental analysis of the surface vibration, airborne sound and acoustic emission analysis responses in time domain and frequency domain analysis include RMS value, Kurtosis and mean value showed good repeatability. The AE measurement response showed the best repeatability, followed by surface vibration and airborne response.

Theoretical study shows that the self-aligning spherical journal bearing system under radial load generated surface vibration, airborne sound and acoustic emission responses that originated from external force excitation such as fluctuating loads due to system misalignment or unbalance and internal excitation such as asperity in boundary or mixed operation. These excitations generate structure-borne vibration and acoustic emission. The structure-borne vibration dynamic responses then radiated airborne sound. Airborne sound also originated from oil pressure fluctuation and flow turbulence. The surface vibration and airborne sound frequency responses occur at frequencies $< 100\text{kHz}$ and the acoustic emission frequency responses appear at high frequencies $>100\text{kHz}$.

The amplitude and frequency of surface vibration, airborne sound and acoustic emission is influence by radial load, shaft speed and surface quality of journal and bearing components themselves. The quality of asperity contact between journal and bearing may be due to manufacturing defect, lubricant and surface deterioration over time during operation.

The experiments and analysis of the surface vibration, airborne sound and acoustic emission characteristics of the self-aligning spherical journal bearing indicate that there is a positive correlation between the spectrum mean value of surface vibration, airborne sound and acoustic emission with radial load and speed. Meanwhile, when use higher lubricant viscosity creates lower surface vibration, airborne sound and acoustic emission mean amplitude.

Investigation of lubricant deterioration due to water contaminant indicated that when use higher concentration contaminant in the lubricant generates higher spectrum mean value of surface vibration, airborne sound and acoustic emission responses.

The surface deterioration experiment showed that there is a clear significant difference in the frequency domain of surface vibration, airborne sound and acoustic emission between a scratched surface and a normal surface journal bearing.

The surface vibration, airborne sound and acoustic emission frequency characteristic for scratches and lubricant deterioration creates different peak amplitudes and different frequency. The larger the scratch generate the greater the amplitude and higher frequency.

From of the three measurement systems used, acoustic emission is the most sensitive and a better detect of the bearing fault than followed by vibration and air-born sound measurement system. Therefore the acoustic emission measurement technique can be integrated with surface vibration, airborne sound for rotating machinery/engine condition monitoring. Using surface vibration, airborne sound and acoustic emission monitoring the symptoms of early damage at low, medium or high frequency can be detected and more severe and catastrophic failure can be prevented, and finally very high maintenance costs can be eliminated.

DECLARATION

No portion of the work presented in this thesis has been submitted in support of an application for another degree or qualification of this or any other university or other institute of learning.

DEDICATION

This thesis is dedicated for my father, mother, wife (Endah) and daughters (Dias and Tya) for their unwavering support and encouragement throughout my study.

ACKNOWLEDGEMENTS

I would like to sincerely thank my academic supervisor, Prof. Andrew Ball for his inspiration, guidance and making so many valuable experiences possible. Without his help and advice this research could not have been undertaken.

I would also like to express my gratitude to Dr Fengshou Gu as my supervisor, for his sincere help both academic and personal.

I would also like to many thanks to the Government of Indonesia in this regard the Ministry of National Education through the Directorate General of Higher Education and Bandung State Polytechnic which has provided scholarships for this study.

Finally, special thanks go to all my family and friend for their support and encouragement.

COPYRIGHT

1. The author of this thesis owns any copyright in it and he has given the University of Huddersfield the right to use for any administrative, promotional, educational and/or teaching learning process.
2. Copies of this thesis, either in full or in extracts, may be made only in accordance with the regulation of the University library.
3. The ownership of any patents, design, trademarks and any and all other intellectual property right except for the copyright and any reproduction of copy right, which may be described in this thesis, may not be owned by author and may be owned by third parties. Such intellectual property rights and reproductions cannot and must not be made available for use without the prior written permission of owners of the relevant intellectual property right and/or reproduction.

CHAPTER ONE

INTRODUCTION

1.1 Background

Complex industrial machinery such as heat engines, turbo-machinery and manufacturing or production machinery consists of many components, a key element is the transmission system used for transmitting power, movement and torsion from one place to another.

A bearing is a machine component which supports the machine load, and is a key in ensuring safe and efficient operation. There are two broad types of bearings widely used in machinery: journal and roller bearings. A common journal bearing is simply a cylindrical sleeve containing a lubricating fluid which surrounds a rotating shaft and prevents metal to metal contact.

Researchers have studied the vibro-acoustic and acoustic emission characteristics of rolling bearings and cylindrical sliding bearings, but studies of surface vibration, airborne sound and acoustic emission for self-aligning spherical journal bearings are still very limited publications.

A self-aligning spherical journal bearing consist of a spherical plain bearing having a spherical contact surface which permits the bearing to move freely in all directions. This gives it the capability to self-align, which means it can accommodate a degree of misalignment. This bearing uses an oil ring lubrication system. The self-aligning spherical journal bearing (SASJB) is a relatively new type of journal bearing and is shown in Figure 1.1 (Arvis, 2009).

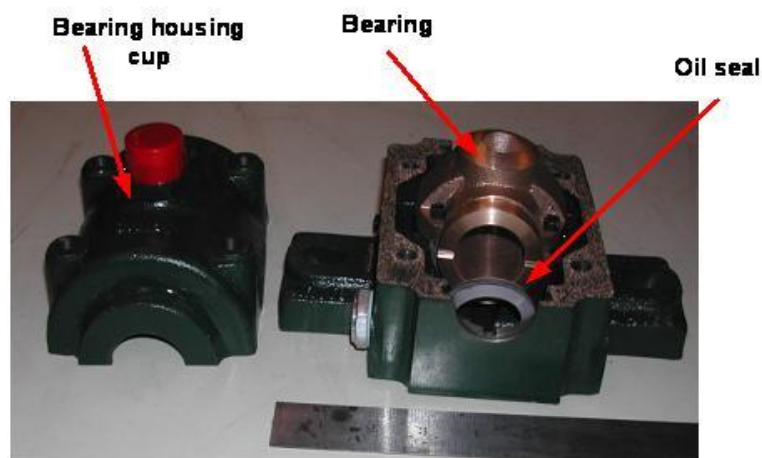


Figure 1. 1 Self-aligning spherical journal bearing

Previous study has shown that most engine or machinery problems are caused by bearing failure, with over 40% of motor failures in machines of 100HP (75kWatt) or more, due to bearing problems (Schoen *et al.*, 1995).

An analysis of typical failures in electrical motors suggests that over half of all faults in the rotor and/or stator, and approximately 40% of all failures are bearing related (Shreve, 2003). Induction machine failure surveys have found the most common failure mechanism to be bearing related faults (40%), stator related (36%) and other faults (22%) (Sin *et al.*, 2003).

Aircraft accident investigation has indicated that the Super Stallion Helicopter CH-53E accident during a test flight was caused by a rotor bearing failure (Tepler and Baldor, 1996).

Flood (2007) showed that 13% of all mechanical seal failures are the consequence of distress that originated with bearing problems.

Above information give information that most damage of the electrical machine and the machine power is caused by bearing faults. Therefore an intensive of bearing monitoring is required.

The bearing may be relatively cheap but because it transmits high power it may fail catastrophically if damaged, which could include not only loss of production and complete loss of machine power, but also serious health and safety issues. Based on the time frame in which the event occurs failure can be classified as catastrophic, intermittent, out of tolerance and maladjustment (Kreith, 1998).

In an hydraulic system, the stage of the system malfunction caused by contamination can be categorized as degradation failure, transient or intermittent failure and finally catastrophic failure (Babcock *et al.*, 2003).

By bearing condition monitoring, early faults and symptoms of failure can be detected and the catastrophic failure avoided.

1.2 Motivation and Topic of Research

The most commonly used techniques for monitoring bearings are lubrication analysis, surface vibration, airborne sound analysis, acoustic emission analysis and bearing performance analysis.

Many condition based maintenance and non-destructive testing techniques can be applied to manufacturing, petroleum refining, chemical and associated industries. A survey of CM

systems in industry showed that industry typically used vibration analysis in 17.29% of cases, oil analysis 13.20%, infra-red thermograph 11.57%, human senses 10.75%, motor current analysis 9.00%, dye penetrant examination 8.64%, ultrasonic thickness testing 8.53%, ultrasonic crack detection 7.36%, magnetic particle inspection 6.54%, acoustic emission analysis 4.56%, and other methods 2.56% (Higgs *et al.*, 2004).

Lubricant analysis has been widely used since the 1960's after railway companies in the United States first introduced this method in the late 1940's (Poley, 2007).

Vibration analysis is one of the most commonly used CM techniques in industry. It has the great advantage that it yields relevant data in a quantitative format and can be operated remotely in real-time. Based on the measured signal, pre-set alarm limits can be triggered automatically (Roylance, 2003).

Ahmadi and Mollazade (2009) used vibration condition monitoring for bearing fault diagnosis of a mine stone crusher and the results indicated that such a technique was effective for machine fault prediction and diagnosis. Choy and his co-workers successfully used vibration monitoring to identify and quantify bearing damage in a rolling bearing (Choy, *et al.*, 2005).

Shiroishi and his companion succeeded in detecting damage of the outer race on a rolling bearing using vibration analysis by combining the high frequency resonance technique (HFRT) and adaptive line enhancement (ALE) (Shiroishi, *et al.*, 1999).

Vibration monitoring has also been used to monitor and diagnose faults in a reciprocating engine (DeBotton, 2000), rotating machine (Pandey, 2011), an electrical motor (Monavar, 2008) and a gear box (Saravanan, 2009).

DeCamillo and co-workers investigated the characteristics of a tilt pad journal bearing (DeCamillo, *et al.*, 2008).

However the literature search revealed relatively little information regarding the application of vibration analysis to journal bearings particularly self-aligning spherical journal bearings.

Acoustic or sonic analysis is the measurement of sound pressure waves generated by component contact inside equipment and radiated from the surface of the machine. Its application in industry with respect to monitoring bearing faults is relatively new (Grible, 2006).

Airborne sound from journal bearings is generated mainly by mechanical contact between journal or shaft and bearing. Sound also can be generated by hydrodynamic sources. Airborne sound is characterized by its amplitude and frequency, and while it has been used for noise control for health, safety and comfort purposes in places of work such as noise monitoring on aircraft (Genesca *et al.*, 2011) and acoustic monitoring on a diesel engine (Jiang, 2008).

Acoustic emission (AE) is an inspection technique which detects elastic waves generated by such sources as cracking, cleavage, fretting and so forth. To treat AE waves theoretically, elasticity dynamics is needed to model AE sources and solve the wave propagation equations (Ohtsu, 2000). AE may be used to investigate or to measure the transient elastic energy wave that is generated from rapid strain energy caused by deformation or damage within or on the surface. Dickershof (2006) investigated lubrication regimes in sliding bearings using acoustic emission. They reported that AE analysis is an appropriate measurement procedure to detect incipient failure of sliding bearings with correlation between the emitted acoustic signal and the energy dissipated in the sliding metallic contact. AE has been widely used in a number of fields to monitor the wear in bearings. When the wear increases, the asperity contact also increases, which will produce more vibration and acoustic emission. AE has also been used to detect and estimate rolling bearings defects (Abdullah, 2006).

Holford and co-workers used AE for crack detection in aircraft construction (Holford, 2009).

Thermography is a predictive maintenance technique that can be used to monitor the condition of plant machinery, structure, and systems. It uses instrumentation designed to monitor the emission of infrared energy to determine operating temperature. By detecting areas of elevated temperatures, an experienced technician can locate incipient problems within the machine and/or plant (Mobley, 2002).

Previous researchers have studied the vibration characteristics of hydrodynamic journal bearings in the lower frequency range ($f \leq 20$ kHz) and the higher frequency range ($f \geq 100$ kHz) for monitoring and detecting damage in ball and journal bearings. These studies give relatively little information regarding acoustical properties of noise radiated from the bearings (Rho *et al.*, 2003).

Previous researchers have studied low, medium, high and very high frequency vibration, airborne sound and AE characteristics of a hydrodynamic journal bearing but these studies give relatively little information regarding to the surface vibration, airborne sound characteristics for self-aligning spherical journal bearings, nor has comprehensive condition monitoring been found of a particular self-aligning spherical bearing journal.

This research will investigate a new type journal bearing – the self-aligning spherical journal bearing and will focus on the using of surface vibration, airborne sound and acoustic emission analysis at low, medium, high and very high frequency ranges simultaneously for early fault detection and diagnosis.

Thus the title of this research is "**An Investigation of Surface Vibration, Airborne Sound and Acoustic Emission Characteristics of a Journal Bearing for Early Fault Detection and Diagnosis**".

1.3 Research Aims and Objectives

The aim of this research is to develop on line condition monitoring technique for journal bearing based on surface vibration, airborne sound and acoustic emission measurements. To achieve this aim main objectives have been set as follows:

1. To design comprehensive test system including mechanical, electrical and measuring systems for testing a self-aligning spherical journal bearing under different operating conditions.
2. To develop surface vibration, airborne sound signal generation models for understanding the dynamic behaviours of a self-aligning spherical journal bearing.
3. To develop a monitoring measurement and analysis system for journal bearing condition monitoring.
4. To study the characteristics of surface vibration, airborne sound and acoustic emission signal response of the self-aligning spherical journal bearing under the influence of radial load and speed variation.
5. To investigate the characteristics of the surface vibration, airborne sound and acoustic emission response of the self-aligning spherical journal bearing under different oil viscosities such as ISO VG 32, ISO VG 68 and SAE 90.

-
6. To investigate the characteristic of surface vibration, airborne sound and acoustic emission due to lubrication deterioration caused by different water contaminant in the lubricant 0%, 1.25% and 2.5%.
 7. To investigate the characteristic of surface vibration, airborne sound and acoustic emission due to the bearing surface deterioration caused by scratching.
 8. To develop MatlabTM codes for processing and analysing the data sets from the accelerometers, microphones and AE sensors in the time, frequency and time-frequency domains.
 9. To provide guide lines for further research and development of surface vibration, airborne sound and AE characteristic for self-aligning spherical journal bearing for early fault detection.

1.4 Outline of Thesis

This thesis is organised into eight chapters according to the logical connection involved in achieving the research objectives. The following is a brief description of each chapter:

Chapter one is the introduction and contains background, motivation and title of the research topic, the research aims and objectives and an outline of thesis.

Chapter two explains journal bearing types, lubricant selection for journal bearing, lubrication system, journal bearing faults and failures modes and journal bearing monitoring methods and techniques.

Chapter three describes the surface vibration, airborne sound and AE sources of a self-aligning spherical journal bearing including bearing components.

Chapter four describes the experimental facilities; the test rig and its components including the electrical motor drive, the torque load system, the instrumentation and data acquisition systems and analysis software, the self-aligning spherical journal bearing, the seeded journal bearing faults and the experimental program.

Chapter five examines the repeatability analysis of the test rig and characteristics of the measured surface vibration, airborne sound and acoustic emission of the self-aligning spherical journal bearing with radial load and speed variation.

Chapter six presents the lubricant quality monitoring through surface vibration, airborne sound and acoustic emission characteristics on uncontaminated and water contaminated lubricant in the self-aligning spherical journal bearing.

Chapter seven reports the scratched surface monitoring through surface vibration, airborne sound and acoustic emission on the self-aligning spherical journal bearing.

Chapter eight presents the conclusions and reviews the achievements of the project against the aim and objectives, describes the contribution to knowledge made by the research, suggests possible future work and list of publications.

CHAPTER TWO

JOURNAL BEARINGS, FAILURE MODES AND MONITORING TECHNIQUES

2.1 Bearing types

Bearings are machine components used to transmit power and to move a certain parts, and also for load support. This may be achieved by some form of rolling motion or by some form of sliding action. Based on this fundamental difference, bearings may be divided into two broad classes namely Rolling Bearings (RB) and Sliding Bearings (SB). In the rolling bearing, rolling elements are located between inner and outer rings as shown in Figure 2.1.



Figure 2. 1 Rolling bearing

The rolling bearing consists of four parts: an outer ring, an inner ring, the rolling elements and the retaining cage or separator. With ball bearings the outer ring and the inner ring are concentric with each other and separated by the insertion of balls circumferentially at equal distances.

Basic types of rolling bearings commonly used in machine can be divided into ball bearings, cylindrical roller bearings, barrels or spherical roller bearings, taper roller bearings and needle roller bearings (Klebanov, *et al.*, 2008). Based on the direction of the loads, rolling bearings can be classified into radial bearings and thrust bearings and also can be grouped as cylindrical bore and taper bore bearings.

A journal bearing also known as a plain bearing or sleeve bearing is a bearing without any rotating element but with a sliding component as shown in Figure 2.2.



Figure 2. 2 Journal bearing

(Berry, 2005)

2.2 Journal bearing

A journal bearing is a bearing in which a shaft rotates freely in a supporting metal sleeve or shell with a layer of oil or grease separating the two parts due to fluid dynamic effects. Journal bearings are used to support high radial loads and are used for low to high speeds. Typical applications include large milling systems, engine crankshafts, gearboxes, and shaft bearing supports (Johnson, 2001). Journal bearing or sleeve bearing may be grouped into five basic types: plain cylinder bore, two lobe bore, four lobe bore, four pad tilting and five pad tilting bearings (Finley *et al.*, 2001). However the journal bearings can also be divided into solid, bushed, split, thrust (Khurmi and Gupta, 2005), and the new self-aligning spherical journal bearing.

2.1.1 Solid bearings

The simplest journal bearing is a shaft rotating in a hole bored in the machine housing. However the hole has to be prepared as a bearing surface and this can be done by using hardened steel in the bearing. Solid journal bearings are used where a removable cap is not required.



Figure 2. 3 Solid journal bearing
(Royersford, 2001)

2.1.2 Bushing

Bushing is a journal bearing where a bush is inserted to act as a sleeve, see Figure 2.4. The bush will be of a softer material such as bronze and will be replaced when its wear is deemed excessive. Some common types of bushing include flanged and split bushes.



Figure 2. 4 Simple bronze bushing

Flanged bushings are a sleeve bushing with a flange extending radial outward at one end, see Figure 2.5. The flange on the bush is usually to provide a thrust bearing surface.



Figure 2. 5 Flanged bush

(Aurora, 2010)

The split bushing is composed of a pair of semi cylindrical halves, each provided with a ridge and a groove on the contact surfaces to allow them to be fitted together accurately and easily. Split bushings are used as components in larger power transmission devices. Split bushings aid in the absorption of shock, minimize the need for additional lubrication, reduce noise and vibration, and reduce the maintenance required for optimal operation. A split bearing and housing is shown in Figures 2.6 and 2.7.



Figure 2. 6 Split flange bushing

(Arvis, 2009)

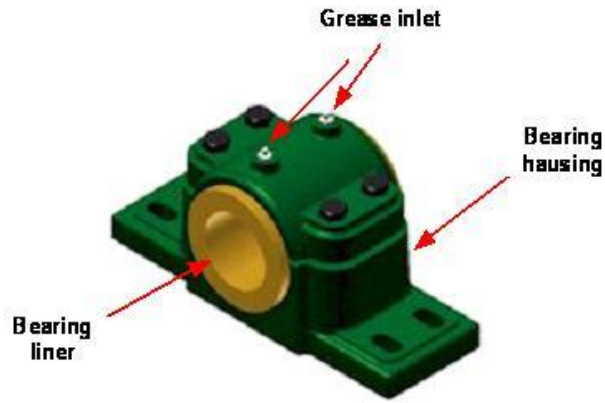


Figure 2. 7 Schematic of split long flange bushing

(Arvis, 2009)

2.1.3 Thrust bearing

A thrust journal bearing is used to support shafts subjected to an axial load. Thrust bearings are sub-divided into pivot bearings and collar bearings. The pivot bearing is a thrust vertical bearing where the loaded shaft rest on a foot step of the bearing, see Figure 2.8. The collar bearing can be for a vertical or horizontal shaft through the bearing with single or multiple collars.



Figure 2. 8 Pivot bearing

(Khurmi and Gupta, 2005)

2.1.4 Tilting pad bearing

Tilting pad or pivoting shoe bearings consist of a journal or shaft rotating within a shell made up of curved pads. The housing is split its long centre line with a number of shoes and a pad fitted under the rim of each shoe that allows the shoes to tilt, see Figure 2.9. Each pad is independently aligned with the surface curvature of the shaft (Scott, 2005).



Figure 2. 9 Radial and thrust pad bearing
(Kingbury, 2010)

2.1.5 Self-aligning spherical journal bearing

The self-aligning journal bearing consist of a spherical plain bearing have a spherical contact surface which permits the inner ring to move freely in all directions. This gives it the capability to self-align, which means it can accommodate a degree of misalignment. Self-aligning journal bearings and housings have a split spherical journal bearing, housing and seal. This bearing is suitable for high speeds and is quiet in operation. The bearing shells can be replaced without the need to dismantle the whole unit from the shaft. This bearing uses an oil ring lubrication system. The spherical self-aligning journal bearing is a relatively new type of journal bearing which is produced by Arvis bearings and is shown in Figure 2.10 (Arvis, 2009).



Figure 2. 10 Self-aligning spherical journal bearing

2.2 Journal bearing lubrication

There are no rolling elements in journal bearings. Their mechanical design and construction may be relatively simple, but the hydraulic theory of these bearings can be complex. Journal bearings consist of two components separated by a lubricant film. The most common cause of premature bearing failure is probably loss or inadequate lubricant. Inadequate lubrication may come from wrong type of lubricant, too little and too much lubricant or wrong frequency of lubricant top-up. If the lubricant film is thick enough to separate the contacting surfaces the friction coefficient will be reduced and the fatigue life of the bearing will be extended.

2.2.1 Lubricant selection

Selection of the proper lubricant is a crucial to prevent premature failure in the journal bearing. Lubricant selection is the starting point in the pursuit of right lubrication application. Many criteria should be considered when selecting a lubricant for a machinery, equipments or components.

Journal bearings are lubricated by a fluid lubricant, where full fluid lubrication gives complete separation between journal bearing surface and shaft, therefore the friction coefficient is low.

The minimum information required for the determination of proper viscosity ISO grade for journal bearing includes speed of shaft (rpm), operation temperature of the oil in the bearing and approximate pressure loading (Pa or Psi) (Johnson, 2008).

There are a number of tables that can be used for ISO viscosity grade lubricant selection for journal bearing.

Table 2.1 provides an ISO viscosity grade lubricant selection based on oil temperature and shaft speed (rpm) for medium pressure such as for automotive or reciprocating engines, about 20.7 to 35 MPa (3000 to 5000 Psi). For most of industrial application the pressure range is between 690 to 2070 kPa (100 to 300 Psi).

Table 2. 1 Viscosity selection for medium pressure.

(Johnson, 2008)

Shaft speed (rpm)	Operating oil temperature (°C)			
	20-50	60	75	90
800	ISO 68	ISO 100	ISO 150	
1200	ISO 46	ISO 68	ISO 100-150	
1800	ISO 32	ISO 46	ISO 68-100	ISO 150
3600	ISO 32	ISO 32	ISO 46-68	ISO 68-100
10000	ISO 32	ISO 32	ISO 32	ISO 32-46

Table 2.2 also provide ISO viscosity grade selection based on bearing or oil temperature and shaft speed.

Table 2. 2 Viscosity selection in general

(Scott, 2005)

Shaft speed (rpm)	Bearing/oil temperature (°C)			
	0-50	60	75	90
300 to 1500	ISO 32	ISO 68	ISO 100-150	
1800	ISO 32	ISO 32-46	ISO 68-100	ISO 100
3600	ISO 32	ISO 32	ISO 46-68	ISO 68-100
10000	ISO 32	ISO 32	ISO 32	ISO 32-46

The selection of appropriate absolute lubricant viscosity grade (cP) based on shaft surface velocity (m/s) and bearing pressure load (kPa or kN/m²) is shown in Figure 2.11.

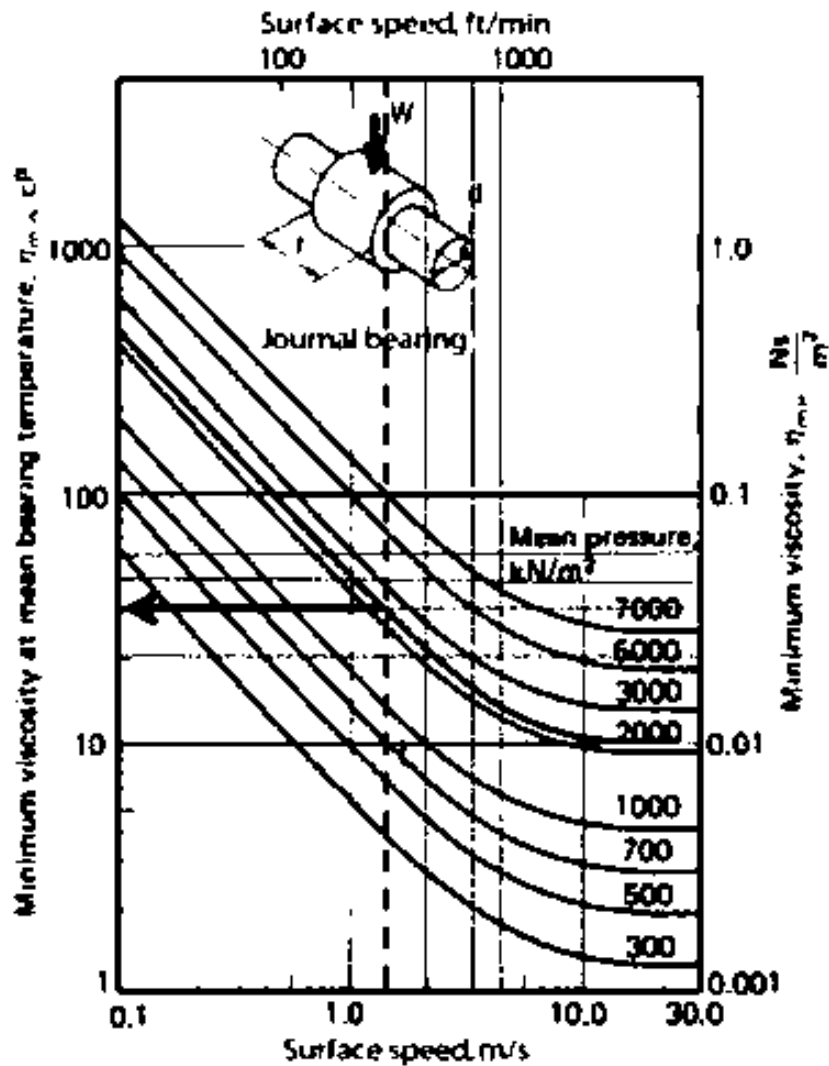


Figure 2. 11 Selection of lubricant viscosity

(Neale, 2001)

The two tables and the figure show that for journal bearing operating at 1450 rpm, the lubricant with viscosity kinematic specification of ISO VG 32 and 46 or with minimum kinematics viscosity of 28.8 cSt and 41.4 cSt are appropriate (Noria, 2001).

The figure 2.11, tables 2.1 and 2.2 indicate that the higher the shaft speed, the lower the lubricant viscosity required and that the higher the operating temperature of equipment or machinery the higher the lubricant viscosity that is required.

2.2.2 Lubricant supply methods

Journal bearing are usually oil lubricated, but for low speed equipment grease may be used. Common types of journal bearing lubrication system are; hand oiling, drip and wick feed, ring and collar feed, bath and splash lubrication and pressure feed (Neale, 2001)

Hand oiling is used for low speed and cheap journal bearings only. Drip feed lubrication is feed of lubricant based on gravity and the lubricant reservoir is usually of glass or Plexiglas.

Oil ring lubrication is where lubrication of the bearing is by means of a ring riding on the rotating shaft which brings up oil from the top of the oil reservoir into which it dips. The ring has an inner diameter about 1.5 times that of the shaft. The journal bearing is slotted to accommodate the ring, see Figure 2.12.

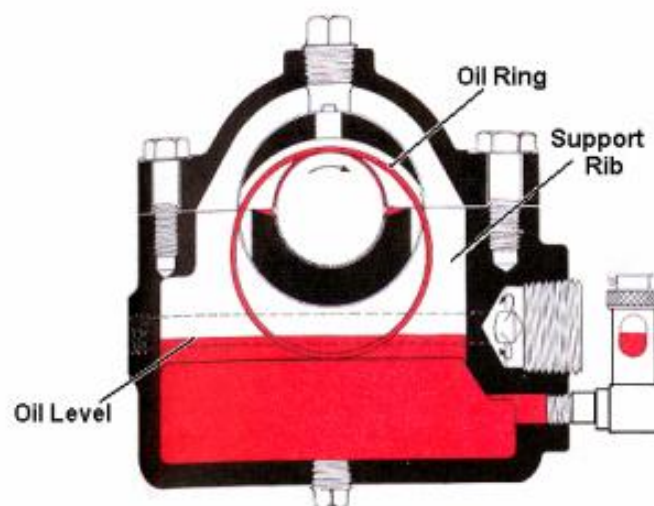


Figure 2. 12 Ring oil lubrication

(Bloch, 2005)

Oil collar lubrication or disk feeding is where a rigid collar which is integral with the shaft or journal dips into the oil reservoir. During rotation it carries the oil and throws it off into a small clearance on both sides of the collar after which the oil flows by gravity through the oil hole and groove to the bearing surface as shown in Figure 2.13

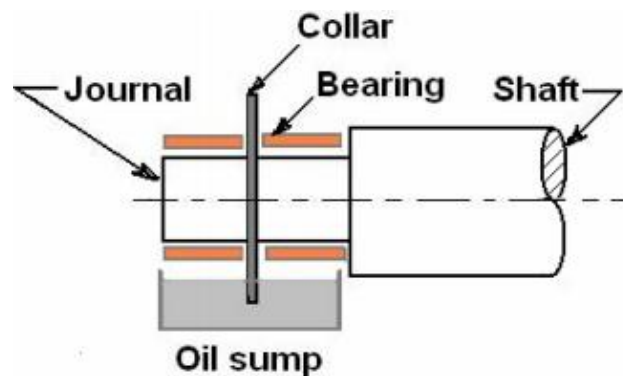


Figure 2. 13 Oil collar lubrication

(Gopinath, no date)

In the oil bath lubrication system the components in contact are sealed in a chamber part filled with oil. The oil level in the chamber is such that the parts are partly submerged and when the submerged components rotate they pick up oil and splash it over the contacting components (Joice, 1995).

In splash lubrication oil is splashed by rapidly moving parts from the oil pan or oil trays. The oil is thrown upward as droplets or fine mist and provides an adequate oil supply to the bearing.

In pressured oil feeding, pressure of a pump is used to supply oil to a circumferential groove in the main bearing. Such a system is used with bearings that operate under heavy loads and high speed.

2.2.3 The lubrication regimes

The coefficient of friction of a bearing is very important, because it determine the life time of bearing. The coefficient of friction for full lubricated journal bearing is a function of bearing modulus, diametral clearance ratio and bearing length to diameter ratio. The bearing modulus depend on the absolute viscosity of the lubricant an as well as angular speed and bearing pressure (Khurmi and Gupta, 2005).

The lubrication regimes can be distinguished by using the Stribeck curve. This curve plots the relationship between the coefficient of friction (f) and the bearing parameter or modulus $\eta N/p$, where η is the absolute viscosity of the lubricant in kg/m.s, N is the shaft speed in rpm and p is the pressure on the projected area in Pa.

The Steinbeck curve shows how the coefficient of friction changes with lubrication regime: boundary lubrication, mixed-film lubrication and hydrodynamic lubrication.

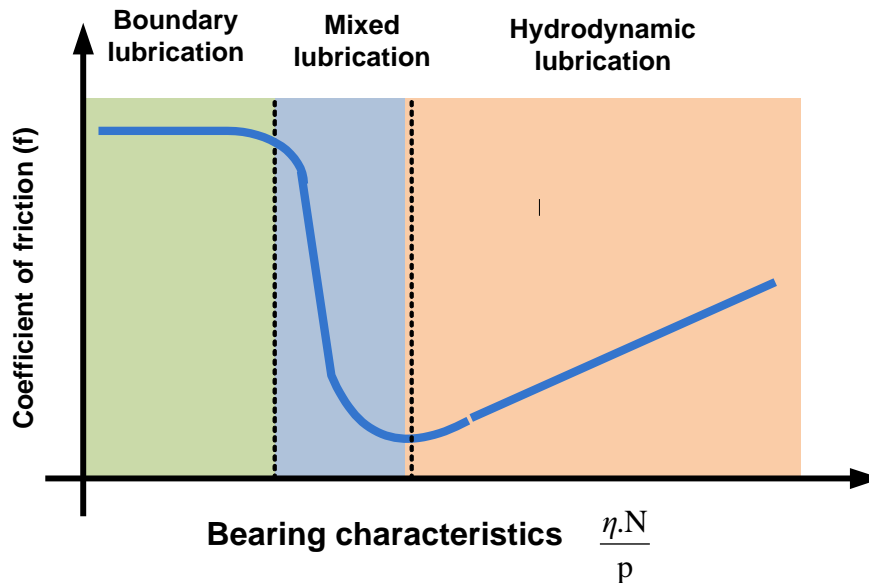


Figure 2. 14 The Stribeck curve

(Hori, 2006)

Boundary lubrication occurs when the lubricating film has the same thickness as the surface roughness (R_a). The high points of asperities on the solid surfaces will contact each other. Boundary lubrication occur when the pressure on the lubricated contact too high, the running speed too low or the surface roughness too great.

The surface films vary in thickness from 5×10^{-9} to 50×10^{-9} m, the minimum film thickness of a mixed lubrication regime is less than the surface roughness ($h < R_a$) (Hamrock, 2006). On the smoothest machined surfaces the height of asperities is about 25×10^{-9} m (Hamrock, 2006).

Mixed lubrication occurs between the boundary and hydrodynamic lubrication range. The fluid film thickness is slightly greater than the surface roughness ($h > Ra$), so that there is very little asperity or high point contact, but the surfaces are still close enough together to have an affect on each other. The minimum film thickness of a mixed lubrication regime is $h_{\min} \sim 10^{-9}$ m and the maximum thickness at the commencement of the hydrodynamic lubrication regime is $h_{\min} \sim 10^{-6}$ m (Dennis and Smith, 1994).

Hydrodynamic lubrication means that the load-carrying surfaces of the bearing are separated by a relatively thick film of lubricant which prevents metal-to-metal contact. Hydrodynamic lubrication does not depend upon the introduction of the lubricant under pressure. The film pressure is created by the moving surface itself pulling the lubricant into a wedge-shaped zone at a velocity sufficiently high to separate the surfaces against the load on the bearing. Hydrodynamic lubrication is also called full-film, or fluid, lubrication (Nisbett, 2008).

Another lubrication system for journal bearings is hydrostatic lubrication which is the process of lubrication using pressure from an external pump to separate journals and bearing surfaces.

2.3 Journal bearing failures

Bearings are small and relatively cheap components of an engine or machine, however failure of a machine bearing commonly leads to serious problems including the need for a complete overhaul. The early detection of the symptoms of faults that could lead to failure in journal bearings is crucial to allow repair to be made in time to prevent possible catastrophic failure.

The bearing damage that often occurs in journal bearings includes scratching, wiping, wear and fatigue. The most common causes of journal bearing failure are associated with inadequate lubrication, improperly machined component and overloading.

Clevite has stated that the eight most common causes of premature machine bearing failure are the ingress of dirt 45%, mis-assembly 13%, misalignment 13%, insufficient lubrication 11%, overloading 8%, corrosion 4%, improper journal finish 3% and others 3% (Clevite, 2002). In practice premature bearing failure is often due a combination of several of these factors.

2.3.1 Scratching

The scratching of journal bearing can be caused by solid contaminant in the lubricant. Solid contaminant from outside in the form of sand and from the machine itself can form wear particle that scratch the surface of the journal bearing.

The large solid contaminant particles such as dirt, dust and metallic hard particles present in the lubricant embed in the soft material bearing lining displacing bearing material and creating a high spot. The high-spot make contact with journal cause a rubbing action that can lead to the rupture of bearing lining. This problem can create high friction, high vibration and noise. Illustration of a scratched journal bearing is shown in Figure 2.15.



Figure 2. 15 Scratch marking on bearing surface

(Clevite, 2002)

2.3.2 Wiping

Wiping is minor rub on the bottom of journal bearing subject to a vertical load (see Figure 2.16). The lubrication breakdown can cause wiping damage and loss of clearance before the hydrodynamic lubricating film has developed. The lubrication breakdown may be influenced by inadequate supply of lubricant, using a lubricant of too low viscosity grade for the application and also fluid contaminant present in the lubricant. Loss of clearance in the journal bearing causes wiping at the bearing centre.



Figure 2. 16 Wiping damage

(Neale, 2008)

Inadequate supply of lubricant can occur when using lubricant with too low a viscosity, when the bearing temperature is too high, when there is misalignment between the shaft and the bush, and excessive load.

2.3.3 Wear

Wear is loss of surface material due to surface contact. Wear can be divided into abrasive wear, adhesive wear, erosion wear and corrosive wear. Abrasive wear is usually due to small particle contamination and is the most common form of wear in lubricated machinery. Two-body abrasion occurs when the metal surface roughness on one surface cuts directly into a second metal surface.

Adhesive wear is the transfer of material from one contacting surface to the other. It occurs when high loads, temperatures or pressures causes the asperities of two metal surfaces to come into contact and can result in small spot-welds then the immediately shearing of the metal in these areas.

Erosion could be considered a form of abrasive wear. It occurs principally in high-velocity, fluid streams where solid particle debris becomes entrained in the lubricant (Scott, 2008).

Corrosion is often caused by the contamination of lubricants in service. Corrosion wear is surface damage resulting from exposure to a reactive environment (Scott, 2008).

2.3.4 Fatigue

Fatigue damage takes place when the journal bearing is under concentrated cyclic loading of misalignment, eccentricity, imbalance, bent shaft, thermal and vibration. The fatigue mechanism occurs more rapidly when repeated bending of the bearing is involved. Imperfect cylindrical geometry of the journal bearing is also a cause of localized loading of engine bearings with consequent wear.

One form of wear is subsurface fatigue which occurs after many working cycles application at high-stresses in the metal. This causes small cracks in the subsurface of the metal, which then propagate to the surface, resulting in small pieces of surface metal being removed. Surface fatigue results in hairline cracks in the surface of the bearing which may appear to open in the direction of rotation. Pieces of bearing may spill out or appear to be pulled away in the direction of rotation, see Figure 2.17.



Figure 2. 17 Mechanical fatigue

(Noria, 2004)

2.3.5 Eccentric bearing

An eccentric bearing is one kind of the imperfect bearing geometry. Eccentric bearings can be caused by manufacturing error but also can be operation system. An eccentric bore fault of the journal bearing is a cause of localized high loading of the bearings with consequent wear. The localized high loading of journal bearing creates bearing geometrical problems such as eccentric oval, taper and ellipse bearing bores.



Figure 2. 18 Wear pattern caused by a tapered journal

(Clevite, 2002)

2.4 Review of journal bearing monitoring techniques

Journal bearings are considered superior to rolling element bearings in vibration absorption, shock resistance, quietness and long life. All these characteristics arise because the journal bearing is supported along its shaft on a thin oil film (Hori, 2006). The smaller outside diameter of a journal bearing compared with that of a rolling element bearing is often beneficial.

The interaction contact between two surfaces in relative motion and how different monitoring techniques can be used to detect and diagnose wear-related failure is shown in Figures 2.19 and 2.20. As the first surface (under load) approaches the second, the interface between them becomes a closely interrelated system influencing the way the surfaces slide over each other. As the sliding starts, any fluid lubricant will shear and the viscous response to surface discontinuities will produce pressure in the fluid. If the pressure is sufficient to balance the applied load, sliding will occur with no solid contact between the surfaces.

Increasing the load causes the fluid film to decrease in thickness and high spots on the surface can protrude through the lubricant layer, sliding will occur but now with contact between the surfaces which will erode them and cause particle wear debris in the lubricant (Glaecer *et al*, 1992).

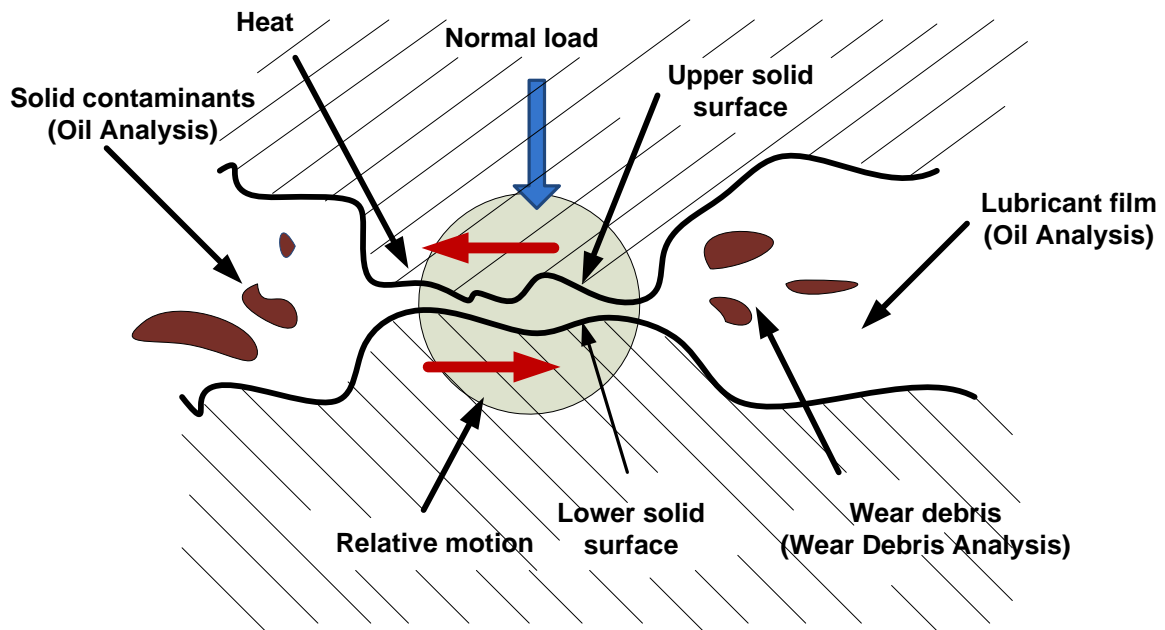


Figure 2. 19 Interaction contact between two surfaces in relative motion

(Roylance, 2003)

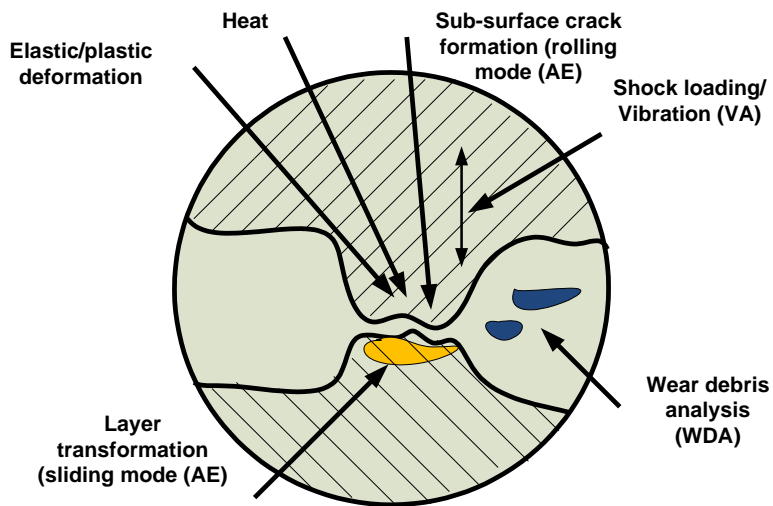


Figure 2. 20 Deployment of monitoring techniques in the early wear regime

(Roylance, 2003)

The most commonly used monitoring techniques deployed throughout industry for monitoring bearings are lubrication analysis, surface vibration, airborne sound analysis and bearing performance but the human senses can also be used detect the symptoms of machine component faults include journal bearings.

2.4.1 Monitoring using the human senses

The first methods for monitoring and inspection of machines used the human senses of touch, sight, hearing and smell. Most, if not all, maintenance personal use at least one human sense to monitor machines. Mobley has sensibly argued they should always make a concerted effort to increase the sensitivity of their own senses as experience is generally the best teacher (Mobley, 2004)

The human senses may be able to detect the difference between healthy and faulty bearings but are generally not sensitive to small changes, and have the inherent problem of being subjective and cannot be expressed in quantitative terms. However, this method remains viable and should be included in modern monitoring systems (Mobley, 2002).

2.4.2 Lubrication analysis

Lubricant monitoring analysis is comparable to blood analysis for human beings and is an important method of predictive maintenance. It can be used to assess the condition of the lubricant and detect the symptoms of early failure of machinery or components, and thus avoid expensive consequences and prolong the machine or equipment life.

The lubricant condition is influenced by the presence of contaminants which may originate from external sources such as water, dust/silica or from internal sources such as metal worn away from machine components. The contamination present in the lubricant reflects the machinery or equipment health. The contamination also may change the physical and chemical property of oil and finally cause degradation of the lubricant.

The general parameter used for lubrication monitoring analysis is viscosity and the tests used are viscosity index test, TAN (Total Acid Number) or TBN (Total Base Number) and water contaminant concentration test. A cleanliness test also called particle counting analysis is used for determining the number of particles in the oil and is expressed in the ISO cleanliness code. Spectrum oil analysis is used to determine the material present in the wear debris in the lubricant for example Fe, Cr, Cu, Sn, etc, and is usually expressed in ppm (part per million).

Ferrography analysis is used for determining size and form of the solid particle in detail. Using these tests it is possible to characterize the wear process (Almeida, 2003).

2.4.3 Vibration analysis

Vibration analysis is one of the most commonly used CM techniques in industry. Vibration analysis has been established and proven as a comprehensive technology to identify a variety of problems. A good vibration condition monitoring program can detect problems and help determine the cause and allows time for appropriate corrective action before equipment failure (Hamernick, 2006)

Using vibration analysis the condition of a machine can be monitored constantly and detailed analysis may be made regarding the health of machine and any faults which may occur or have been arisen (Jayaswal *et al.*, 2008).

Some of the common faults that can be detected using vibration monitoring analysis are unbalance, bent shaft, eccentricity, misalignment, looseness, belt drive problems, gear defects, bearing defects, electrical faults, oil whirl, cavitations and shaft cracks (Girdhar, 2004)

Excessive vibration can cause damage to structures and machine sub-assemblies, resulting in mis-operation, excessive wear, or even fatigue failure. Bearing vibration occurs from many elements in various modes and frequencies simultaneously. Vibration analysis is used to assess the condition of machine bearings and diagnose any problem. Vibration analysis technique is capable of covering a wide range of machine diagnostics and faults within the bearing (Ahmad, 2009).

The vibration parameters are displacement (m), velocity (m/s) and accelerations (m/s^2 or g). The vibration velocity is usually measured in the frequency range of 10 to 1000 Hz.

Measurement should be displacement, velocity or acceleration. Each of which has amplitude and frequency. The amplitude of vibration in the machine is a measure of vibration magnitude displacement on the bearing. The amplitude value may be used to trigger an alarm for high vibration and stop the machine if the vibration exceeds the safe limit.

The frequency of the vibration indicate number of rate the vibration amplitude occurring. The frequency also tells what kind of the vibration sources. The frequency is commonly expressed in Hertz (Hz) or cycle over second.

For measuring bearing vibration, a vibration acceleration sensor is used which determines the acceleration of the measured point relative to a reference system.

The vibration acceleration sensor is the best tool for determining the force from machine vibration. The accelerometer uses a piezoelectric crystal under tension and compression displacement to convert mechanical energy into an electrical signal. The piezoelectric sensors are very good vibration transducers available for industry application. They are solid, usable over a wide temperature range and resist damage from severe shock and vibration (Moblely, 2002)

Accelerometer mounting is very important because it will affect the vibration measurements. Improperly mounting accelerometers on the machine can lead to erroneous data and permanent damage to the accelerometer.

Ideally accelerometer should be mounted on a place closed to vibration source such as on the bearing housing. The accelerometers mounted on bearing housing should provide three-way readings of the acceleration, in the horizontal, vertical and axial directions (Commtest, 2006).

In practice the process of vibration analysis requires gathering complex machine data. The vibration signal originates from many sources of vibration. Each source generates its own signal. The final signal is the sum of the individual signals and is displayed as a composite signal.

The final signal can be displayed in the time domain, frequency domain or in the time frequency domain. The bearing condition can be determined by comparing between the RMS amplitude values of frequency domain signal with an ISO severity chart. The vibration sources can be explained by spectrum analysis.

2.4.4 Acoustic or airborne sound analysis

Airborne sound (AS) can be a loud low frequency or a soft high frequency sound. The human ear can detect a very wide range of both sound levels and frequencies ranging from about 20 to 20 kHz. AS will invariably be a composite formed from a combination of numerous different frequency sources.

The amplitude of the sound wave can be expressed as sound intensity level or sound pressure level. Sound intensity level is the power per unit area per unit time of the sound wave and expressed in Watt/m^2 . It indicates the total acoustic power emitted by the source. The sound pressure is expressed in Pascal (Pa), but usually a logarithmic scale is used where the units are decibels (dB). Sound pressure of a sound wave can be measured using acoustic/sound transducer or microphone.

2.4.5 Acoustic emission analysis

AE may be used to investigate or to measure the transient elastic energy wave that is generated from the rapid release of strain energy caused by deformation or damage within or on the surface of a material. The AE signal is a result of the surface of the material releasing strain energy caused by a deformation which may originate from the interaction of two surfaces that are in relative movement such as occurs in a journal bearing or rolling bearing (Mba, 2003).

AE can be used to identify the presence of bearing defects before they appear in the vibration acceleration range. The signal detected in the AE frequency range represents bearing defect rather than other defects, such as imbalance, misalignment, looseness and shaft bending. AE parameters such as RMS and AE counts can be used for detecting bearing damage, while numerous diagnostic technique such as wavelet, higher order statistics, neural networks etc., could be applied to aid diagnosis (Mba, 2003).

Dickershof *et al.*, (2006) investigated lubrication regimes in a sliding bearing using AE. They reported that AE analysis is an appropriate measurement procedure to detect incipient failure in sliding bearings with correlation between the emitted signal and the energy dissipated in the sliding metallic contact.

AE sensors are piezoelectric with a number of specifications available: general purpose sensors, wide band sensors, low frequency sensors, medium frequency sensors, differential sensors and high temperature sensors which can be used according to the requirements (PAC, 2010).

Based on the shape of the time-domain of the AE signal there are three types of AE: burst, continuous and mixed, see Figure 2.21. Of course, the differences between the three types of signal are arbitrary, if the bursts are frequent enough the burst type signal will appear continuous. And, in fact, many apparently continuous AE signals are composed of a multitude of overlapping bursts. The intensity of AE activity depends on the properties of

the material involved. Factors that tend to increase the amplitude of the AE are high strength, high strain rate, low temperature, thick section, brittleness, and whether the material is cast (Miller and McIntire, 1987).

The acoustic emission energy magnitude is influenced by external load, component materials, roughness or asperity, geometrical occurrence and lubricant viscosity. The increasing of these parameters may create the acoustic emission energy amplitude to increase except for lubricant viscosity.

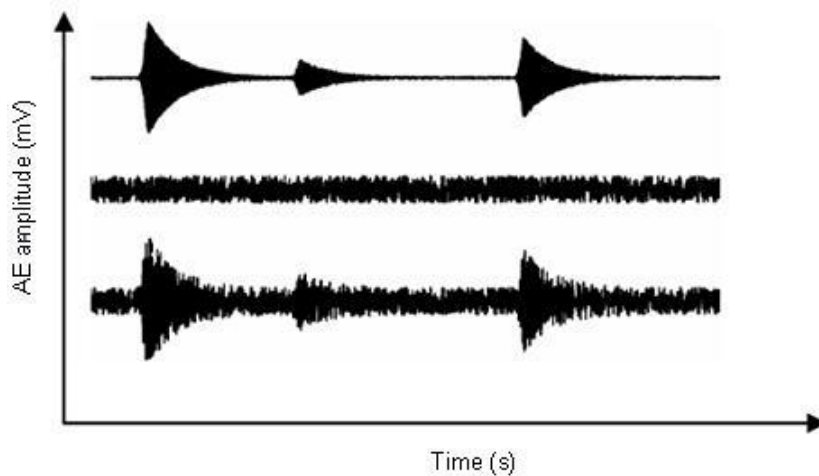


Figure 2. 21 AE signal types

From top down: burst, continuous and mixed (Price *et al.*, 2003)

Another effect on the AE process is the Kaiser effect. This is a special phenomenon concerning crack growth. Once a defined stress has been applied to a sample and then removed, AE will not be induced again in that sample until the level of applied stress exceeds that of the defined stress (Miller and McIntire, 1987). This phenomenon affects the AE generation process as when a rotating component passes a fault in a bearing which generates stress in the material.

The parameters which can be extracted from the signal depend on the type of the signal. For the burst type of signal the parameter are: the duration of the AE event, AE counts, AE count rate, AE energy, AE peak amplitude and the signal rise or decay time, see Figure 2.21. (Mechefske *et al.*, 2002).

An AE event may be defined by the detected AE signal. The AE count is the number of times an AE signal crosses a given threshold limit. AE count rate is a rate at which AE counts occur. AE peak amplitude is the peak value attained by the signal waveform during the AE event. The duration (t_{AE}) is the time between the first and last crossings of the AE threshold. Energy in an AE signal corresponds to the energy released by the AE source (Mechefske *et al.*, 2002).

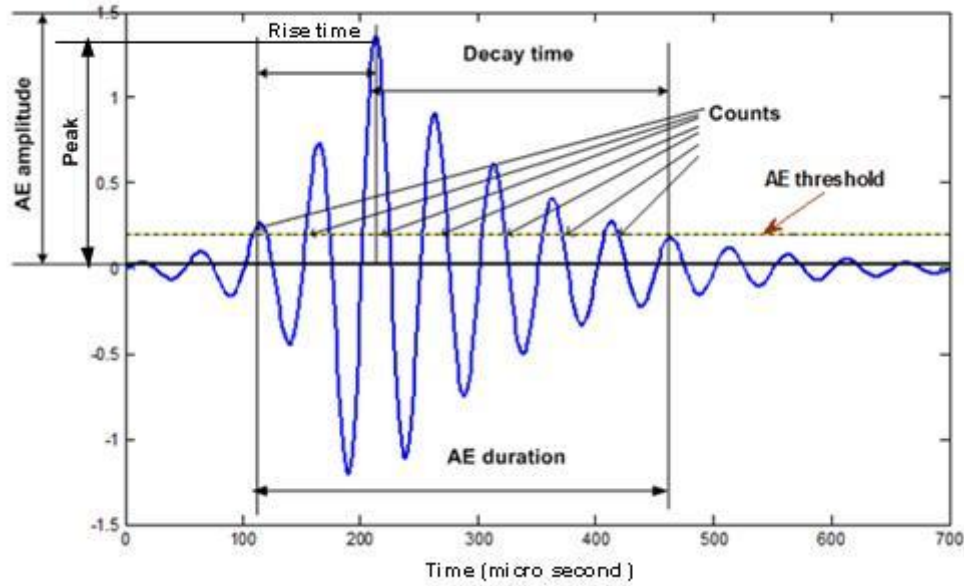


Figure 2. 22 A burst AE signal and the characteristic parameters

Based on the Figure 2.22, the number of AE counts (c_{AE}) is 7, the AE amplitude $\cong 1.4$, AE duration

(t_{AE}) is $\cong 345 \mu s$.

AE count rate (cr_{AE}) can be determined by:

$$cr_{AE} = \frac{c_{AE}}{t_{AE}} \quad (2.1)$$

$$cr_{AE} = \frac{7}{345 \cdot 10^{-6}}$$

$$cr_{AE} = 20000 / s$$

The characteristic of an AE signal such as frequency, amplitude, duration time, growth and decay rate time are influenced by the mode of generation and are very different for different materials and machine components (Mechefske *et al.*, 2002).

2.5 Analysis of surface vibration and airborne sound signals

The main purpose of the analysis of vibration signals is to determine the magnitude of the vibration generated and the source of the vibration. Success in vibration analysis depends on the data acquisition system and processes used to measure the amplitude and frequency of the individual components, relative phases of the vibration signal, and trend of the overall vibration level (Shreeve, 1995).

Machine vibration monitoring techniques are usually based on the time-domain, frequency-domain, time-frequency domain and quefrency (cepstrum) techniques. Time and frequency domain techniques consist of waveform and statistical analysis (Rao, 2004).

2.5.1 Time-domain analysis of vibration signals

The time waveform is the raw unprocessed signal obtained from the vibration transducer, and is a graph of amplitude of the vibration signal as a function of time. The time-domain signal is complex because it is the sum of all the individual frequency components that are present, and is a visual representation of the instantaneous value of the motion.

When performing fault diagnosis using the time-domain vibration signal, statistical methods are invariably applied. The most common statistical parameters are root mean square (RMS), crest factor (CF), peak value (PK), skewness (SK) and kurtosis (KT) (Kim *et al.*, 2007). However, today the entropy spectrum (EN) and probability density function (PDF) are increasingly popular.

Root mean square (RMS) is a measure of the energy content of a signal. The root mean square of a variable X is the square root of the arithmetic mean or average of the square of the X value. For a set of data number X_1, X_2, \dots, X_n , X_{RMS} is defined as:

$$X_{RMS} = \sqrt{\frac{\sum_{i=1}^n X_i^2}{n}} \quad (2.2)$$

Where X_i is the value of variable X at instant i , and n is the number of data points.

Peak value (PK) is the maximum absolute value of the waveform. For a set of data number X_1, X_2, \dots, X_n , PK is expressed as (Kim *et al.*, 2007):

$$X_{PK} = \max(|X|) \quad (2.3)$$

Where $|X|$ is the absolute value of X .

The crest factor (CF) is a measure of the number and sharpness of the peaks in the signal and might be used to determine whether a signal contains repeated impulses. A high CF value for the vibration signal from a bearing would usually be taken to be an indication of a fault. The CF is the ratio of the peak value (X_{PK}) to the RMS value (X_{RMS}) of a waveform (Kim *et al.*, 2007):

$$CF = \frac{X_{PK}}{X_{RMS}} \quad (2.4)$$

Skewness (SK) is a measure of the lack of symmetry in the data distribution. For data set X_1, X_2, \dots, X_n , SK is given by (Marques de Sa, 2007):

$$SK = \frac{\sum_{i=1}^n (X_i - \bar{X})^3}{(n-1)S^3} \quad (2.5)$$

Where \bar{X} is the mean of data set X_1, X_2, \dots, X_n , and S is the standard deviation of the distribution (De Caurcey, 2003):

$$S = \sqrt{\frac{\sum_{i=1}^n (X_i - \bar{X})^2}{n}} \quad (2.6)$$

Kurtosis (KT) is a measure of whether the data is peaked or relatively flat. Usually it is compared with the Gaussian or Normal distribution. For data X_1, X_2 until X_n , the formula for kurtosis is given by the following equation (Kim *et al.*, 2007):

$$KT = \frac{\sum_{i=1}^n (X_i - \bar{X})^4}{(n-1)S^4} - 3 \quad (2.7)$$

Where, the symbols have their usual meanings.

If KT is negative then the distribution is flatter than the Gaussian, if KT is positive it means the distribution is more peaked than the Gaussian.

Entropy EN is a measure of the uncertainty associated with a random variable. If X_1, X_2, \dots, X_n form a dataset, the formula for the Shannon entropy may be expressed as (Kim *et al.*, 2007):

$$EN(X) = -\sum_{i=1}^n p(X_i) \cdot \log_2 p(X_i) \quad (2.8)$$

Where $p(X_i)$ is the probability of variable X having the value X_i .

The probability density function (PDF) is commonly used for time-domain analysis. The PDF of a continuous random variable is a function which can be integrated to obtain the probability that the random variable takes a specific value in a given interval.

The PDF for the normal distribution of a continuous variable X_i can be expressed as (Mendenhall and Sincich, 2007):

$$f(x) = \frac{1}{S\sqrt{2\pi}} \exp\left(\frac{-(X_i - \bar{X})^2}{2S^2}\right) \quad (2.9)$$

Where, the symbols are having their usual meaning.

The probability for $a < X_i \leq b$ may be expressed as: (Norton and Karzub, 2003)

$$P(a \leq X_i \leq b) = \int_a^b f(x) \cdot dx \quad (2.10)$$

2.5.2 Frequency-domain analysis of vibration signal.

Spectrum or frequency-domain signal is a plot of amplitude of vibration signal as a function of frequency. The vibration signal of a machine is generated both by the individual components and by their assembling and installation. Each component in a working machine will generate specific identifiable frequencies, thus a given frequency spectrum can often be attributed directly to corresponding machine components (Rao, 2004).

Quefrequency domain or cepstrum analysis is the result of taking the Fourier transform of such a dB power spectrum; it is the spectrum of the logarithmic power spectrum. The cepstrum is often used to detect periodicities, such as harmonics, in the spectrum.

If the power spectrum, $S_x(\omega)$, of the time signal, $x(t)$, is expressed as (Rao, 2004):

$$S_x(\omega) = |F\{x(t)\}|^2 \quad (2.11)$$

Then the power ceptrum, $Cp_x(\tau)$, is a real valued function and is the inverse of the Fourier transform of the square of the logarithm of the power spectrum of the signal (Norton and Karzub, 2003):

$$Cp_x(\tau) = F^{-1}\{\log_{10} S_x(\omega)\}^2 \quad (2.12)$$

Power ceptrum analysis is usually used as a complementary tool to identify components which are not readily identifiable by spectral analysis alone.

Trending analysis is used to predict the likelihood of occurrence of future events, e.g. the RMS amplitude of the time-domain vibration signal is monitored and plotted over time, and if the magnitude exceeds a certain critical level then remedial action is taken.

However the vibration signal of a machine while generated by the individual components will also be affected by their assembly, installation and interaction. By comparison of the actual frequency domain signal with a signal from a healthy machine the status condition (good, satisfactory, unsatisfactory or unacceptable) may be determined.

2.6 Summary

Summary of bearing type:

The function of bearing is to support other machine components. Based on the nature of contact, the bearing can be classified into rolling bearing and journal bearing. Journal bearing is superior to rolling bearing and is used to support high radial load at low, medium and high speed. The journal bearing can be divided into solid bearing, bushing, flange bush, split flange bushing, pivot, tilting pad and self-aligning spherical journal bearing. The self-aligning spherical journal bearing can accommodate misalignment.

Summary of journal bearing lubrication:

Lubricant is a very important component in the bearing system. The most common premature bearing failure initiates from lubrication problems. Selection of lubricant can be considered based on speed, load and temperature operation. Journal bearing under medium load, normal temperature operation and medium speed ISO VG 32 or ISO VG 46 of lubricant can be applied. The self-aligning spherical journal bearing applies oil ring

lubrication. The process of journal bearing lubrication system there are three kinds of lubrication regimes such as boundary, mixed and hydrodynamic regimes. Hydrodynamic lubrication is the bearing surface fully be separated by lubrication oil film and generate minimum vibro-acoustic and acoustic emission amplitude responses.

Summary of journal bearing failure:

Premature bearing failure is often due to a combination of contaminant, miss-assembly, misalignment, insufficient lubrication, over loading, corrosion and others. These factors will create the journal bearings damage includes scratching, wiping, wear and fatigue. The premature bearing failure initiates from contaminant or inadequate lubricant, if these case can be identified as early as possible the severe failure and catastrophic can be prevented.

Summary of journal bearing monitoring techniques:

Based on the interaction contact between two surfaces under load in relative motion, the monitoring techniques in the early wear regime include lubricant monitoring, vibration monitoring, airborne monitoring and acoustic emission may be applied. Vibration monitoring is most commonly used condition monitoring in industry, but vibration measurement only detect signal at low until medium frequency. Airborne sound also can be used for monitoring for bearing condition at medium frequency. Higher airborne sound amplitude indicates the machine or equipment condition. The airborne sound may originate from gas, air or fluid pressure fluctuation, also from structural vibration sound. In practice the source of airborne sound high amplitude some time difficult to be analyzed. Acoustic emission may detect signal at high frequency that be caused asperity contact between bearing and shaft which is indication of the early fault and lubrication degradation in a journal bearing. There surface vibration, airborne sound and acoustic emission monitoring techniques can be associated to get effective and comprehensive monitoring techniques for journal bearing.

Summary of surface vibration, airborne sound and acoustic emission signal analysis:

Machine surface vibration, airborne sound and acoustic emission monitoring techniques based on the time domain and frequency domain. Time domain and frequency domain techniques consist of waveform and statistical analysis. The time waveform is the raw unprocessed signal from accelerometer. The statistics parameters analysis are root mean square, crest factor, peak value, skewness, and kurtosis and probability density factors. The statistic parameter analysis cannot be used to determine the natural frequency of source of signal.

Spectrum or frequency domain signal is a plot of vibration amplitude against frequency. Spectrum analysis is able to detect the amplitude and natural frequency characteristic of vibrating components. If the value of amplitude still cannot be identified well the power spectrum analysis is required. Mean value of spectrum amplitude and comparison spectrum analysis also used to determine influence of a few experiment parameters of vibro-acoustic and acoustic emission such as radial load, speed and fault variations.

CHAPTER THREE

SURFACE VIBRATION, AIRBORNE SOUND AND ACOUSTIC EMISSION

SOURCES IN A SELF-ALIGNING SPHERICAL JOURNAL BEARING

3.1 Introduction

Self-aligning spherical journal bearings have spherical plain bushings that have an inner bore and outer spherical sliding surfaces in contact. It can support large radial loads and tolerate small misalignment. There are many types of spherical bushings, but they are often divided into steel-on-steel, steel-on-bronze, bronze-on-steel and maintenance-free types. The structure of a self-aligning spherical journal bearing unit is shown in Figure 3.1. It mainly consists of a self-aligning spherical journal bearing and a bearing house. The inner sleeve of the bearing operates as a normal journal bearing which is subjected to motion and radial load, the spherical surfaces on the outer surface allows misalignment of the shaft in the inner sleeve.

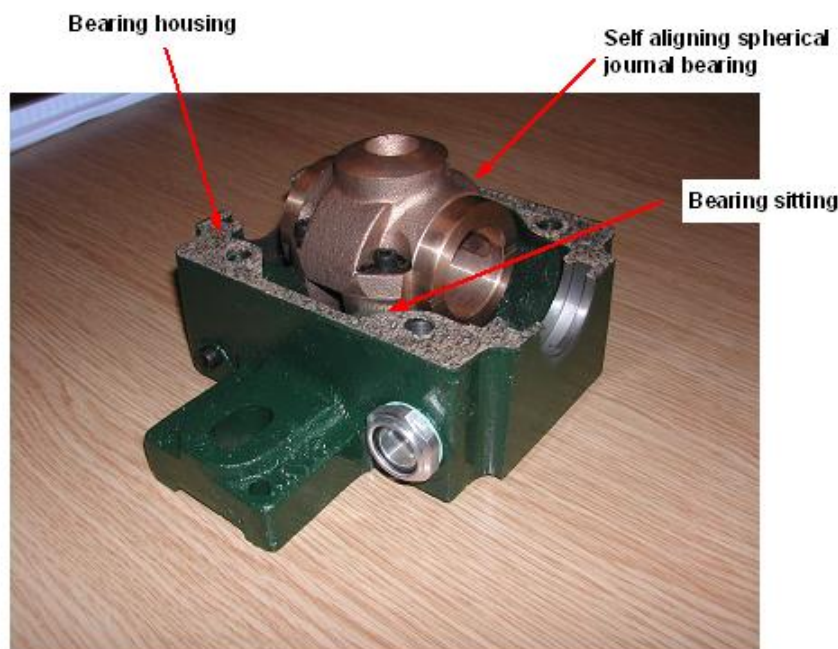


Figure 3. 1 Self aligning spherical journal bearing components

Based on this structure and operating process, its dynamic responses of surface vibration, airborne sound and acoustic emission can be understood as shown in Figure 3.2. There are two main excitation sources: external forces such as fluctuation loads from system misalignment and imbalance, and internal excitations such as the asperity contact in boundary operation. These excitations will cause structure-borne vibrations and acoustic emissions of the bearing vibrations system. These structure-bore dynamic responses then radiate airborne sound. In addition fluid dynamics such as oil pressure fluctuations and flow turbulences also produces airborne sounds.

The vibration system of journal bearing is formalised with two distinctive phases: normal hydrodynamic lubrication and boundary lubrication. There is a high speed motion between the shaft and a bearing sleeve. Because of this relative motion between these components their contacting surfaces may be separated each other by a layer of lubricant. On the other hand the motion between the spherical surface and its seating on bearing housing is very tiny and the contacting surfaces may have only a very thin lubricant film.

In normal operation, i.e. excluding the instability of lubrication which is often resulted from inadequate system design and configuration, the hydrodynamic lubrication occurs between the shaft and bearing surfaces. It means that the oil film formed by hydrodynamic lubrication process can separate shaft and bearing perfectly. The dynamic parameters: stiffness and damping is thus due to oil properties only.

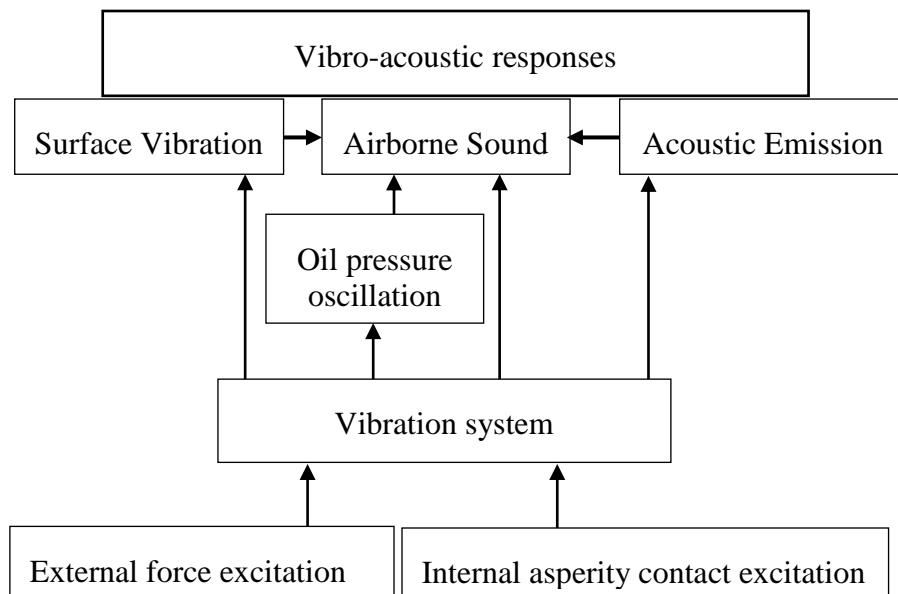


Figure 3. 2 Vibro-acoustic responses generation process

However, the contact between spherical bearing and bearing is a mixed lubrication system because of small hydrodynamic effects. It means that these two surfaces cannot be completely separated and there will be high degree of asperity contact. Therefore, the dynamic parameter: stiffness and damping are determined not only by oil properties but also surface finish quality and material properties.

With these understandings, the vibration system of journal bearing between shaft and bearing can be described as a mass damping system, while contact between the bearing with the bearing housing due to mainly direct contact or asperity contact can be represented as micro vibration damping stiffness systems.

Thus a self-aligning spherical journal bearing operating under radial load (F) and angular speed (ω) can be modelled as Figure 3.3 for understanding the generation processes of surface vibration, airborne sound and acoustic emission.

The surface vibration and airborne sound in journal bearings are excited from two main kinds of sources. These are excitations due to primary sources and excitation due to secondary sources. The first sources are structural and manufacturing defects which are inherent in both the manufacturing quality and the configuration of bearing installation. The second source in journal bearing can be asperity contact between journal and bearing due to abnormal operations.

It is well known that acoustic emission is the phenomenon of transient elastic wave generation in a material under stress. When some materials are subjected to stress above a certain level, a rapid release of strain energy takes places in the form of elastic waves (Bonnes and McBride, 1991).

Acoustic emission occurs in journal bearings due to direct contact between the journal and the bearing. Direct contact is due to operation of the journal bearing under mixed lubrication regimes, so that the surface contact cannot be separated perfectly by the oil film. In other words, lubrication system in the journal bearing is combination between boundary and hydrodynamic lubrication regimes. Acoustic emission responses occur randomly at high frequencies.

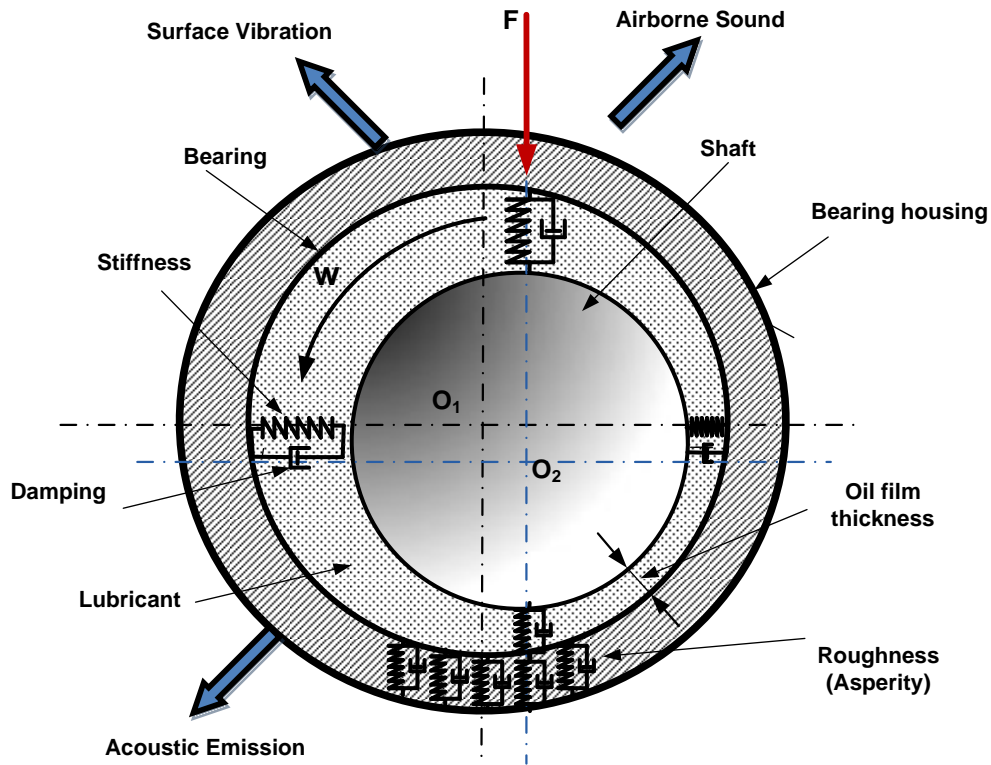


Figure 3. 3 Surface vibration, airborne sound and AE generation

Airborne sound response that occurs in journal bearings can be derived from the journal bearing component vibration, pressure fluctuation in the journal bearing and the direct contact between the journal and the bearing surface.

Premature failure often occurs in journal bearings due to both fluid and solid contaminants. These contaminants cause surface deterioration and change the surface roughness on the journal bearing and increase the asperity contact number.

Asperities present in the journal and bearing can cause a mechanical component to generate surface vibration, airborne sound and acoustic emission. Vibro-acoustic frequency response and acoustic emission caused by asperity contact occurs at high frequencies. The number of asperity contacts influenced by the quality of asperity contact, quality of lubricant and lubrication regime.

In hydrodynamic lubrication regime the journal and bearing are completely separated so there is no asperity contact at all. The vibro-acoustic and acoustic emission amplitude responses in this lubrication regime are thus very small.

The mixed lubrication regime is when the asperities are not fully separated, depending on the quality of lubricant or film oil layer, speed, pressure and quality of surface. When the bearing is not lubricated or lacks adequate lubrication the number asperity contacts increases and the vibro-acoustic and acoustic emission responses increase. Asperity contact in journal bearings is not simple because it involves aspect tribology and the local micro-structure including deformation manufacturing defect.

The surface vibration, airborne sound and acoustic emission amplitude in the journal bearing is influenced by the contact surface quality of machine component itself. The quality of asperity contact between journal and bearing may come from manufacturing defect and surface deterioration during operation time.

3.2 Surface vibration sources

As explained earlier the vibration occurring in journal bearings is caused mainly by mechanical problems such as external misalignment and unbalanced forces, internal oil pressure and impulsive excitation due to asperity contact between the journal and the bearing.

3.2.1 Vibration model

To understand the influences on vibration responses, a vibration model including these forces was developed based on their generation mechanisms. The self-aligning spherical journal bearing vibration system consists of shaft mass (m_s), stiffness between shaft and bearing (k_{sb}), the damping coefficient between shaft with the bearing (c_{sb}); the mass of the bearing (m_b), bearing stiffness between bearing and housing (k_{bh}), damping coefficient between bearing and bearing housing (c_{bh}); the mass of the bearing housing (m_h), equivalent stiffness of bearing housing (k_h) and equivalent damping coefficient of bearing housing (c_h). When the asperity contact occurs between the shaft and bearing surfaces, the contact dynamic parameters for each micro spring-damper and stiffness are denoted as k_{icsb} and c_{icsb} , and between bearing and house is k_{icbh} and c_{icbh} . Moreover, asperity contact creates new excitations. When asperity contact occurs, the interactions between asperity peaks produce

elastic deformation and restoration. This effect will lead to micro impulsive forces $F_{1s}(t) \dots F_{ns}(t)$ that act on to contact masses and cause corresponding high frequency vibration responses.

The free body diagrams and vibration model for vibration motion in vertical direction can be represented as in Figure 3.4.

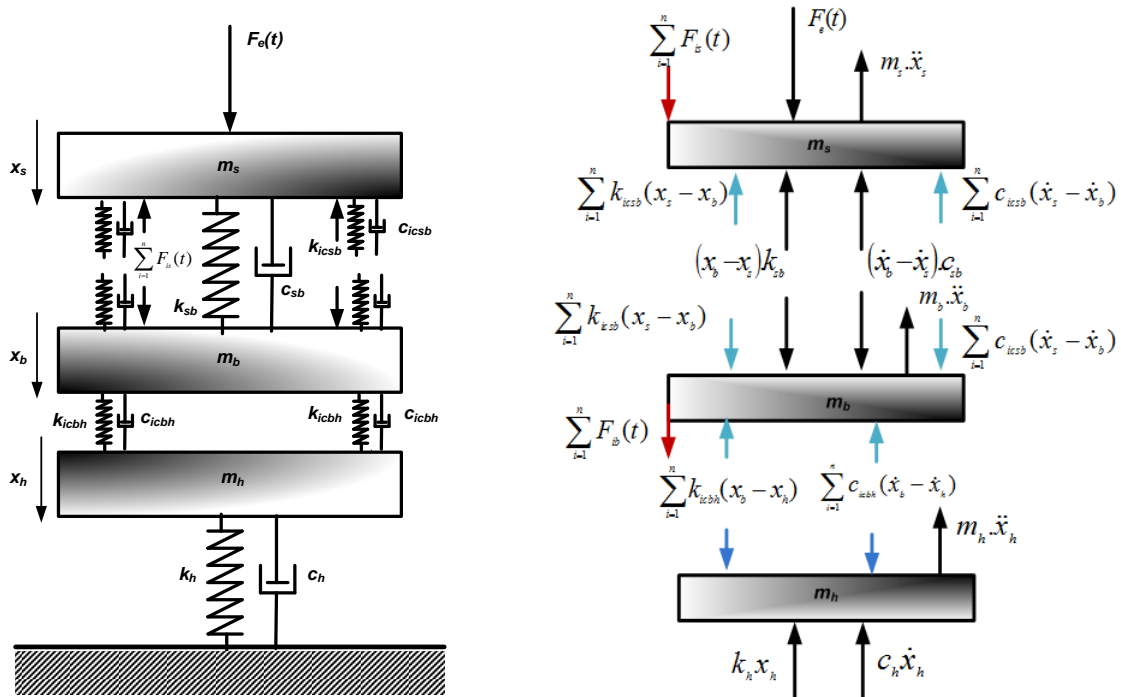


Figure 3. 4 Free body diagram of self-aligning spherical journal bearing

According to the signs for each response, the three governing equations for the system can be derived, assuming $x_s > x_b$:

$$\begin{aligned}
 & m_s \ddot{x}_s + c_{sb}(\dot{x}_s - \dot{x}_b) + k_{sb}(x_s - x_b) \\
 & + \sum_{i=1}^n c_{icsb}(\dot{x}_s - \dot{x}_b) + \sum_{i=1}^n k_{icsb}(x_s - x_b) = F_e(t) + \sum_{i=1}^n F_{is}(t)
 \end{aligned} \tag{3.1}$$

$$\begin{aligned}
 & m_b \ddot{x}_b - c_{sb}(\dot{x}_s - \dot{x}_b) - k_{sb}(x_s - x_b) - \sum_{i=1}^n c_{icsb}(\dot{x}_s - \dot{x}_b) - \sum_{i=1}^n k_{icsb}(x_s - x_b) \\
 & + \sum_{i=1}^n c_{icbh}(\dot{x}_b - \dot{x}_h) + \sum_{i=1}^n k_{icbh}(x_b - x_h) = \sum_{i=1}^n F_{ib}(t)
 \end{aligned} \tag{3.2}$$

$$m_h \ddot{x}_h + c_h \dot{x}_h + k_h x_h - \sum_{i=1}^n c_{cbn} (\dot{x}_b - \dot{x}_h) - \sum_{i=1}^n k_{cbh} (x_b - x_h) = 0 \quad (3.3)$$

In Equations (3.1) - (3.2) the equivalent stiffness and damping coefficients are the combination of stiffness and damping effects of two surfaces.

Obviously, high amplitude external and internal forces will produce large vibration responses. However the vibration responses measured from the surface of bearing house can be influenced by the combined effect of the stiffness and damping values in different parts.

3.2.2 Responses due to external forces

To understand vibration responses due to external forces, the vibration model can be simplified for the case of hydrodynamic lubrication when the asperity contact effect can be ignored in Equations (3.1) and (3.2). In addition, external dynamic forces usually occur in the low frequency range (<1000Hz) and high frequency effects due to asperity contacts for shaft and bearing surfaces can be ignored. However, for full representation of the vibration measurement process, the mean values of stiffness (\bar{k}_{cbh}) and damping (\bar{c}_{cbh}) for the faces between our surface and house surface can be considered. This will lead to:

$$m_s \ddot{x}_s + c_{sb} (\dot{x}_s - \dot{x}_b) + k_{sb} (x_s - x_b) = F_e(t)$$

$$m_s \ddot{x}_s + c_{sb} \dot{x}_s - c_{sb} \dot{x}_b + k_{sb} x_s - k_{sb} x_b = F_e(t) \quad (3.4)$$

$$m_b \ddot{x}_b - c_{sb} (\dot{x}_s - \dot{x}_b) - k_{sb} (x_s - x_b) + \bar{c}_{cbh} (\dot{x}_b - \dot{x}_h) + \bar{k}_{cbh} (x_b - x_h) = 0$$

$$m_b \ddot{x}_b - c_{sb} \dot{x}_s + c_{sb} \dot{x}_b - k_{sb} x_s + k_{sb} x_b + \bar{c}_{cbh} \dot{x}_b - \bar{c}_{cbh} \dot{x}_h + \bar{k}_{cbh} x_b - \bar{k}_{cbh} x_h = 0$$

$$m_b \ddot{x}_b - c_{sb} \dot{x}_s + (c_{sb} + \bar{c}_{cbh}) \dot{x}_b - \bar{c}_{cbh} \dot{x}_h - k_{sb} x_s + (k_{sb} + \bar{k}_{cbh}) x_b - \bar{k}_{cbh} x_h = 0 \quad (3.5)$$

$$m_h \ddot{x}_h + c_h \dot{x}_h + k_h x_h - \bar{c}_{cbh} (\dot{x}_b - \dot{x}_h) - \bar{k}_{cbh} (x_b - x_h) = 0$$

$$m_h \ddot{x}_h - \bar{c}_{cbh} \dot{x}_b + (c_h + \bar{c}_{cbh}) \dot{x}_h - \bar{k}_{cbh} x_b + (k_h + \bar{k}_{cbh}) x_h = 0 \quad (3.6)$$

Equations 3.4 and 3.5 may be expressed in matrix form:

$$\begin{bmatrix} m_s & 0 & 0 \\ 0 & m_b & 0 \\ 0 & 0 & m_h \end{bmatrix} \begin{bmatrix} \ddot{x}_s \\ \ddot{x}_b \\ \ddot{x}_h \end{bmatrix} + \begin{bmatrix} c_{sb} & -c_{sb} & 0 \\ -c_{sb} & (c_{sb} + \bar{c}_{cbh}) & -\bar{c}_{cbh} \\ 0 & -c_{bh} & (c_h + \bar{c}_{cbh}) \end{bmatrix} \begin{bmatrix} \dot{x}_s \\ \dot{x}_b \\ \dot{x}_h \end{bmatrix} + \begin{bmatrix} k_{sb} & -k_{sb} & 0 \\ -k_{sb} & (k_{sb} + \bar{k}_{cbh}) & -\bar{k}_{cbh} \\ 0 & -\bar{k}_{cbh} & (k_h + \bar{k}_{cbh}) \end{bmatrix} \begin{bmatrix} x_s \\ x_b \\ x_h \end{bmatrix} = \begin{bmatrix} F_e(t) \\ 0 \\ 0 \end{bmatrix} \quad (3.7)$$

Determination of frequency natural of vibration motion equation in a journal bearing can be calculated by assuming a free un-damped surface vibration system and a harmonic solution of the form:

$$x = ue^{j\omega t}; \dot{x} = u\omega je^{j\omega t}; \ddot{x} = -u\omega^2 e^{j\omega t} \quad (3.8)$$

Matrix of free un-damped vibration system yields:

$$\begin{bmatrix} m_s & 0 & 0 \\ 0 & m_b & 0 \\ 0 & 0 & m_h \end{bmatrix} \begin{bmatrix} \ddot{x}_s \\ \ddot{x}_b \\ \ddot{x}_h \end{bmatrix} + \begin{bmatrix} k_{sb} & -k_{sb} & 0 \\ -k_{sb} & (k_{sb} + \bar{k}_{cbh}) & -\bar{k}_{cbh} \\ 0 & -\bar{k}_{cbh} & (k_h + \bar{k}_{cbh}) \end{bmatrix} \begin{bmatrix} x_s \\ x_b \\ x_h \end{bmatrix} = \begin{bmatrix} 0 \\ 0 \\ 0 \end{bmatrix}$$

$$-\omega^2 \begin{bmatrix} m_s & 0 & 0 \\ 0 & m_b & 0 \\ 0 & 0 & m_h \end{bmatrix} e^{j\omega t} + \begin{bmatrix} k_{sb} & -k_{sb} & 0 \\ -k_{sb} & (k_{sb} + \bar{k}_{cbh}) & -\bar{k}_{cbh} \\ 0 & -\bar{k}_{cbh} & (k_h + \bar{k}_{cbh}) \end{bmatrix} e^{j\omega t} = \begin{bmatrix} 0 \\ 0 \\ 0 \end{bmatrix}$$

(3.9)

If λ is Eugenvalue and expressed as:

$$\lambda = \omega^2 \quad (3.10)$$

The matrix yields to:

$$-\lambda \begin{bmatrix} m_s & 0 & 0 \\ 0 & m_b & 0 \\ 0 & 0 & m_h \end{bmatrix} + \begin{bmatrix} k_{sb} & -k_{sb} & 0 \\ -k_{sb} & (k_{sb} + \bar{k}_{cbh}) & -\bar{k}_{cbh} \\ 0 & -\bar{k}_{cbh} & (k_h + \bar{k}_{cbh}) \end{bmatrix} = \begin{bmatrix} 0 \\ 0 \\ 0 \end{bmatrix} \quad (3.11)$$

Tabel 3. 1 Journal bearing parameter data

Mass of shaft (kg)	$m_s=1.75$
Mass of bearing (kg)	$m_b=0.35$
Mass of bearing housing (kg)	$m_h=6.0$
Damping coefficient between shaft and bearing (N/(m/s))	$c_{sb}=0.35$
Damping coefficient between bearing and housing (N/(m/s))	$c_{bh}=0.45$
Damping coefficient bearing housing (N/(m/s))	$c_h=0.35$
Mean damping coefficient between bearing and housing (N/(m/s))	$c'_{cbh}=0.4$
Stiffness between shaft and bearing (N/m)	$k_{sb}=140$
Stiffness between bearing and housing (N/m)	$k_{bh}=600$
Stiffness of bearing housing (N/m)	$k_h=5000$
Mean stiffness between bearing and housing (N/m)	$k'_{cbh}=2800$

Eigen value analysis is used to determine the frequency responses of surface vibration analysis. Based on journal bearing parameter data (Table 3.1), by using Eigen analysis, the results for the natural frequencies are $\omega_1=7.9$ kHz, $\omega_2=28.4$ kHz and 47.7 kHz.

In the journal bearings system unbalance problems may be caused by manufacturer's error or due to bearing damage such as cracks or wear. With an unbalanced mass the resulting centrifugal force is a function of the unbalanced mass (m_o), the distance of the location of unbalance to shaft axis or eccentricity (e) and angular speed (ω) and a direction vector. The magnitude of centrifugal force due to unbalance in the vertical direction is:

$$F_c = m_0 e \omega^2 \sin(\omega t) \tag{3.12}$$

Tabel 3. 2 Journal bearing operation parameter data

Mass of unbalance (kg)	$m_0=0.05$
Eccentricity (m)	$e=d/4$
Speed (rpm)	$n=1450$
Diameter of shaft (m)	$d=0.035$

From Table 3.1 and added the data bearing operation parameters shown in Table 3.2, using ordinary differential equation 45 (ODE 45) program the time domain vibration response can be obtained as shown in Figure 3.5, and the frequency domain vibration responses as shown in Figure 3.6.

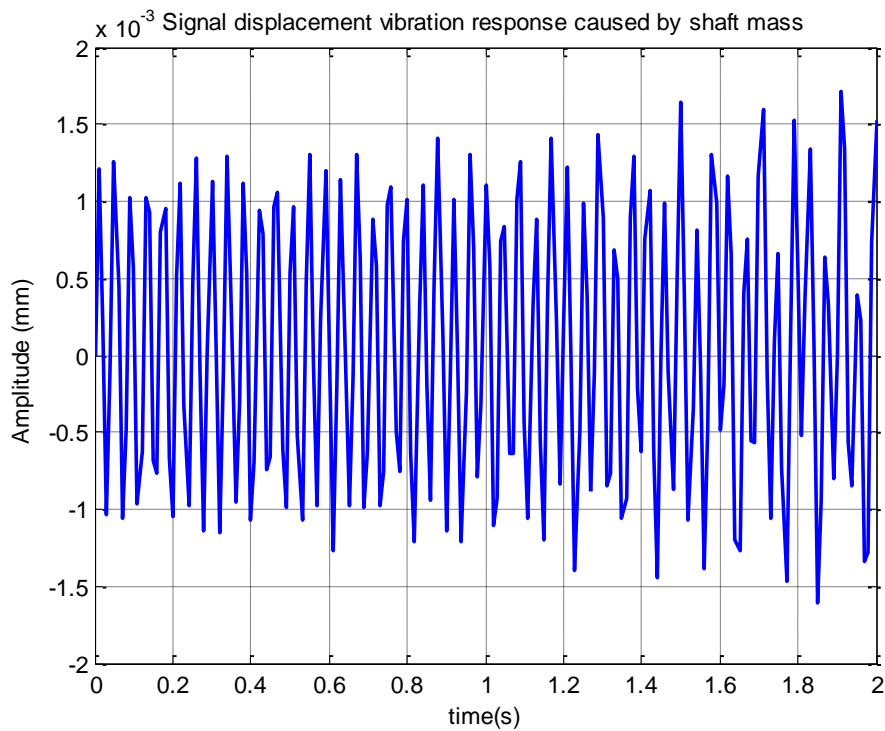


Figure 3. 5 Calculated time domain response due to unbalance

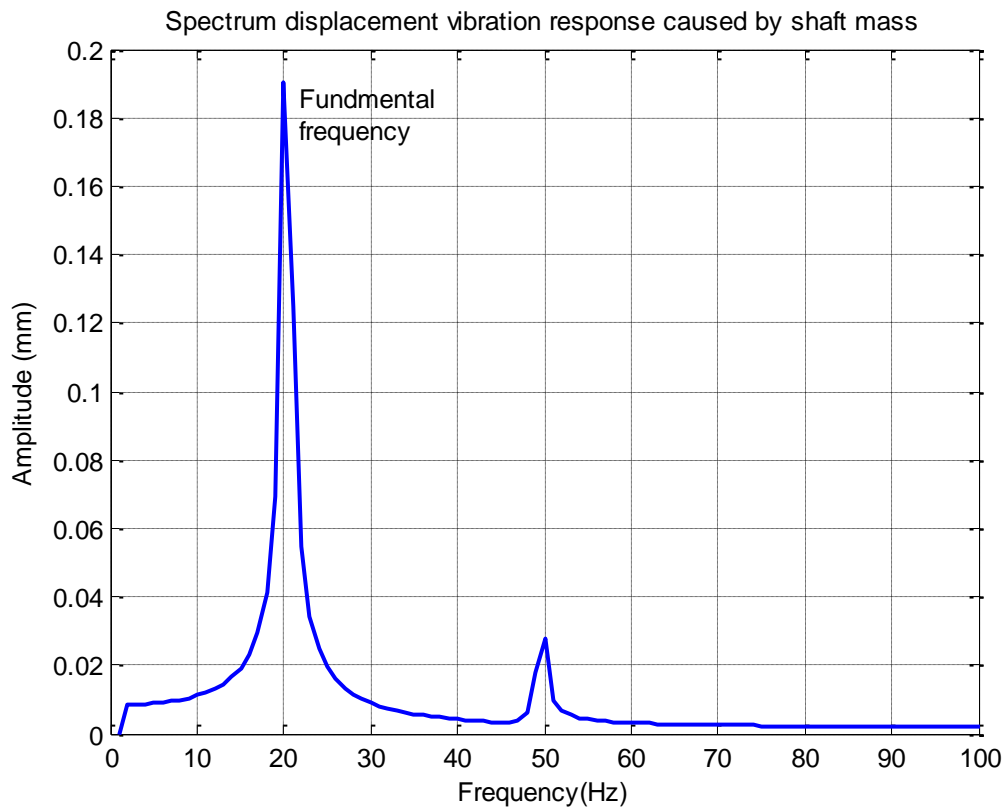


Figure 3. 6 Calculated spectrum response due to unbalance

Figure 3.6 shows that the peak amplitude due to unbalance occurs at 20 Hz. The amplitude is determined by the amount of unbalance caused by manufacturing errors or damage such as wear and cracks or other surface deterioration. The frequency at which the peak occurs is the first frequency fundamental or shaft speed. The next high amplitude occurs at the second harmonic of frequency fundamental.

The journal bearing damping coefficient and stiffness coefficient may change due to lubricant deterioration of contaminant over the life time of the lubricant. The journal bearing damping and stiffness coefficients may also change due to surface deterioration due to wear and scratching. The change of damping and stiffness coefficients will influence the vibration amplitude and frequency response.

The effect of damping coefficient on the vibration spectrum response is shown in the Bode diagram in Figure 3.7.

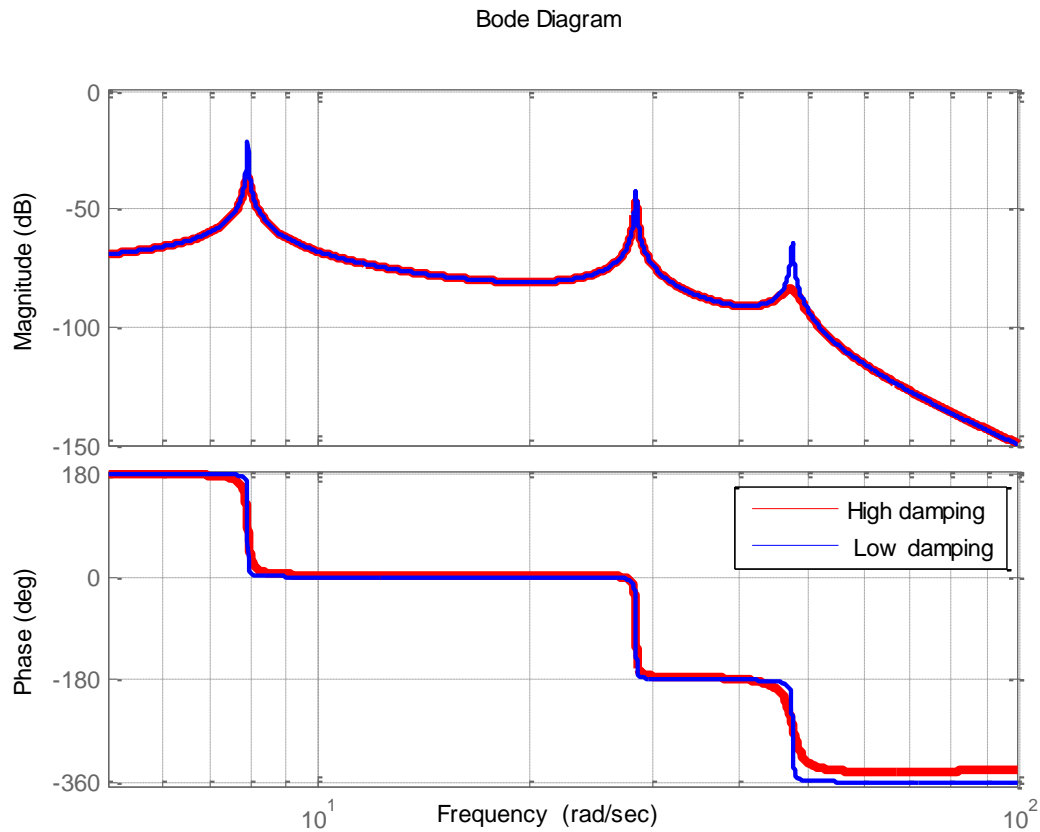


Figure 3. 7 Frequency responses in different damping coefficients

Figure 3.7, shows that when the journal bearing damping coefficient changes the amplitude of the frequency response also changes. The greater the damping coefficient creates the lower the amplitude, and vice versa is.

Figure 3.8 shows the vibration frequency response of the journal bearing when the stiffness is changed due to, for example, lubricant deterioration or surface deterioration.

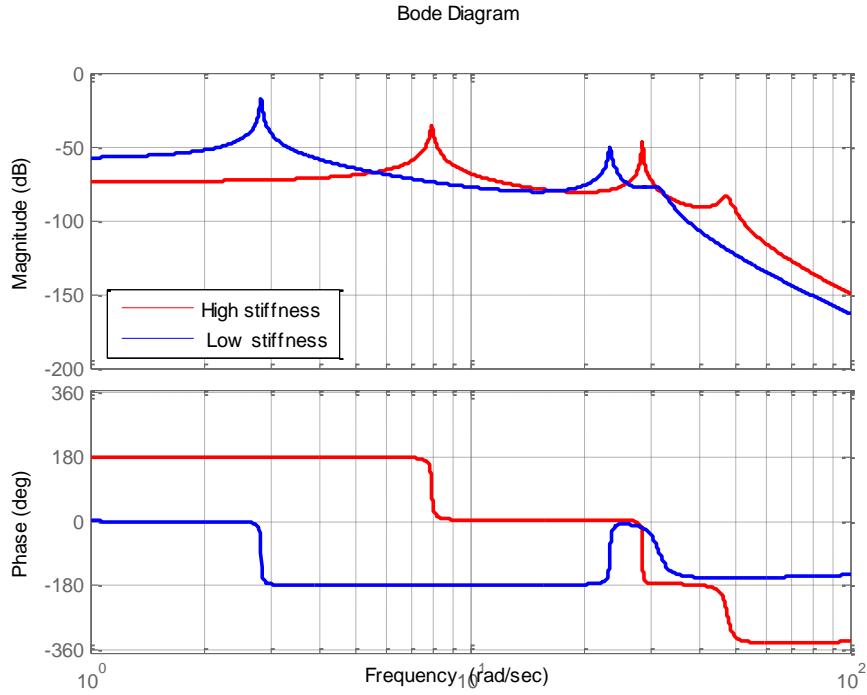


Figure 3. 8 Frequency responses in different stiffness

Figure 3.8 shows that when the stiffness coefficient changes the frequency response changes significantly in terms of both amplitude and resonant frequencies. The greater stiffness coefficient generates high amplitude at the frequency.

3.2.3 Responses due to asperity contact

When the bearing is under abnormal operation, high levels of asperity contact occur in shaft-bearing interface. This means the effect of additional stiffness and damping due to asperity contact has to be included to describe the system, i.e. in the model the stiffness

between shaft and bearing becomes $k_{sb} + \sum_{i=1}^n k_{icsb}$ and the damping coefficient

becomes $c_{sb} + \sum_{i=1}^n c_{icsb}$.

Moreover, because of this asperity contact, a new vibration source has to be formalised and

expressed as the asperity excitation $f_c(t) = \sum_{i=1}^n f_{icsb}(t)$. As this excitation process is very

close to that of AE excitations it will be modelled in Section 3.4 as an AE energy release.

For this source the induced vibration response, $f_c(t)$ is modelled to be proportional to energy release rate.

3.3 Airborne sound sources

3.3.1 Lubricant pressure fluctuation

The generation of hydrodynamic oil pressure in the journal bearing due to shaft rotation creates noise. In the journal bearing, sound or acoustic wave travels in the radial direction from the component outwards through the lubricant (fluid), the bearing housing (solid) and the surrounding air.

A schematic of the self-aligning journal bearing under a hydrodynamic lubrication state is presented in Figure 3.9

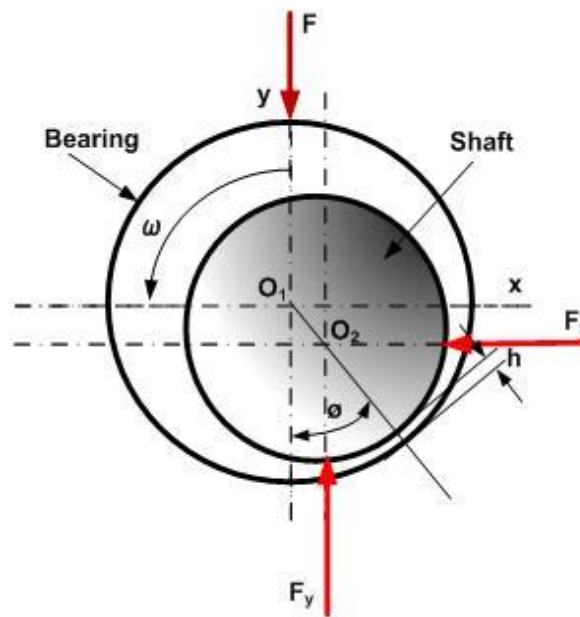


Figure 3.9 A schematic of the self-aligning journal bearing under hydrodynamic lubrication

As shown in Figure 3.9, with h , η , and V denoting the film thickness, oil absolute viscosity and linear velocity respectively, the Reynolds equation for pressure p distribution in a journal bearing under steady condition may be expressed as (Rho *et al.*, 2003):

$$\frac{\partial}{\partial x} \left(h^3 \frac{\partial p}{\partial x} \right) + \frac{\partial}{\partial z} \left(h^3 \frac{\partial p}{\partial z} \right) = 6\eta V \frac{\partial h}{\partial x} + 12\eta \frac{\partial h}{\partial t} \quad (3.13)$$

If the radius of the shaft is denoted by R and the relations $x=R\theta$ and $V= \omega R$ are used, then the Reynolds equation can be expressed as:

$$\frac{1}{R^2} \frac{\partial}{\partial \theta} \left(h^3 \frac{\partial p}{\partial \theta} \right) + \frac{\partial}{\partial z} \left(h^3 \frac{\partial p}{\partial z} \right) = 6\mu\omega R \frac{\partial h}{R\partial \theta} + 12\mu \frac{\partial h}{\partial t}$$

$$\frac{1}{R^2} \frac{\partial}{\partial \theta} \left(h^3 \frac{\partial p}{\partial \theta} \right) + \frac{\partial}{\partial z} \left(h^3 \frac{\partial p}{\partial z} \right) = 6\mu\omega \frac{\partial h}{\partial \theta} + 12\mu \frac{\partial h}{\partial t} \quad (3.14)$$

For a long journal bearing, the pressure distribution is given by: (Rho *et al.*, 2003).

$$p(\theta) = \frac{6\eta VR}{c_r^2} \frac{\varepsilon(2 + \varepsilon \cos \theta) \sin \theta}{(2 + \varepsilon^2)(1 + \varepsilon \cos \theta)^2} \quad (3.15)$$

Where c_r is radial clearance (m), ε is eccentricity ratio, and θ is contact angle (rad). Equation (3.15) shows that the oil pressure produces fluctuations with time because the operating parameters such as speed and load are time-varying. In addition, bearing conditions such as the clearances and lubrication quality can also alter the pressure fluctuation characteristics.

In the journal bearing, sound or acoustic waves travels in the radial direction from the component outwards through the lubricant (fluid), the bearing housing (solid) and the surrounding air, see Figure 3.10.

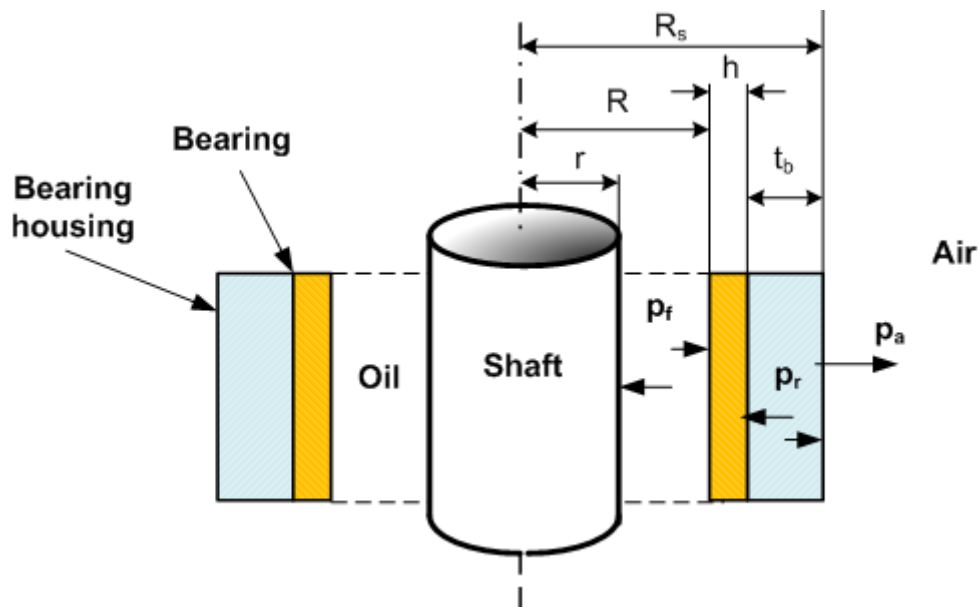


Figure 3. 10 Journal bearing acoustic transmission

The relationship between oil pressure fluctuation p_f , pressure reflected wave p_r in the bearing and bearing housing and pressure transmitted wave p_a (Pa) into the surrounding air may be written as (Rho and Kim, 2003):

$$p_a = p_f \frac{2Z_b}{Z_b + Z_a} \quad (3.16)$$

Where the acoustic impedance of bearing Z_b ($\text{kg/m}^2\cdot\text{s}$) is proportional to bearing density ρ_b (kg/m^3) and sound speed in bearing material is c_b (m/s).

$$Z_b = \rho_b c_b \quad (3.17)$$

The acoustic impedance of the surrounding air Z_a ($\text{kg/m}^2\cdot\text{s}$) is proportional to air density ρ_a (kg/m^3) and sound speed in air c_a (m/s).

$$Z_a = \rho_a c_a \quad (3.18)$$

The amplitude of sound pressure fluctuation level in oil is measured by its RMS value is:

$$p_{f\text{ rms}} = \sqrt{\frac{1}{T} \int_t^{t+T} (p - p_m)^2 .dt} \quad (3.19)$$

Where p is the instantaneous pressure in the oil, and P_m is the mean pressure of the oil defined as:

$$p_m = \frac{1}{T} \int_t^{t+T} p .dt \quad (3.20)$$

p_m is the mean pressure of oil (Pa); T is the period of steady state response(s).

The sound pressure level in the fluid film, L_p , may be expressed in dB (Adams, 2001):

$$L_p = 20 \log_{10} \frac{P_m}{P_{ref}} \quad (3.21)$$

Where: L_p : Pressure level in fluid film (dB), and P_{ref} is the reference pressure (2×10^{-5} Pa).

If the sound pressure level at the outer bearing housing is p_a (Pa) then the sound level transmitted into the air in a radial direction at the outer bearing housing L_{pa} (dB) can be written as:

$$L_{pa} = 20 \log_{10} \frac{P_a}{P_{ref}} \quad (3.22)$$

The average sound pressure level, L_{pab} , transmitted to air through bearing and bearing housing in the radial direction at outer surface of bearing housing may be expressed as: (Rho and Kim, 2003).

$$L_{pab} = 10 \log_{10} \left(\int_A 10^{0.1 L_{pa}} dA \right) \quad (3.23)$$

Where: A is the surface area of the bearing.

The influence of the design parameters (see Table 3.3) on the airborne sound responses by geometric parametric calculation are presented in Figure 3.11.

Tabel 3. 3 Geometrical journal bearing parameter

Dynamic viscosity of lubricant ISO VG 32 (cSt) or (mm^2/s)	$\eta=32$
Dynamic viscosity of lubricant ISO VG 46 (cSt) or (mm^2/s)	$\eta=46$
Dynamic viscosity of lubricant ISO VG 68 (cSt) or (mm^2/s)	$\eta=68$
Oil density (kg/m^3)	$\rho=850$
Shaft diameter (mm)	$d=35$
Length of bearing (mm)	$L=75$
Speed (rpm)	$N=1450$
Eccentricity ratio	$\varepsilon=0.7$

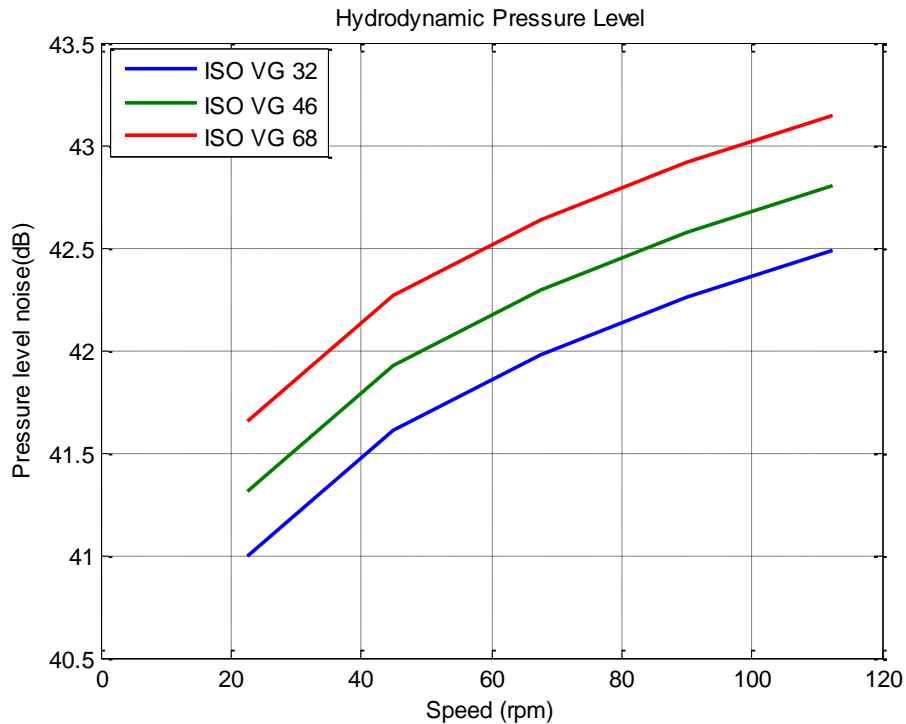


Figure 3. 11 Bearing pressure level (dB) in three different viscosities

Figure 3.11 shows that there is a positive correlation between the speed of rotation of the bearing and airborne pressure level. When speed increases airborne pressure levels also rise.

3.3.3 Bearing roughness excitations

Friction airborne sound is the sound radiated when two rough surfaces contact each other under speed and load as can happen without an adequate layer of lubricating oil between shaft and bearing. The friction airborne sound can be classified in two types depending on the contact pressure. When the contact pressure is high, the contact and amplitude of airborne sound is strong. When the contact pressure is light, the amplitude of noise is weak (Akay, 2002).

The friction noise can originate as stick slip due to asperity contact. The airborne sound is produced by vibration response of the coupled solids (Emira *et al.*, 2011).

Fundamental studies on friction noise can be founded in Ben Abdelounis and his companion, who showed that under normal light load and rough surface the vibration level increases as the logarithm of the product of surface roughness and the sliding speed, with shock frequencies occurring between antagonist asperities at sliding surface speed (Ben Abdelounis *et al.*, 2011).

The relationship between surface roughness, sliding speed and airborne sound level is given by (Ben Abdelounis *et al*, 2011):

$$L_v = 20 \log \left[\left(\frac{R_{a2}}{R_{a1}} \right)^n \left(\frac{V_2}{V_1} \right)^m \right] \quad (3.24)$$

Where : L_v is noise or airborne sound level (dB), R_{a2} is mean arithmetic surface roughness for second component (μm), R_{a1} is mean arithmetic surface roughness for first component (μm), V_1 is velocity of first components and V_2 is velocity of second component. The exponent n and m are independent and they are respectively of $0.82 \leq n \leq 0.97$ and $0.95 \leq m \leq 1.22$.

When considering the apparent asperity contact area, the radiated airborne sound power could be proportional to roughness, sliding speed and apparent contact area is expressed in the following general equation:

$$P_{ra} \propto R_a^\alpha V^\beta A_c^{\frac{\lambda_a}{10}} \quad (3.25)$$

Where: P_{ra} is the radiated airborne sound power, R_a is mean arithmetic surface roughness, V is sliding speed, A_c is apparent contact area, λ_a is exponent expressed in dB/decade, α and β are independent exponents.

The equation for the radiated airborne sound power indicates that the amplitude of sound power will increase with contact surface roughness, contact area and speed.

Use of improper lubricant viscosity will influence the contact area. If less viscous lubricant (caused by water contaminant) or improper lubricant is used then the contact area can increase and generate higher radiated airborne sound amplitude.

In the event of journal bearing damage due to the surface scratching or wearing, the roughness index increases, thereby increasing the amplitude of the radiated airborne sound.

3.3.4 Component vibration

Vibrations of journal bearing components are vibrating solid surfaces in contact with a prime mover that radiate sound to the environment around the bearing.

The radiation airborne sound power is proportional to the vibrating area and the mean square vibrating velocity (Gerges *et al*, 2013):

$$P_{as} = \rho_a c_s A_v \bar{V}^2 \eta_{rad} \quad (3.26)$$

Where: P_{ra} is the radiated sound power (Watt); ρ_a is the air density (kg/m^3); c_s is the speed of sound (m/s); A_v is the vibrating area (m^2), \bar{V} is mean square vibrating velocity (m/s) and η_{rad} is the radiation efficiency.

3.3.5 Fluid flow turbulence

Oil turbulence in the journal bearing also generates airborne sound, especially at high sliding speeds. Oil turbulence can be generated by interaction of the fluid and moving solid objects such as the shaft in the journal bearing.

The aerodynamic airborne sound power generated by turbulent flow is a function of the flow velocity (Gerges *et al.*, 2013):

$$P_{rat} \propto U^{\lambda_u} \quad (3.27)$$

Where: P_{rat} is radiated sound power (Watt); U is the flow velocity (m/s); λ_u is 6 to 8.

Thus doubling of the flow velocity (U), increases the sound power by a factor 2^6 to 2^8 , that is by a factor between 64 and 256.

3.4 Acoustic emission sources

3.4.1 Asperity contact excitation

As shown in the schematic and free-body diagram (Figure 3.4) external loads on the bearings cause acoustic emission in addition to surface vibration and airborne sound. The frequency responses occur at a high frequency and random.

AE is the phenomenon of transient elastic wave generation in a material under stress. When some materials are subjected to stress above a certain level, a rapid release of strain energy takes places in the form of elastic waves which can be detected by an AE transducer (Choudury and Tandon, 2000).

AE has been detected from tribological components such as bearings which rub against or slide over each other, generating friction and wear (Kolubaev *et al.*, 2010; Cludema, 1996). The sources of AE signals generated by mechanical loading and failure of materials include such friction effects as plastic deformation, change in surface structure and appearance of

wear debris and formation of fatigue pits, so AE signal analysis may be of use in detecting journal bearing early failure.

When two solid bodies are in contact with each other, the true contact between them occurs at only a limited number of asperities. The pressures on those points are high and this asperity contact was found to be the main source of AE in sliding friction (Bonnes and McBride, 1991). In journal bearing operation the coefficient of friction depends on the operating condition and AE analysis is an appropriate measurement to detect incipient failure of sliding bearings because of the correlation between friction, emitted signal and energy dissipated in the sliding metallic contact which results in a substantial increase of the signal amplitude in the frequency range around 100 kHz. Damage or failure can be recognized independently by contact geometry, sliding speed, shell and lubricant temperatures (Dickerhof *et al.*, 2006).

There will be a relationship between AE and power loss; if the increase in AE signal is due to increased asperity contact there will be increased friction and increased power loss. (Ali *et al.*, 2008).

Solid surfaces are covered by asperities which have a random height distribution. Figure 3.12 shows contact areas for an ideal smooth surface and a second rough surface (Fan *et al.*, 2009).

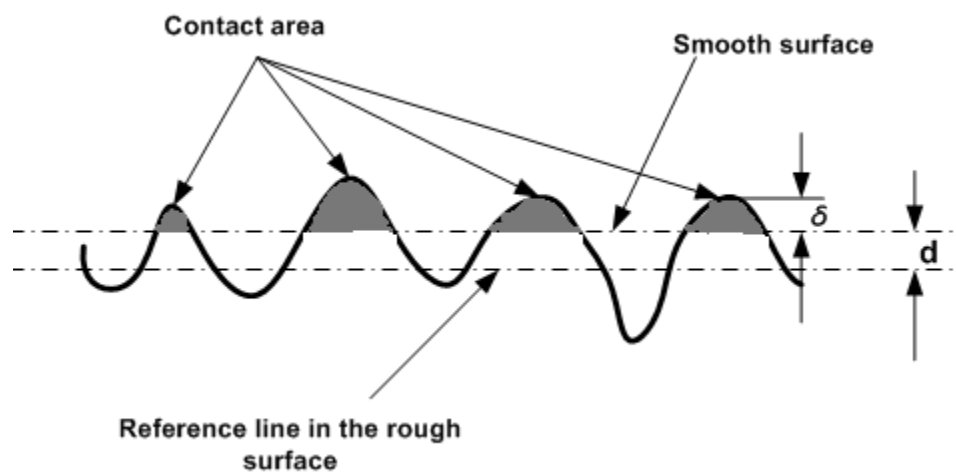


Figure 3. 12 Contact of rough and smooth surfaces

Surface roughness (R_a) is the RMS of the height of the individual asperities, R_{a1} , etc. N is number of asperities. (Ford, 1993).

$$R_a = \sqrt{(R_{a1}^2 + R_{a2}^2 + \dots + R_{an}^2) / N} \quad (3.28)$$

If z is the variable representing the height distribution of the surface, and the cumulative probability that the random variable z will not exceed a specific value of D exists we will have a probability density function $f(z)$ that can be expressed as (Stolarski, 1990):

$$P(0 \leq z \leq D) = \int_0^D f(z) dz = 1 \quad (3.29)$$

Where $P(0 \leq z \leq D)$ is the probability that the height of the asperity will lie between 0 and D .

If two surfaces approach each other so that the distance between their smooth surface planes is d (see Figure 3.12) which is less than the height of the asperities, those asperities higher than d will support the load.

The proportion of the asperities with a height greater than d and less than D will be (Fan *et al*, 2009):

$$P(z > d) = \int_d^D f(z) dz = \int_d^{\infty} f(z) dz \leq 1 \quad (3.30)$$

If the total number of asperities per unit area is n , and the number of asperities per unit area in contact (height greater than d) is n_a then:

$$P(z > d) = n_a / n \quad (3.31)$$

Assume each asperity is deformed the same amount by the load (W). If the area of contact is A_i , then the average load on each asperity in contact will be:

$$W_i = \frac{W}{n_a A_i} \quad (3.32)$$

where: W_i is the average load for each asperity (N), W is external total load (N), A_i is asperity contact area (m^2) and n_a is number of asperities per unit area ($1/m^2$).

3.4.2 Acoustic emission energy release

If the asperities of two components surfaces contact each other under influence of an external load and slide over each other, the stored elastic energy can be expressed as (Fan *et al.*, 2009):

$$E_{ei} = \int W d\delta \quad (3.33)$$

where: E_{ei} is the stored elastic energy (J), W is the applied load (N) and $d\delta$ is consequent deformation (m).

The contact between journal bearing and shaft is the contact between two parallel cylinders. The maximum deflection of the asperities in the contact area between two parallel cylinders is influenced by total load W (N), radius of each of the cylinders (R_1 and R_2 (m)), half-length of bearings in contact, L (m), half wide of bearing contact b (m) and equivalent modulus of elasticity E' (N/m^2). The maximum deformation δ (m) may be written (Stachowiak *et al.*, 2001):

$$\delta = 0.319 \left(\frac{W}{EL} \right) \left[\frac{2}{3} + \ln \left(\frac{4R_1 R_2}{b^2} \right) \right] \quad (3.34)$$

The stored of energy of elasticity E_{ei} (J) is the applied load W (N) multiplied by consequent deformation $d\delta$ (m). From Equation (3.34) the change in deformation $d\delta$ with change in load dW is:

$$d\delta = 0.319 \left(\frac{1}{EL} \right) \left[\frac{2}{3} + \ln \left(\frac{4R_1 R_2}{b^2} \right) \right] dW \quad (3.35)$$

where E' (N/m^2) is the effective elasticity of the two materials whose surfaces are in contact each other.

Equation (3.35) for $d\delta$ is substituted into Equation (3.33), for E_{ei} and integrated:

$$E_{ei} = 0.319 \left(\frac{1}{EL} \right) \left[\frac{2}{3} + \ln \left(\frac{4R_1 R_2}{b^2} \right) \right] \int W dW$$
$$E_{ei} = \frac{0.319W^2}{2} \left(\frac{1}{EL} \right) \left[\frac{2}{3} + \ln \left(\frac{4R_1 R_2}{b^2} \right) \right] \quad (3.36)$$

The equivalent elastic modulus for two different solid materials in contact, E' , is given by (Stachowiak *et al.*, 2001) and depends on the Poisson ratio for the two materials (ν_1 and ν_2 respectively), and the modulus of elasticity for the two materials (E_1 and E_2).

$$\frac{1}{E'} = \frac{1}{2} \left(\frac{1-\nu_1^2}{E_1} \right) + \left(\frac{1-\nu_2^2}{E_2} \right) \quad (3.37)$$

The relation between stored energy of elasticity in a pair of asperities in contact, E_{ei} and the maximum deformation δ can be expressed using Equation (3.36) for E_{ei} and Equation (3.34) for δ .

Equation (3.36) is divided by Equation (3.35) yields to:

$$\frac{E_{ei}}{\delta} = \frac{W}{2}$$

$$E_{ei} = 0.5W\delta \quad (3.38)$$

If $\delta = z-d$, the mean value of energy of elasticity for one asperity contact can be expressed as (Fan *et al.*, 2009):

$$E_{ei} = 0.5W(z-d) \quad (3.39)$$

The total of the stored energy of elasticity, E_e , due to asperity contact for contact area A is (Fan *et al.*, 2009):

$$E_e = An_a E_{ei} \quad (3.40)$$

Substitute Equation (3.39) for E_{ei} into Equation (3.40) for E_e :

$$E_e = An_a 0.5W(z-d) \quad (3.41)$$

The contact between the shaft surface and journal bearing “hole” is as shown in Figure 3.13 and may be likened to two parallel cylinders in concave contact.

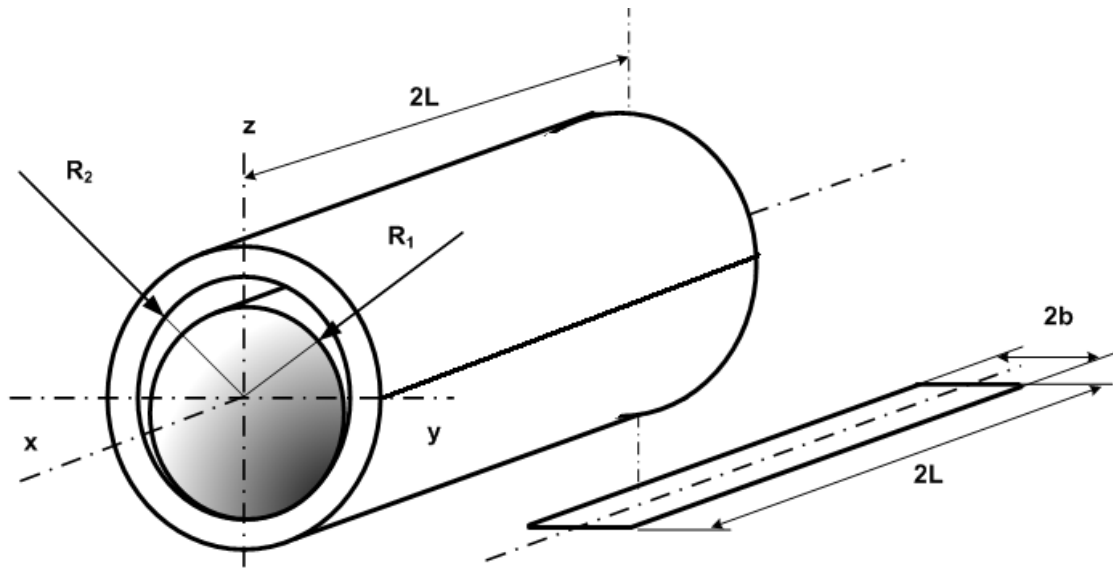


Figure 3. 13 Contact between shaft surface and journal bearing

The first body is the hole in a journal bearing with radius $R_{1x} = \infty$ and $R_{1y} = R_1$. The second body is the cylinder shaft surface with radius $R_{2x} = \infty$ and $R_{2y} = R_2$. These are in contact with each other. The equivalent radius of curvature of contact is (Stachowiak *et al.*, 2001):

$$\frac{1}{R'} = \left(\frac{1}{R_{1x}} + \frac{1}{R_{1y}} \right) - \left(\frac{1}{R_{2x}} + \frac{1}{R_{2y}} \right) \quad (3.42)$$

For the given values of R_{1x} , R_{1y} , R_{2x} and R_{2y} :

$$\frac{1}{R'} = \frac{1}{R_1} - \frac{1}{R_2} \quad (3.43)$$

If the velocity of sliding motion of the surfaces in contact is V (m/s) and the Hertzian contact width for the asperities is $2b$ (m), the time t (s) required to release an individual asperity is:

$$t = \frac{2b}{V} \quad (3.44)$$

For two parallel cylinders in concave contact, as shown in Figure 3.13, under radial load W (N), radius of first cylinder is R_1 (m), radius of second cylinder is R_2 (m), a half-length of cylinder L (m), equivalent radius of two cylinder radius is R' (m) and equivalent Young's modulus of the two materials is E' (Pa), the Hertzian contact half width of between two parallel cylinders in concave contact is (Stachowiak *et al.*, 2001):

$$b = \left(\frac{4WR'}{\pi LE'} \right)^{\frac{1}{2}} \quad (3.45)$$

Equation (3.45) for b substituted into Equation (3.44) for t, gives the release time as:

$$t = \frac{2}{V} \left(\frac{4WR'}{\pi LE'} \right)^{\frac{1}{2}}$$

$$t = \frac{2.26R'^{\frac{1}{2}}}{V} \left(\frac{W}{LE'} \right)^{\frac{1}{2}} \quad (3.46)$$

Introducing C_o into Equation (3.34) for δ gives:

$$\delta = 0.319 \left(\frac{W}{E'L} \right) C_o$$

Where:

$$C_o = \left[\frac{2}{3} + \ln \left(\frac{4R_1R_2}{b^2} \right) \right]$$

Rearranging gives

$$\left[\frac{W}{E'L} \right]^{\frac{1}{2}} = \frac{1}{0.319C_o} \left[\frac{E'L}{W} \right]^{\frac{1}{2}} \delta$$

On substituting this value of $\left[\frac{E'L}{W} \right]^{\frac{1}{2}}$ into Equation (3.46) gives the time release as a function of deflection yield:

$$t = \frac{2.26R'^{\frac{1}{2}}}{0.319C_oV} \left(\frac{E'L}{W} \right)^{\frac{1}{2}} \delta$$

$$t = \frac{7.08}{C_oV} \left(\frac{E'LR'}{W} \right)^{\frac{1}{2}} \delta \quad (3.47)$$

If $\delta = z-d$, the mean of the release time for one asperity contact t' can be expressed as:

$$t' = \frac{7.08}{C_oV} \left(\frac{E'LR'}{W} \right)^{\frac{1}{2}} (z-d) \quad (3.48)$$

The release rate of the energy of elasticity \dot{E}_e (J/s) can be calculated as:

$$\dot{E}_e = \left(\frac{E_e}{t'} \right)$$

$$\dot{E}_e = 0.5An_aW(z-d) \frac{C_oV}{7.08} \left[\frac{W}{E'LR'} \right]^{\frac{1}{2}} \frac{1}{(z-d)}$$

$$\dot{E}_e = 0.07 A n_a V W \left[\frac{2}{3} + \ln \left(\frac{4R_1 R_2}{b^2} \right) \right] \left[\frac{W}{E' L R'} \right]^{\frac{1}{2}}$$

$$\dot{E}_e = 0.07 A n_a V W \left[\frac{W}{E' L R'} \right]^{\frac{1}{2}} \left[\frac{2}{3} + \ln \left(\frac{4R_1 R_2}{b^2} \right) \right] \quad (3.49)$$

Where \dot{E}_e is the release rate of the elastic energy (W), A is asperity contact area (m^2), n_a is number of asperity (peaks/ m^2), V is sliding motion velocity (m/s), W is radial load (N), E' is equivalent elasticity modulus of the two materials (N/m^2), L is a half-length of bearing (m), R' is equivalent radius of cylinder (m), R_1 is shaft or journal radius (m), R_2 is bearing bore radius (m) and b is a half width of the two cylinder contact (m).

The effect of linear velocity and radial load the elastic energy release rate on self aligning journal bearing can be determined by considering the geometrical design parameters of the journal bearing. Data for the geometrical design parameters of the journal bearing are given in Table 3.4.

Tabel 3. 4 Journal bearing geometrical design parameter data

Number of asperity area density ($1/mm^2$)	n_a : 16025 (Abdo, 2006)
Nominal shaft diameter (mm)	$d=35$
Length of bearing (mm)	$L=75$
Shaft speed (rpm)	$N=1450$
Radial load 1 (N) or (bar)	$W_1= 400$ or (2)
Radial load 2 (N) or (bar)	$W_2= 1000$ or (10)
Radial load 3 (N) or (bar)	$W_3= 1800$ or (20)
Equivalent modulus of elasticity (N/mm^2)	$E'=38700$

Effect of speed on the elastic energy release rate for three different radial loads can be seen in Figures 3.14 and 3.15.

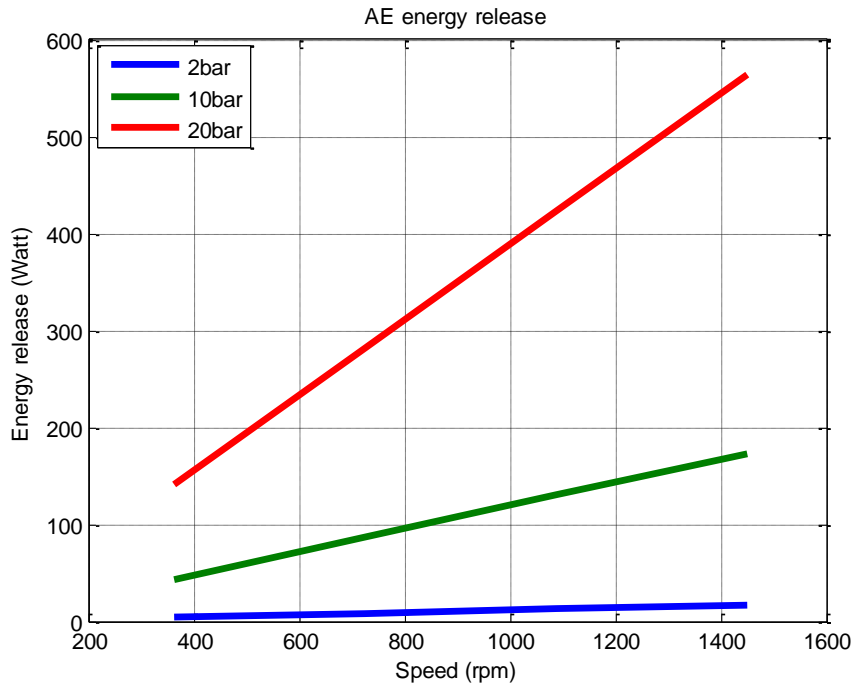


Figure 3. 14 Energy release under three different load variation

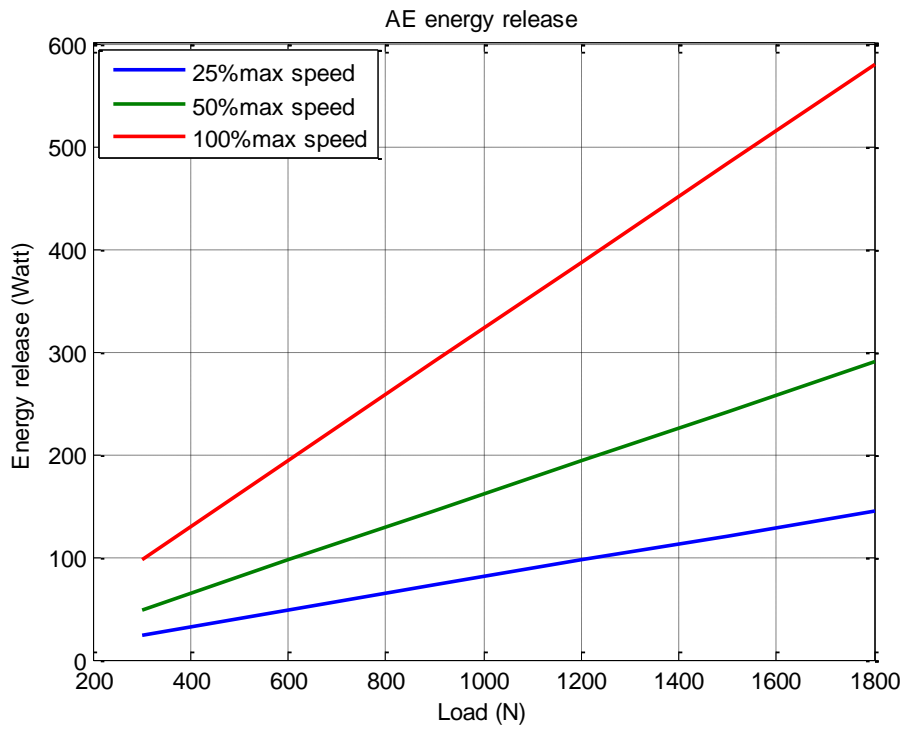


Figure 3. 15 AE Energy release under three different speed variation

The Figures 3.14 and 3.15 shows that the AE energy releases are influenced by speed and radial load. Under higher radial load will generate higher AE energy release, also for increasing of speed.

Lubricant viscosity also affects the AE released, when using a more viscous lubricant asperity contact number declines as the surfaces are more separated by the layer of lubricant, therefore energy released also reduced.

Water contaminants in the lubricant can reduce oil viscosity and decrease the layer of lubricant so that the asperity contact increases and AE energy released is also increased.

Effect of journal bearing surface damage will increase the amount of asperity contact so that energy AE or AE amplitude response also increases.

CHAPTER FOUR

EXPERIMENTAL FACILITIES

4.1 Introduction

To confirm the theoretical understanding gained in Chapter 3, a journal bearing test system was developed for an experimental study of the bearing's dynamic responses under different operating conditions including typical bearing faults. In the meantime, it will be used for developing appropriate data analysis methods to extract useful information for early fault detection and diagnosis.

The test system as developed has three subsystems: a mechanical subsystem which is capable to simulate typical bearing operating conditions, an electrical control subsystem which allows the mechanical subsystem to be controlled for different test programs, and a measurement subsystem which allow both operating condition data and dynamic response data of the testing bearing to be recorded for further analysis.

4.2 Test rig construction and components

The mechanical system was designed to operate two journal bearings simultaneously. It consists of a three phase AC driving motor, couplings, torque load system, hydraulic ram, hand pump, two SA35M self-aligning spherical journal bearings, load cell and main drive shaft. As shown on Figure 4.1 these components are installed on a base frame.

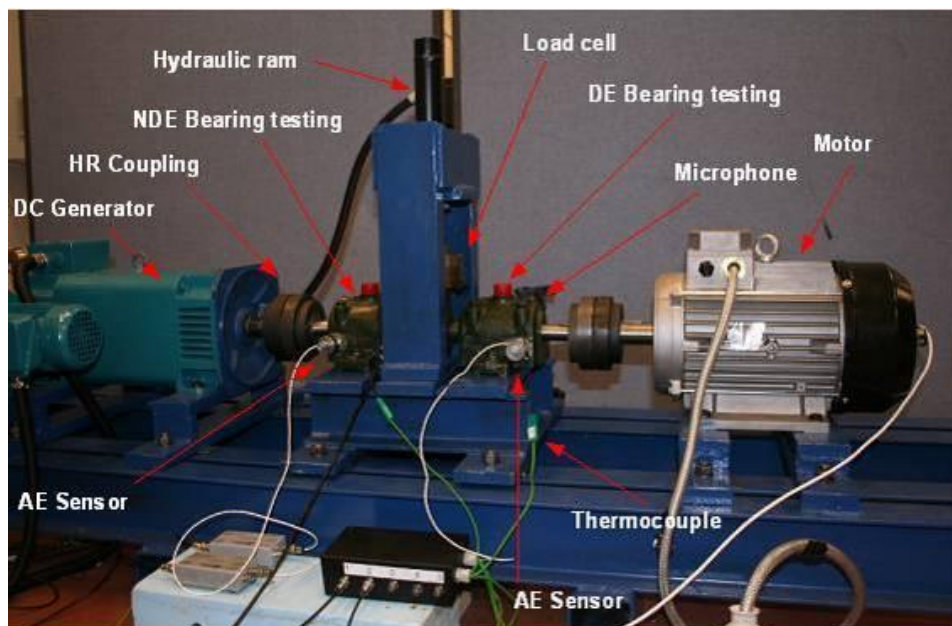


Figure 4. 1 Test rig construction

The torsion load is a DC generator placed at the end of the rig. The electrical drive motor is connected to the main test rig and DC generator by a hard rubber coupling.

4.2.1 Testing bearings

The two SA35M self-aligning spherical journal bearings to be tested were mounted at the drive end (DE) and non-drive end (NDE) of the drive train. The self-aligning spherical journal bearing is shown in the figure 4.2.



Figure 4. 2 Self-aligning journal bearing SA35M

To maintain axial displacement at DE and NDE bearings a pair of washers is installed. The washer in addition to functioning as a stopper to prevent axial movement also serves as a thrust bearing. The self-aligning spherical journal bearing assembly, including the washer, is shown in Figure 4.3.

The preliminary experiments showed that high radial loading of the journal bearings loading generated high temperature. Reducing the heat generated in the loaded bearing, loading bearing replaced by two cylinders rolling bearing.

Table 4.1 gives the housing dimensions of the self-aligning spherical journal bearing and main performance parameters.

Table 4. 1 Self-aligning journal bearing SA35M housing dimensions

(Arvis, 2009)

Type of bearing	Self-aligning journal bearing
Bearing code	SA35M/S 4170
Diameter of bearing hole (mm)	35
Length of bearing (mm)	76
Spherical diameter of bearing (mm)	82
Maximum load (kN)	10
Maximum speed (rpm)	5000
Lubrication system	Ring lubrication

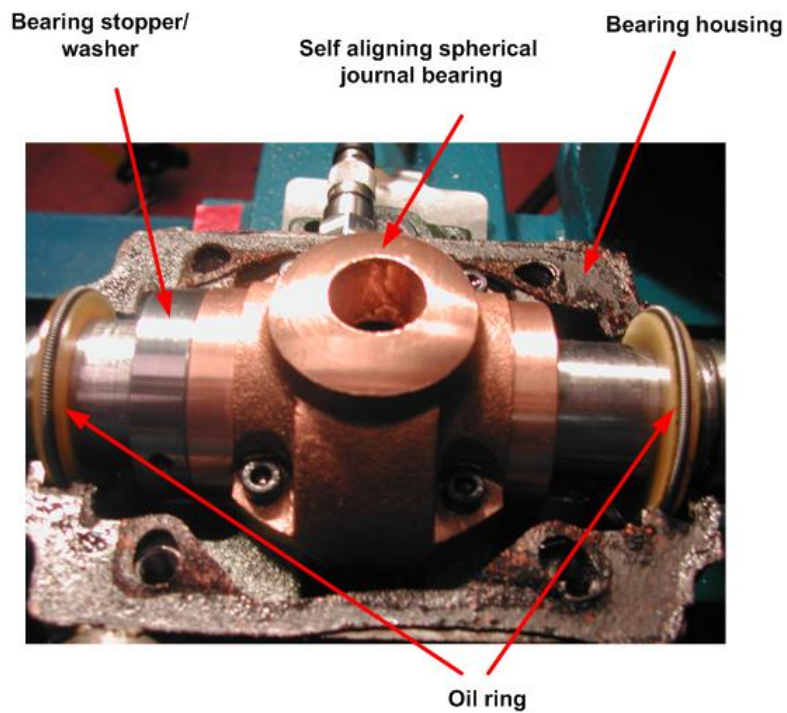


Figure 4. 3 Self aligning spherical journal bearing assembly

4.2.2 AC driving motor

The test rig was driven by a 9 kWatt (12.5 HP), 3-phase, 4 pole electric induction motor at a speed of 1450 rpm with a shaft diameter, 38 mm.

Specification of the test rig motor was:

Table 4. 2 Test rig motor specification

Manufacturer	Clarke
Type of mounting	Foot mounting (B3)
Phase	3 Phase
Pole number/rpm	4 pole/1450 rpm
Starter requirement	20Amp
Power	9kWatt/12.5Hp
Shaft diameter	38mm with standard keyway
Frame size	132

4.2.3 Hydraulic cylinder

The radial load is applied on the bearings by using a hydraulic cylinder system with pressure gauge and load cell and powered by a hand pump. The maximum pressure exerted by the hydraulic cylinder was 380 bar gauge. The specification of hydraulic ram is summarized in table 4.3.

Table 4. 3 Hydraulic ram specification

(Steerforth, 2011)

Manufacturer	Steerforth
Type	Single acting
Stroke (mm)	200
Bore diameter (mm)	40
Rod diameter (mm)	27
Outside diameter (mm)	50
Piston diameter (mm)	30

Pressure in the hydraulic cylinder originated from the hand pump via a hand pump tank as oil reservoir. The hand pump is double stroke and can be flange mounted directly onto a tank. This hand pump is designed to operate a single acting cylinder, an unloading valve is optional. A 0.6 metre lever handle was included as the standard with hand grip. The specification of the hydraulic pump is summarized in Table 4.4.

Table 4. 4 Hydraulic hand pump specification

(HP, 2003)

Manufacturer/model	Hydra products
Type	HPMU12
Displacement (cm ³)	12
Work pressure (bar)	320-380
Height (mm)	166
Total height (mm)	273

The hand pump tank is made of 3 mm steel, and can be mounted using M8 bolts in a vertical or horizontal position. Tank specification is as shown in Table 4.5.

Table 4. 5 Hydraulic pump tank specification

(HP, 2003)

Manufacturer/model	Hydra
Type	RP 408.01
Capacity (litres)	1
Length (mm)	150
Width (mm)	100
Height (mm)	120

The principle of the hydraulic installation specified in Tables 4.4 and 4.5.

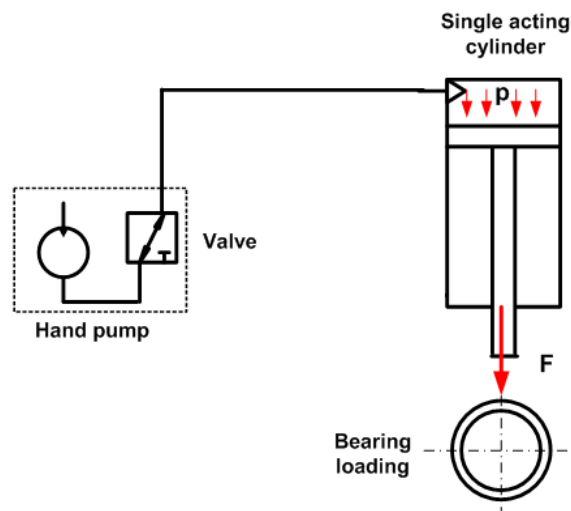


Figure 4. 4 Hydraulic system schematic

This system allows the bearing to be radial loaded from 2.0 Bar to 30 Bar.

4.2.4 Hard rubber coupling

A hard rubber coupling (HRC) is used to connect the electrical motor drive shaft to the bearing testing shaft and at the other end of the gear train to connect the bearing shaft to the DC motor as a torque loading, see Figures 4.1. HRC couplings are used as general purpose couplings with a flexible element which can accommodate a degree of misalignment and absorb vibration. The specification of the HRC130H was:

Table 4. 6 Specification for Fenner Coupling HRC130H
(Maryland, 2008)

Manufacturer	Fenner
Type	HRC130H
Size	130
Bore diameter (mm)	14-42
Outer diameter (mm)	130
Diameter of hub (mm)	105
Length of hub (mm)	18.0
Width of rubber (mm)	36
Taper lock bush size code	1610

Based on the bore size and type, there are three HRC couplings: HRC couplings with type B (cylinder bore), with type F for a taper lock bushing where the widest part of the taper lock bush faces the flexible element, and type H for taper lock bushings where the widest part of the taper lock bush faces away from the flexible element. In this case an H type coupling, HRC130H with taper lock bushing 1610 was used.

4.2.5 DC Generator

The test rig uses a Siemens DC generator as a torsion loader, where the loading is adjusted through the Siemens microcontroller. The magnitude of the load is expressed as a percentage of the maximum power which is 9.9 kW at speed of 2850 rpm, supply voltage 400V and current of 28A.

DC generator was used to provide the torque loads to makes it easier to control the loading. The torque loads and speed control was done using the Siemens Micro Controller system.

4.3 Speed and torque controller

The test rig can be operated at different speeds and different torque loads, so a speed and torque controller was required. A Park 690 AC drive with Siemens Micro Master Controller was installed so that the motor could be run at different speeds and different torque loads.

The Siemens Micro Master Controller was installed on the rig and proved easy to use and was able to deliver torque and speeds accurately. Loading is conducted using a set-up panel screen that includes number of steps, time of operation (minute), AC motor speed (%) and DC torsion load (%)

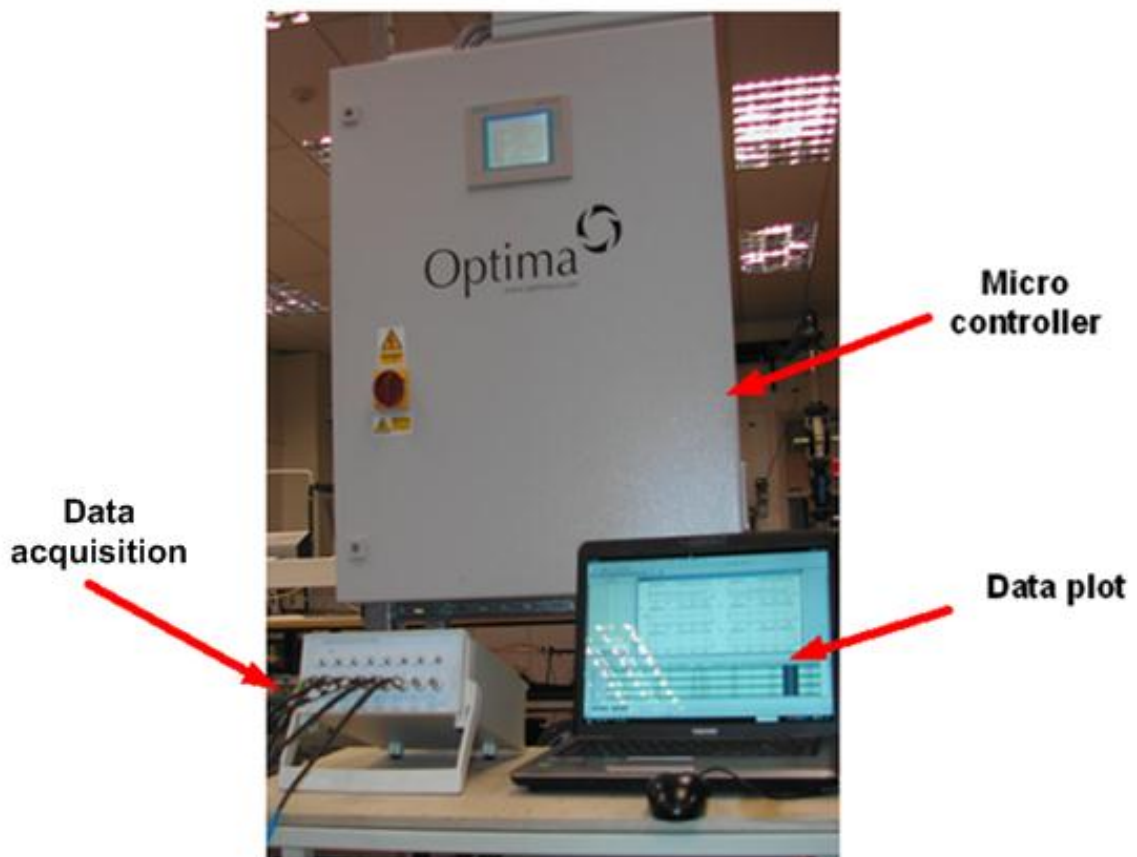


Figure 4. 5 Siemens Micro Master Controller and data acquisition system

4.4 Data acquisition and measurement systems

The data acquisition system (DAS) consisted of two sets of multiple channels of ADC converters with associated software for collecting vibration, acoustic and AE data.

In the vibration monitoring system, the relevant hardware was the vibration transducer which has a useful frequency band up to 10 kHz, an amplifier and/or pre-amplifier, and a data acquisition card (DAC) installed in a PC. The amplifier increases the vibration signal and serves to isolate the processing and display equipment from unwanted interference from the vibration pick up.

The software allows data acquisition with different triggering modes, which is convenient for viewing the data in real time and saving data to the hard drive. In addition, DAC has basic data analysis capabilities such as correlation, synchronised time averaging and spectrum analysis of data.

4.4.1 Data acquisition system for vibration and airborne sound

In these experiments the DAS system was a Sinocera YE6232B, a 16-channel high speed data acquisition system which recorded all the measurements data at a sampling rate of 96 kHz, see Figure 4.6.



Figure 4. 6 Sinocera YE6232B

Table 4. 7 Technical specifications of the Sinocera
(GST, DAQ,2010)

DAQ system manufacturer	Sinocera YE6230B
Number of Channels	16 channels. Selectable voltage/IEPE input.
A/D conversion resolution	16 bit
Sampling rate (maximum)	100kHz per channel parallel sampling
Input range	±5V
Gain	Selectable, either 1, 10 or 100
Filter	Anti-aliasing filter
Signal frequency range	30 kHz
Interface	USB 2.0
Software	YE7600

The data acquisition system is supported by general purpose YE76000 software for data acquisition, conditioning and analysis as part of the data acquisition system. This software supports the YE6232B and allows users to set up parameters for data acquisition, data conditioning, data formatting, real-time analysis and signal sources. It also possesses efficient data storage and fast data conversion to Matlab format; 16 bit with 16 channels. It has the capability of real time domain analysis, frequency domain, statistical analysis and time-frequency domain. It also allows selection of acquisition modes: oscilloscope, manual continuous and triggered.

Vibration transducers

The vibration transducer is used to measure machinery or structural vibration by converting vibration energy into a measurable voltage. Velocity pickups, accelerometers and eddy current or proximity probes can be used for vibration measurement. Today accelerometers are by far the most popular vibration transducers used with rotating machinery (Girdhar and Scheffer, 2004).

The accelerometers attached to the test rig were Sinocera model CA-YD-185TNC. Two were attached to the NDE bearing, in the horizontal direction. These are piezoelectric devices with integrated electronics in which a piezoelectric material responds to mechanical deformation by developing an electrical charge across its surfaces. A charge amplifier is used to produce a voltage which is directly proportional to the applied mechanical stress. The specification of the accelerometer is given in Table 4.8.

Table 4. 8 Specification of the Sinocera accelerometer model CA-YD-185TNC

(GST,Accelerometer,2010)

Manufacturer	Sinocera
Type	Accelerometer (piezoelectric)
Model	CA-YD-185TNC
Frequency range	0.5Hz to 5000Hz
Voltage Sensitivity	4.96mV/ms ²
Temperature range	-20°C to 120°C

The accelerometers were attached to the bearing housing casing using a threaded bronze stud. The vibration transducers were each connected to the DAS as described above and then to the computer via a USB port.

Acoustic sensors

The acoustic sensor or microphone is used to measure the airborne sound radiated from journal bearing to its surrounding.

When a component of machine vibrates in the presence of air, the air molecule at the surface will start to vibrate as well. The vibration transmits through the air as oscillating pressure at frequency and amplitude depend on the original sound source. A microphone is designed to convert pressure oscillations to electrical signals which can be saved and analyzed to get information on the nature and characteristic of the sound source.

The piezoelectric microphone is one kind of microphone that can be used for test and measurement purposes. The piezoelectric microphone uses a quartz or ceramic crystal structure. This type of microphone is able to gain very high amplitude pressure range. The output voltage of piezoelectric is proportional to the pressure exerted on it.

The microphones were used are Sinocera model BAST YG 201 07067 for the DE bearing and model BAST YG 201 07065 for the NDE bearing. The microphones were placed 220 mm away from the accelerometer pick up. The microphone was directly connected to the DAS and then connected with the computer by USB.

Table 4. 9 Specifications of the Sinocera microphone model BAST YG 201

(BAST, 2007)

Manufacturer	Sinocera
Name	BAST YG 201 07067 with ICP Microphone
Type	CHZ 211 serial 0069
Frequency response	20Hz to 100 kHz \pm 0.2 dB
Dimensions	\varnothing 12.7 mm x 70 mm
Sensitivity	49.5 mV/Pa
Maximum output voltage	5.0 Vrms
Operating temperature	-40°C to +80 °C

4.4.2 Data acquisition system for AE

The AE data acquisition system use PAC PCI-2 commercial data acquisition system. The PCI-2 AE System is a 2-channel data acquisition and digital signal processing system on a single full-size 32-bit PCI-Card. The PAC PCI-2 data acquisition board is shown in Figure 4.7. (PAC, 2009)



Figure 4. 7 PCI-2 AE System board

In the operation of data acquisition, waveform transfer and processing is supported by the Windows platform of PACwin Suite. The PAC Windows platform consisting of AEwin™, which can be run in standard Windows such as Windows 98, 2000 and XP. The sampled AE waveforms can be continuously transferred to the hard disk. Hence the AE signal can be saved up to the capacity of the hard disk in the computer. The PCI-2 AE system specification is shown in Table 4.10.

Table 4. 10 Specifications of the PCI-2 AE system specification

(PAC, 2009)

Manufacturer	Physical Acoustic Corporation
AE input	2 channels
Input impedance	50 ohm or 1000 ohm
Frequency response	1kHz-3MHz
Minimum noise threshold	17dB
ADC Type	18bit 40 MSPS per channel maximum
Dynamic range	>85dB
Sample rate	100kS/s-40MSPS
Operating temperature	5°C to +45 °C
DC Power	12Volt, 1.0 amps

Advanced analysis can use the Mathlab™ code for configuring the AE signal and streaming data system as shown in Figure 4.8.

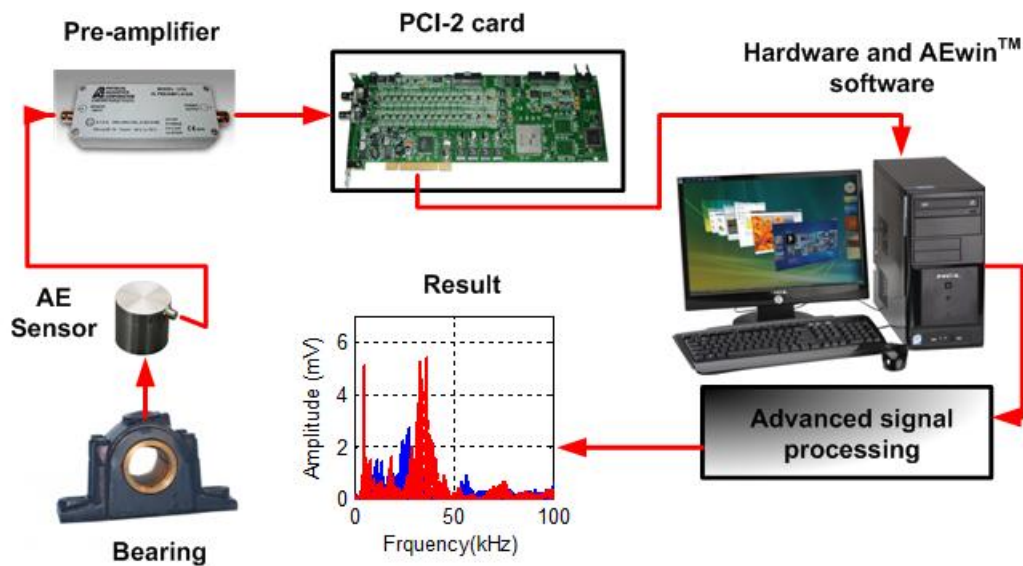


Figure 4. 8 AE signal measurement and data streaming system configuration

The acoustic emission sensor is a transducer that converts the mechanical energy carried by the elastic wave into an electrical signal. The transducer most used in acoustic emission application is the piezoelectric transducer. The AE transducer used here the wide band model PAC WD FQ 35 with sample frequency 1 MHz. The specification of AE transducer is as shown in Table 4.11.

Table 4. 11 AE transducer specification

(PAC, 2010)

Manufacturer	Physical Acoustic
Type	Wideband AE Sensor
Model	WD FQ 35
Peak sensitivity	64.50 dB ref 1V/ μ bar
Frequency response	Peak frequency 263,67 kHz
Frequency range	100kHz-1MHz
Operating range	-45° C to 125 °C
AE DAS	AEwin™ for PCI2 version

The output signal from AE-sensor was pre-amplified by 40 dB through a preamplifier 20/40/60 dB gain.

4.4.3 Load cell

The load cell converts mechanical force into an electric signal. In this test it is used to measure the radial force imposed on the bearings by the hydraulic ram. The specification of the Sinocera model CL-YB-11.5kN load cell is given in Table 4.12. This type of load cell is essentially a high precision strain gauge.

Table 4. 12 Sinocera load cell specification

(GST, Load Cell, 2010)

Manufacturer	Sinocera
Name	Weight Transducer (Strain Based)
Type	CL-YB-11
Sensitivity	1.5mV/N
Linear range	0-5kN
Overload	150%
Operating temperature	-20 to +60°C
Material	Special alloy steel
Output connection	Five core shielded cable

4.4.4 Temperature sensor

For measuring the temperature on the bearings being tested, TC Ltd commercial type K thermocouples were used. These are miniature (1.5 mm diameter) mineral insulated thermocouples with miniature flat pin plug connected to the data acquisition system through a preamplifier and distributor. The specifications of the thermocouple are shown in Table 4.13.

Table 4. 13 Thermocouple specification

(TC, 2009)

Manufacturer	TC Ltd
Type	K
Sheath diameter	1.5 mm x 250 mm
Sheath material	321 Stainless Steel
Operating range	-100° C to 800 °C

4.4.5 Pressure sensor

A radial load is imposed on the bearing testing measured using load cell and pressure transducer. The pressure transducers used to measure the radial load from the hydraulic pump are strain gauge pressure transmitters RS 249 3836. The strain gauges are small components that are fixed to a surface that is strained. The change in length of the element caused by external pressure or external force produces change in the electrical resistance. The electrical resistance change is processed and converted into a voltage. The specification of the pressure transmitter is presented in table 4.14.

Table 4. 14 Pressure transmitter specification

(RS)

Manufacturer	RS
Type	249 3836
Supply	10V dc
Output	0-100 mV
Operating range	40bar G

4.4.6 Shaft encoder

Encoder or speed transducer is widely used for measuring the output speed of rotating objects such as electrical motors, turbines and internal combustion engines. This encoder is a sensor produces signals due to rotation movement of such items as an electrical motor shaft. The DC type of encoder or tachometer generates a voltage directly proportional to the shaft speed. The encoder is coupled and installed to the electrical end of the motor shaft. The encoder used is economic for small devices, has a long life and very small torque ball bearings. Specification of the encoder is shown in Table 4.15.

Table 4. 15 Encoder specification
(Hengstler, 2001)

Manufacturer	HENGLER
Type	RI 32
Mounting	Round flange
Number of pulses	100
Shaft diameter	5mm
Maximum speed	6000 rpm
Operating temperature	-10 – 60°C
Supply voltage	DC 5V±10%

4.5 Seeded faults

Most premature bearing faults (45%) is caused by the presence of impurities in the lubricant (Clevite, 2002). Water, fuel and gas contamination of the lubricant may result in inadequate lubrication and eventually cause wear. Solid contaminants cause immediate damage (e.g. scratching) to the bearing surface.

The information contained in the surface vibration, airborne sound and acoustic emission responses for self-aligning journal bearing due to viscosity variation and lubricant surface deterioration were investigated in a series of experiments which imitated bearing deterioration due to water contamination of the lubricant and scratched surface bore.

4.5.1 Water contaminated lubricant

Water in oil creates rust and sludge, change in viscosity, foaming, acidity and decrease of lubricant film strength. Water contamination accelerates the aging process resulting in,

amongst other things, corrosion, reduced lubricant film strength, damaged components and premature aging of the oil (Noria Corporation, 2003). The potential sources of water contamination in lubricating oil including leakage from cooler, condensation of atmospheric humidity, coolant jacket leak and contamination from top-up oil or during oil changes.

The mixing of lubricant ISO VG 46 with water was done manually by using a chemical measuring tube. Concentration of water and lubricant were as follows 0%, 1.25% and 2.5%.

4.5.2 Surface scratch

Scratching is a problem that is often found in journal bearing failures, see Section 2.9. A scratch is a step change in the local roughness in the surface of a journal bearing. It also means a change the distribution and size of the local asperities which can lead to changes in amplitude and frequency of vibration, noise and AE emitted from the bearing.

To obtain information in a controlled way on the surface vibration, airborne sound response to the presence of a scratch an artificial or imitation scratch was introduced into the bearing. The artificial scratch was made by cutting a circumferential scratch on the surface bearing bore every two millimetres along the length of bearing using a lathe cutting tool. The journal bearing with seeded with a scratch fault which was 0.05 mm deep and 0.1 mm wide, see Figure 4.20.

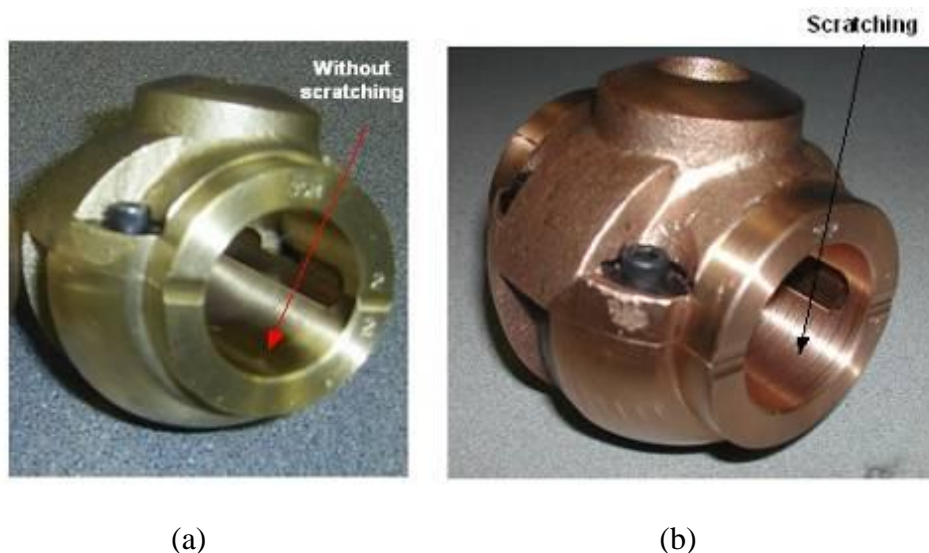


Figure 4. 9 Self-aligning spherical journal bearing, normal and with seeded scratch

4.6 Experimental procedure

This study investigated the changes in vibration, airborne sound and AE signal characteristics of a self-aligning spherical journal bearing fault due to lubricant viscosity variation, lubricant and surface deterioration. The lubricant deterioration is due to water contaminant in three concentrations 0%, 1.25%, and 2.5% by volume.

The surface deterioration is due to circumferential scratches each 0.05 mm deep and 0.1 mm wide. The surface vibration, airborne sound and AE characteristics of the self-aligning spherical journal bearing will also be functions of radial load and speed and lubricant viscosity.

4.6.1 Radial load and speed variation.

Because the SA35M self-aligning spherical journal bearing is relatively new, there was little information available regarding its response to changes in radial load, speed and lubricant viscosity. Thus the aim of this experiment was to obtain surface vibration, airborne sound and acoustic emission characteristics of the self-aligning spherical journal bearing due to variation in radial load, shaft speed and lubricant kinematic viscosity.

The initial experiments consisted of two set of tests: the first was for four speeds 362.5 rpm (25% of the maximum speed of 1450 rpm), 725 rpm (50% of the maximum speed), 1087.5 rpm (75% of the maximum speed) and 1450 rpm (maximum speed). At each speed there were three different radial loadings: 2bar, 10bar and 20bar. Through all the tests the bearing was lubricated with specified lubricant ISO VG 32.

The tests were performed start save at a temperature of 22.5°C, so that the effect of temperature on the surface vibration, airborne sound and acoustic emission responses can be reduced.

The sensors used have been described in Sections 4.3.1 (accelerometers), (microphone) and 4.3.2 (AE sensor). The accelerometers were attached to the bearing housing casing by a threaded bronze stud and the microphones were placed 220 mm behind the accelerometer. The AE sensors were placed on the horizontal surface of the bearing housing.

4.6.2 Lubricant viscosity variation

The test rig used to determine the effect of viscosity variation on surface vibration, airborne sound and acoustic emission with the same speed and loading parameters as in the first sets of tests but with four different lubricants: ISO VG 32 (as a reference) and lubricants ISO VG 46, ISO VG 68 and SAE 90.

4.6.3 Lubricant deterioration due to water contaminant

This series of experiments used the test rig to investigate the characteristics of the surface vibration, airborne sound and acoustic emission response from the SA35M self-aligning spherical journal bearing it was tested using lubricant ISO VG 46 with four levels of water contamination 0%, 1.25% and 2.5% by volume. The tests were conducted under constant radial load of 2bar, 10bar and 20bar with speed 25%, 50%, 75% and 100% of maximum speed (1450rpm). This test also was performed on the test rig.

4.6.4 Scratching surface deterioration

These experiments were used to investigate the characteristics of the surface vibration, airborne sound and acoustic emission signals for the SA35M self-aligning spherical journal bearing with surface deterioration caused by scratching.

The experiment program investigating the effects of surface deterioration was done by comparing the surface vibration, airborne sound and acoustic emission signals from two otherwise identical journal bearings for the same speed and load but with and without the seeded fault. The two bearings are shown in Figure 4.2, the bearing with the seeded faults is at the drive end (DE) and the normal bearing is at the non-drive end (NDE).

The scratched surfaces experiments were conducted under constant torsion load of 2 bar, 10 bar and 20 bar under speeds of 25%, 50%, 75% and 100% maximum speed. The bearing was lubricated by specified lubricant ISO VG 32.

The analysis is done by comparing the surface vibration, airborne sound and acoustic emission responses of the scratched bearing with that of the reference bearing. Tests of the reference bearing were conducted by installing normal bearing on both DE and NDE under same load and speed conditions.

4.6.5 Summary of experiment procedure

Summary of experiment procedure can be shown in table 4.16 and 4.17.

Table 4. 16 Experiment procedure for repeatability and viscosity variation

No	Experiment type	Speed (%)	Radial load (Bar)
1	Repeatability	25	2, 10 and 20
		50	2, 10 and 20
		75	2, 10 and 20
		100	2, 10 and 20
2	Viscosity variation ISO VG 32	25	2, 10 and 20
		50	2, 10 and 20
		75	2, 10 and 20
		100	2, 10 and 20
	ISO VG 68	25	2, 10 and 20
		50	2, 10 and 20
		75	2, 10 and 20
		100	2, 10 and 20
	SAE 90	25	2, 10 and 20
		50	2, 10 and 20
		75	2, 10 and 20
		100	2, 10 and 20

Table 4. 17 Water contaminant in oil and scratching surface bearing

No	Experiment type	Speed (%)	Radial load (Bar)
3	Water contaminant in oil ISO VG 46 % water contaminant	25	2, 10 and 20
		50	2, 10 and 20
		75	2, 10 and 20
		100	2, 10 and 20
	1.25% water contaminant	25	2, 10 and 20
		50	2, 10 and 20
		75	2, 10 and 20
		100	2, 10 and 20
	2.5% water contaminant	25	2, 10 and 20
		50	2, 10 and 20
		75	2, 10 and 20
		100	2, 10 and 20
4	Scratching surface bearing Normal surface bearing	25	2, 10 and 20
		50	2, 10 and 20
		75	2, 10 and 20
		100	2, 10 and 20
	Scratching surface bearing	25	2, 10 and 20
		50	2, 10 and 20
		75	2, 10 and 20
		100	2, 10 and 20

CHAPTER FIVE

SURFACE VIBRATION, AIRBORNE SOUND AND ACOUSTIC EMISSION CHARACTERISTICS OF A SA35M SELF-ALIGNING SPHERICAL JOURNAL BEARING UNDER DIFFERENT OPERATION

5.1 Introduction

To develop more effective methods for the detection of developing faults in self-aligning spherical journal bearings, this chapter investigates surface vibration, airborne sound and acoustic emission signals from such bearings under different operating conditions. The study of changes in radial load, rotation speed and the quality of the lubricant give a fuller understanding of the physical processes of feature development in bearings.

All the tests were performed on the test rig described in Chapter 4.1 using two SA35M self-aligning spherical journal bearings as described in Section 4.1.1. Experiments were carried out with the journal bearings installed on the driven (DE) and non-driven (NDE) sides of the load cell see Figure 4.1. The accelerometer CAY-YD-187 TNC, microphone BAST YG 201 and the data acquisition system Sinocera YE6230B were used in the experiment, were described in Section 4.3.

The acoustic emission experiments used a Physical Acoustic Corporation (PAC) Model WD FQ 35 and WD FQ 36 is as described in Section 4.3.2. The Data Acquisition System and tools for measurement and analysis tools are AEwinTM for PCI2 version E1.55 pre amplified by 40 dB, with sampling rate 1MHz and record length for 10 second.

The experiment for determining the effect of speed and radial load on surface vibration, airborne sound and acoustic emission characteristics was performed for radial loads of 2 bar, 10 bar and 20 bar. Each experiment the motor speed was operated at 25%, 50%, 75% and 100% of the maximum of 1450 rpm.

To reduce the influence of temperature on the vibration, acoustic and acoustic emission signals the initial data collection was always carried out at the same temperature of 22.5 °C.

Installation of instrumentation measurement such as accelerometer, microphone and acoustic emission sensors are as shown in Figure 5.1.

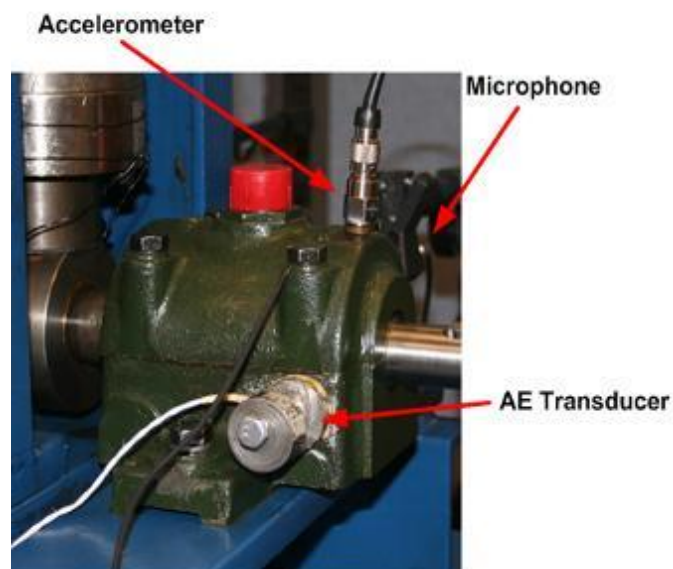


Figure 5. 1 Instrumentation measurement installation

Each experiment was performed 3 or 4 times to get a good reliability and repeatability of data. Statistical parameters such as RMS value and Kurtosis value for the time and frequency domains were used for descriptive and comparative analysis of the surface vibration, airborne sound and acoustic emission spectra.

5.2 Repeatability of experimental results

The result of repeatability test is divided in to surface vibration, airborne sound and acoustic emission measurement result. Each measurement result the time domain, RMS means value, kurtosis, spectrum and mean value of spectrum and comparative analysis are applied.

5.2.1 Surface vibration

Figure 5.2 is the time domain surface vibration (SV) signal of the two self-aligning spherical journal bearings DE and NDE for three tests operated at 100% speed with radial load 10 bar and use lubricant ISO VG 32.

Figure 5.2 shows no significant difference between the first, the second and third experiments.

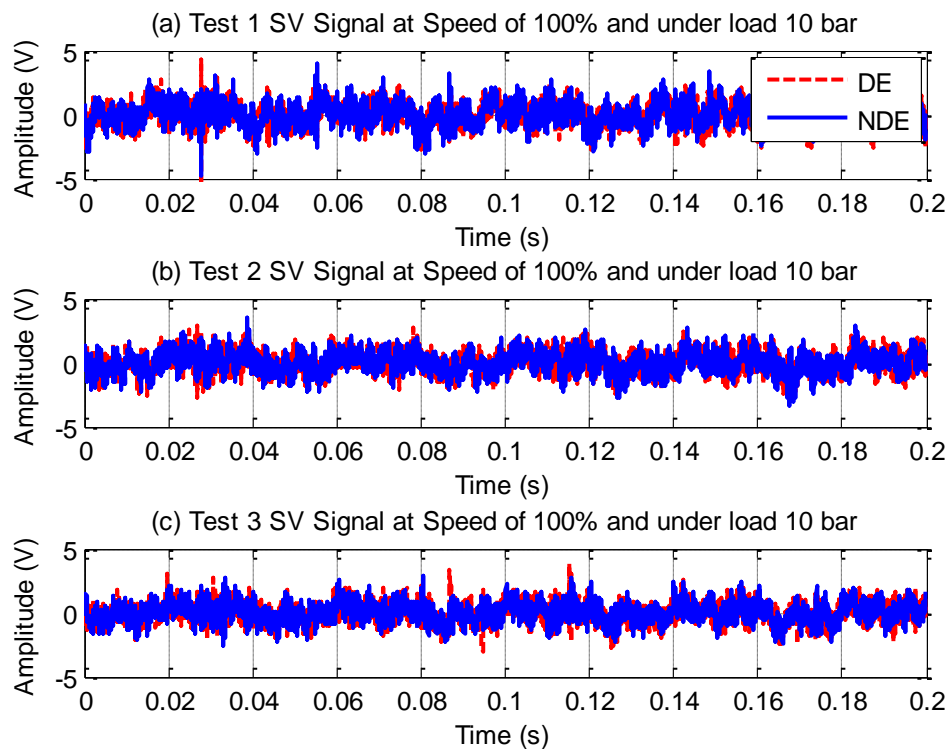


Figure 5. 2 SV signal of bearing under 10bar radial loads for three tests

Experimental repeatability can also be seen from the SV RMS of the raw signal as shown in Figure 5.3

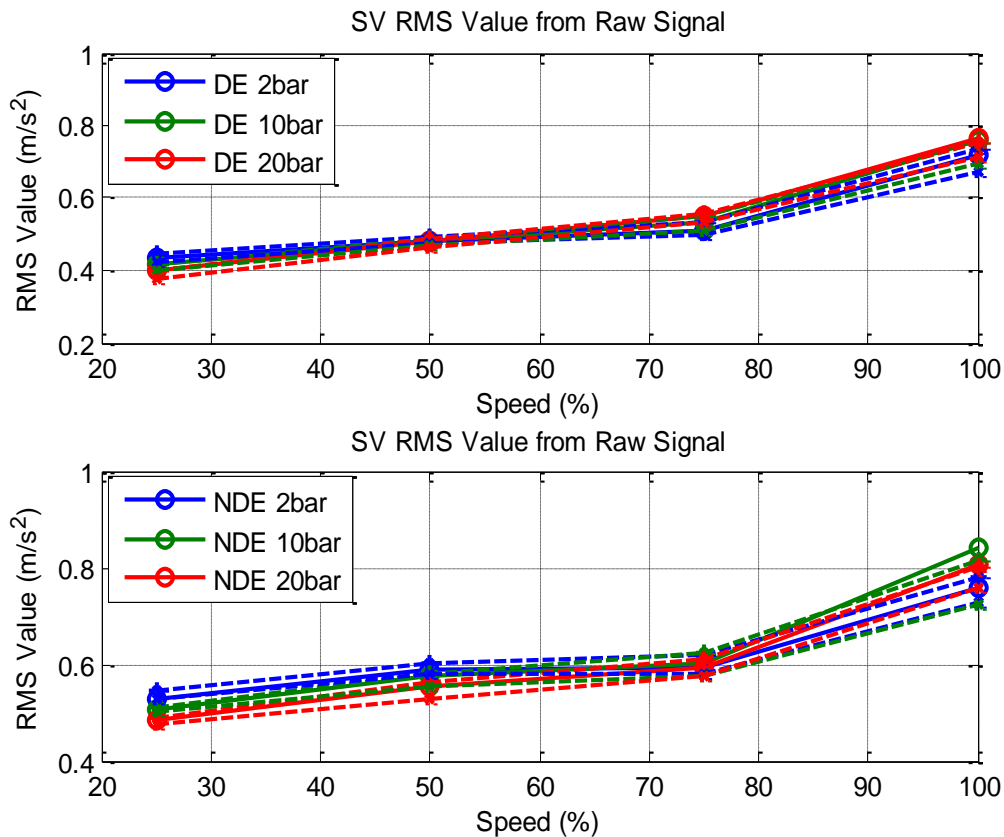


Figure 5. 3 SV RMS value from raw signal of DE and NDE bearing under three loads and four speeds for three test runs

The SV RMS values from the raw signal indicates that while the influence of speed is clear to see, particularly from 75% to 100% of maximum speed, the variation in radial load do not give significant difference because the RMS values obtained at the different loads overlapped. These variations occur due to the difficulty of precisely controlling the radial load because lack of sensitivity in the pressure transducer allows a small pressure drop in the hydraulic system.

Figure 5.4 is the SV frequency domain signal for the journal bearings operating at 100% maximum speed and 20 bar radial load for three test runs.

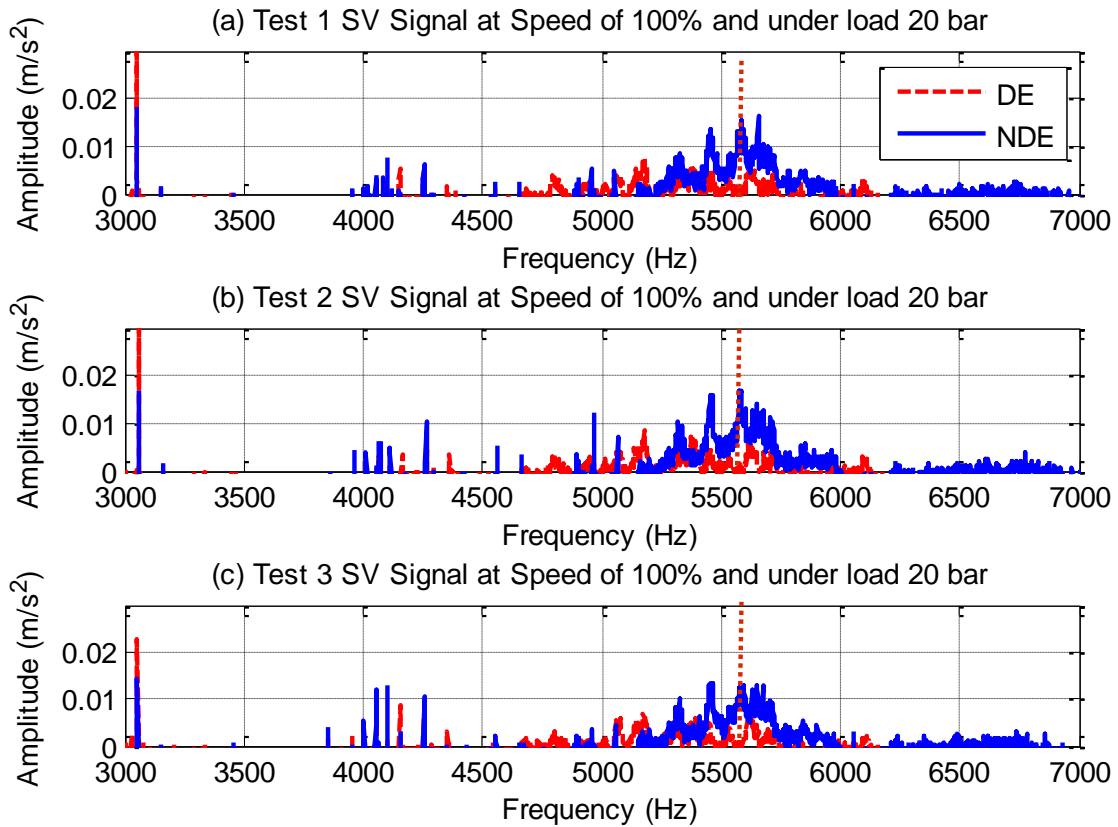


Figure 5. 4 SV spectra of DE and NDE bearing under 20 bar load and 100% maximum speed

The spectrum of the surface vibration is shown in Figure 5.4 and in general it can be seen that there is a small difference in pattern and peak amplitude at 5.6 kHz of the spectra between the first, second and third experiments.

Figure 5.5 shows surface vibration RMS values for different loads and speeds for both DE and NDE bearings which also demonstrate experimental repeatability.

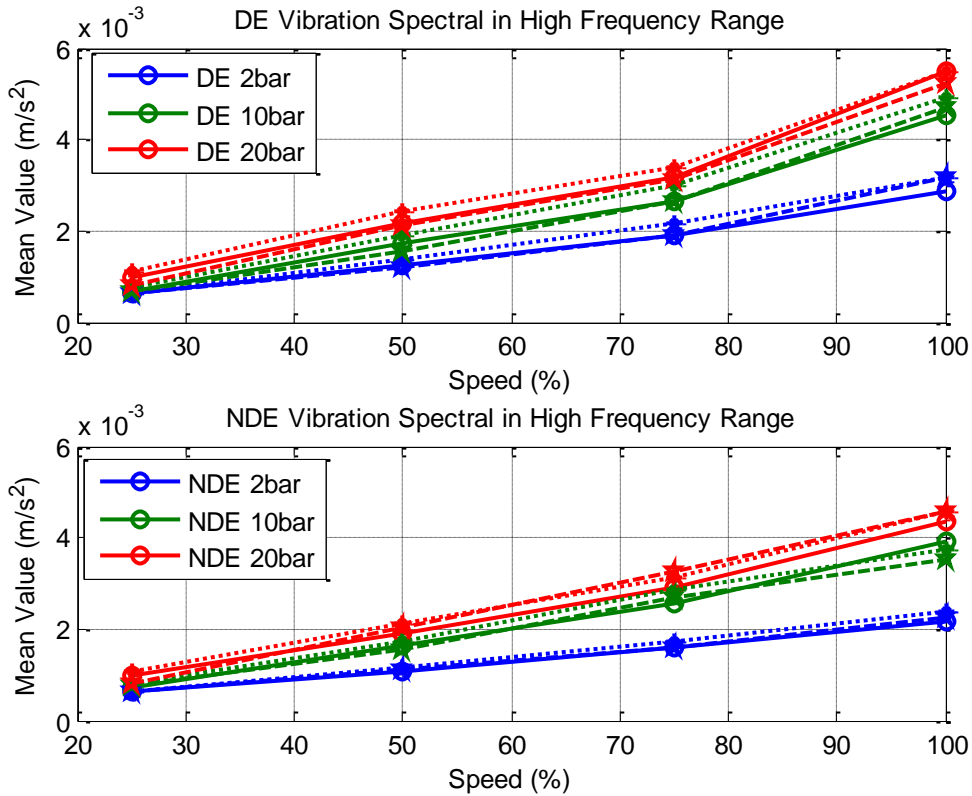


Figure 5. 5 SV mean spectrum response value on bearing under different load and speeds for three test runs

The SV RMS value on DE and NDE bearings for different speeds and three radial loads shows repeatability under the experimental limitations mentioned above and, importantly, at speeds above the minimum the ranges of the measurements do not overlap.

5.2.2 Airborne sound

Figure 5.6 shows the time domain of airborne sound (AS) signal for the DE and NDE bearings. The figure shows no significant differences between the three test results which is confirmed by the RMS value of airborne sound for both DE and NDE bearings obtained under three loads and at four speeds, see Figure 5.7. It can be seen that the plots for the tests are difficult to distinguish because they overlap. As with the vibration signal the RMS level initially increases with speed, but unlike the vibration signal, the RMS value for the airborne sound drops at greater than 75% of the maximum speed. This case is caused by improving of lubrication system.

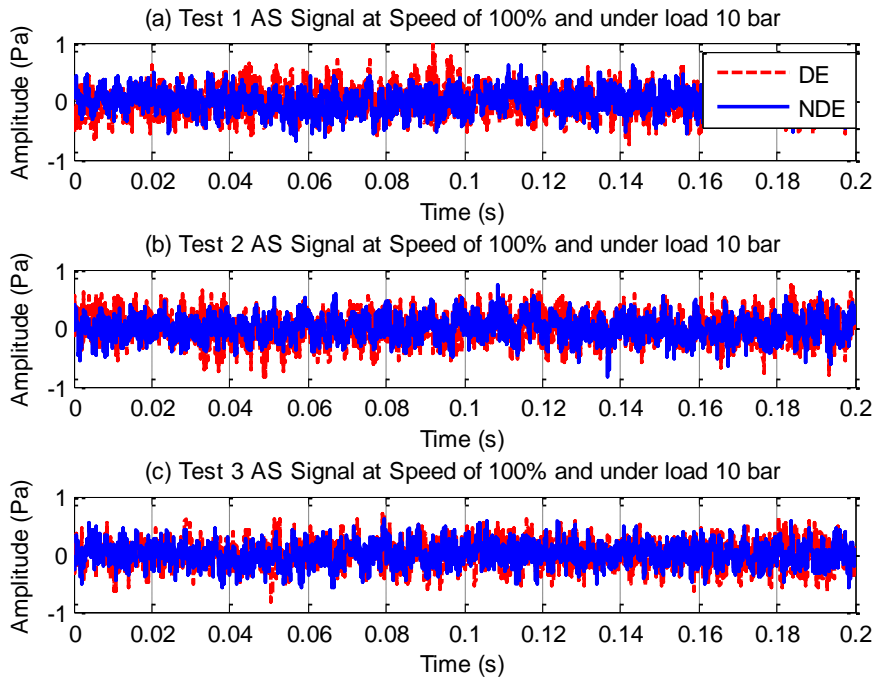


Figure 5. 6 AS signal for DE and NDE bearings under 10bar radial loads at maximum speed for three test runs

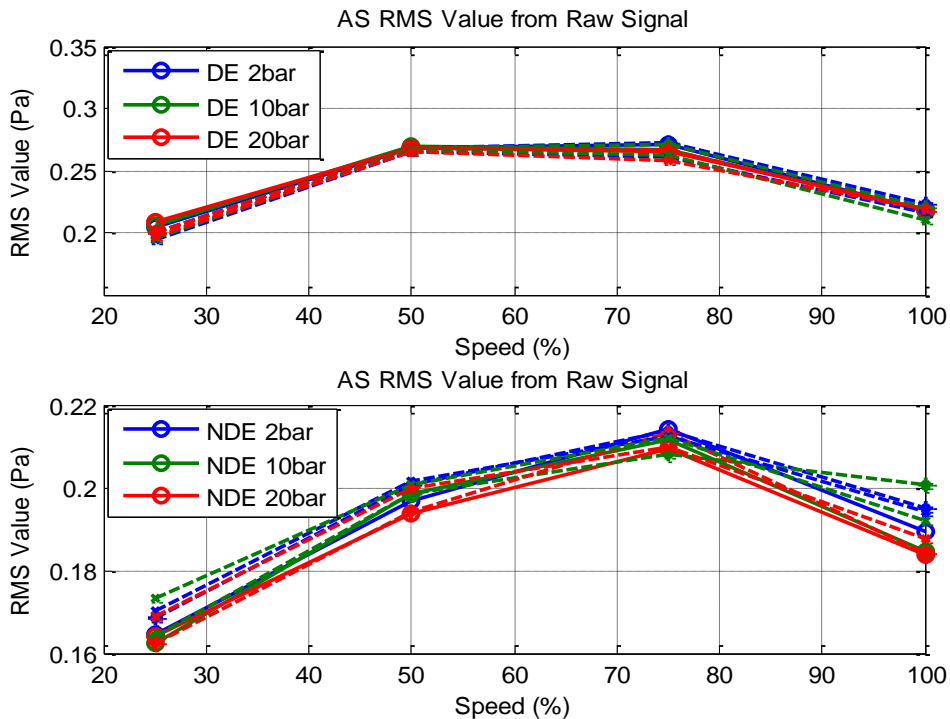


Figure 5. 7 AS RMS values from raw time domain signals for DE and NDE bearings under three loads and four speeds for three test runs

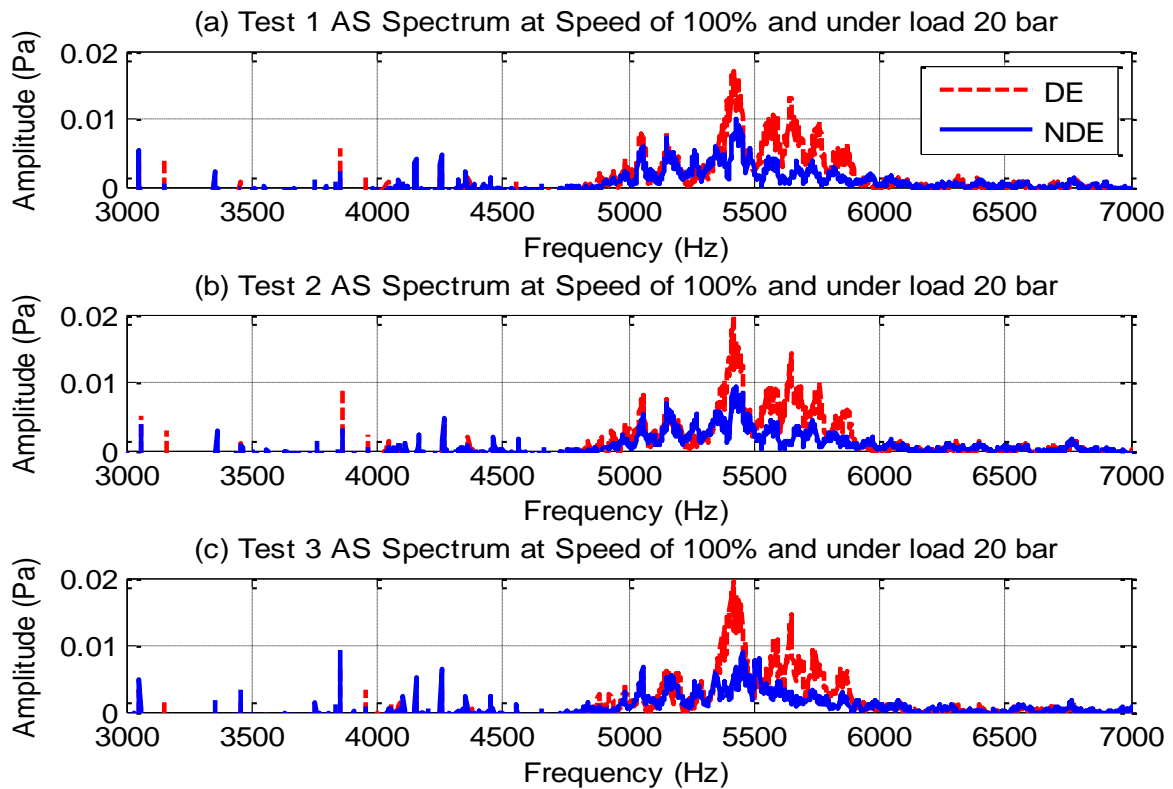


Figure 5. 8 AS spectra for DE and NDE bearings under maximum load and at maximum speed for three tests runs

Figure 5.8 shows the AS spectra obtained for the DE and NDE bearings at 100% speed and 20 bar radial load for three test runs. It can be seen that the three spectrums are within experimental repeatability.

Figure 5.9 shows the AS means spectra for DE and NDE bearing under different speeds and radial loads. As with the vibration signal the mean value initially increases with speed, but unlike the vibration signal the mean value for the airborne sound drops at after 75% of the maximum speed. The figure shows that the variability in measurement with change in radial load means that it is not possible to distinguish significant differences between test runs for different loadings.

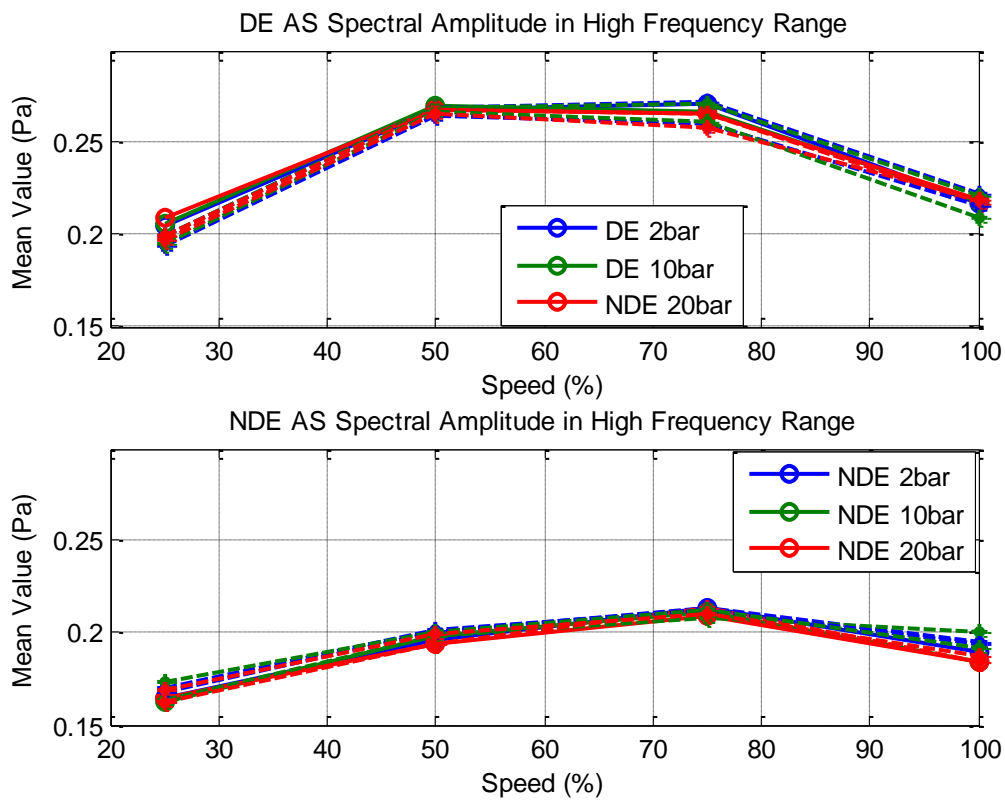


Figure 5. 9 AS mean spectra for DE and NDE bearing under different speeds and radial load.

5.2.3 Acoustic emission

Figure 5.10 shows the amplitude of the time domain signals of the acoustic emission (AE) of the self-aligning spherical journal bearings when operated at 100% speed with three radial loads; 2 bar, 10 bar and 20 bar using lubricant of ISO VG 32. Three tests runs were performed.

Figure 5.10 also indicates that the AE signal is a mix of burst and continuous types and that signal amplitude increased with increasing radial load. It means that more and larger AE events are generated at high radial load.

The three AE signals in the three tests show no significant difference. Based on the figure it was concluded that the AE signal repeatability was good.

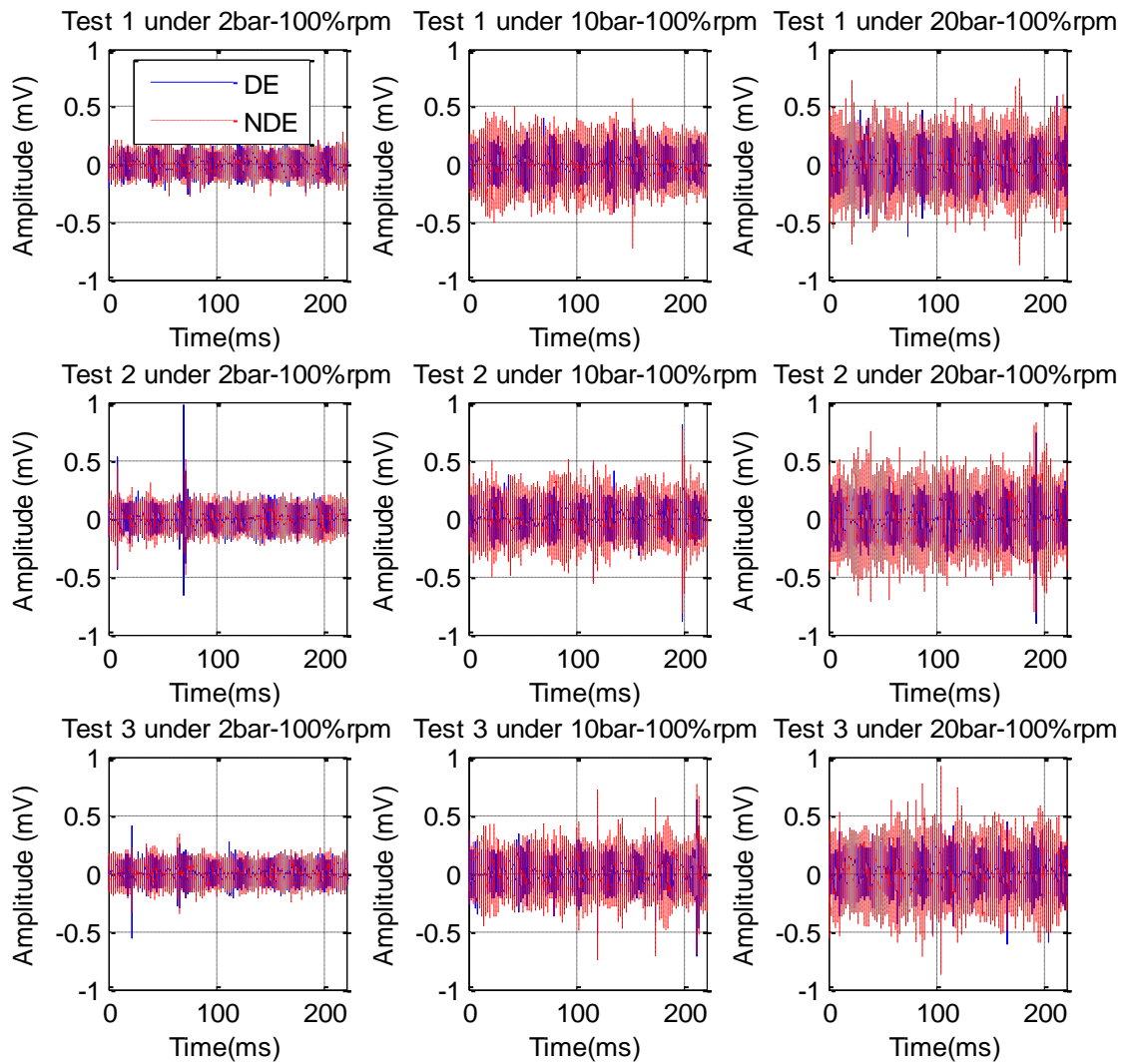


Figure 5. 10 AE time domain signal for DE and NDE bearing under three loads at maximum speed for three test runs

Figure 5.11 shows the time domain AE RMS value for three test runs of the DE and NDE bearings for three radial loads at four speeds.

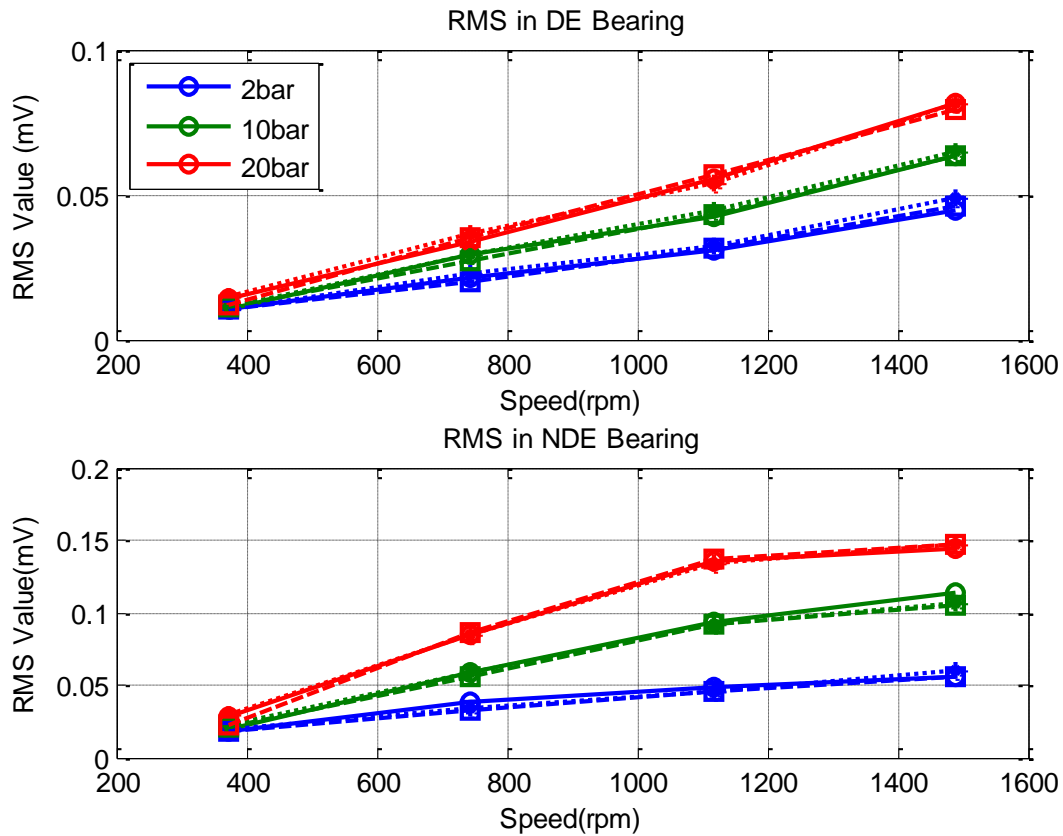


Figure 5. 11 AE RMS values for DE and NDE bearings in three loads at four speeds for three test runs

Figure 5.11 clearly shows that increase in load gives a significant increase in time domain AE RMS amplitude and that as the speed increases the AE RMS amplitude also increases. It can be seen that the results for each load and speed are not significantly different and this is taken to mean the repeatability of AE RMS amplitude tests is very good. It can also be seen that the results at each speed and load (except possibly at the lowest speed) are substantially different from each other.

Figure 5.12 shows the frequency domain of AE signal of a journal bearing under three radial loads 2 bar, 10 bar and 20 bar at 100% speed for three test runs at frequency range of 1-100kHz.

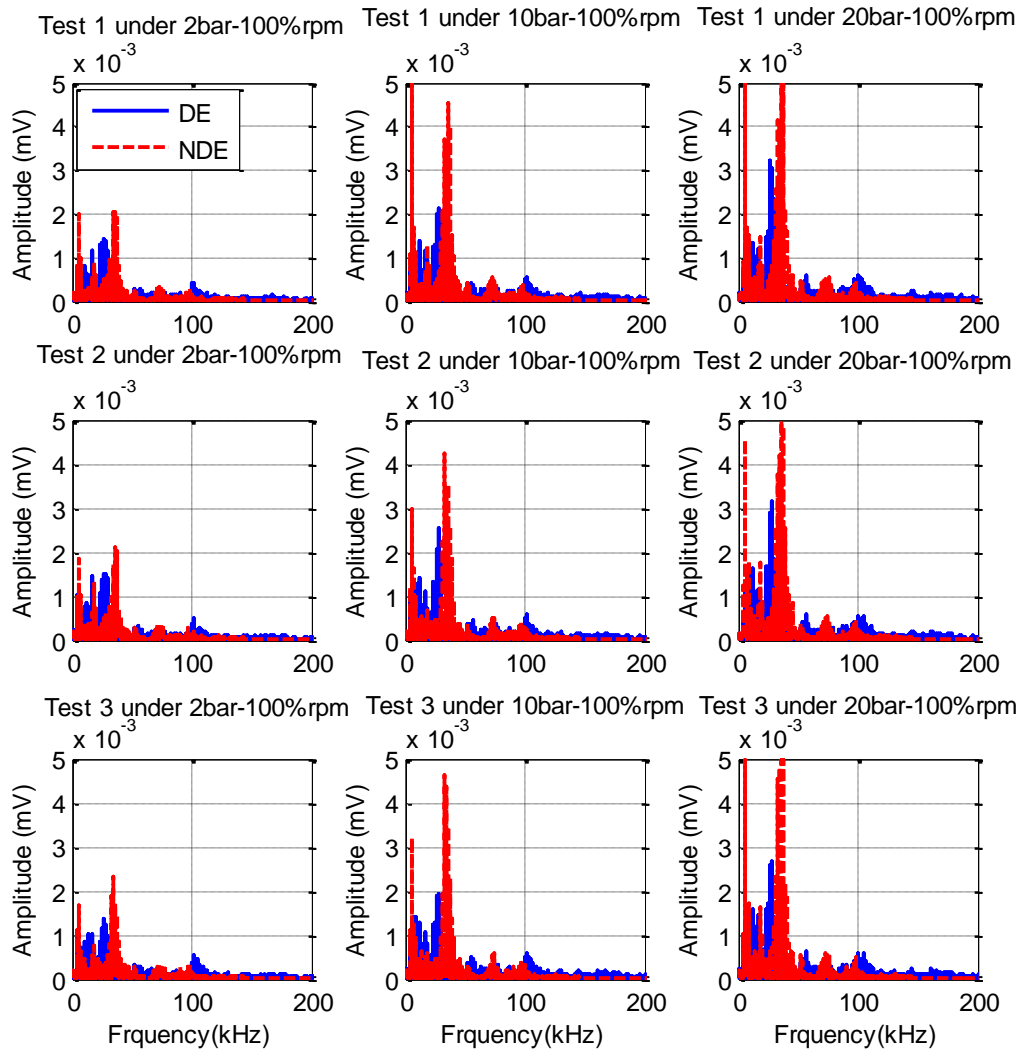


Figure 5. 12 AE spectra for DE and NDE bearings under three loads at 100% speeds for three test runs

Figure 5.12 shows that AE peaks occur at about 5.2 kHz and 36.6 kHz, with a high amplitude range between 2.5 kHz and 42 kHz. The figure shows that when the radial load increases the peak value also increases. The comparison of AE spectra in the three test runs shows no substantial difference in either pattern or amplitude. This is taken to mean the repeatability of the AE experiment is satisfactory.

Figure 5.13 is the mean value of the AE spectrum for three radial loads on the bearing for four speeds and three test runs.

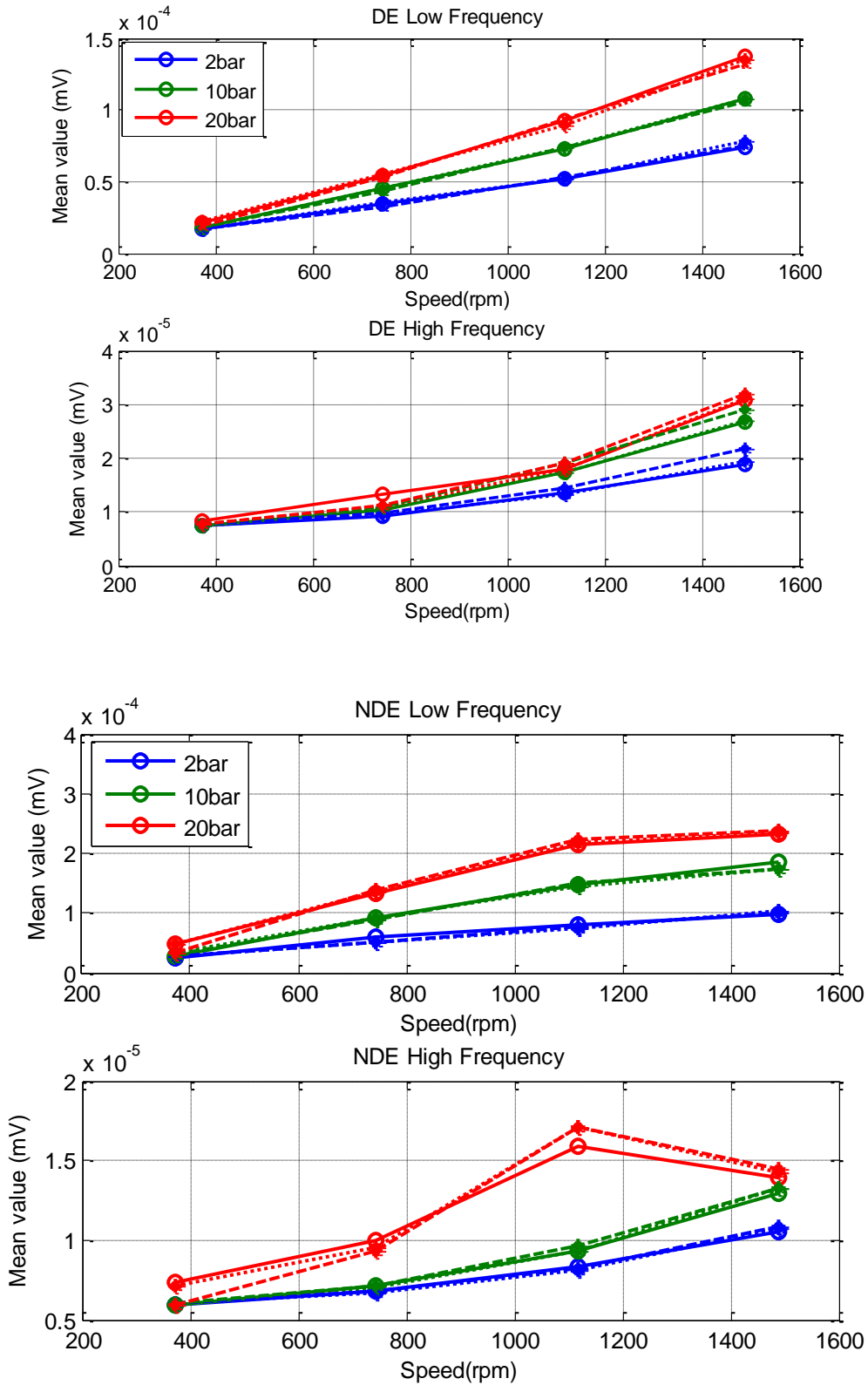


Figure 5. 13 AE mean value for DE and NDE bearings in three loads at four speeds for three test runs

Figure 5.13 shows that AE mean response for the NDE journal bearing for two frequency ranges; low frequency (20 kHz-90 kHz) and high frequency (90 kHz-320 kHz) has good repeatability but with some small variation at maximum load for the high frequency measurement probably due to small variation in load due lack of sensor sensitivity. The frequency ranges were selected based on the spectrum pattern shown in Figure 5.12 which shows high amplitudes in the frequency range 20 kHz-90 kHz, but greater than 90 kHz the AE amplitude is lower than amplitude at less than 90 kHz.

From Figures 5.2 to 5.13 for SV, AS and AE responses in both time and frequency domains it is concluded that overall repeatability is quite acceptable, although not 100%. It is suggested that the imperfection in repeatability is due mainly to radial load leakage in the hydraulic system because of the lack of sensitivity of the pressure transducer and as a secondary effect the difficulty of controlling the temperature of the local environment although the experiment always started at 22.5°C.

The AE response shows the best repeatability, followed by SV and then the AS.

Determination of the surface vibration, airborne sound and acoustic emission responses characteristics is done by averaging of three sets of experiment data.

5.3 Surface vibration characteristics

This section presents the results obtained from the investigation of SV characteristic of a self-aligned spherical journal bearing due to speed and radial load variation using lubricant ISO VG 32.

5.3.1 Time domain analysis

Figure 5.14 shows the time domain of the SV acceleration raw signal of the DE and NDE self-aligning journal bearing for three kind of radial loads at 100% of maximum speeds.

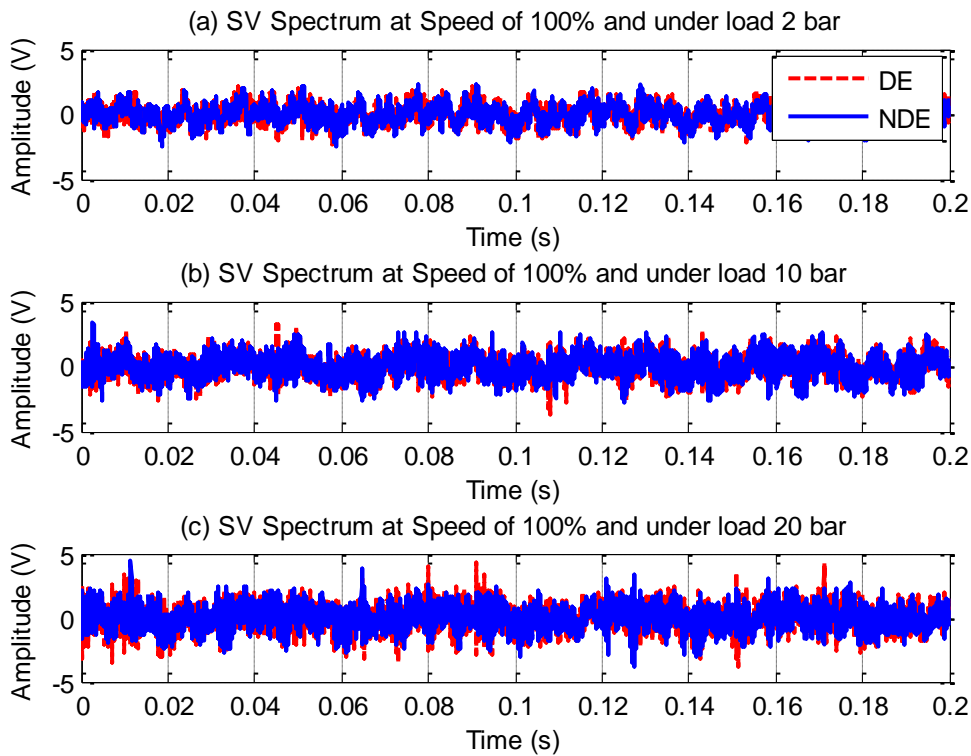


Figure 5. 14 SV signal for DE and NDE bearings for three radial loads at maximum speed

Figure 5.14 shows that the SV amplitude for self-aligning journal bearings at 100% of motor speed increases with radial load. The figure indicates that there is small difference in amplitude between DE and NDE bearings which might be due to their different positions and starting conditions. The influence of radial load and speed on the vibration response can be seen in statistical parameter and spectrum analysis.

Figure 5.15 is the Kurtosis value for the time domain raw signal for DE and NDE bearings for different speeds and radial loads.

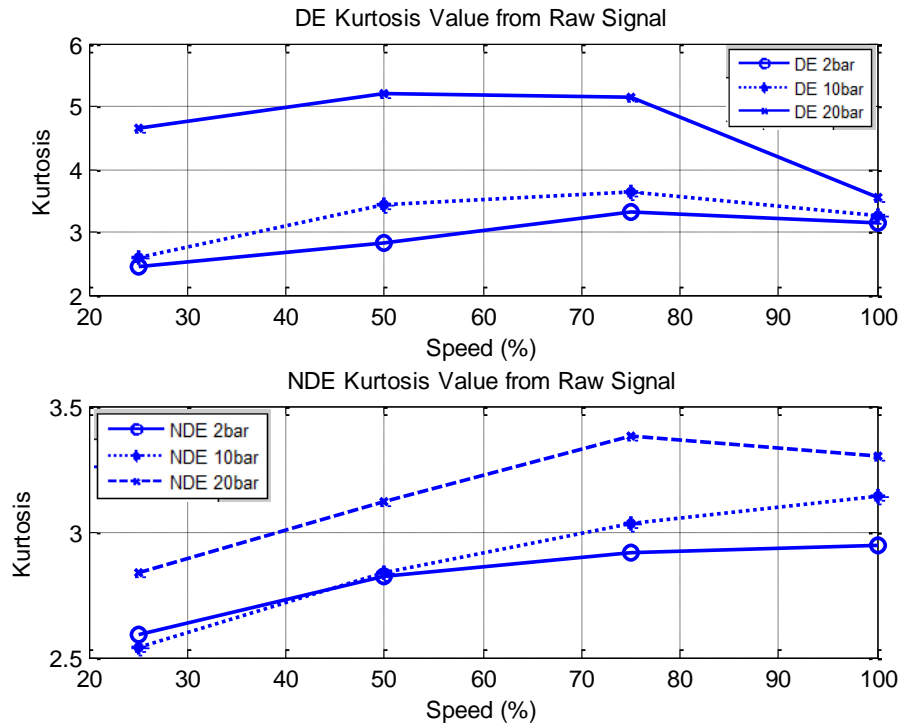


Figure 5. 15 Kurtosis values of raw SV time domain signal for both DE and NDE bearings.

Figure 5.15 shows that the Kurtosis value is affected by the speed, increasing with speed at low speeds but levelling off or falling as the speed approaches its maximum value. The figure shows that for the DE bearing Kurtosis increased with load, but this was not the case for the NDE bearing. Radial load does not appear to influence the Kurtosis value in a consistent manner.

The Kurtosis value lies between 2.0 and 3.4 for the NDE bearing which indicates that the sampled amplitude distribution was close to Gaussian, but for the DE bearing the range was between 2.5 and 5.1 which indicates that only at the highest speed was the sampled amplitude distribution close normal distribution or closed Gaussian because Kurtosis close to 3.

Figure 5.16 is the SV RMS value of the time domain of the raw signal for DE and NDE bearings under three different radial load and four speeds

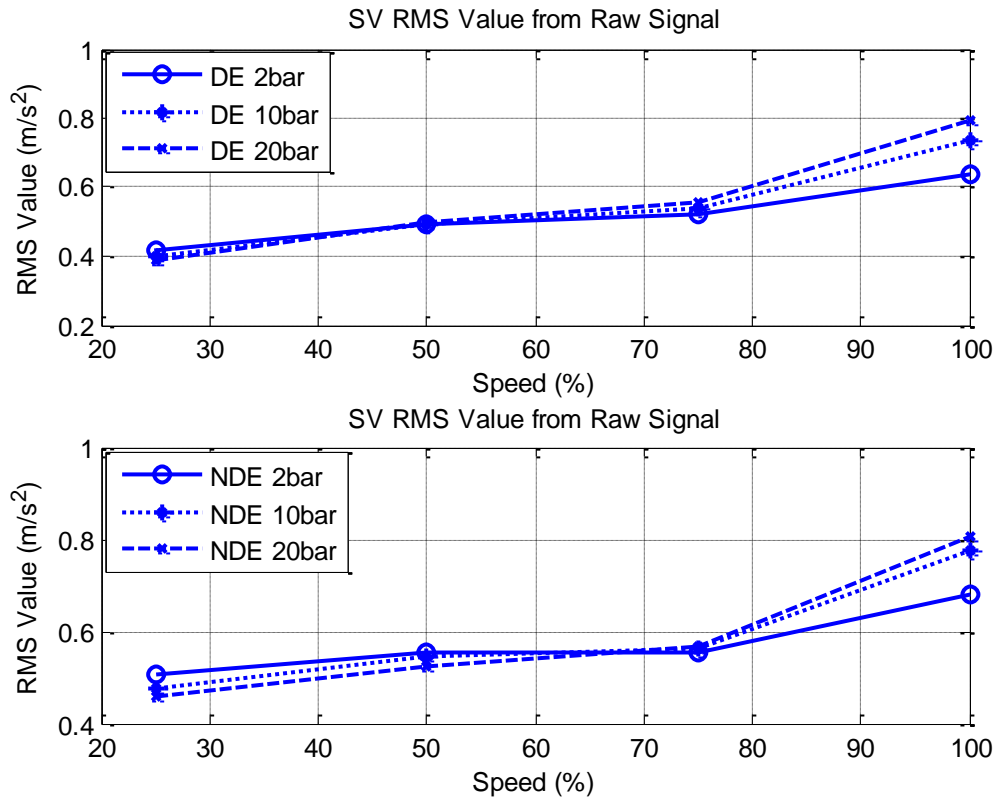


Figure 5. 16 SV RMS value for time domain signal for both DE and NDE bearings for three radial loads and four speeds

Generally Figure 5.16 shows a small positive correlation between speed and SV RMS value for the raw signal time domain, but at maximum speed the RMS value increases significantly. Only at maximum speed does there appear to be a significant differences in SV RMS values with radial load. For identifying the effect of radial load against SV RMS value it is necessary to use the SV spectrum or SV spectrum analysis for getting an accurate analysis.

5.3.2 Frequency domain analysis

SV spectra for the DE and NDE journal bearing for three radial loads at 25% of the maximum speed are shown in Figure 5.17 and at maximum speed in Figure 5.18.

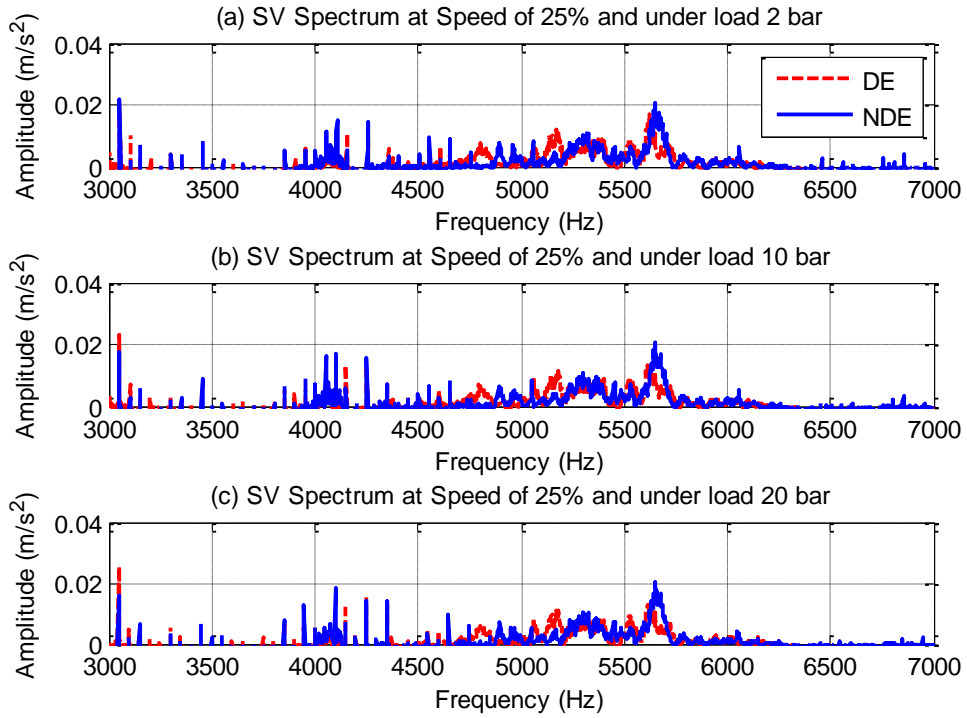


Figure 5. 17 SV spectra for DE and NDE bearings under three radial loads at 25% maximum speed

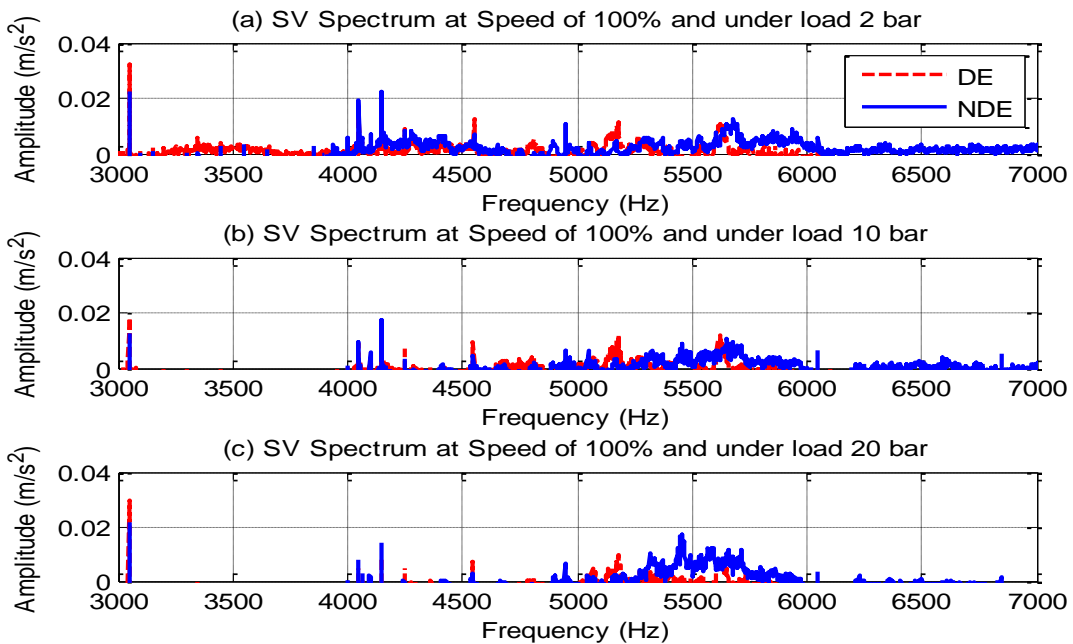


Figure 5. 18 SV spectra for DE and NDE bearings under three radial loads at maximum speed

Figure 5.18 show that there are small differences in SV responses at the DE and NDE bearings. This is due to differences in the initial conditions and respective loads of the two bearings. High amplitudes can be seen in the frequency spectrum for both bearings in the range 3 kHz to 6 kHz. It can be seen that when the bearings operate at low speed (25%) and low load (2 bar), Figure 5.17, the bearings generated similar amplitude vibration to those obtained when the bearings operated at low speed with medium radial load of 10 bar.

Figure 5.19 shows the mean value of SV spectrum for the frequency range between 4 kHz and 7 kHz, for DE and NDE for three radial loads and four speeds. As can be seen as the speed increases the vibration amplitude also increased. There are substantial differences in SV bearing responses in DE and NDE bearings under different radial loads; 2 bar, 10 bar and 20 bar

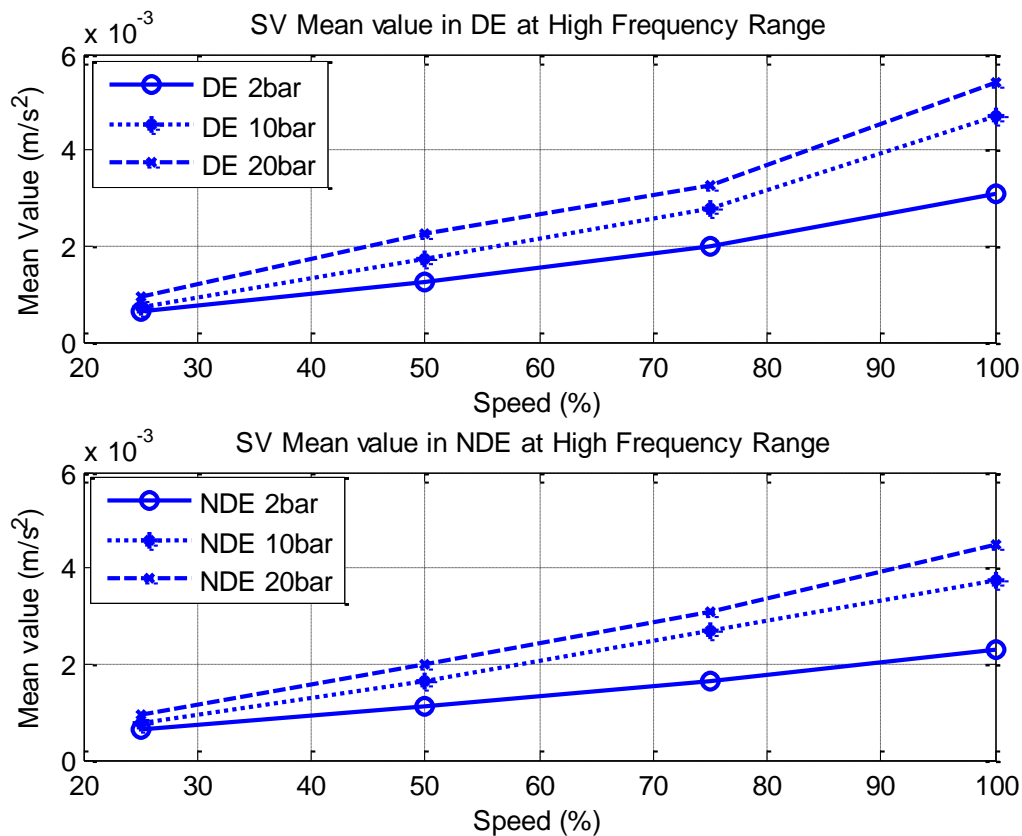


Figure 5. 19 SV mean value of spectrum (high frequency range 4 kHz to 7 kHz) for DE and NDE bearings under three radial loads at four speeds

According to existing surface vibration theory the SV RMS value, the amplitude of vibration is a function of the speed of shaft according to a quadratic equation relationship, while the effect of radial load on the vibration acceleration amplitude corresponding to a linear equation.

5.4 Airborne sound characteristics

The experiment for determining the effect of speed and radial load on airborne sound (AS) characteristics of the DE and NDE self-aligning journal bearings were performed in parallel with SV measurements. Thus the radial loadings were 2 bar, 10 bar and 20 bar and the speeds were 25%, 50%, 75% and 100% of the maximum. Lubricant ISO VG 32 was used in both DE and NDE bearings.

5.4.1 Time domain analysis

The AS time domain raw signals for DE and NDE bearings for maximum speed and three radial loads are shown in Figure 5.20 which shows that the AS amplitude for both bearings show no significant difference due to radial load.

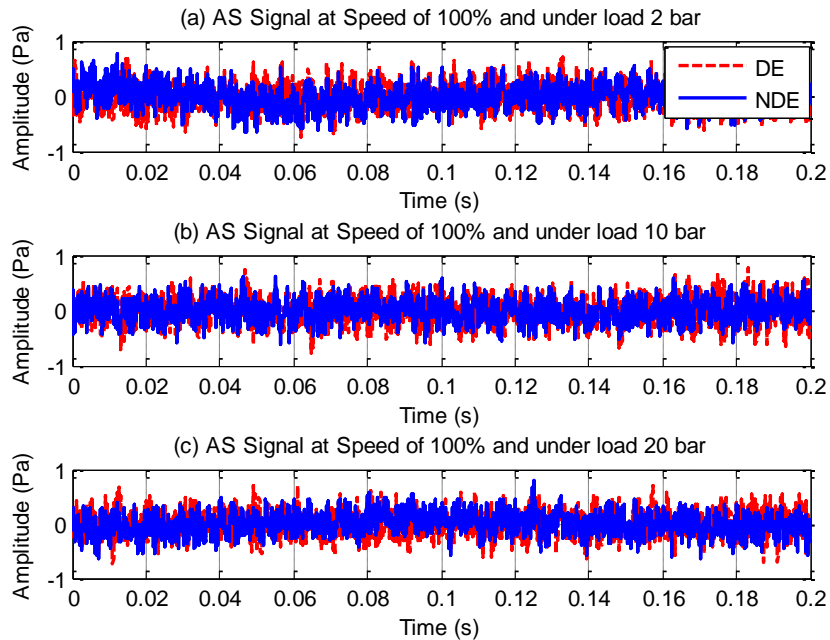


Figure 5. 20 AS signals for DE and NDE bearings for maximum speed and three radial loads

Figure 5.21 shows the effect of speed and radial load on the RMS of the raw time domain AS signal. It can be seen that initially as the speed increases the RMS amplitude of the AS slowly increases but at maximum speed, the AS amplitude increases relatively sharply. When the radial load on the bearing increased from 2 bar to 10 bar no significant change in the AS RMS levels were observed. But when increasing the load from 10 bar to 20 bar a substantial decrease in RMS level was noted. This phenomenon is due to improving lubrication film.

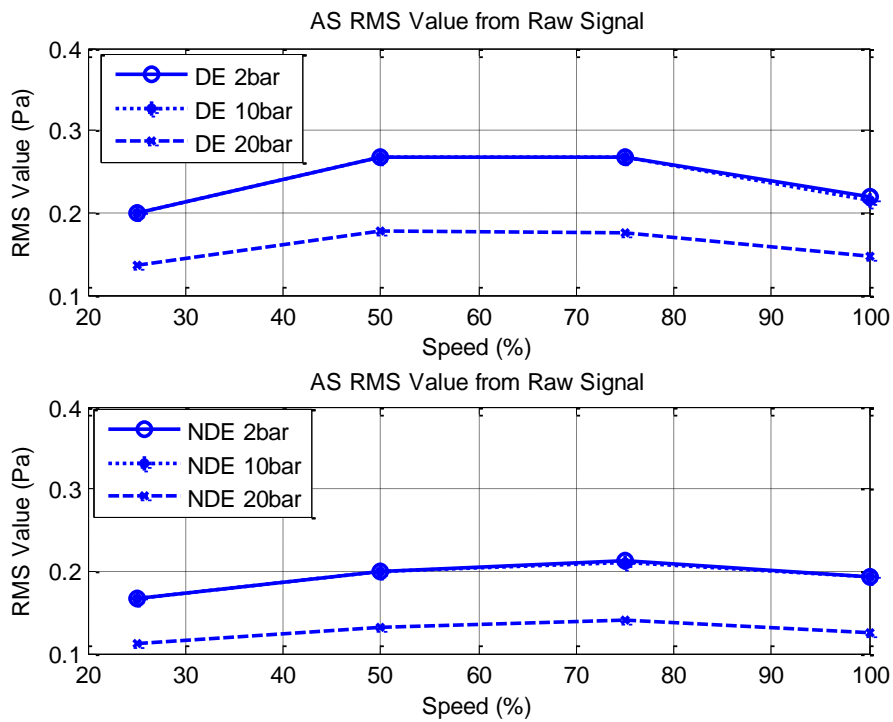


Figure 5. 21 AS RMS value of raw signal for DE and NDE bearing for four speeds and three radial loads

Figure 5.22 shows the Kurtosis for the AS time domain raw signal for three radial loads and four speeds.

Figure 5.22 shows that, overall, when speed increased the Kurtosis for the DE bearing tended to increase. No precise or clear trends were observed for the Kurtosis for the NDE bearing. The effect of increasing the radial load was unclear and depended upon the speed of the bearing for both bearings. The figure shows that Kurtosis value for both the DE and NDE bearings varied between about 2.95 and 3.05 indicating a Gaussian distribution.

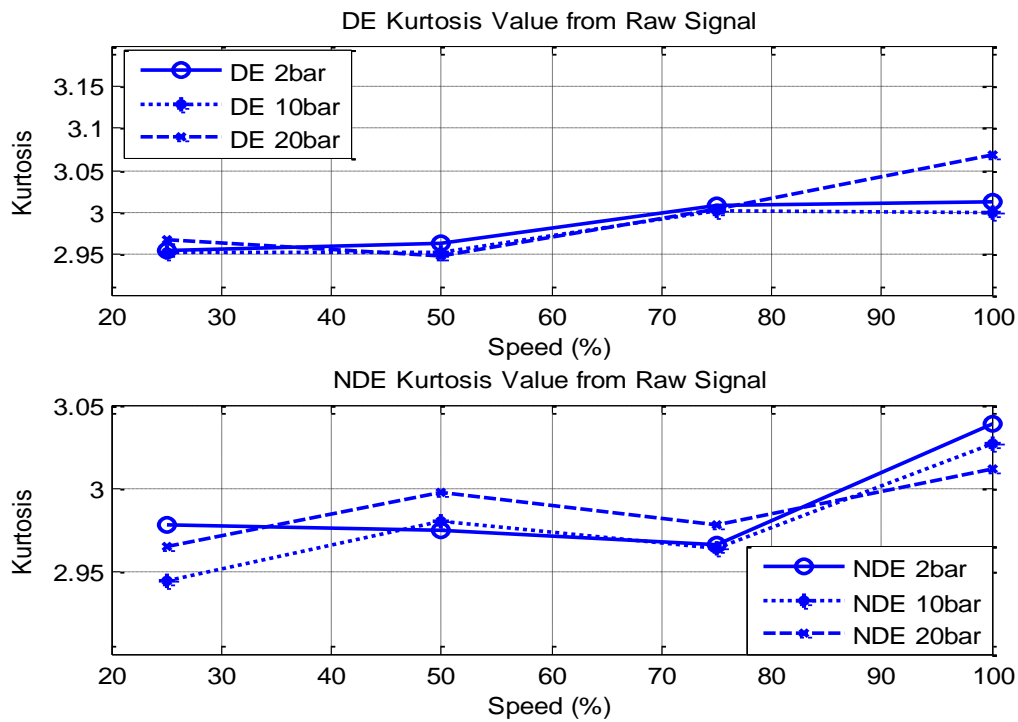


Figure 5. 22 Kurtosis value of AS time domain raw signal in DE and NDE bearings for three radial loads and four speeds

5.4.2 Frequency domain analysis

The spectrum of the AS for the DE and NDE bearings for three radial loads at low speed (25% of maximum speed) is shown in Figure 5.23 which indicates that radial load does not significantly affects the AS amplitude response. The AS large peak amplitudes occur at high frequency range 4.75 kHz up to 6.5 kHz and highest amplitude state at frequency 5.4 kHz

Clearly there is a difference in the AS signal between the DE and NDE bearings. This is due to differences in bearing condition and radial load on the bearing.

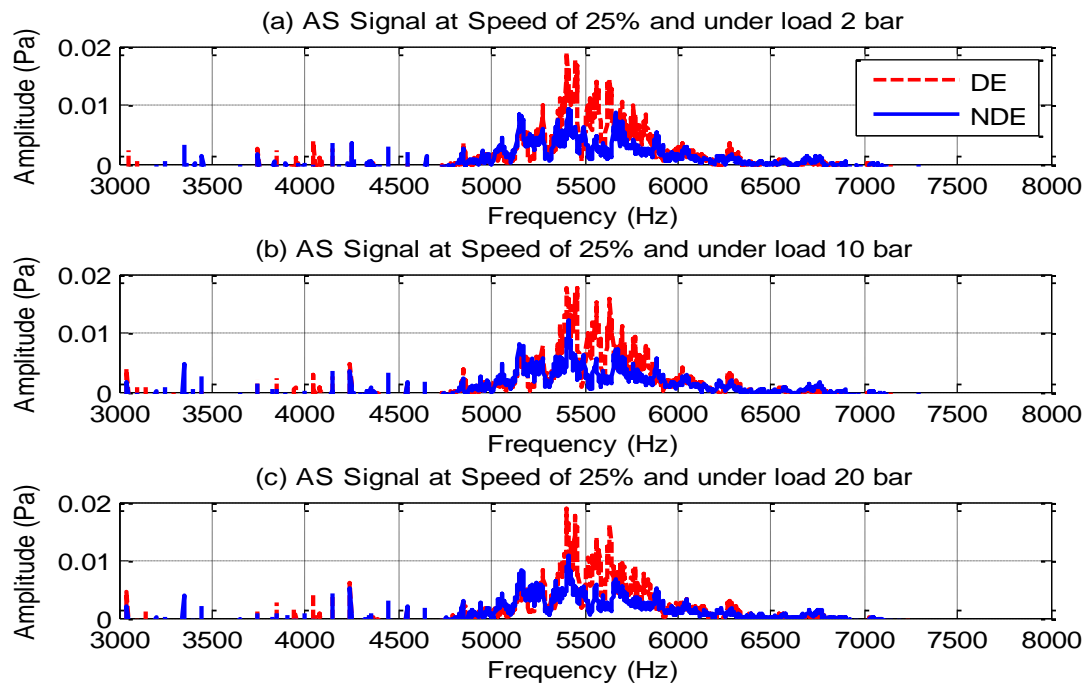


Figure 5. 23 AS spectra for DE and NDE bearings under three radial loads at speed 25% maximum

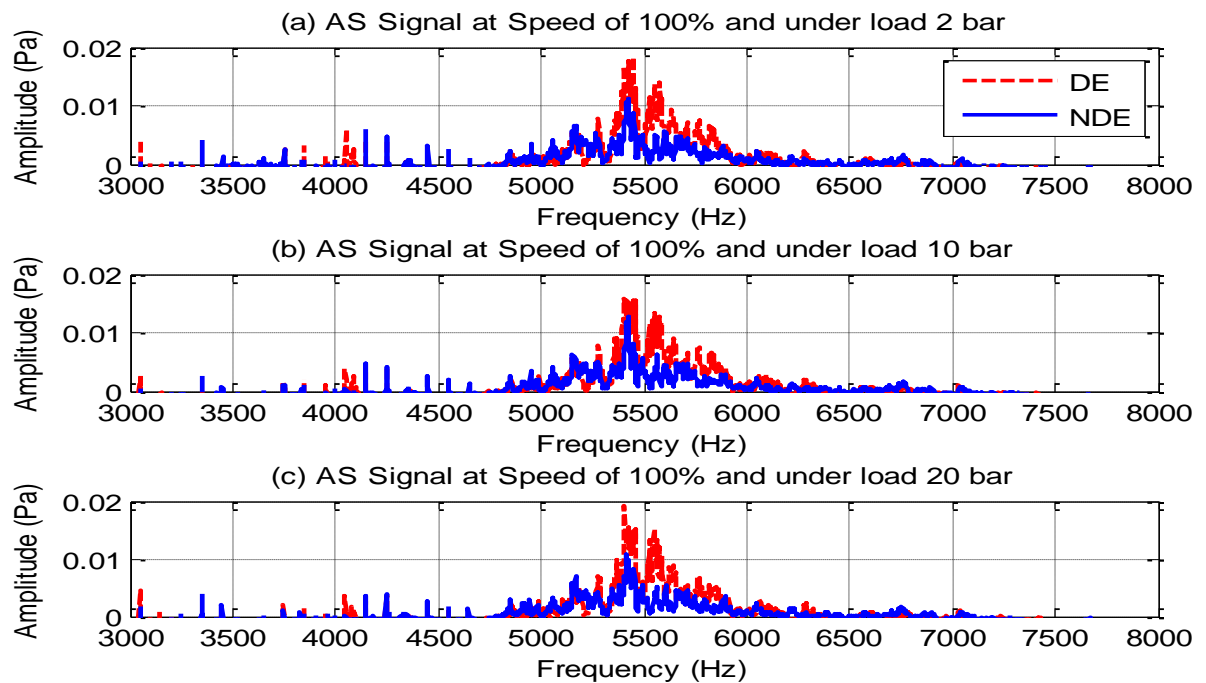


Figure 5. 24 AS spectra for the DE and NDE bearings at maximum speed and three radial loads

Figure 5.24 is the AS signal spectra from the DE and NDE bearings at maximum speed and three radial loads. The figure shows that the radial load does not affect to the AS spectrum amplitude significantly.

Confirmation can be seen on the RMS AS spectrum amplitude for speed variation as shown in Figure 5.25.

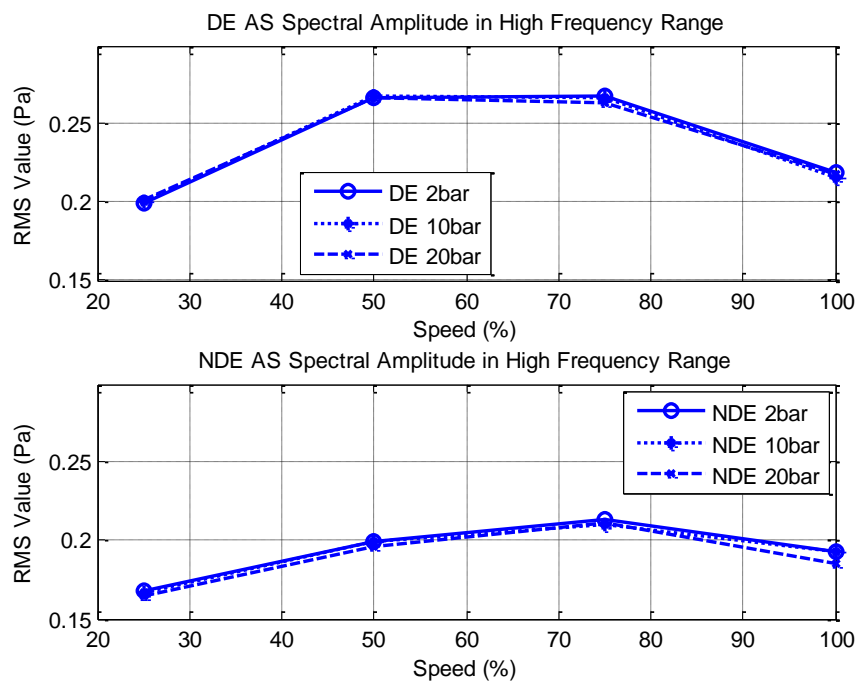


Figure 5. 25 AS mean value of spectrum (7 kHz to 18 kHz) for DE and NDE bearings for three radial loads and four speeds

Figure 5.25 shows the effect of speed on the AS RMS for the high frequency (7 kHz to 18 kHz) spectrum response for both DE and NDE bearings for three radial loads and four speeds. Both the figures show the same general “concave” shape, an initial increase in AS RMS amplitude followed by a decrease when the speed reached maximum. The figure also indicates that the effect of radial load on the AS RMS amplitude was not significant.

5.5 Acoustic emission characteristics

This section describes the results obtained using AE to detect the effects of radial load and rotation speed on the two bearings installed on DE and NDE sides of the hydraulic ram. The AE sensor was mounted on bearing housing in the horizontal direction.

The initial set of experiments was to test the effects of three radial loads and four drive speeds. The viscosity grade of the lubricant was ISO VG 32. As with the surface vibration and airborne sound analysis, the determination of AE characteristics used both time and frequency domain analysis and AE mean analysis.

5.5.1 Time domain analysis

The raw AE time domain waveforms for DE and NDE bearings are shown in Figure 5.26 and 5.27 for three radial loads; 2 bar, 10 bar and 20 bar with 50% and 100% of maximum speed respectively.

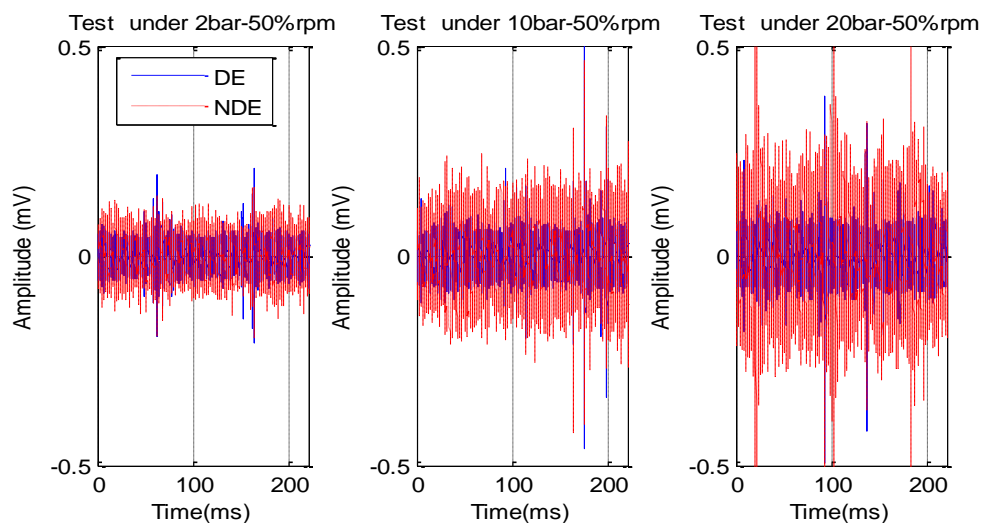


Figure 5. 26 AE signal for DE and NDE bearing for three radial loads at 50% maximum speed

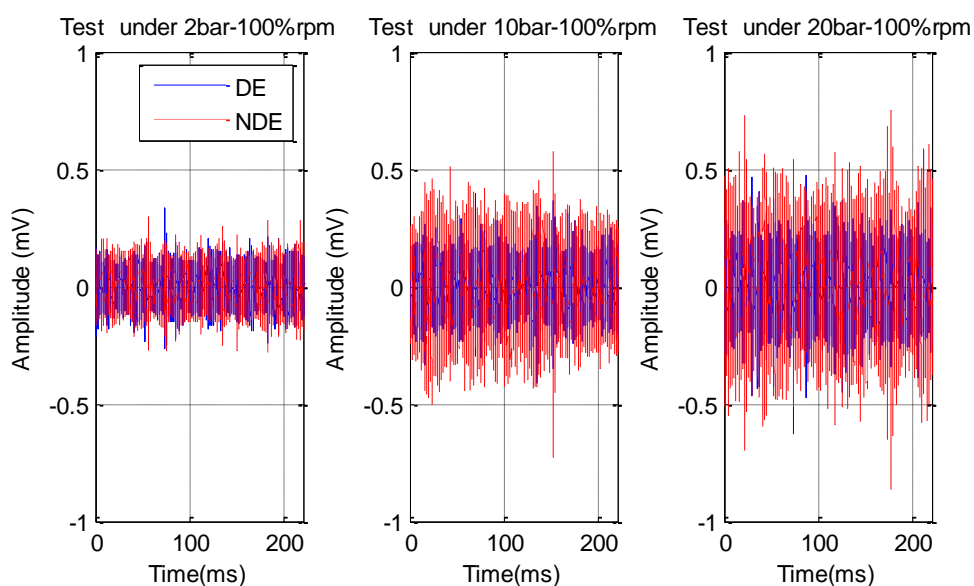


Figure 5. 27 AE signal for DE and NDE bearing for three radial loads at maximum speed

Figures 5.26 and 5.27 indicate that the AE response is a mix of burst and continuous signals, and that the amplitude increases with increasing radial load; more and larger AE events are generated at higher speeds. The AE signals for the two bearings (DE and NDE) are different due to different initial conditions and different installed positions.

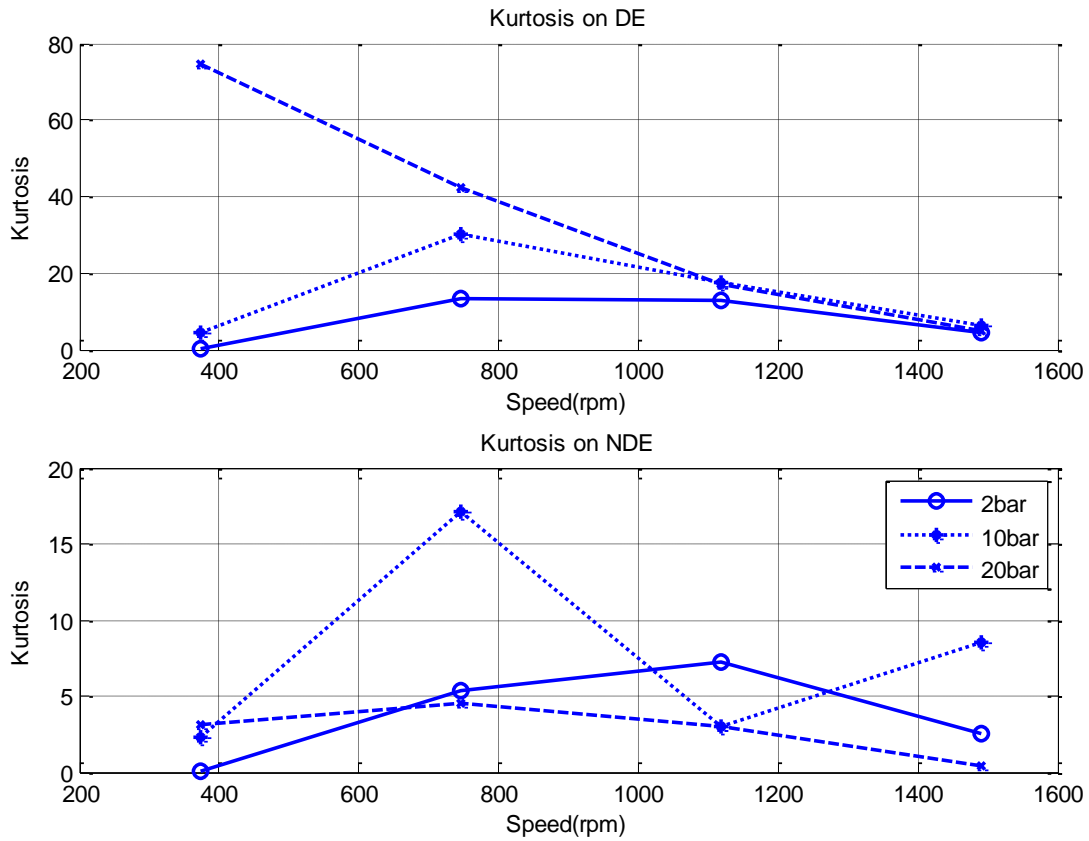


Figure 5. 28 Kurtosis values of raw AE signal for both DE and NDE bearings for three radial loads and four speeds

Figure 5.28 shows the Kurtosis value obtained from the raw AE time domain signal for both bearings for three load and four speeds. The figure shows that the Kurtosis for the DE bearing generally exhibits values > 3 , thus the distribution of data of AE signal is non-Gaussian. However, for the NDE bearing 7 of the 12 measurements are < 3 , suggesting that the distribution of data is close to the Gaussian distribution.

The high values of Kurtosis can be explained by the fact that AE signals, even when described as continuous, are a series of impulses which means the Kurtosis – which is a measure of the peakedness of the signal – will return a high value.

The trends in Kurtosis with load for the DE and NDE bearings are difficult to be drawn a general conclusion.

The Figure 5.29 shows the RMS mean value of the AE signal response for the DE and NDE bearing for four different speeds and three radial loads.

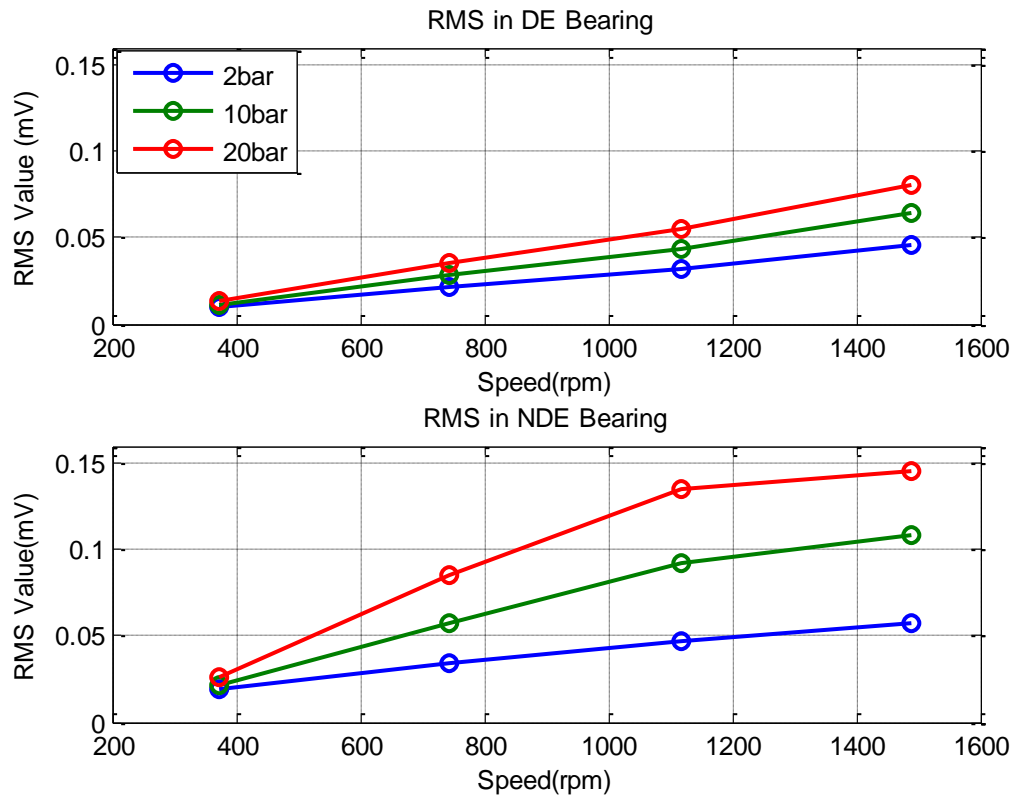


Figure 5. 29 AE RMS value from raw signal for DE and NDE bearings for four different speeds and three radial loads

Figure 5.29 shows a positive correlation between speed and the AE RMS response for the raw signal. The figure also shows significant increase in AE amplitude with increase in radial load.

5.5.2 Frequency domain analysis

Figures 5.30 and 5.31 are the AE spectra for DE and NDE bearing for three radial loads at 100% of maximum speed respectively in different range of frequency.

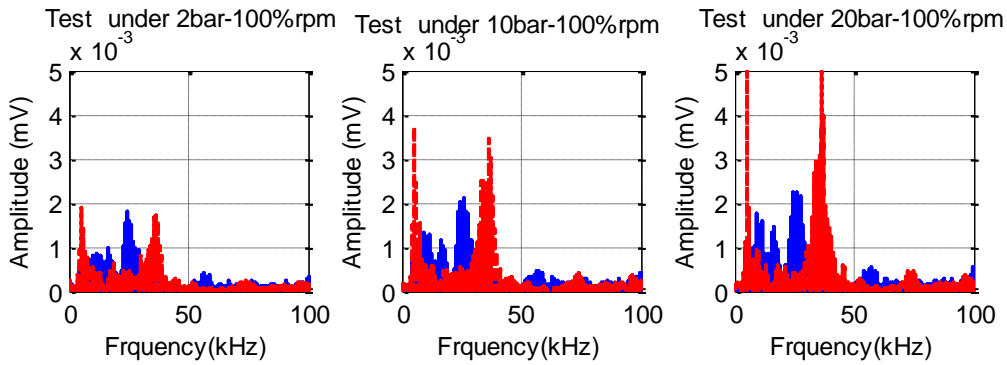


Figure 5. 30 AE spectra for DE and NDE bearing for radial load 20 bar at 100% maximum speed at frequency range 1-100kHz

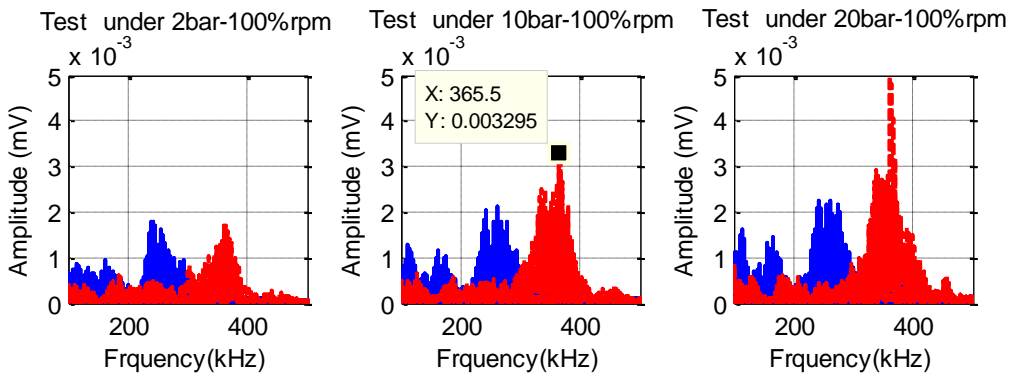


Figure 5. 31 AE spectra for DE and NDE bearing for radial load 20 bar at maximum speed at frequency range 100-500kHz

Figures 5.30 and 5.31 show that increasing in radial load generates higher AE signal amplitude. The figures also show that for both DE and NDE bearings as speed increased so did the amplitude of the peaks in the spectrum. The figures indicate that high amplitude peaks are present at frequency of 365.5 kHz.

Figure 5.32 shows the mean value of the AE spectrum in the DE bearing at low frequency range 20 kHz to 90 kHz and at high frequency range 90 kHz up to 320 kHz. The mean value in the NDE bearing at low and high frequency range for three radial loads and four speeds is shown in figure 5.33.

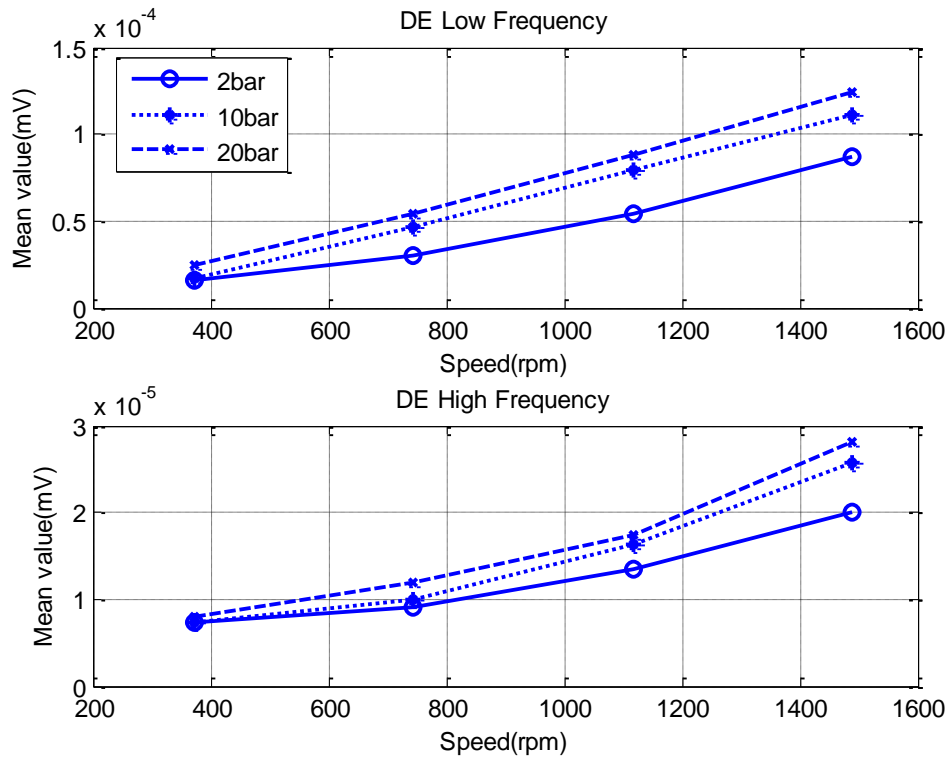


Figure 5. 32 AE mean amplitude for low (20 kHz to 90 kHz) and high frequency (90 kHz to 320 kHz) ranges for the DE bearing for three loads and four speeds

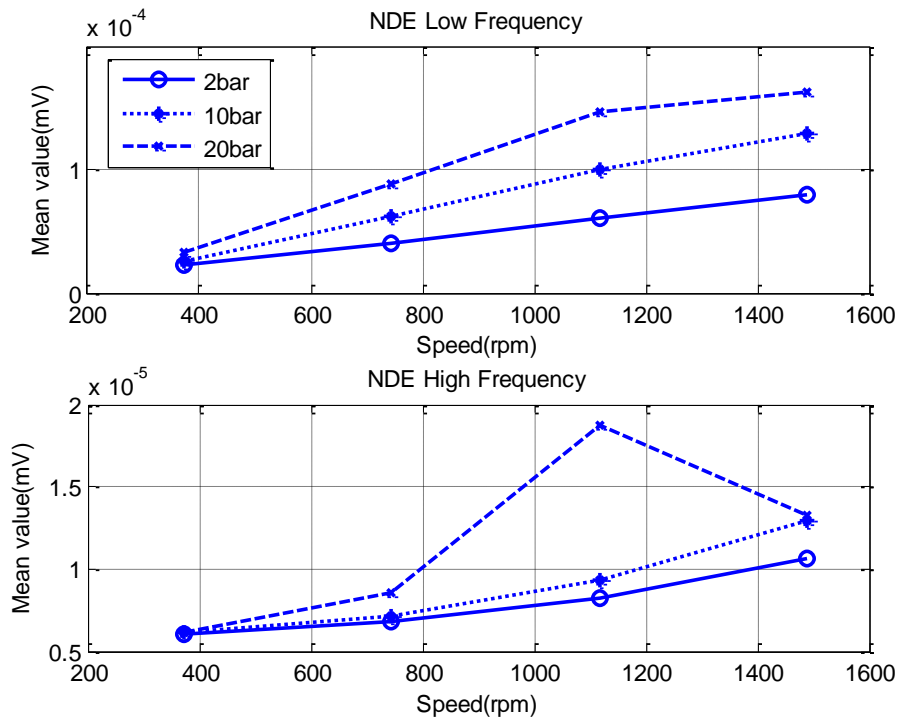


Figure 5. 33 AE mean amplitude for low (20 kHz to 90 kHz) and high frequency (90 kHz to 320 kHz) ranges for the DE bearing for three loads and four speeds

Both figure show that for both bearings the mean value of the AE spectrum increased as speed increased. When radial load is increased, the AE mean amplitude also increased.

As mentioned in Chapter 3 the magnitude AE energy generated in the journal bearing is affected by the radial load and speed. The released AE energy increases with radial load and is linearly influenced by the speed.

Based on the relationship between speed, radial load and amplitude; the SV, AS and AE signals show that the magnitude of the RMS value for each of the three type of signals increased with increase in radial load and speed.

5.6 Discussion of load and speed characteristics

Repeatability, signal characteristics of surface vibration, airborne sound and acoustic emission responses in a self-aligning spherical journal bearing under different speed and load are as follows:

5.6.1 Repeatability

As described in Chapter 4 the test rig used for this study is a new test rig, so it was necessary to analyze the repeatability of the response to establish a correct result every time an experiment is run.

To determining the repeatability of surface vibration, airborne sound and acoustic emission testing responses, it is necessary to run the measurement system 3 to 4 times for each specific data collection. The acquired data is then further processed using MatlabTM software for analysis. Analyses used include time domain analysis such as the RMS value of the raw signals, and in the frequency domain the mean value of the spectrum over a given bandwidth.

The repeatability of the surface vibration signal indicates that there is no significant difference between the first, second and third tests from the analyses in the time and frequency domains. The repeatability for airborne sound and acoustic emission signals were similar.

The repeatability of the RMS value of the raw signal of the surface and airborne sound for the three kinds of experiments cannot be identified because the each graphic coincidence and they are plotted close to each other.

The spectra for the three measurements showed no significant difference.

The mean values for the spectral analysis of the surface vibration and acoustic emission indicate that the repeatability of the responses for light, medium and heavy loads are very good. However, the mean value of the response for the spectral airborne sound cannot be identified.

From the three measured parameters it is shown that acoustic emission responses have the best repeatability rate followed by a surface vibration and airborne sound respectively.

5.6.2 Radial load characteristics

In the time domain analysis, the responses of the surface vibration and airborne sound indicate that the radial load has no significant impact on the amplitude of the responses. But the effect of radial load on the acoustic emission signal's amplitude is significant and noticeable.

The analysis of the RMS value of the raw signal of surface vibration and airborne sound indicates that the effect of radial load on both signals is difficult to be distinguished. However, the analysis of the RMS values of the acoustic emission signal shows very clearly that there is a positive relationship. When the radial load increases the AE RMS value from raw signal also increases.

The effect of radial load against Kurtosis values for the surface vibration and airborne sound does not show a significant difference when the load is varied although the Kurtosis value is approaching 3 and close to the Gaussian data distribution pattern. The effect of radial load on AE Kurtosis value also cannot be distinguished. The Kurtosis value on the acoustic emission signal response is very high due to the essentially burst types of signal.

The effect of radial load on the AE spectrum responses is very obvious and significant, but on the surface vibration and airborne sound spectrum the influence of the radial load on the amplitude and spectrum pattern is not significant.

The spectrum mean value for the high frequency bands for surface vibration and acoustic emission show a highly significant response to radial load, but the airborne sound response cannot be identified. The measurements indicate that the acoustic emission once again has the best sensitivity responses followed by the surface vibration and airborne sound.

5.6.3 Speed characteristics

The effect of speed variations on the surface vibration, airborne sound and acoustic emission responses can be analysed using the RMS value, Kurtosis and spectrum mean value. There is a positive correlation between the speed and the RMS value of the surface vibration, airborne sound and acoustic emission responses. When the speed is increased the RMS value of the raw signal for vibration and acoustic emission surface also increases.

The effect of speed on the kurtosis value for the surface vibration, airborne sound and acoustic emission responses could not be identified.

The spectrum mean value analysis shows that there is a positive correlation between the speed and the mean amplitude of the spectrum of the surface vibration and acoustic emission responses. When the speed is increased the spectrum of the mean values of the surface vibration and acoustic emission responses also increases.

The mean value of the airborne sound spectrum initially showed a positive correlation with speed, but after reaching a speed of 75%, the maximum the mean spectrum amplitude decreased. This could be due to the improved lubrication system on the journal bearing.

The third parameter measurement again showed that the acoustic emission response has the best response followed by the surface vibration.

The best parameter that shows the influence of radial load and speed on the surface vibration, airborne sound and acoustic emission spectrum responses is the mean spectrum value for the high frequency range.

5.6.4 Frequency characteristics

Surface vibration, airborne sound and acoustic emission have different frequency responses.

Spectrum analysis on the surface vibration (see Figures 5.4, 5.17 and 5.18) showed that high amplitude responses are dominant at frequencies between 3 kHz and 6 kHz. Peaks with the largest amplitudes are located at frequencies around 3.1 kHz, 4.1 kHz and 5.7 kHz.

The spectra of the airborne sound response (see Figures 5.8, 5.23 and 5.24) show that high amplitudes dominate in the frequency band between 4.8 kHz and 6.1 kHz with the largest amplitude peak located at 5.4 kHz.

The spectra of the acoustic emission response (see Figures 5.12, 5.30 and 5.31) show that maximum amplitudes appear in the ranges from 3 kHz up to 12 kHz, and 12 kHz up to 50 kHz. The peak amplitudes occur at frequencies 5.6 kHz and 36 kHz.

Surface vibration, airborne sound and acoustic emission in a journal bearing caused by asperity contact occur in the higher frequency spectra and with random temporal distribution. Journal bearing surface imperfections can be expressed by its roughness level between bearing contact surfaces.

The AE Kurtosis of the journal bearings shows high values. This means that the signal data pattern is of a non-Gaussian distribution. The AE signals of journal bearings are formed from the combination of continuous and burst type responses originating from the surface asperities – the making and breaking of welds. The impulse signal or hit occurs due to the level of imperfections or early fault on the contact surfaces of the shaft and journal bearing also the journal bearing side surface with the stopper surface. Amani also founded that the Kurtosis value for the AE signal in gear transmission is greater than 10 in the early stages of wearing and in the final stages the Kurtosis value increases to over 100 (Amani, 2004).

The other SV, AS and AE characteristics of a journal bearing are also influenced by the quality or viscosity of the lubricant, this investigation will be presented in Chapter 6.

5.7 Summary of load and speed characteristics

Based on the result investigation and discussion of the self-aligning spherical journal with radial load and speed variation it can be summarized as follows:

5.7.1 Repeatability experimental results

It is indicated that overall repeatability of the measurements is acceptable, although not 100% match both for surface vibration and acoustic emission responses. It is suggested that the imperfection in repeatability is due mainly to radial load leakage in the hydraulic system and lack of sensitivity of the pressure transducer. The AE response shows the best repeatability, followed by surface vibration and then the airborne sound measurement.

5.7.2 Surface vibration, airborne sound and acoustic emission characteristics

Surface vibration, airborne sound and acoustic emission characteristics of a self-aligning spherical journal bearing vary with radial load and speed as follows.

The effect of speed and radial load on surface vibration:

- There is a positive correlation between the speed and the RMS value of the raw signal.
- The influence of the radial load on the RMS value from the raw signal cannot be detected.
- SV Kurtosis value due to speed variations shows a distribution that was close to Gaussian, but is not consistent regarding the different radial load variation.
- High amplitude dominates at frequencies from 3 kHz up to 6 kHz.
- High amplitude peaks occur at frequencies of 3.05 kHz, 4.05 kHz and 5.6 kHz.
- The effects of speed and radial load variation on the spectrum mean value are clear and significant.

The effect of speed and radial load variation on airborne sound response:

- There is a positive correlation between speed and the RMS value of the raw signal.
- The effect of radial load on the RMS value of raw signal was not detected.
- AS Kurtosis value was close to that for a Gaussian distribution, but it did not distinguish between different radial loads.
- High amplitude peaks dominated the AS spectrum from 4.75 kHz to 6.5 kHz, with the highest amplitude peak at 5.4 kHz.
- There was a positive correlation between speed and spectrum mean value but after the speed reached 75% of the maximum, the spectrum mean value slightly decrease. The influence of radial load cannot be identified.

Effect of speed and radial load on acoustic emission:

- There is a positive correlation between speed and radial load on AE RMS value from the raw signal and significant differences between in different load.
- AE Kurtosis had values that were far from Gaussian and were not consistent.

-
- High amplitudes dominated the frequency range between 250 kHz to 425 kHz.
 - The highest amplitude peaks occurred at 365.5 kHz
 - There is a positive correlation between speed and radial load and AE spectrum mean value in both the low and high frequency ranges.

CHAPTER SIX

LUBRICANT QUALITY MONITORING

6.1 Introduction

This chapter describes the result of an investigation into the surface vibration and airborne sound and acoustic emission characteristics of a self-aligning spherical journal bearing as a function of viscosity, an important factor that determines the quality of the lubricant, by using three lubricants meeting specifications ISO VG 32, ISO VG 68 and SAE 90, and contaminating the lubricant by adding known proportions of water.

Lubricating qualities are very important to ensure the longevity of a machine, because early damage or failure may be caused by selecting the wrong lubricant. The qualities of the lubricant influence stiffness, damping coefficient and damping factor of lubricant and they will affect the surface vibration (SV) and airborne sound (AS) response of the bearing. The higher viscosity of lubricant in the journal bearing will generate the SV and AS responses decreasing. When a thinner lubricant is applied greater SV and AS levels will be produced.

The quality of the lubricant will also affect the acoustic emission (AE) response because it will determine asperity contact between surfaces. If the lubricant used on the journal bearing has a higher viscosity, the amount of asperity contact will decrease due to a thicker mean layer of lubricant. Since the amount of energy dissipated in the form of friction is reduced with increase in thickness of the lubricant layer, so the AE energy generated will decrease.

Lubrication systems in engines and machines are similar to the blood circulating system in humans and the condition of the lubricating oil can indicate the health of the machine (Akintunde, 2008). The function of lubrication is to reduce wear and friction, remove contaminants and heat, and to cool the process (Singh, 2002). The condition of the lubricating oil will influence the machine operating system and the working life of engine components especially bearings, both rolling and journal bearings. Lubricant failure, degradation or deterioration can result in the impaired functioning of the bearings.

Lubricant deterioration can be caused by gaseous, fluid or solid contaminants. Solid particle contaminants such as silica and wear particles act as an abrasive which accelerates wear of engine components, decreases efficiency and generates additional heat. As a result the engine consumes extra fuel, develops less power and there is an increase in maintenance cost.

Water contamination in oil can be the root cause of many problems; creating rust and sludge, changing viscosity, depleting additives, decreasing lubricant film strength and so damaging components, causing foaming, premature aging of the oil, etc. (Noria, 2003)

Cantley (1977) developed a figure relating bearing life to water content as measured by a number of tests including crackle or bubble test, the Karl Fischer test and spectrometric oil analysis. Figure 6.1 shows an adaptation of Cantley's findings and illustrates the strong relationship between water content and relative bearing life.

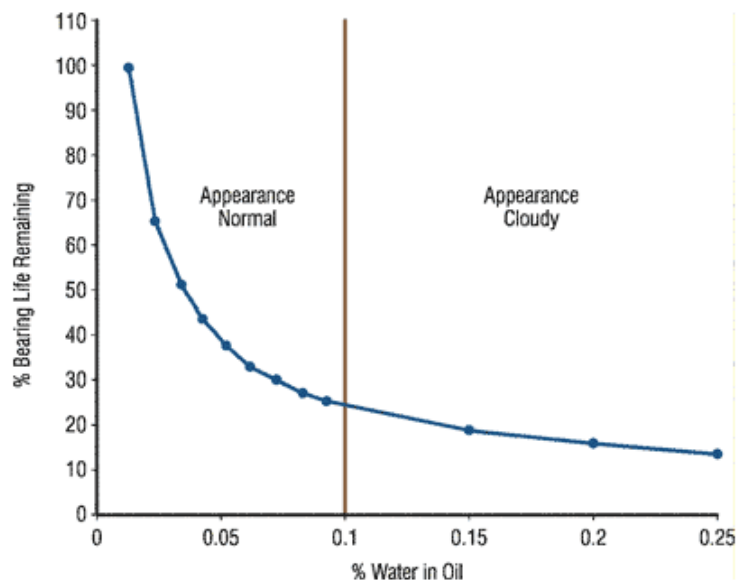


Figure 6. 1 Bearing life with water contamination of lubricating oil

(Noria Corporation, 2001)

Early failure of machinery and equipment often begins with lubricant deterioration which may be caused by the presence of contaminants, especially fluids or water. If water contamination of lubricants can be detected using vibration, airborne sound and/or acoustic emission responses, catastrophic failure can be prevented and risks of failure reduced with gains in safety, economics and finance. Therefore, it is proposed to use the surface vibration and airborne sound and AE characteristics to monitor the lubrication quality in journal bearings.

The temperature of a lubricant has a significant effect on the surface vibration, airborne sound and acoustic emission responses of the bearing thus the data collection was always undertaken under similar temperature conditions at 22.5°C by using temperature sensors and digital thermometer.

The first experiment was a series of tests used three uncontaminated lubricants that met the specifications of ISO VG 32, ISO VG 68 and SAE 90 respectively.

The second experiment was a series of tests used lubricant ISO VG 46 contaminated with the addition of water: 0%, 1.25% and 2.5% (vol/vol).

The bearings on the DE side of the motor and NDE bearing were normal in all tests. The bearing on the DE and NDE side of the motor initially had zero water in the lubricant as reference, and in every test the same contaminated lubricant was used in both bearings. Again three radial loads were imposed (2 bar, 10 bar and 20 bar) and the bearing were tested at 25%, 50%, 75% and 100% of maximum speed (1450 rpm).

The experiment is repeated 3 to 4 times to get a good repeatability. Subsequent analysis was done by calculating the mean value of the three or four data sets. In each case the data was obtained in the time and frequency domains.

6.2 Abnormal lubricating.

6.2.1 Surface vibration analysis

The SV characteristics of a self-aligning spherical journal bearing with quality of lubricant were obtained for “viscosity 1” (ISO VG 32), “viscosity 2” (ISO VG 68) and “viscosity 3” (SAE 90), for abnormal lubricating will be presented in sub-chapter 6.3.

Time domain analysis and frequency domain analysis are used in the surface vibration analysis.

Figure 6.2 show the time-domain of the raw SV acceleration signal of the DE and NDE self-aligning journal bearings for the three lubricants at maximum speed. The first, second and third test represents radial load 2 bar, second test 10 bar and the third test 20 bar.

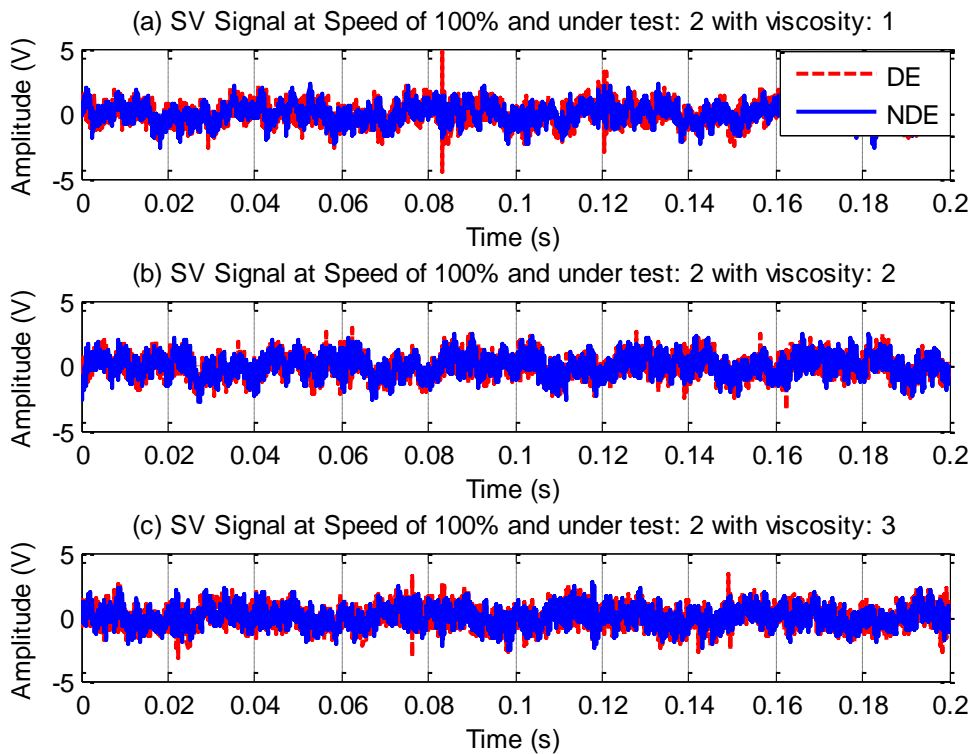


Figure 6. 2 SV signal on bearing for different lubricant viscosities at 100% speed and radial load of 10bar

Figure 6.2 shows that the effect of the quality or viscosity of lubricant cannot be distinguished from the SV amplitude. The figure also indicates a small difference in amplitude between DE and NDE bearing - this may be caused by their different positions and starting bearing condition.

The influence of lubricant quality on SV response was further investigated by statistical parameter analysis: RMS and Kurtosis. Figure 6.3 shows the Kurtosis value of the raw signal for DE and NDE bearings at four speeds, three radial loads and three values of the viscosity.

.

.

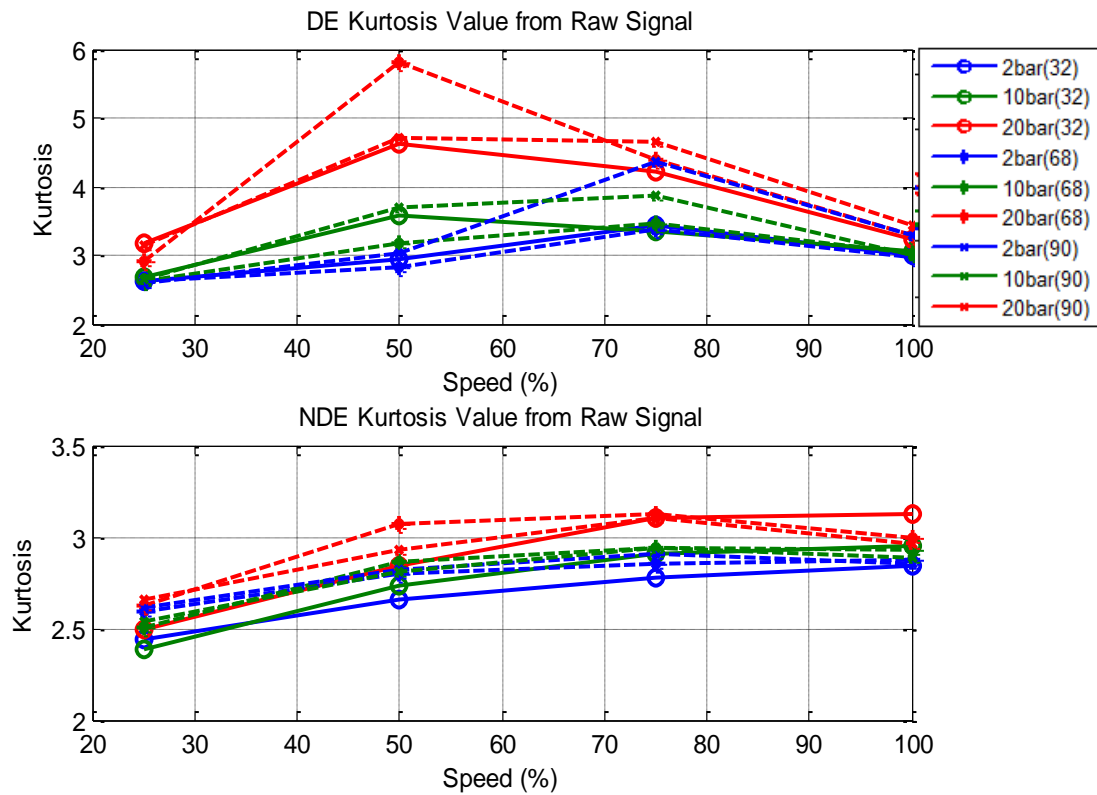


Figure 6. 3 Kurtosis value of raw signal for three different loads, four speeds and three lubricant viscosities

The figure indicates that radial load does not produce a constant effect on the Kurtosis value. The Kurtosis values lie between 2.5 and 5.8 for DE bearing and 2.5 and 3.2 for NDE bearing, which indicates that signal amplitude distribution was close to a Gaussian data distribution for NDE bearings. However, the Kurtosis cannot be used to identify the effect of viscosity under the test conditions and there is no consistent change in Kurtosis with either speed or lubricant.

Figure 6.4 shows the RMS value of the SV signal from the journal bearings as a function of shaft speed, radial load and lubricant. Figure 6.4 shows a small positive correlation between speed and SV RMS value, but the effect of radial load and viscosity variation are difficult to be identified.

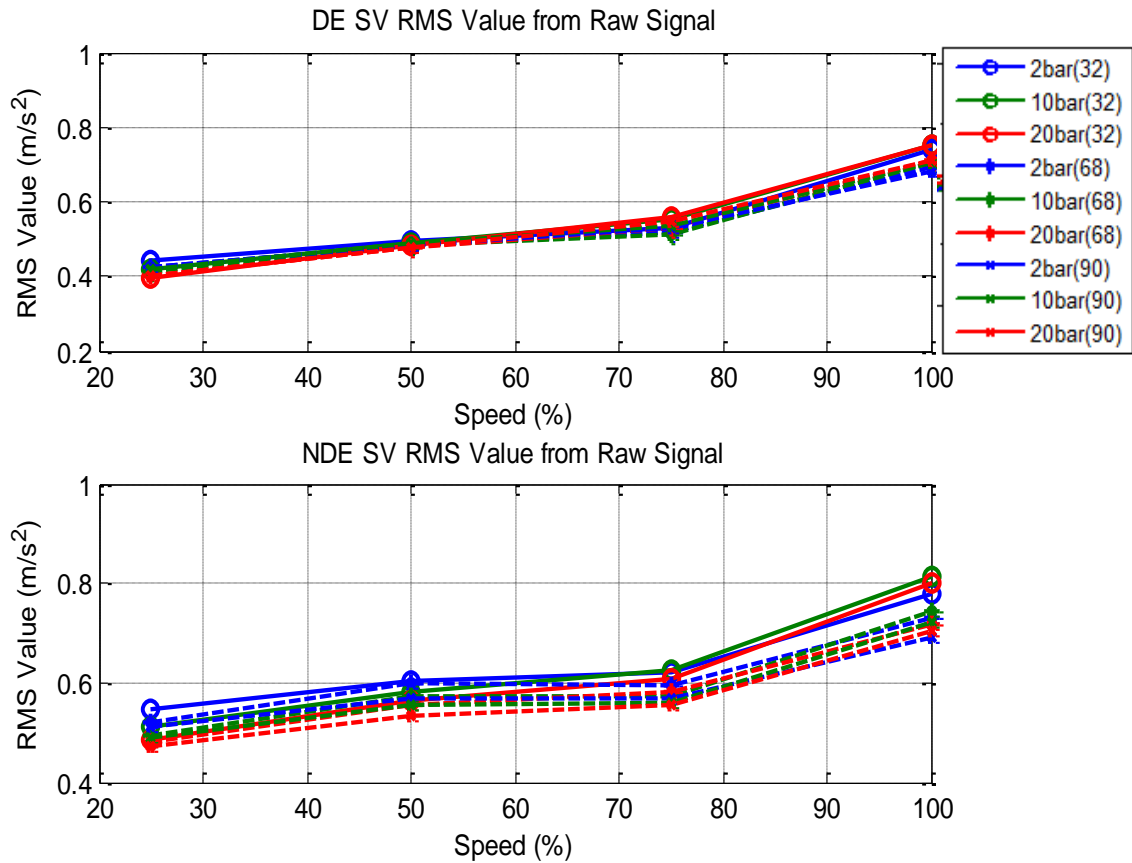


Figure 6. 4 SV RMS value from raw signal in DE and NDE under different speed, radial loads and lubricant viscosity

The SV responses of the DE and NDE journal bearing at 50% maximum speed and 20 bar radial load for the three lubricants ISO VG 32, 68 and SAE 90, are shown in Figure 6.5. It can be seen that there are small differences in SV spectrum responses between the DE and NDE bearings. The NDE spectrum response is higher than the DE response, this is due to differences in the initial conditions and loading of the two bearings.

Individual high amplitude peaks can be seen in the frequency range from about 3.0 kHz up to 4.5 kHz, but between 4.7 kHz and 6.3 kHz there appears a more continuous spectrum with a series of broad peaks. This was the case for all three lubricants.

The peak values generated by the bearing when operated 50% of speed and 20 bar radial load with three kind of viscosity of lubricant occur at frequency 3.05 kHz, 4.05 kHz, 4.1 kHz, 5.3 kHz and 5.7 kHz. The highest amplitude peak occurs at 5.7 kHz

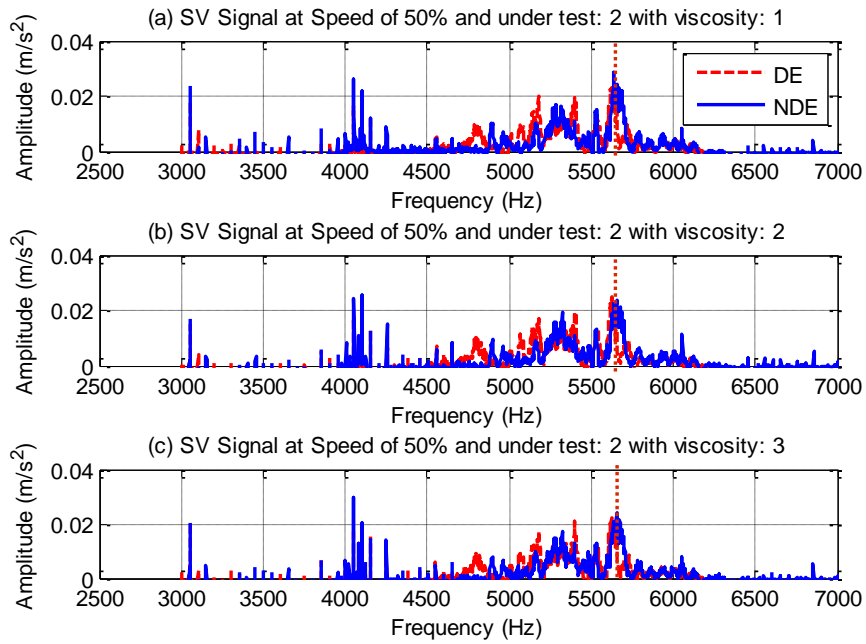


Figure 6. 5 SV spectrum in DE and NDE bearing for three different lubricant viscosities at 50% maximum speed, radial load 20 bar

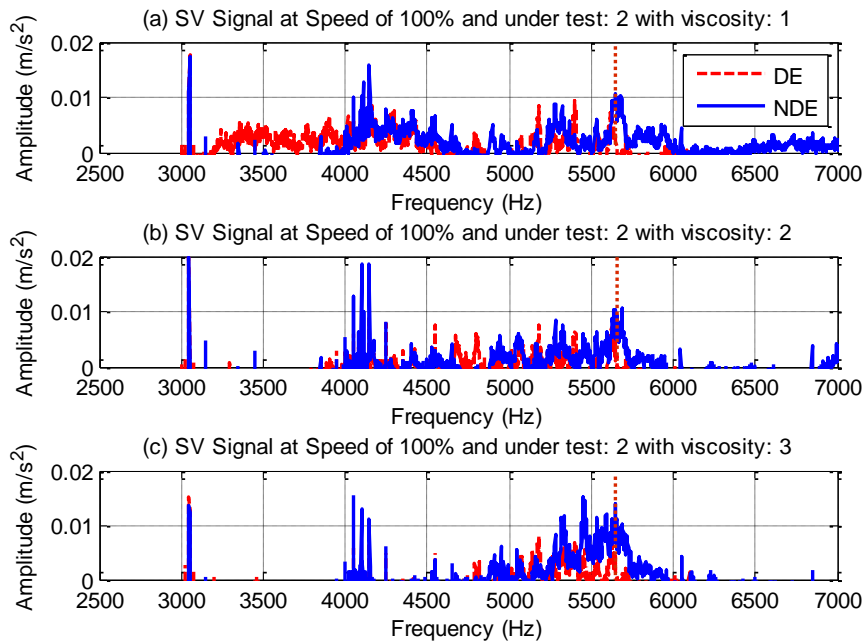


Figure 6. 6 SV spectrums in DE and NDE bearing for three different lubricants at maximum speed, radial load 20 bar

Figure 6.6 is the spectrum of the SV responses for the DE and NDE bearings under radial load of 20 bar and maximum speed of 1450 rpm. The figure shows high amplitude peaks at frequencies from 3.0 kHz to 3.7 kHz and between 3.9 kHz and 6.3 kHz. The peak values generated by the bearing when operated at maximum speed and 20 bar radial load with three different lubricants were at 3.05 kHz, 4.05 kHz, 4.1 kHz and 5.7 kHz. The highest amplitude occurred at 3.05 kHz. Figure 6.6, also shows that a higher viscosity gives a lower peak SV amplitude at 3.05 kHz, from 0.029 m/s^2 to 0.016 m/s^2

Figure 6.7 shows the effect of speed, radial load and lubricant viscosity on the RMS value of the raw SV signal when it has been high frequency filtered (4 kHz to 7 kHz). The most obvious effect that can be seen is a positive relationship between speed and RMS SV amplitude response

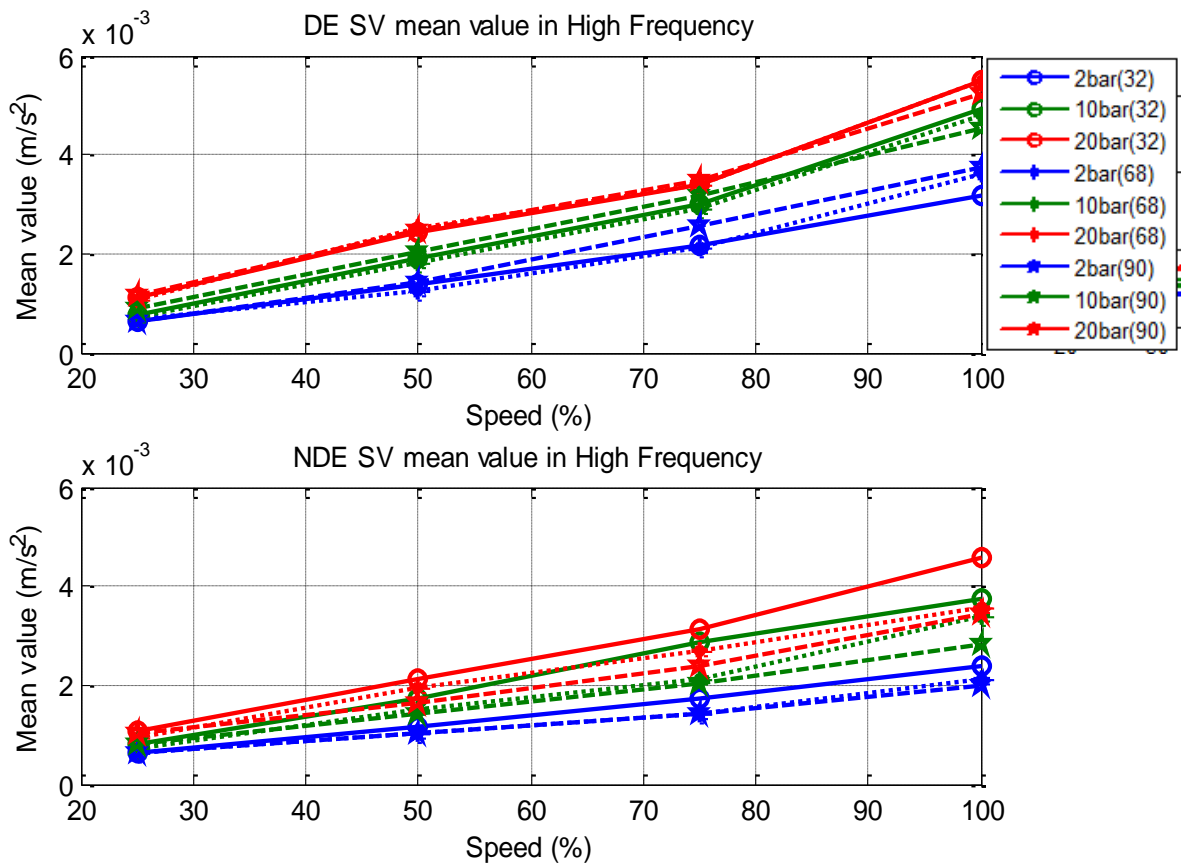


Figure 6. 7 SV mean value in DE and NDE bearing under different speed, radial loads and lubricant viscosity at high frequency

Figure 6.7 also shows that the RMS amplitude of the high frequency SV signal increases with increase in radial load and decreases with increase in lubricant viscosity for both DE and NDE bearings.

6.2.2 Airborne sound characteristics

The airborne sound measurements were performed at the same time as the surface vibration measurements so the conditions are identical: three radial loads - 2 bar, 10 bar and 20 bar, speeds of 25%, 50%, 75% and 100% of the maximum and lubricants conforming to ISO VG 32, ISO VG 68 and SAE 90.

In the airborne sound characteristic also use time domain and frequency domain analysis.

The raw AS signal responses for the DE and NDE bearings for maximum speed and 10 bar radial load for three lubricant viscosities are shown in Figure 6.8. It can be seen that the time-domain of the raw AS signal from DE and NDE bearings do not appear significant different for the different viscosities.

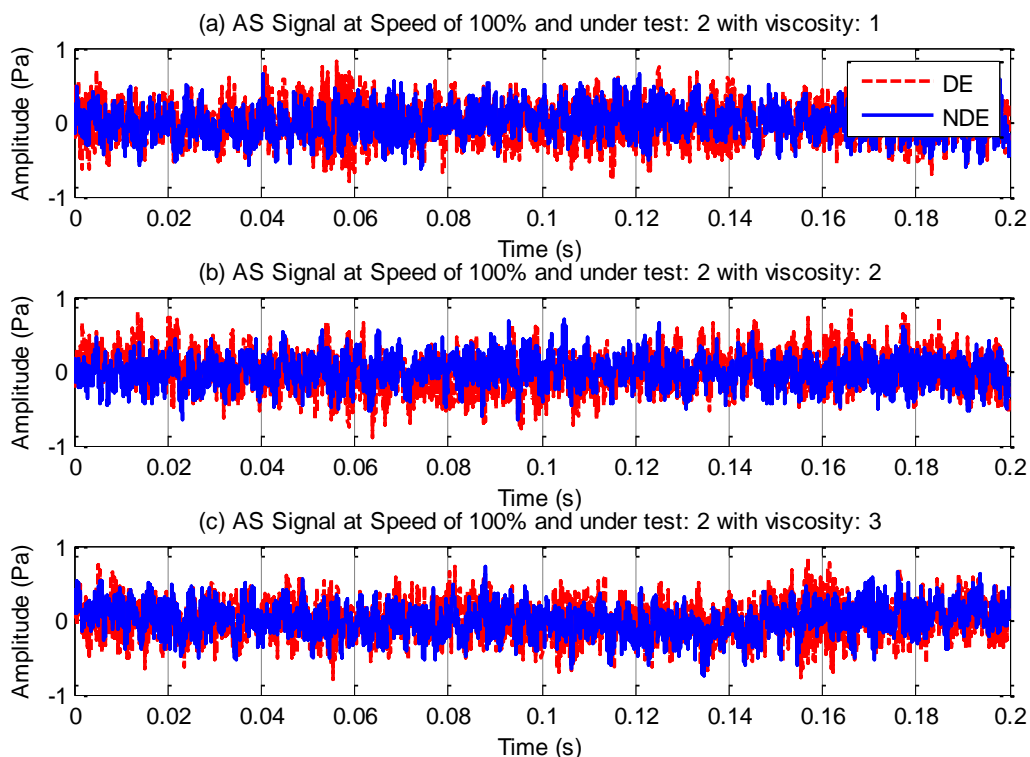


Figure 6. 8 AS signal in DE and NDE bearing under different lubricant viscosity at maximum speed with 10 bar radial load

As in previous discussions (see Sections 5.3 and 5.4) there is little difference in the responses of the SV and AS signals between DE and NDE bearings. The different response may be caused by different condition and unsymmetrical distribution radial load.

Figure 6.9 shows the relationship between RMS of the raw AS signal and speed, radial load and viscosity for DE and NDE bearings.

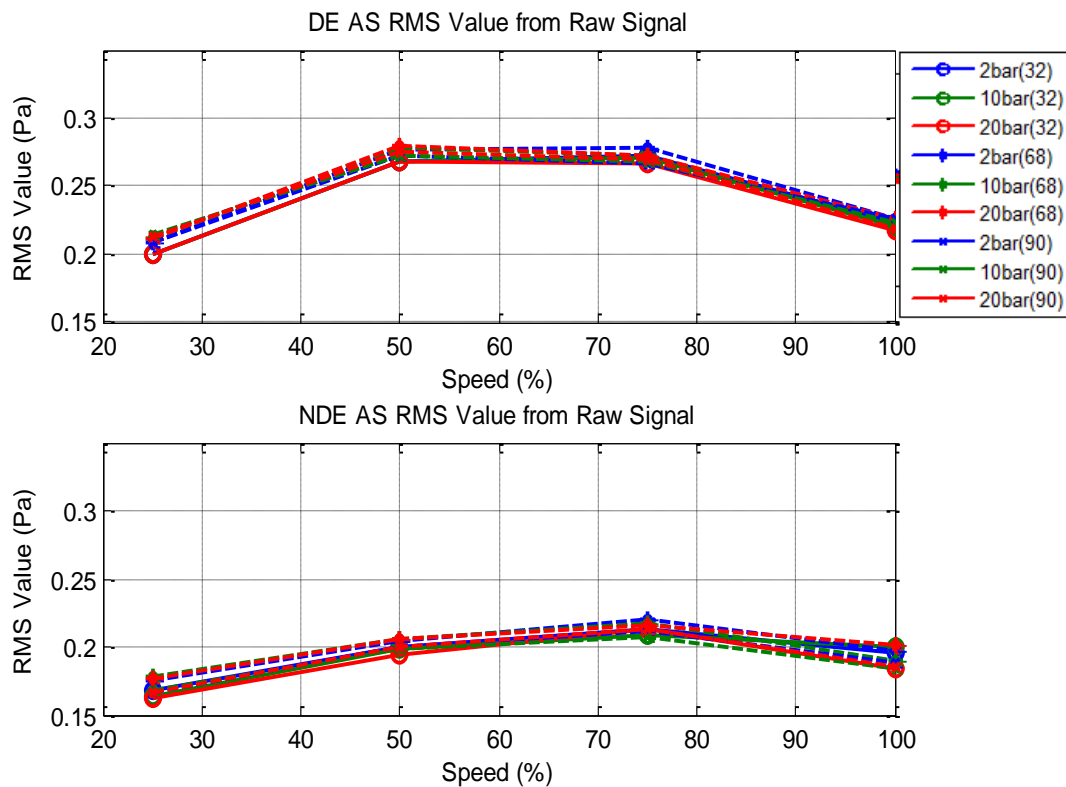


Figure 6. 9 AS RMS value raw signal for DE and NDE bearings under three different loads, four speeds and three viscosities

Figure 6.9 shows that as the speed increases the AS RMS amplitude for both DE and NDE bearings increases initially, but after about 75% of maximum speed, the AS amplitude decreases. This phenomenon may be caused by improved lubrication. When the radial load on the bearing is increased there is no significant change in amplitude. This condition may not be due to the AS signal from the bearings alone but may be due to other components such as cooling fan motor, cooling fan and DC generator motors and DC generator itself.

Figure 6.10 shows the Kurtosis values for the raw AS signal for DE and NDE bearings for variation in radial load, speed and lubricant viscosity

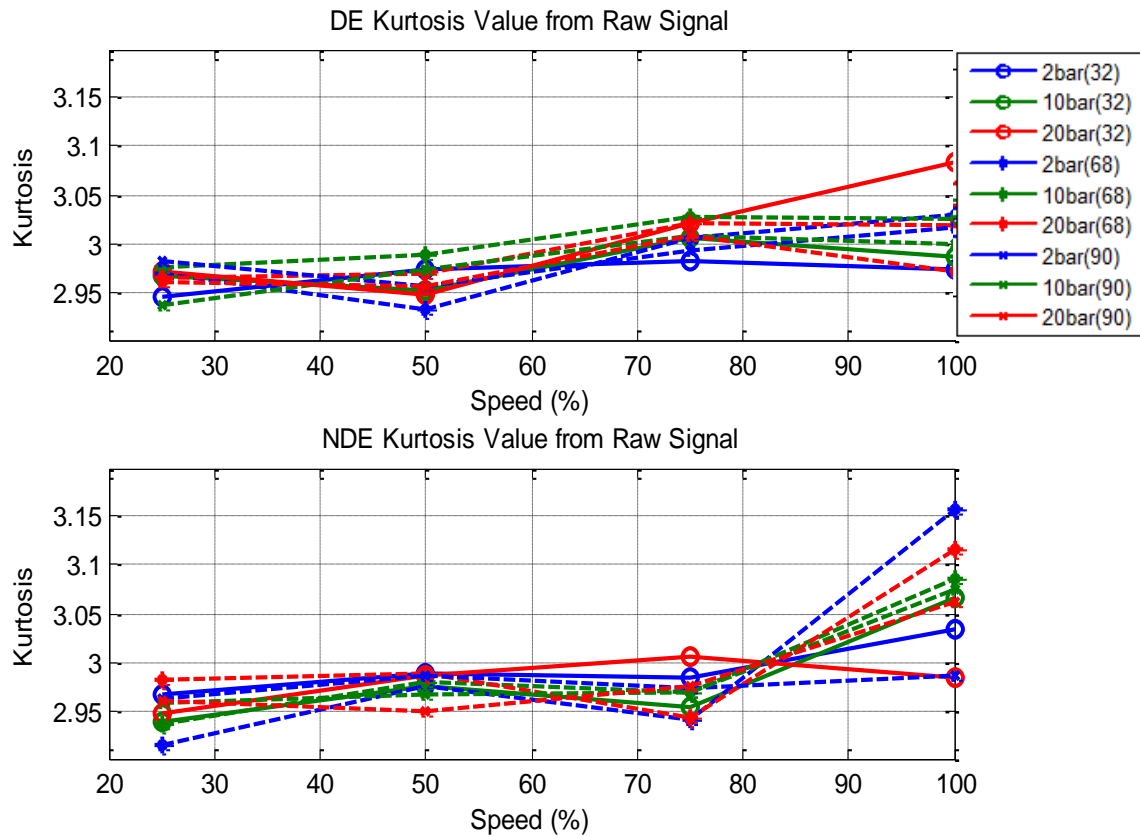


Figure 6. 10 Kurtosis value of AS raw signal for DE and NDE bearings under three different loads, four speeds and three viscosities

Figure 6.10 shows that when speed increases, the Kurtosis value tends to increase but not in a consistent manner. The effects of increasing radial load and varying viscosity are not sufficiently discernible to be useful for condition monitoring. The range of Kurtosis values for DE and NDE bearings were within 2.9 to 3.15, indicating that the data distribution approaches Gaussian.

AS frequency domain response for DE and NDE bearings under a radial load of 10 bar and 50% of maximum speed with three different viscosities is shown in Figure 6.11.

Figure 6.12 is the AS frequency domain response for 10 bar radial load at maximum speed for three different lubricant viscosities.

Figure 6.11 and 6.12 generally indicate that viscosity variation does not significantly affect the AS spectral response. The figures also show that is difficult to distinguish the AS response of journal bearings operating at medium speed (50%) and maximum speed.

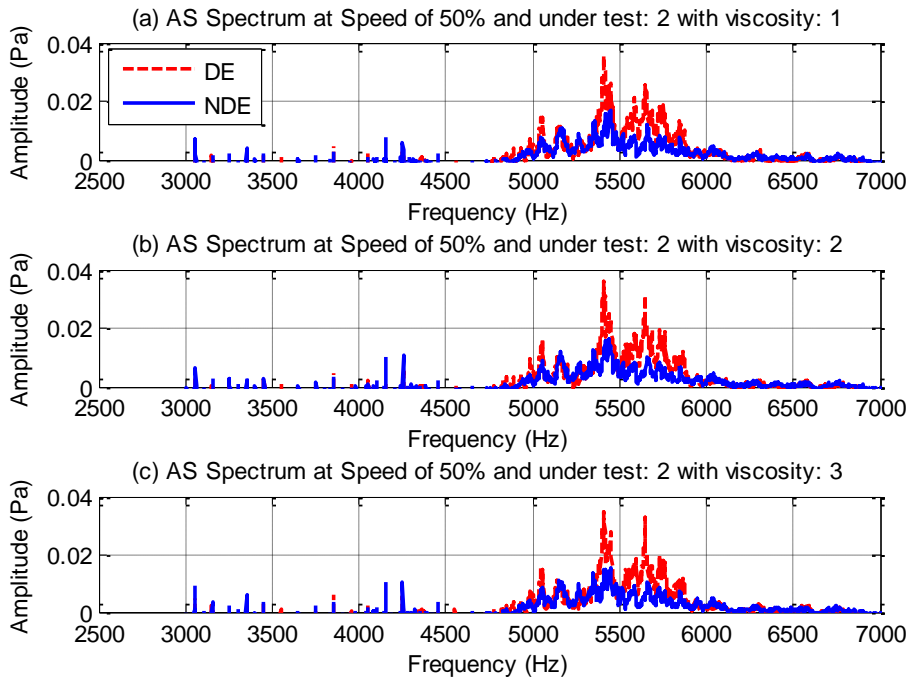


Figure 6. 11 AS spectrum for DE and NDE bearings under 10 bar radial load, at 50% maximum speed for three different lubricant viscosities

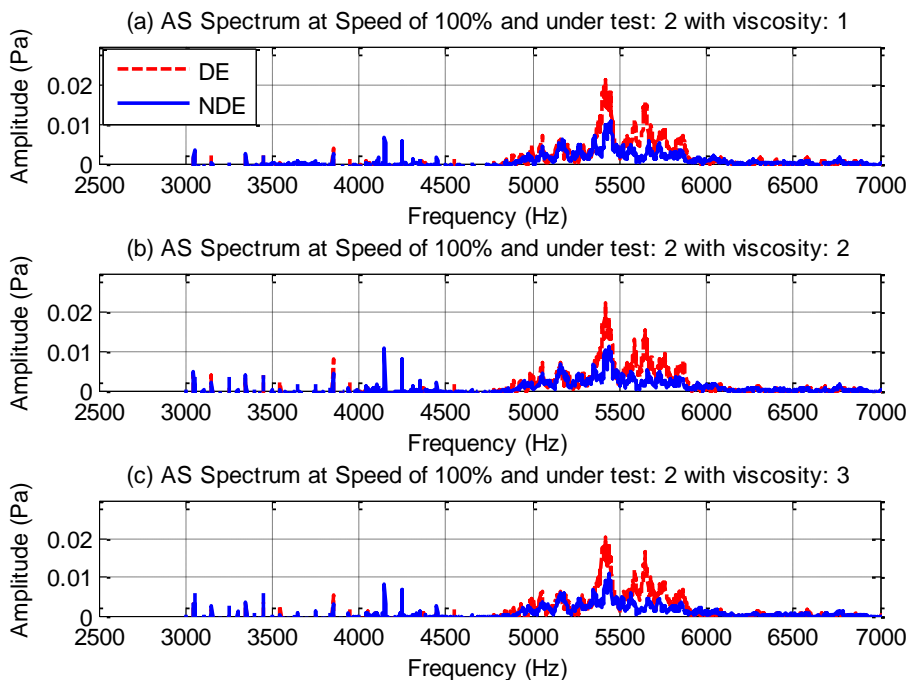


Figure 6. 12 AS spectrum for NDE bearings under 10 bar radial load, at maximum speed for three different lubricant viscosities

Minor peaks in the AS spectrum occur in the range between 3 kHz to 4.5 kHz, but the dominant peaks occur between 4.8 kHz until 6.1 kHz. The highest amplitude peak occurs at 5.4 kHz and followed by the peak at 5.6 kHz.

A clear difference can be seen in the AS spectra between the DE and NDE bearings. This is due to differences of early bearing condition and radial load on the bearing because their positions are not absolutely symmetric with respect to the load, as described previously in Section 6.2.2.1. These differences are due to the test set up they appear in every set of readings.

Figure 6.13 shows the effect of speed, radial load and lubricant viscosity on the AS RMS spectra for DE and NDE bearings for the low frequency range (3 kHz up to 6 kHz).

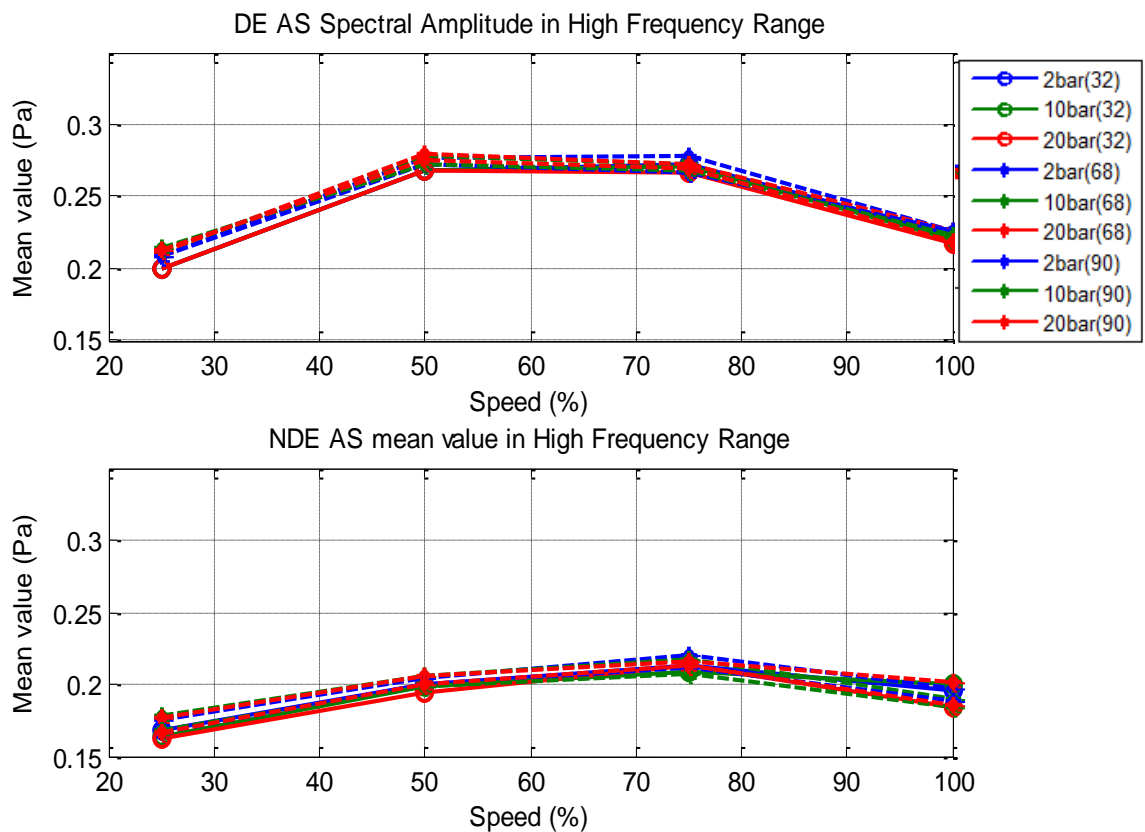


Figure 6. 13 AS spectral mean value (3 kHz to 6 kHz) for DE and NDE bearings for four speeds and three loads with three different lubricants

Figure 6.13 shows the effect of speed on the RMS of the AS low frequency spectrum for DE and NDE bearings with radial load and viscosity. The pattern is much the same as for Figure 6.9, when the speed increases the AS RMS amplitude increased but declined after reaching at speed of about 75% of maximum. The figure also indicates that the effect of radial load and viscosity on the RMS amplitude was small and difficult to identify.

The decreasing of airborne sound RMS value after 75% of speed may be due to a better lubrication system.

6.2.3 Acoustic Emission characteristics

This section describes the results of monitoring using acoustic emission (AE) to detect the effects of change in lubricant viscosity on two SA35M self-aligning spherical journal bearings. The AE sensor and its mounting are described in Section 4.1. The initial set of experiments tested the effects of viscosity for three lubricants meeting specifications ISO VG 32, 68 and SAE 90, three radial loads (2 bar, 10 bar and 20 bar) and four speeds.

As with the SV and AS analysis, AE characteristic due to viscosity variation used time-domain, frequency domain, comparative, include Kurtosis, RMS and mean value analysis.

The time-domain waveforms shown in Figure 6.14 and 6.15 are for raw AE signals for DE and NDE journal bearings under three radial loads, three different lubricant viscosities at 50% and 100% maximum speed.

Figure 6.14 and 6.15 indicate that the AE signal response is a mix of burst type and continuous type and that the amplitude increases with both increasing radial load and rotational speed. The AE time-domain amplitude also shows a significant difference with lubricant viscosity. Lubricants that are less viscous will produce higher AE peak amplitude compared with lubricants that are more viscous. Apart from that the AE responses of DE and NDE bearings are similar and do not differ significantly.

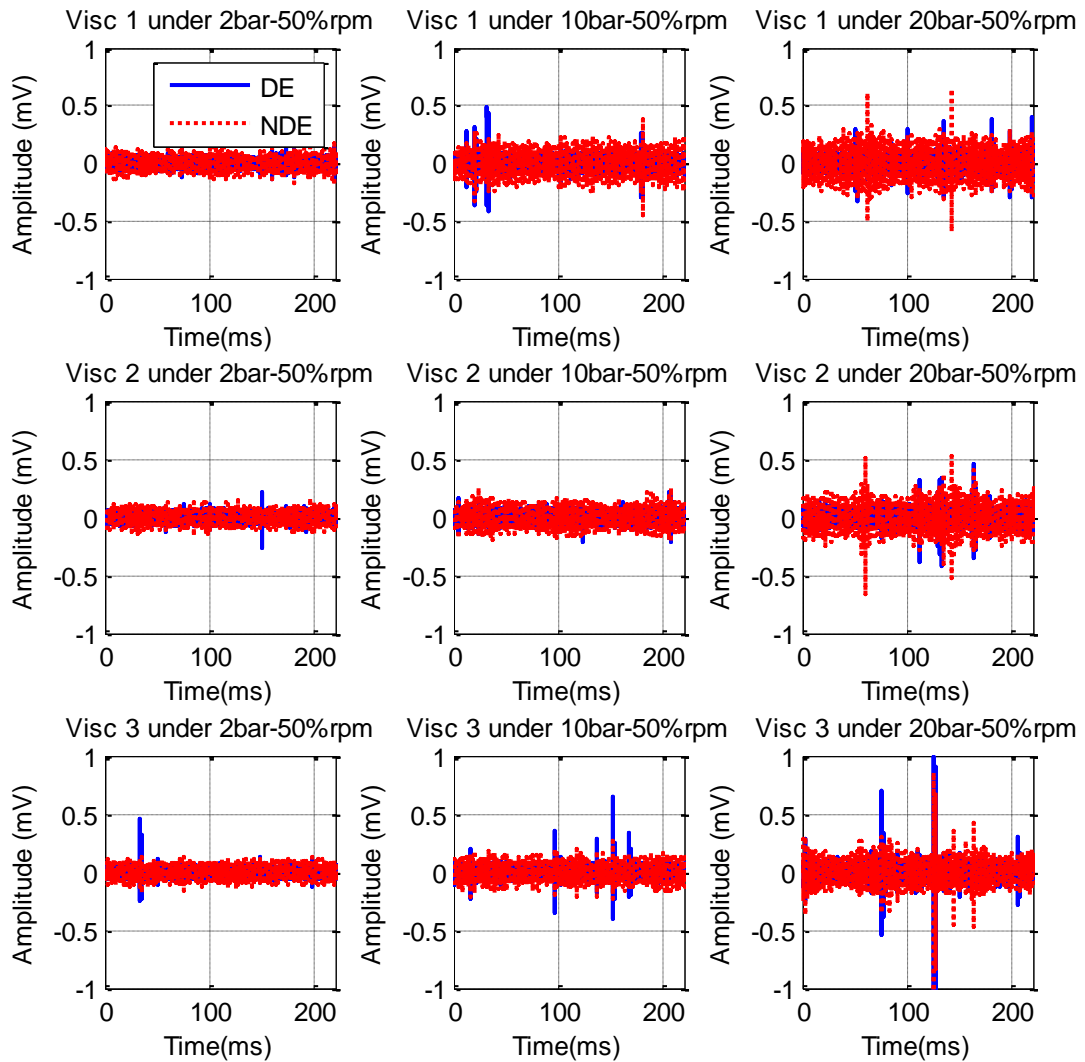


Figure 6. 14 AE signal for DE and NDE bearings under three radial loads and three viscosities at 50% maximum speed

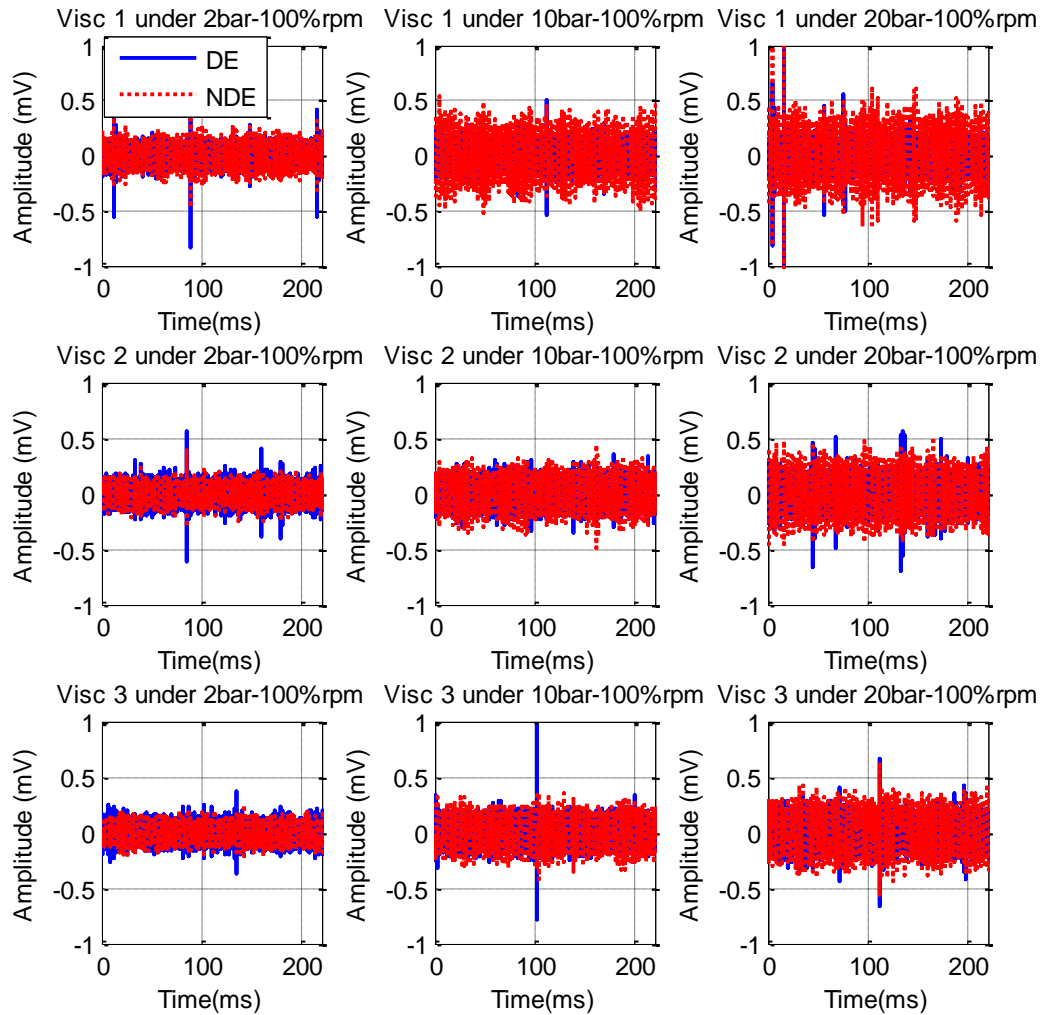


Figure 6. 15 AE signal for DE and NDE bearings under three radial loads and three viscosities at maximum speed

Figure 6.16 shows the RMS value of the AE raw signal for the time-domain with speed, radial load variation and different viscosities for the DE bearing.

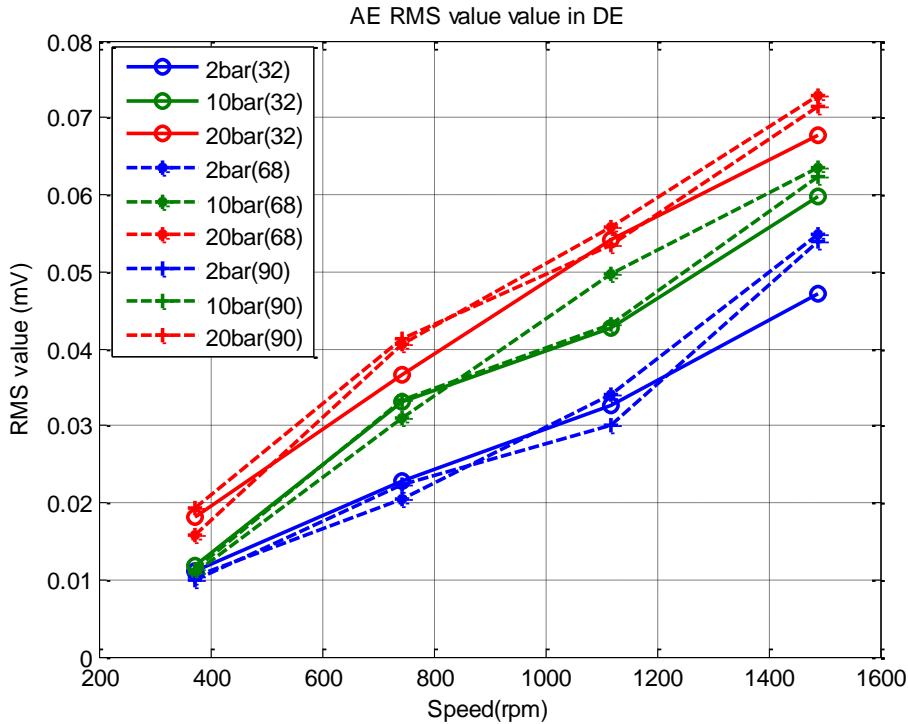


Figure 6. 16 AE RMS value from raw signal for DE bearing under three radial loads, four speeds and three lubricant viscosities

Figure 6.16 shows that there is a positive correlation between shaft speed and AE RMS value of the raw signal for each of the three radial loads; 2 bar, 10 bar and 20 bar. No clear or consistent differences in the RMS value were discerned with change in viscosity.

Figure 6.17 shows the RMS value of the AE raw signal for the time-domain with speed, radial load and three different lubricant viscosities for the NDE bearing. It can be seen there is a clear and distinct increase in the RMS value as the speed increased. It also appears clear that as radial load increases so does the AE RMS. The figure also appears to show that an increase in lubricant viscosity causes a decrease in the AE RMS amplitude of the raw signal. The decrease is quite clear for all three radial loads. This decrease is explained because a more viscous lubricant will decrease asperity contact so AE release is also reduced.

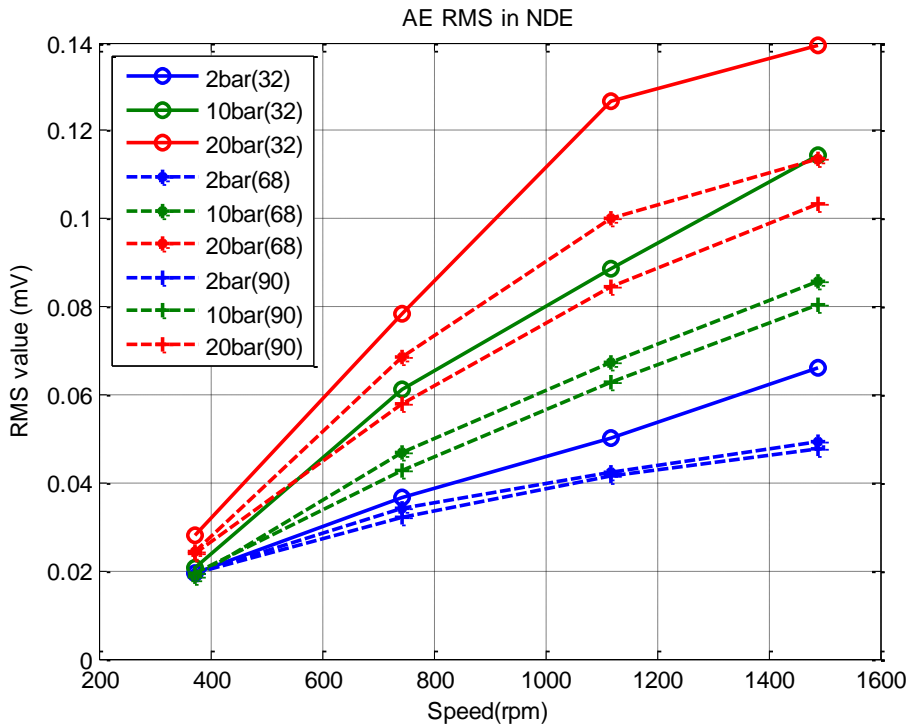


Figure 6. 17 AE RMS value from raw signal for NDE bearing under three radial loads, four speeds and three lubricant viscosities

The RMS values from the raw signal for the NDE bearing show more or less similar results, increasing in RMS value as the speed increased, and increase in AE RMS amplitude when the radial load increased. It is also clear for all radial loads that using a lubricant with a higher viscosity produces a lower AE RMS response, because a more viscous lubricant decreases asperity contact and less AE energy is released.

Figure 6.18 shows the relationship between speed and Kurtosis for the raw data obtained for three radial loads and three different viscosities of the lubricant for DE and NDE bearings. It can be seen that the Kurtosis does not show a consistent pattern. The Kurtosis has very high values caused by the type of signal which consists of continuous and burst type accompanied by multi hit. At the lowest speed the maximum radial load gave the largest Kurtosis value, but there was a clear peak in the Kurtosis at a speed of 50% maximum for the lubricant with minimum viscosity for all loads.

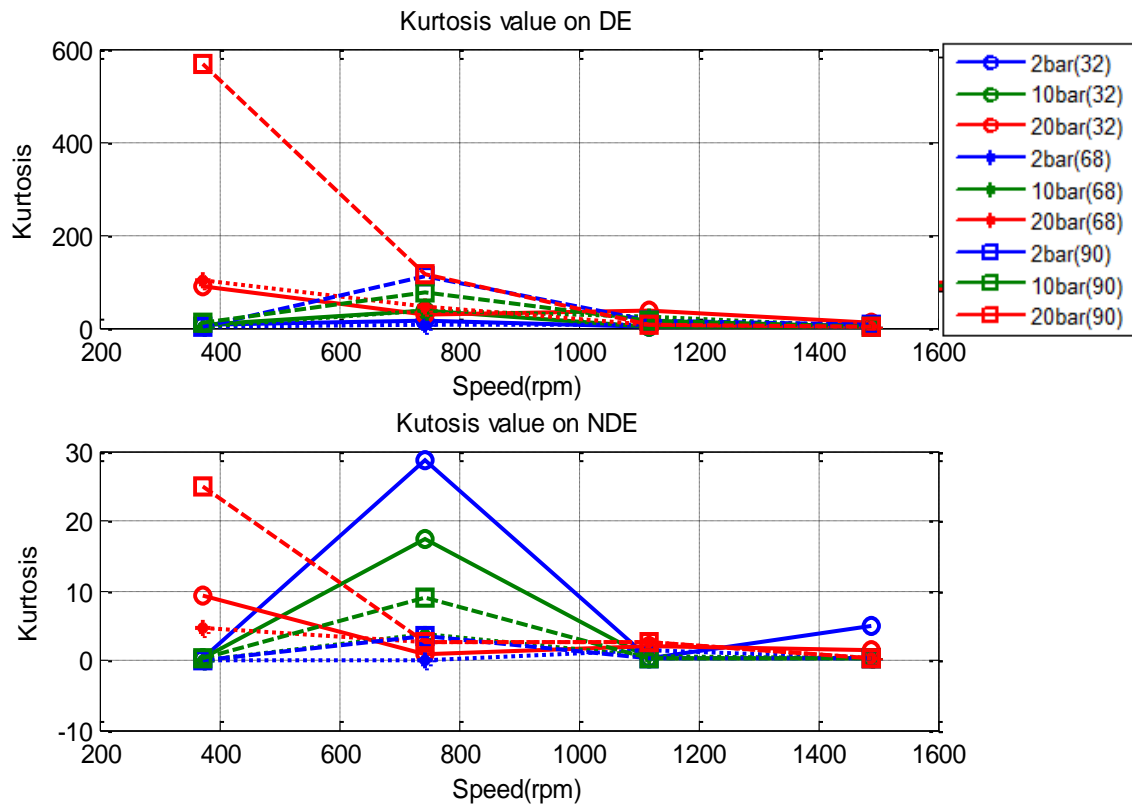


Figure 6. 18 Kurtosis of AE signal from DE and NDE bearing under different radial loads, for four speeds and three lubricant viscosities

6.2.3.2 Frequency domain analysis

The AE spectra for the raw signal from DE and NDE bearings under the three radial loads and for the three lubricant viscosities are shown in Figure 6.19 for 100% maximum speed at frequency range 1-100 kHz

As previously Viscosity 1 represents lubricant with ISO VG 32, viscosity 2 corresponds to ISO VG 68 and viscosity 3 represents SAE 90.

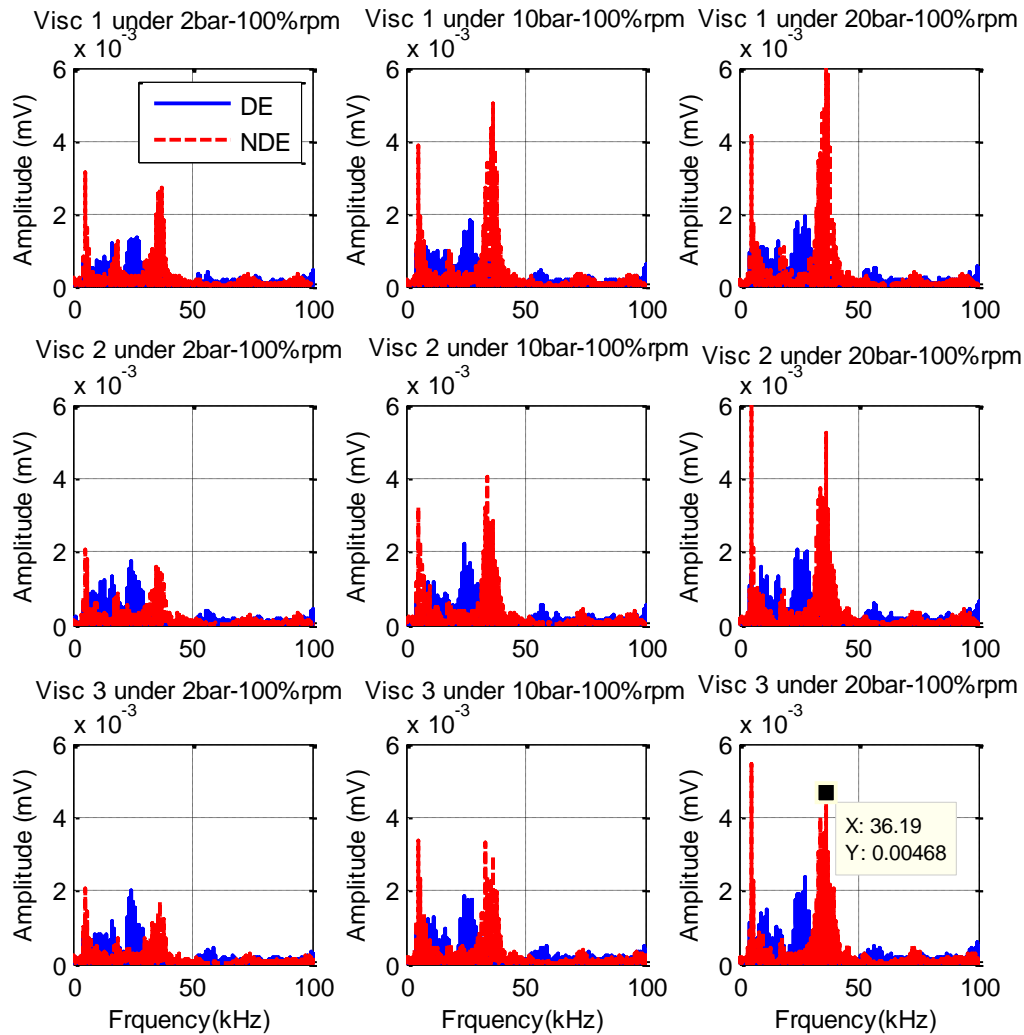


Figure 6. 19 AE spectrum for DE and NDE bearings for three radial loads, three lubricant viscosities at 100% maximum speed at frequency range 1-100kHz

The figures demonstrate that the quality of lubricant affects the amplitude of AE spectrum: a higher viscosity lubricant produces a spectrum with lower amplitude. In this figure high amplitudes occur in the frequency range from about 3.0 kHz to about 50 kHz. Clear peaks appear at frequencies of 5.3 kHz and 36.6 kHz.

Figure 6.20 is AE spectra in DE and NDE bearings under the three radial loads and for the three lubricant viscosities at 100% maximum speed at frequency range 100-500 kHz

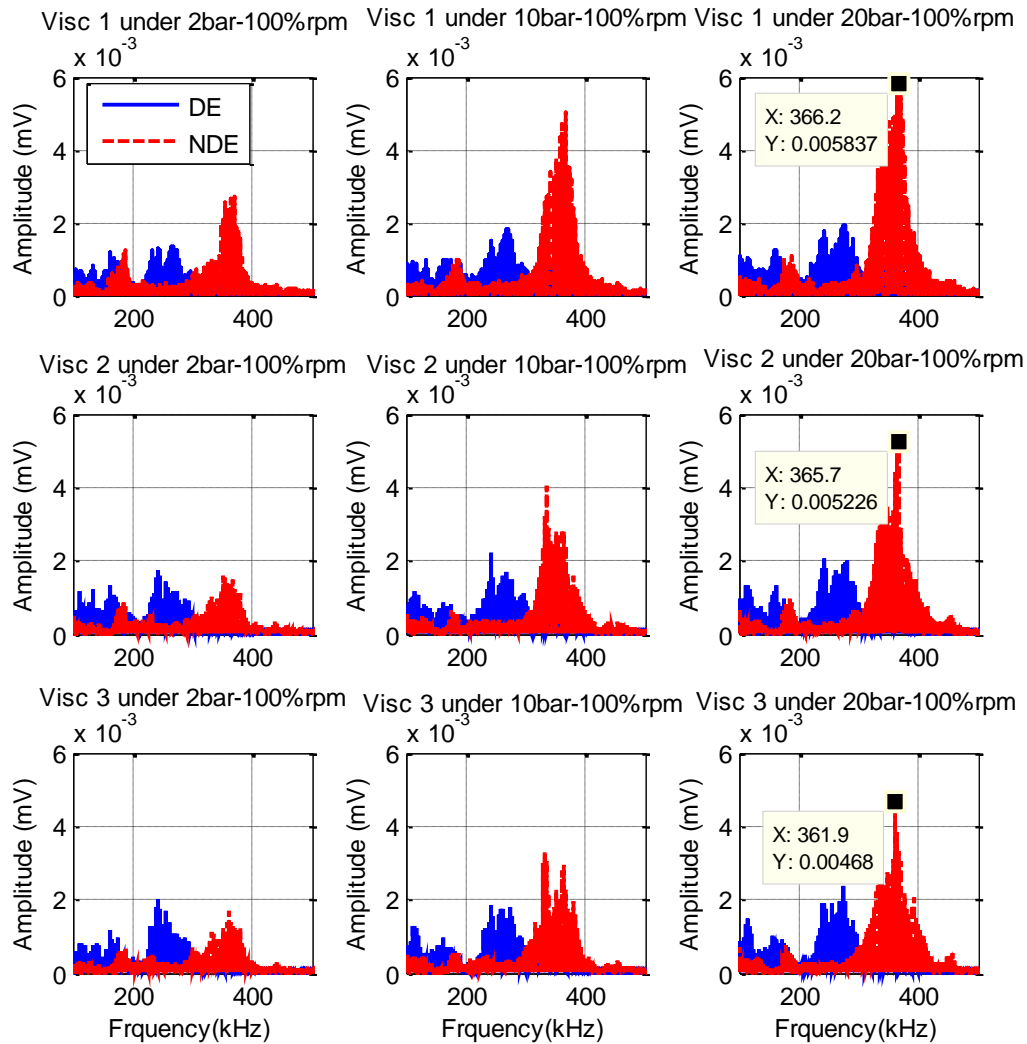


Figure 6.20 AE spectrum for DE and NDE bearings for three radial loads, three lubricant viscosities at maximum speed

The figures also demonstrate that the quality of lubricant affects the amplitude of AE spectrum: a higher viscosity lubricant produces a spectrum with a lower amplitude. The figures show that high amplitudes occur 361.9 kHz.

The highest amplitude under 20 bar radial load at 100% maximum speed with ISO VG 32 is 0.0058 mV at 366.2 kHz. The corresponding value for ISO VG 68 is 0.0052 mV at 365.7 kHz and for SAE 90 is 0.0047 mV at 361.9 kHz. There are significance differences in the AE spectrum amplitudes and frequency for the three different lubricant viscosities.

The effect of viscosity can also be seen in Figure 6.21 which shows the relationship between speed and AE mean value in the (low) frequency range 20 kHz to 90 kHz for the NDE bearing for three radial loads at four speeds. Figure 6.22 is the corresponding figure for the high frequency range 90 kHz to 320 kHz.

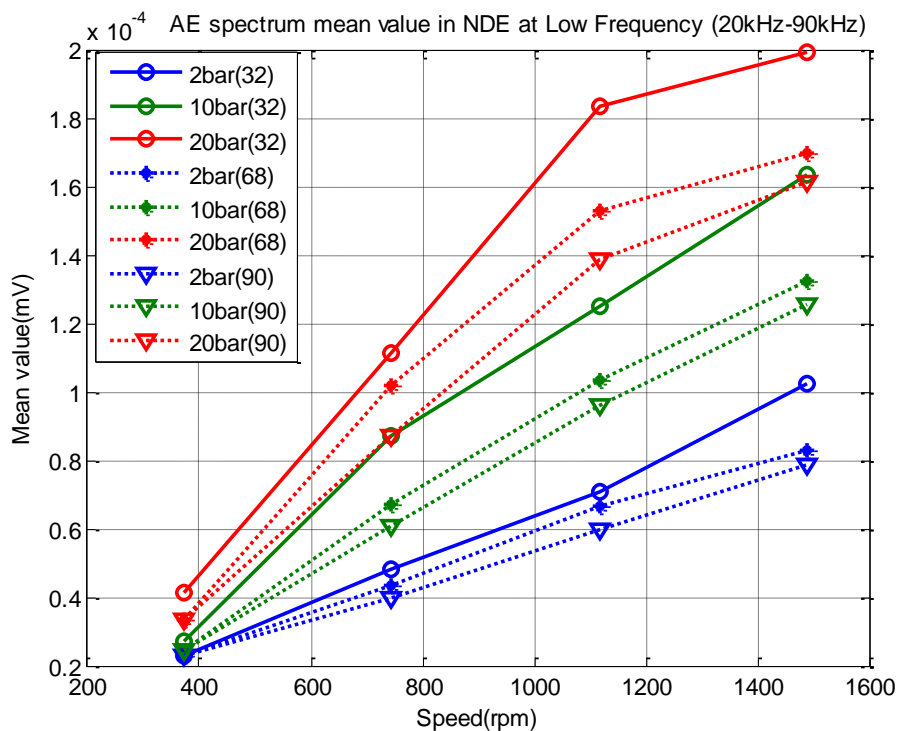


Figure 6. 21 AE mean amplitude in frequency range 20 kHz to 90 kHz for NDE bearing for three radial loads, four speeds and three lubricant viscosities

Figure 6.22 corresponds to Figure 6.21 except that the frequency range is from 90 kHz to 320 kHz. The mean amplitude generally appears to increase with rotational speed for all three loads and lubricants. However, at radial load 20 bar there is a decreasing mean value near maximum speed. It can be seen that generally an increase in radial load produced an increase in the mean AE amplitude.

At 2 bar and 10 bar radial loads the difference in mean AE signals for the different viscosities is not significant. At 20 bar load the lowest viscosity (ISO VG 32) gives the lowest value for mean AE which is caused by out of AE frequency range.

Change in lubricant viscosity may be identified through SV and AE analysis, but with AS this is unlikely.

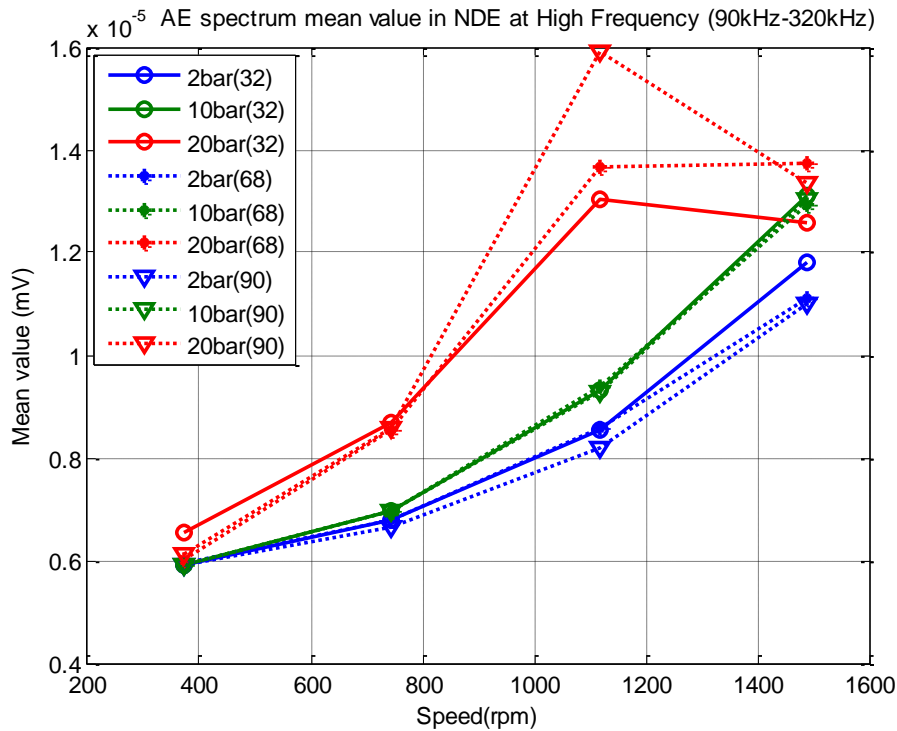


Figure 6. 22 AE mean amplitude in frequency range 90 kHz to 320 kHz for NDE bearing for three radial loads, four speeds and three lubricant viscosities

6.3 Water contaminated lubricant monitoring

A common form of lubricant deterioration is due to water ingress or vapour contaminants. If these contaminants can be detected early possible damage of machinery or machine components can be reduced or avoided. SV, AS and AE analysis is expected to be able to detect the presence of such contaminants in the lubricants used in the given journal bearings.

6.3.1 Surface vibration monitoring

Figure 6.23 represent the raw SV signal from the self-aligning spherical bearing for radial load 10 bar at maximum speed for three different concentrations of water contaminant in the lubricant ISO VG 46, 0.0% (contaminant 1), 1.25% (contaminant 2) and 2.50% and (contaminant 3). Lubricant ISO VG 46 also can be used for journal bearing lubricant under medium load.

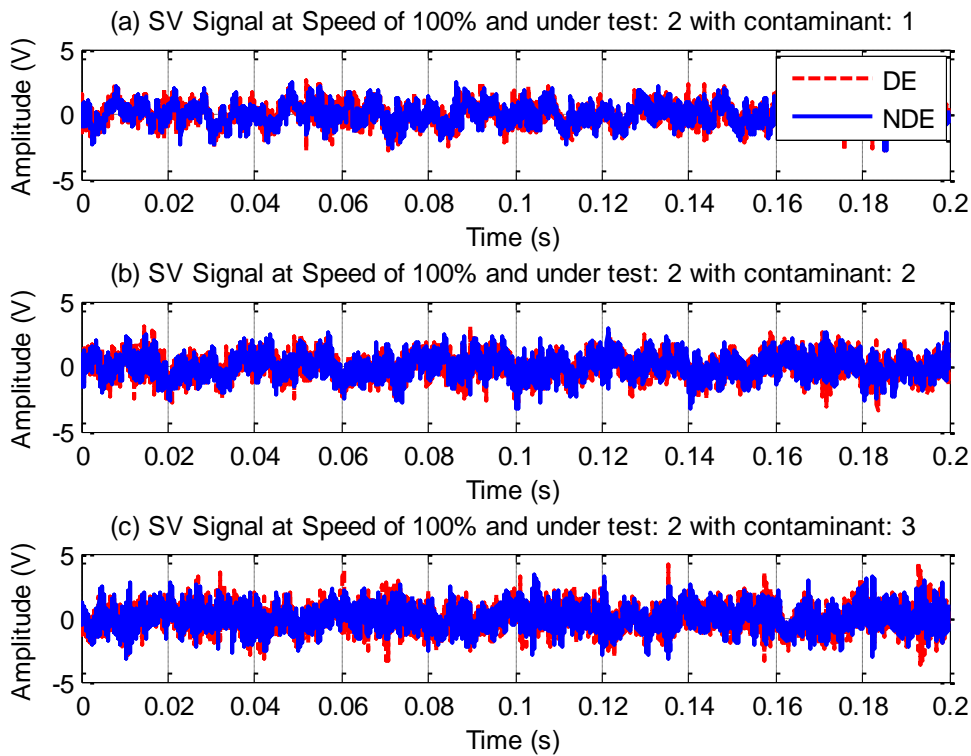


Figure 6. 23 SV signal with three different levels of water contaminant at 100% speed under 10bar radial load

Figure 6.23 shows little or no increase in amplitude of the raw SV signal with increased level of water contaminant in the lubricating oil. There is very little difference between SV signal responses for the DE and NDE bearings.

Figure 6.24 shows the RMS amplitude of the raw SV signal for three radial loads and four speeds for three levels of lubricant contamination. There is very little difference between SV signal responses for the DE and NDE bearings. As previously the RMS level increases with speed, particularly above 75% of maximum speed. No significant differences can be seen due to changes in radial load or level of water contamination. The RMS value of the raw SV signal is not able to detect the effects of the given contaminants in the lubricant.

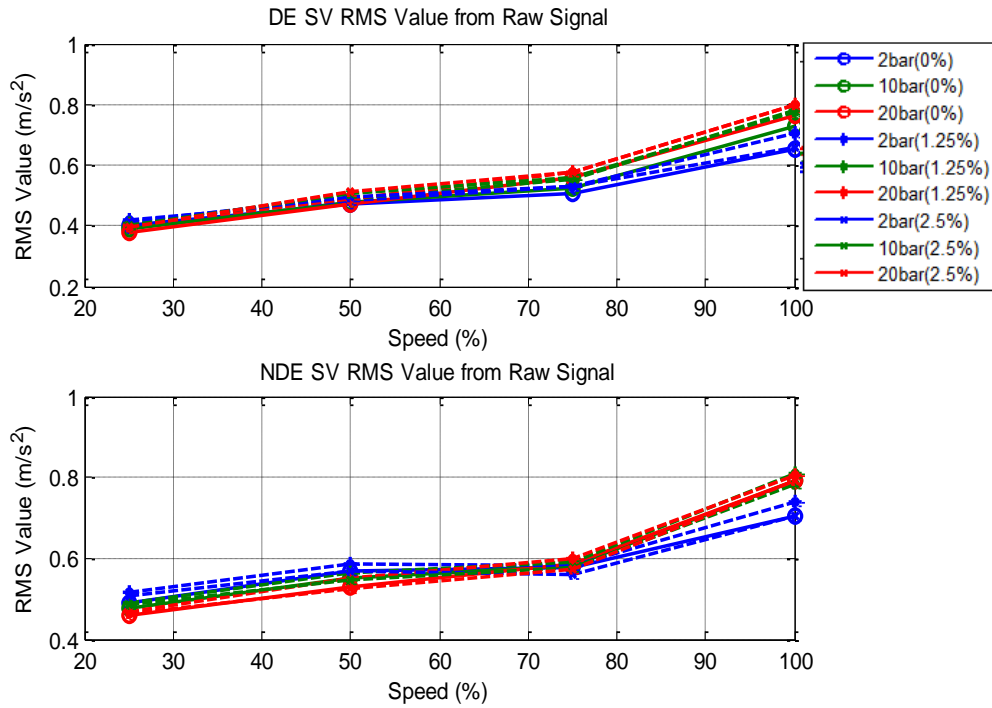


Figure 6. 24 SV RMS of raw signal for four speeds, three radial loads and three levels of contaminant

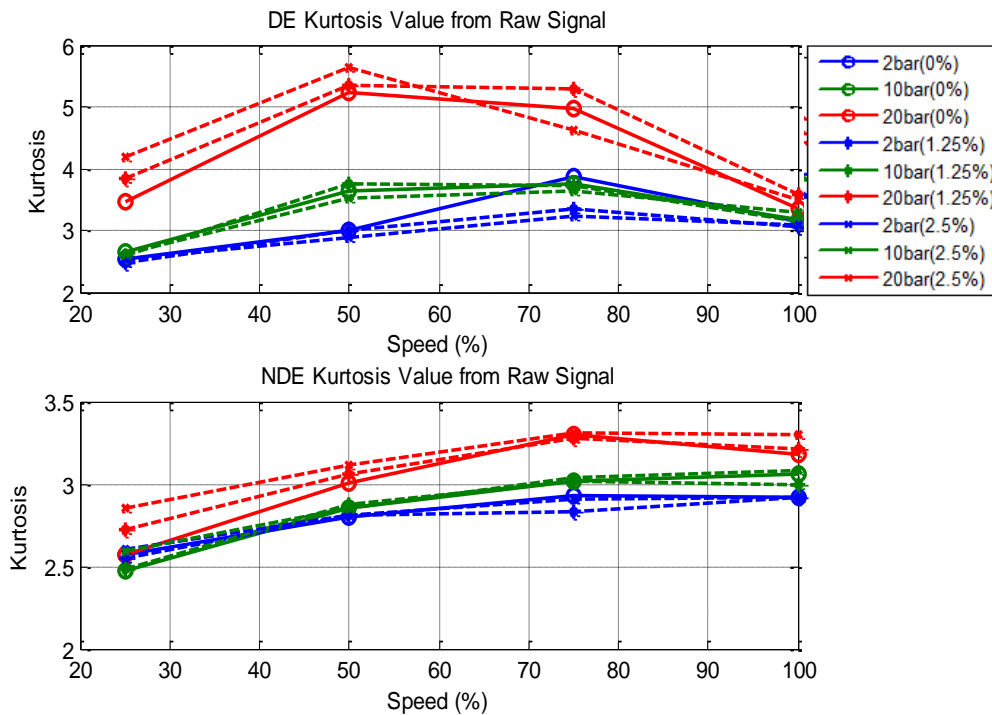


Figure 6. 25 Kurtosis for raw signal from DE and NDE bearings for four speeds, three radial loads and three levels of contaminant

Figure 6.25 shows the Kurtosis values obtained from DE and NDE bearings for the raw SV signal with change in speed, radial loading and lubricant contamination.

It can be seen that effect of speed on Kurtosis values is small and not consistent. The effect of change in level of water in the oil is not significant. The effect of increasing radial load becomes clear only at the maximum load. The Kurtosis value of the DE bearing is between 2.5 and 5.5, and between 2.5 and 3.3 for the NDE bearing. Thus for the NDE bearing the AE signal data has a Gaussian distribution. However the SV Kurtosis analysis cannot detect concentration of water contamination in the lubricant.

Figure 6.26 and 6.27 show SV spectra for DE and NDE bearings under radial load of 10 bar with three levels of water contaminant (0%, 1.25% and 2.5% (vol/vol)) at 50% and 100% maximum speed, respectively.

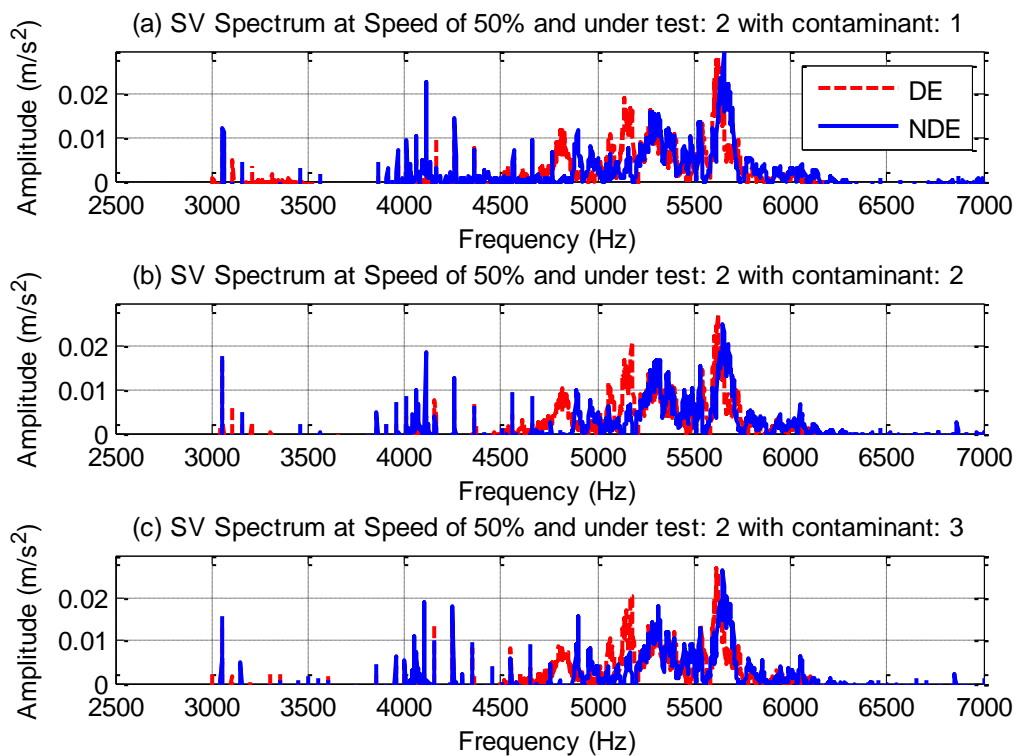


Figure 6. 26 SV spectrum under different water contaminants at 50% speed

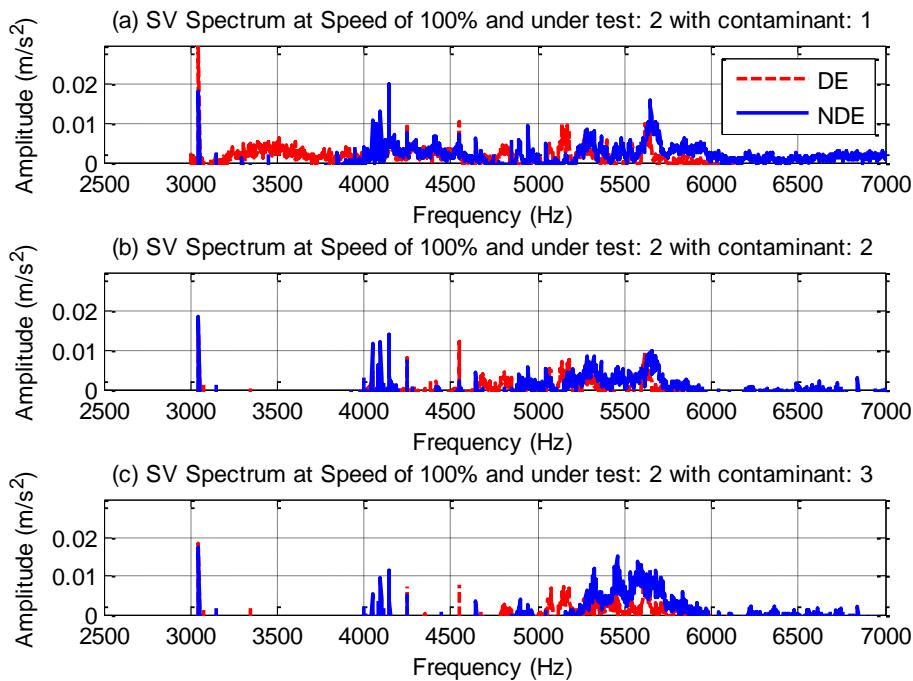


Figure 6. 27 SV spectrum under different contaminants at 100% speed

Figures 6.26 and 6.27 show that SV peaks value occur at 3.0 kHz to 4.5 kHz and then 4 kHz to 6.0 kHz. Peak amplitude appears at 3.1 kHz, 4.1 kHz and 5.6 kHz. The effects of changing the levels of water contaminant from 0% to 2.5 % cannot be identified either at 50% maximum speed or maximum speed. These figures suggest it is not possible to identify contaminants in the lubricant from the SV amplitude alone.

Figure 6.28 shows the relationship between speed, radial load and water contaminant concentration in the lubricant on the SV mean amplitude over the high frequency band 7 kHz to 9 kHz for both DE and NDE bearings.

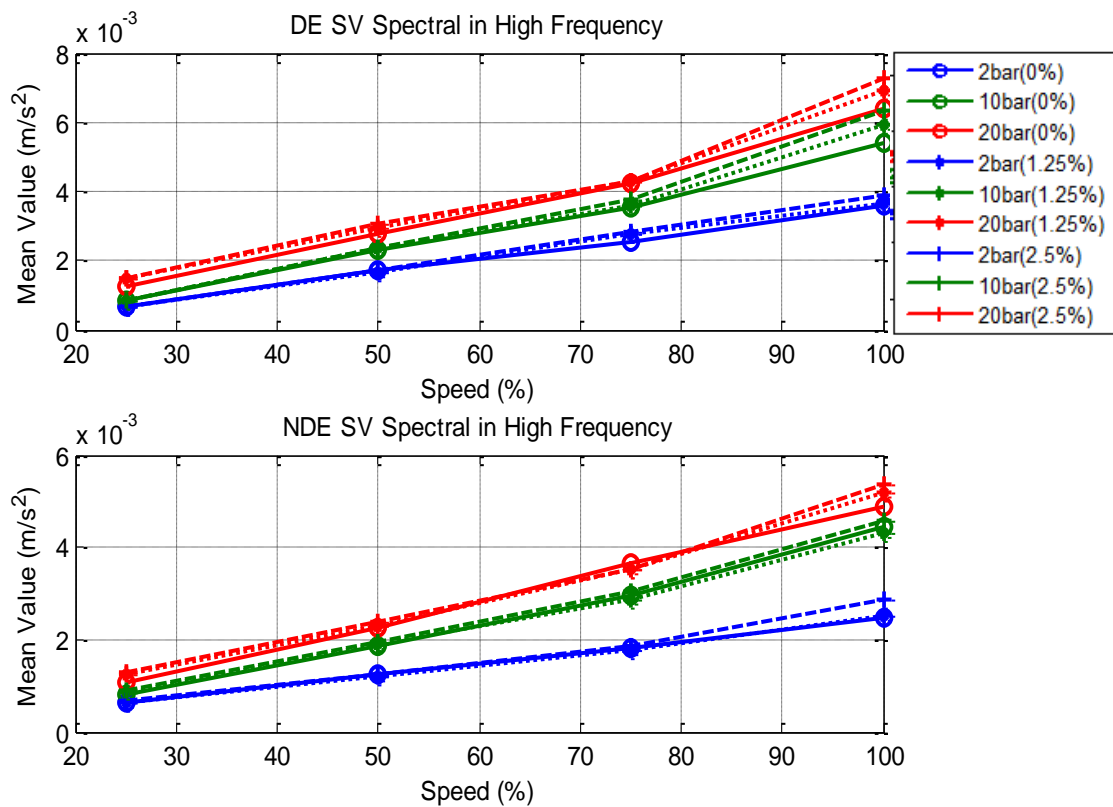


Figure 6. 28 SV mean spectrum 7 kHz to 9 kHz for radial load of 10 bar, maximum speed and three levels of water contaminant

Figure 6.28 again shows a positive correlation between speed and radial load against mean of the SV signal for the high frequency band. However the figure shows that there are no significant differences in amplitude response with increasing water contaminant in the lubricant.

6.3.2 Airborne sound characteristics

Figure 6.29 shows the time-domain AS response for a radial load of 10 bar at maximum speed with different water contaminant concentrations in the lubricant (0%, 1.25% and 2.5% (vol/vol)).

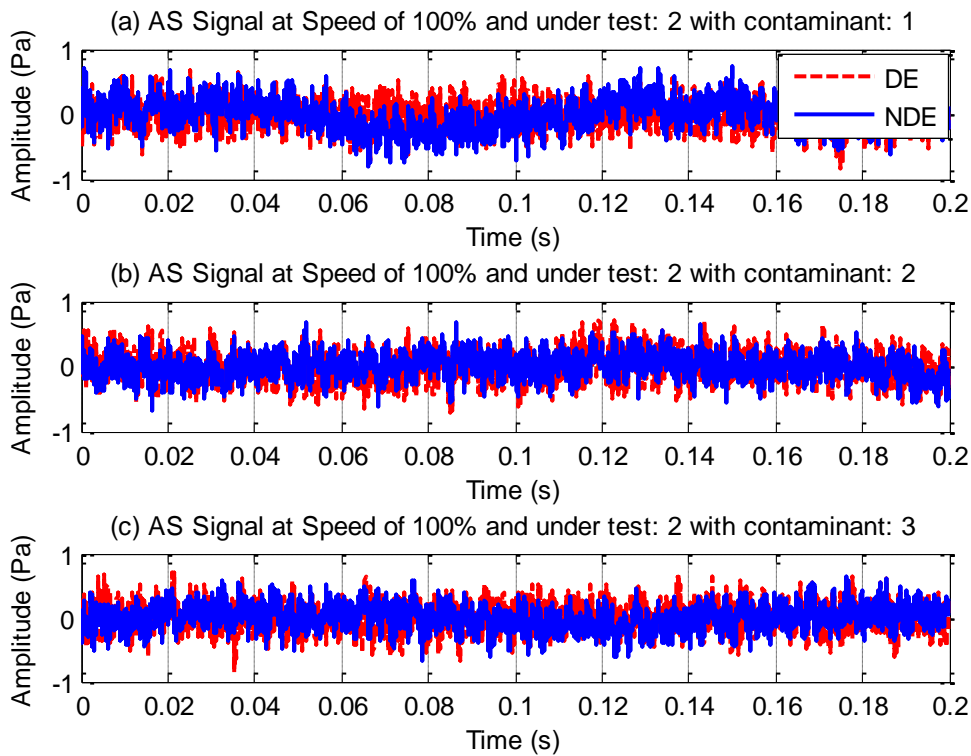


Figure 6. 29 AS signal for three levels of water contaminant concentration, 10 bar radial load at maximum speed

Figure 6.29 shows no significant difference in SV signal pattern regarding water contaminant in the lubricant.

Figure 6.30 is a plot of the relationship between RMS value of the AS signal with three levels of water concentration for DE and NDE bearings with three radial loads and four speeds. It is clear that the results obtained are generally similar to those obtained from previous experiments. There is no consistent relationship between increase in speed and AS RMS amplitude, nor are there any significant changes in AS RMS amplitude with either radial load or concentration of water contaminant.

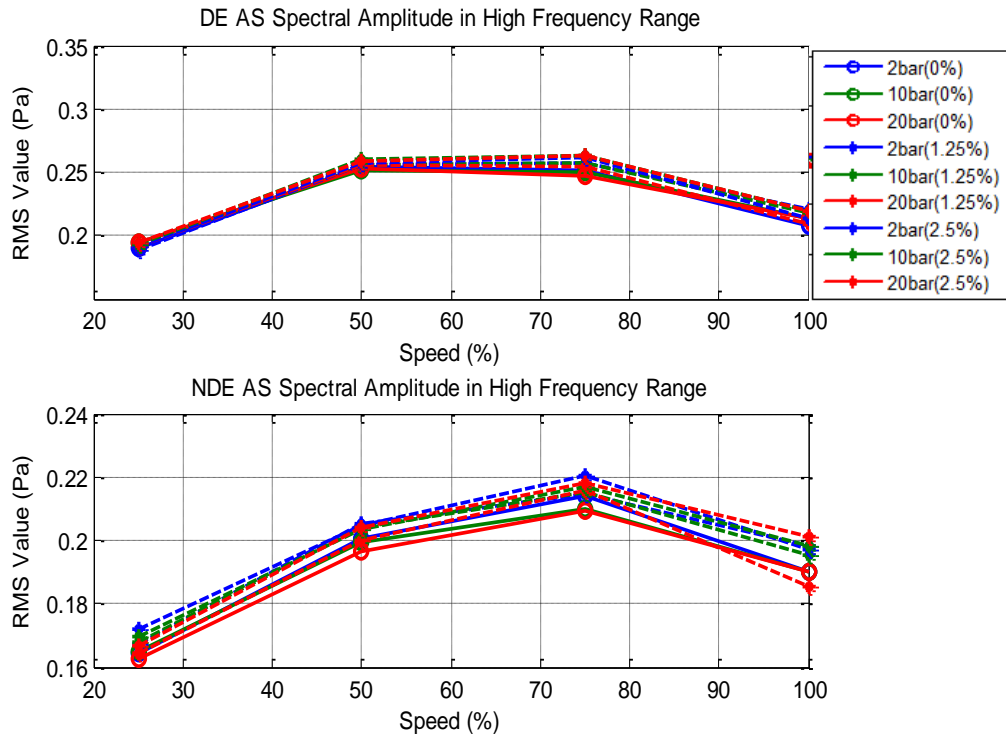


Figure 6. 30 AS RMS from raw signal in different load, speed and water contaminant concentration

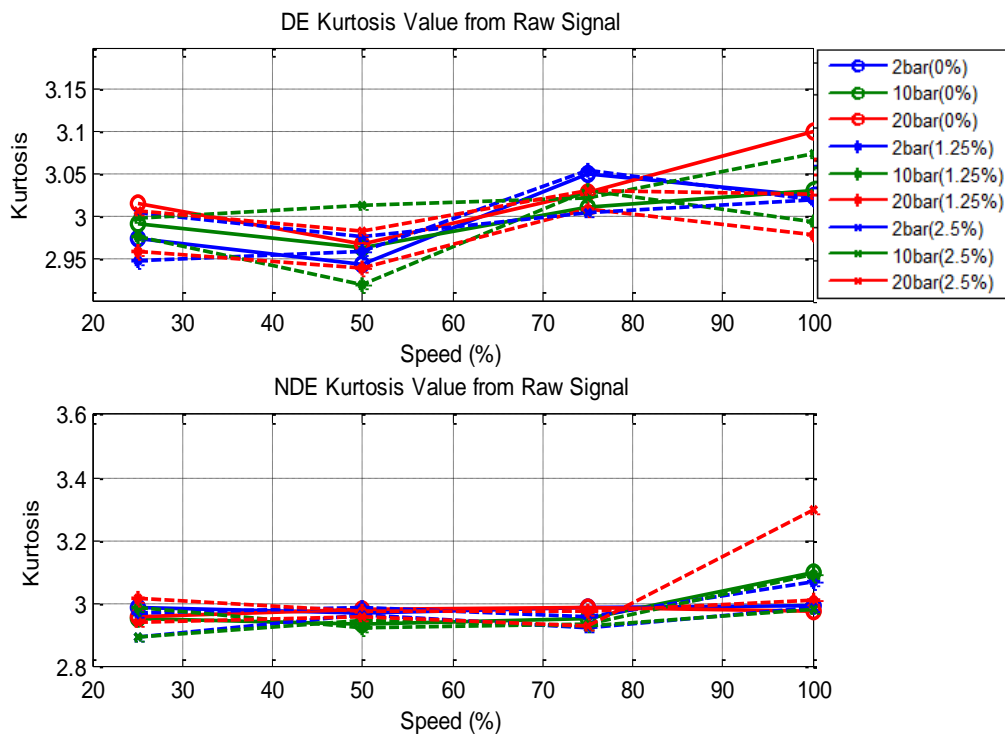


Figure 6. 31 Kurtosis value of in different load, speed and water contaminant concentration

Figure 6.31 shows the Kurtosis for the raw AS signal for the three levels of lubricant contamination for the three radial loads and four speeds.

The results obtained show that there is no significant difference in Kurtosis value regarding variation of water contaminant concentration. Speed has no significant effect on the Kurtosis value for either DE or NDE bearings. The effect of variation in radial load and level of water contaminant on the Kurtosis cannot be identified. Overall the Kurtosis value for both DE and NDE bearings was between 2.9 and 3.3 so the AS data had a Gaussian distribution, but the Kurtosis analysis cannot identify the influence of water contaminant in the lubricant.

6.3.2.2 Frequency domain analysis

Figure 6.32 is AS spectrum for DE and NDE bearings for three different concentrations of water in the lubricant under 10 bar radial load at 50% maximum speed. Figure 6.33 is the corresponding AS spectrum but with maximum speed.

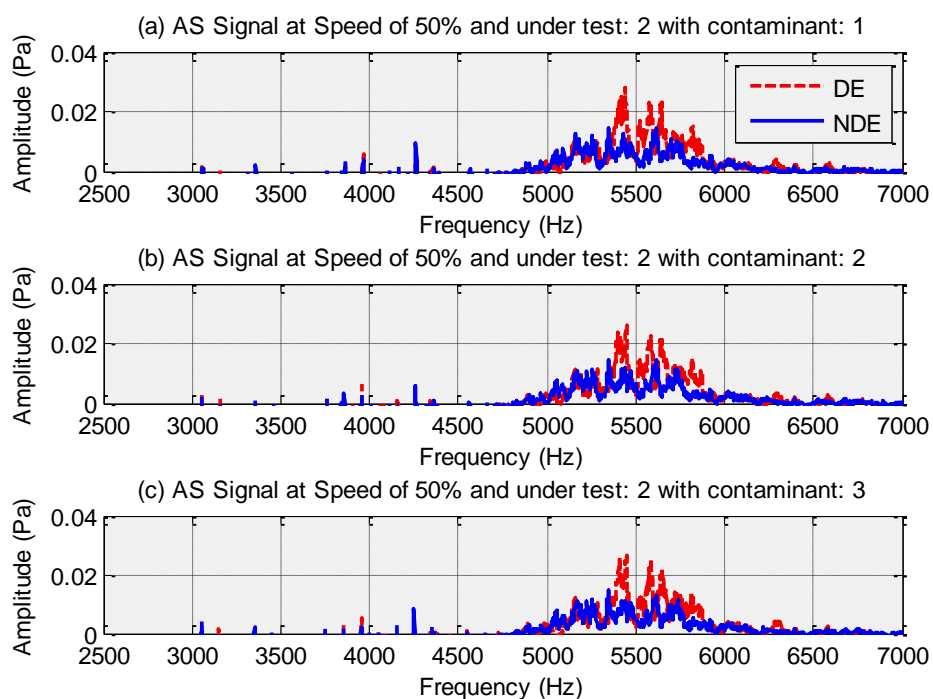


Figure 6. 32 AS spectrum under 10bar radial load at 50% speed with different water contaminant concentration

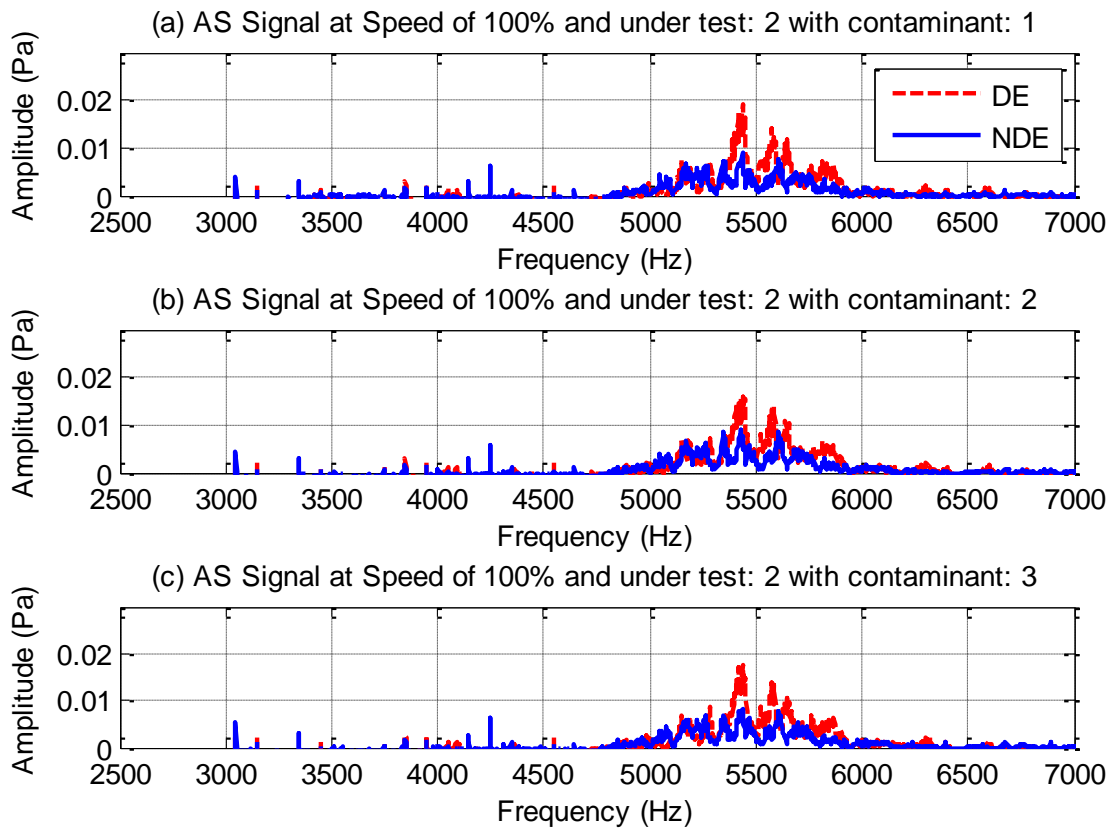


Figure 6. 33 AS spectrum under 10bar radial load at 100% speed with different water contaminant concentration

The spectra show the high amplitudes are dominant between 5.0 kHz to 6.0 kHz with the highest amplitude at 5.4 kHz. The influence of contaminant to the AS amplitude is difficult to be identified.

Figure 6.34 shows the mean amplitude for the high frequency band, 7 kHz to 18 kHz, of the AS spectrum for three radial loads, four speeds and three levels of contaminant.

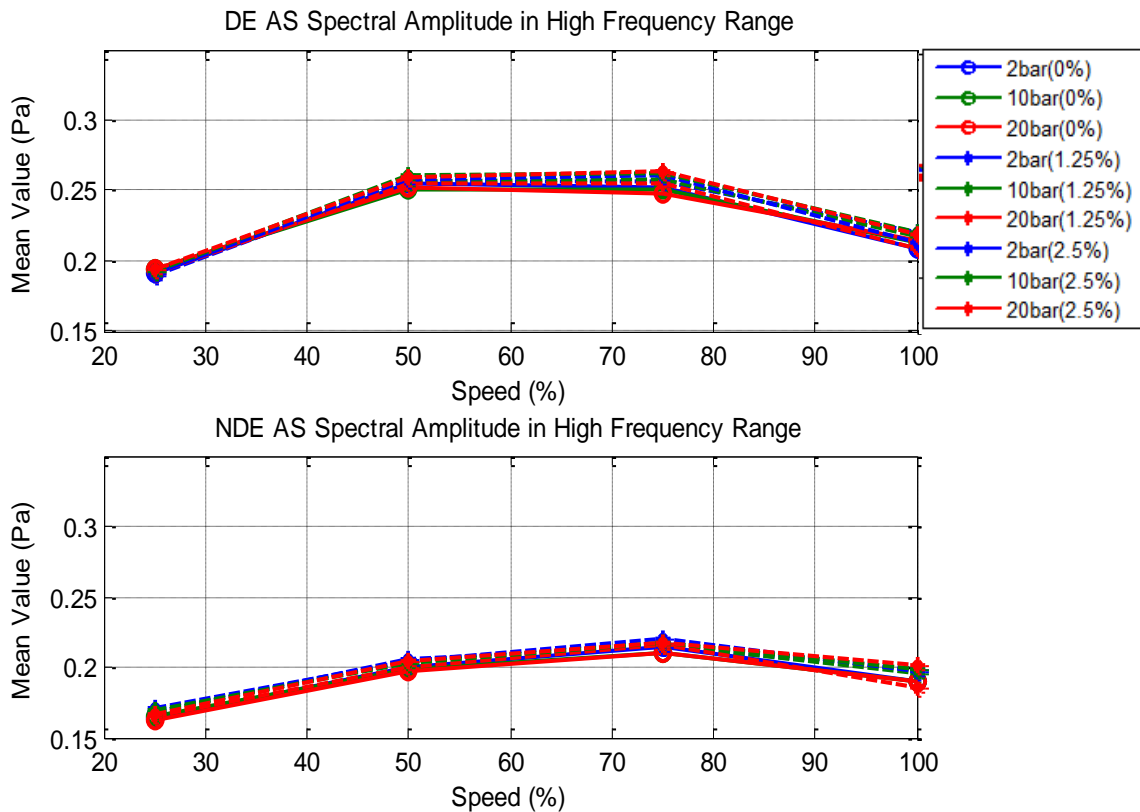


Figure 6. 34 AS mean spectrum with different water contaminant concentration under 10bar radial load and 100% speed

The results obtained are very similar to those obtained earlier, see Figure 6.30. There appears to be no significant change in mean amplitude for this high frequency band with change in radial loading or change in level of contaminant. There is some change in mean value with change in speed but this is not consistent and not useful for the detection of level of contaminant. It is concluded that the AS mean value measurement analysis cannot be used to monitor presence of water contaminant in the journal bearing lubricant.

6.3.3 Acoustic emission characteristics

Figures 6.35 and 6.36 are the time-domains of the raw AE signals for the DE and NDE bearings with water contaminant levels of 0%, 1.25% and 2.5% under different radial loads at 50% and 100% of maximum speed.

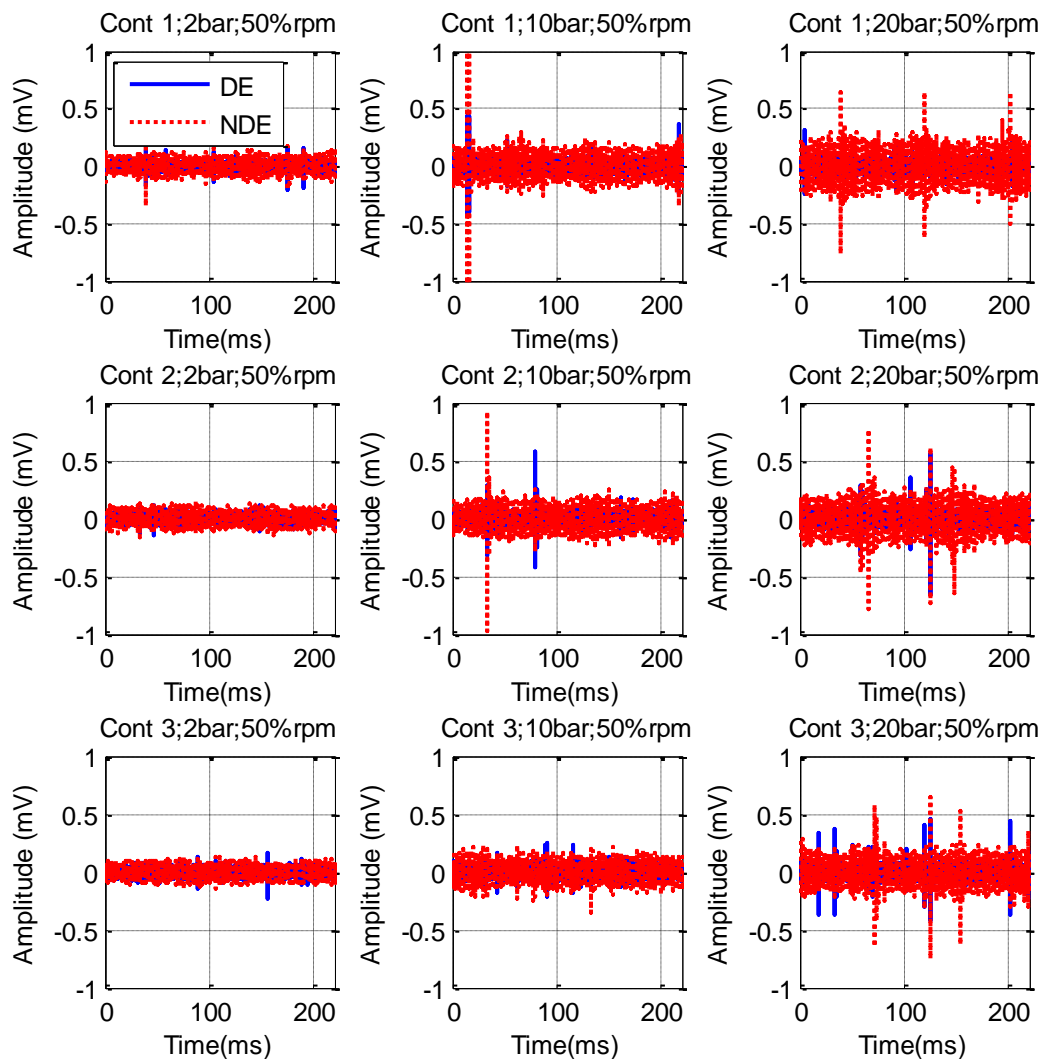


Figure 6.35 signal under different levels of water contamination and load at 50% speed

Figure 6.35 and 6.36 show that the AE signal is both continuous and burst type. The amplitude of the signal clearly and significantly increased with both speed and radial load. The figures also shows that increasing the level of water contaminant in lubrication system create higher amplitude and number of impulse of signal. This increasing of impulse is caused by increasing of asperity contact between surface bearing and shaft.

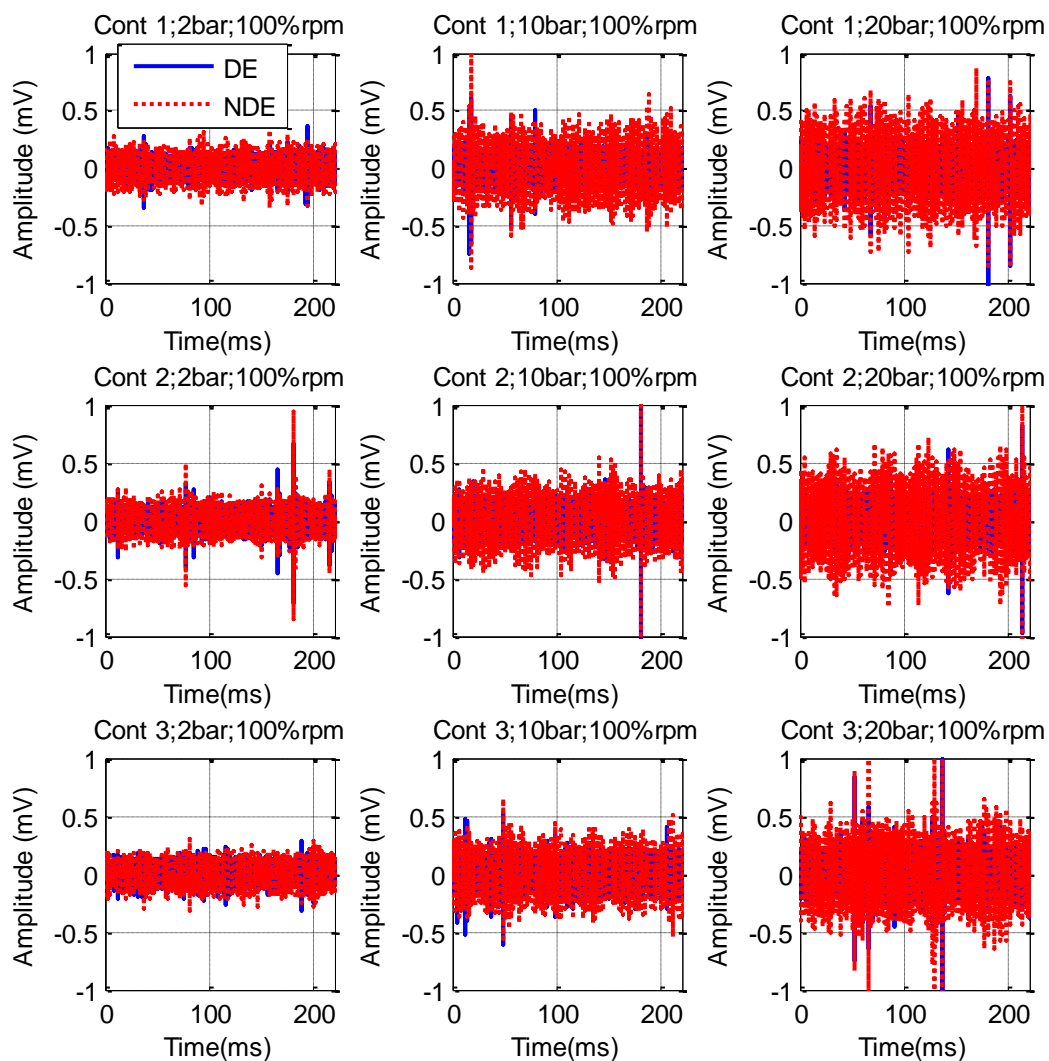


Figure 6. 36 AE signal under different levels of water contamination, and load at 100% speed

Obviously, the direct comparison between AE signal for 0%, 1.25% and 2.5% water contaminant in the lubricant confirms the clear differences between the AE waveforms both the amplitude and impulsive nature of the events forming the signal.

RMS of the AE raw signal from the DE and NDE bearings for four speeds, three radial loads and three level of water contaminant in the lubricant is shown in the Figures 6.37 and 6.38.

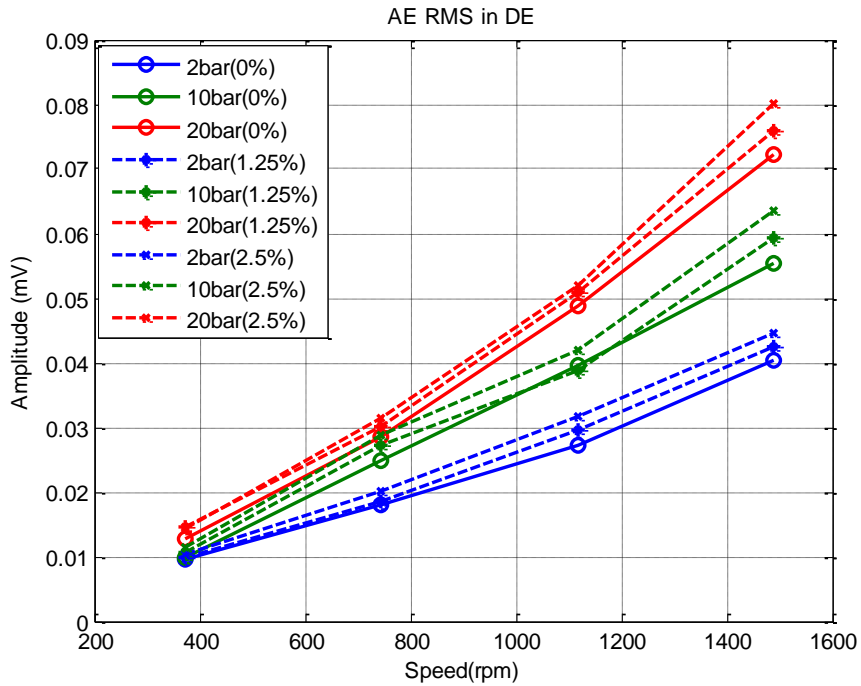


Figure 6. 37 AE RMS from raw signal under speed, radial load and different water contaminant concentration.

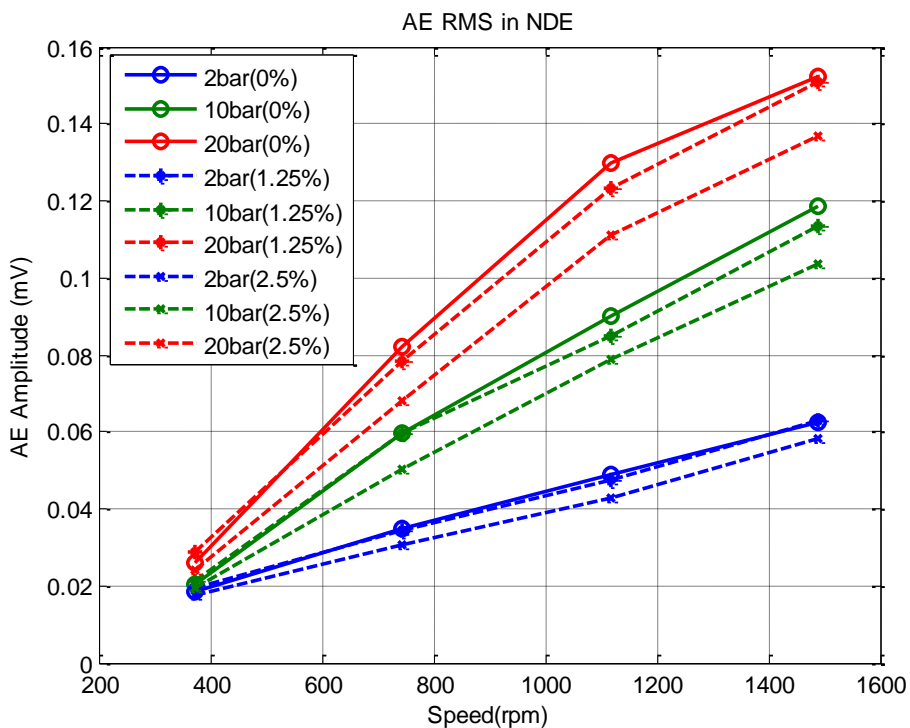


Figure 6. 38 AE RMS from raw signal for NDE bearings for three radial load, four speeds and three water contaminant concentrations.

Figures 6.37 and 6.38 confirm that speed and radial load have a positive correlation with AE RMS response. It can be seen that an increase in the level of concentration of water in the lubricant generate higher amplitude in RMS value in DE bearing, but in NDE bearing indicate that influence increasing of water contaminant to the RMS amplitude value is not consistent.

AE spectra generated by the DE and NDE bearings under three radial loads and three levels of water contaminant concentrations at 100% speed maximum speed at frequency range 1-100 kHz and 100 kHz-500 kHz can be seen in Figures 6.39, and 6.40.

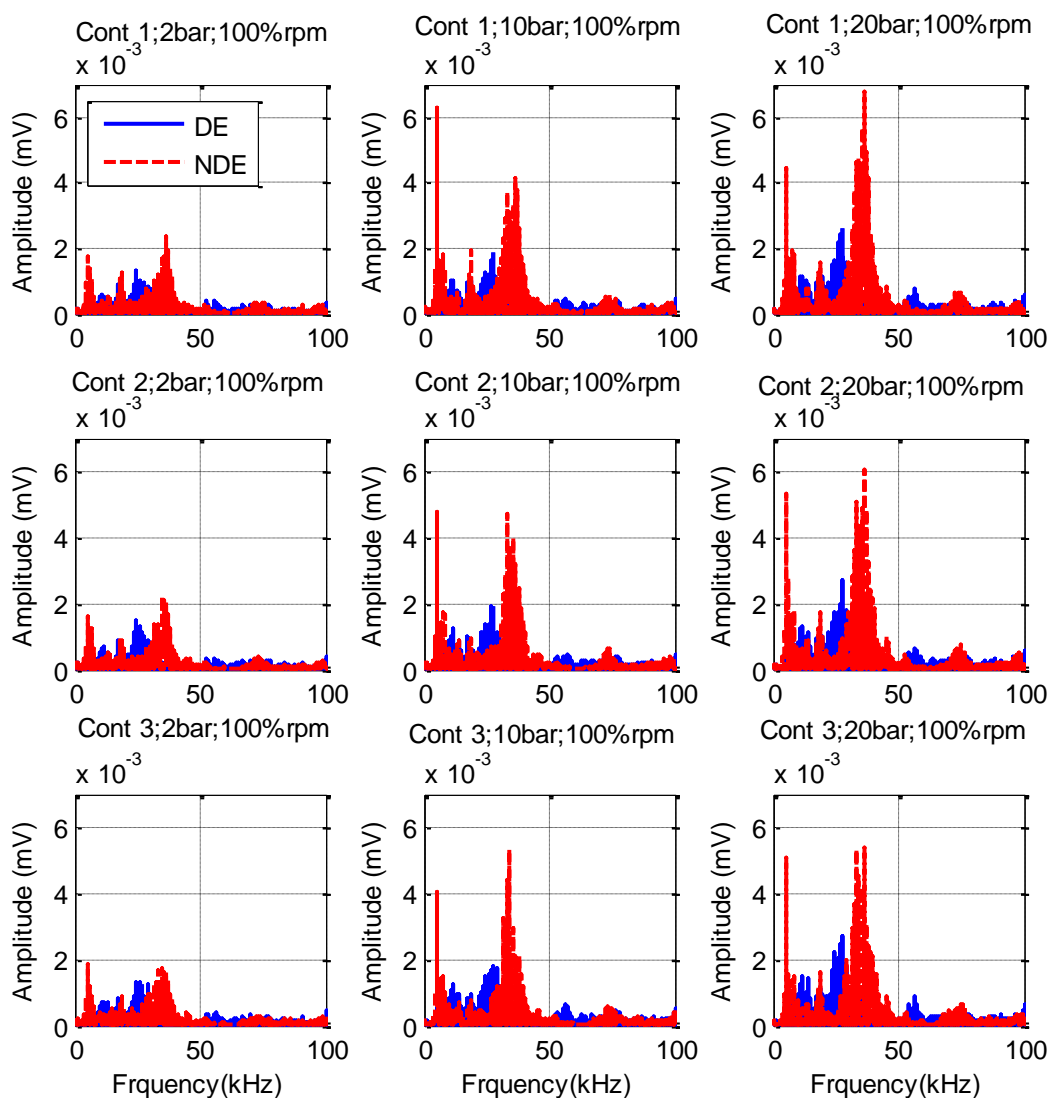


Figure 6. 39 AE spectrum under radial load and different water contaminant concentration at 100% speed.

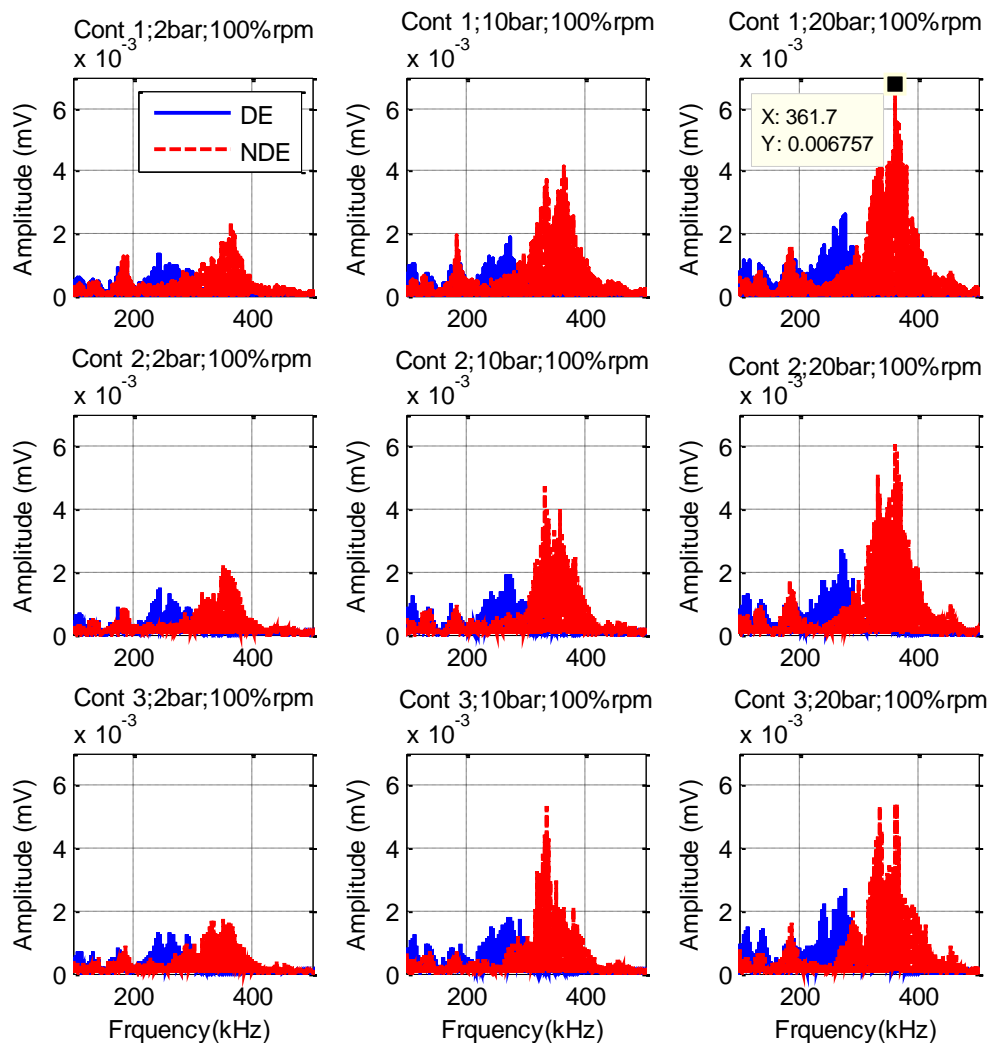


Figure 6. 40 AE spectrum under radial load and different water contaminant concentration at 100% speed in frequency range 100kHz-500kHz.

Figures 6.39 and 6.40 show that increasing the radial load from 2 bar to 10 bar and to 20 bar very clearly increases the peak amplitudes of the AE spectrum, particularly at frequency 36.5 kHz for AE spectrum in frequency range 1-100kHz and at frequency 361.7kHz for spectrum in frequency range 100-500kHz. The effect of increase of speed also has a significant effect on the peak amplitudes of AE spectrum. However, any effect due to water contaminant concentration in the lubrication is difficult to identify at either speed.

Figure 6.41 is the plot of mean value of AE signal amplitude for the frequency range 20 kHz to 90 kHz for four speeds, three radial loads and three levels of water contaminant concentration in the lubricant. It can be seen that mean AE amplitude increases with rotational speed and radial load. The effect of the level of water in the lubricant on the AE mean amplitude is small but can be seen for all three loads at higher speeds. For lower speeds the differences cannot be significant because the lines meet and even cross each other.

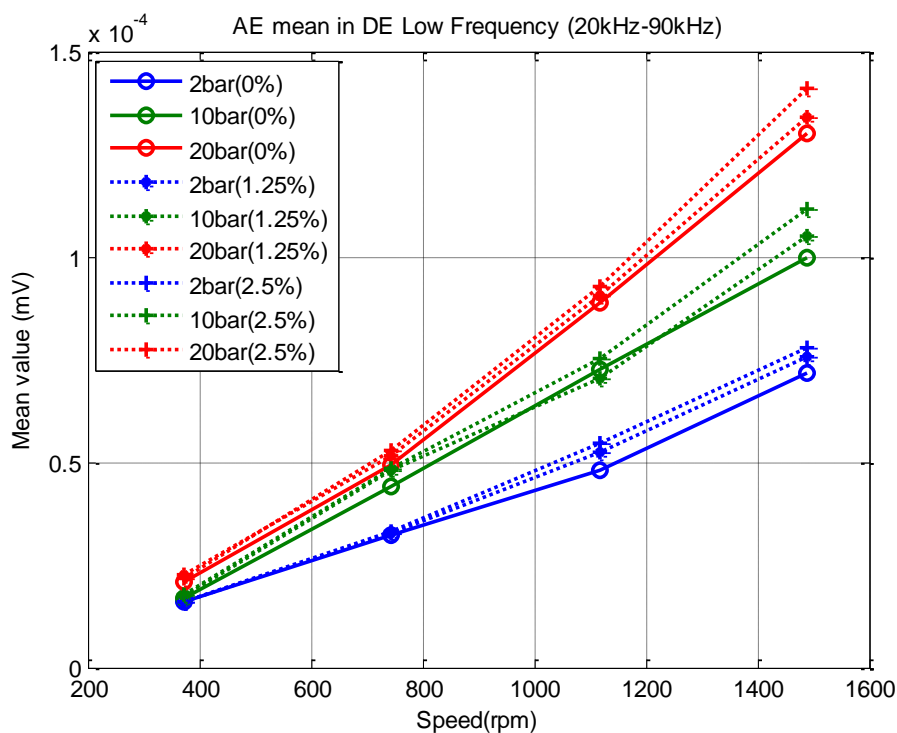


Figure 6. 41 AE mean value in DE bearing under different speed, radial load and with water contamination at frequency range 20 kHz-90 kHz

Figure 6.42 is the plot of mean AE signal amplitude for the frequency range 90 kHz to 320 kHz for four speeds, three radial loads and three levels of water contaminant concentration in the lubricant. Once again it can be seen that mean AE amplitude increases with rotational speed and radial load, but now there is some overlap in these values at lower speeds. The effect of the level of water in the lubricant on the AE mean amplitude can be detected at maximum speed but is not significant below that except at the lowest load (2 bar).

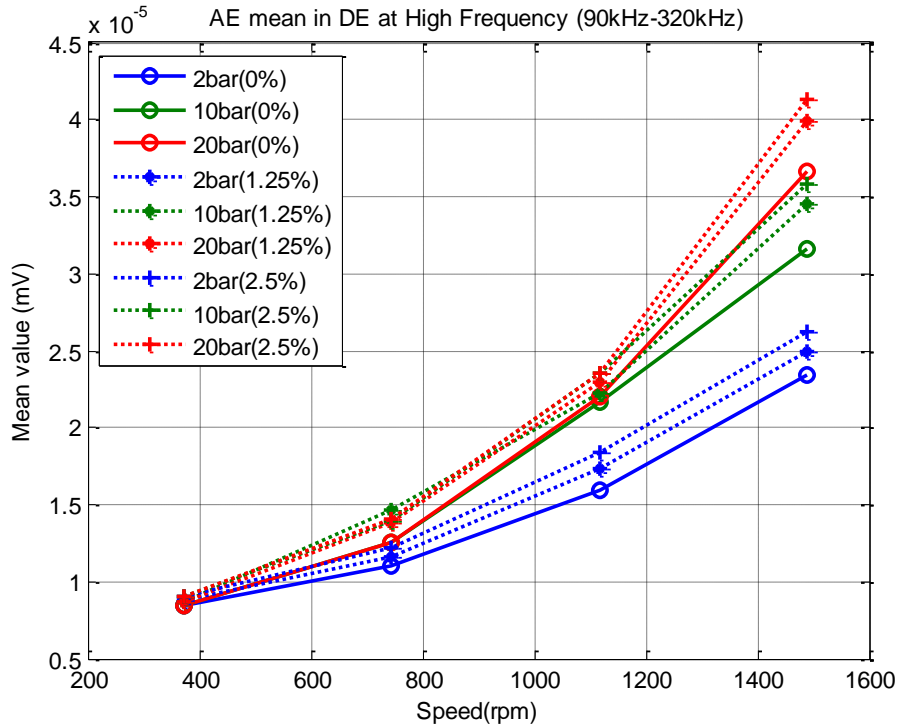


Figure 6. 42 AE mean value in DE bearing under different speed, radial load and with water contamination at frequency range 90kHz-320kHz

Conclusion to be drawn from comparisons of SV, AS and AE characteristics on presence of water contaminant in the bearing lubricant are as follows:

SV raw time-domain and frequency domain signals cannot distinguish between the water contaminated lubricant and uncontaminated lubricant. However, SV RMS measurements using both low and high frequency bands can detect significant differences in the signals when water contaminant is present in the DE bearing.

RMS analysis of the AE time-domain signal shows a positive correlation between water contaminant concentrations in the lubricant and RMS level for the signal from the DE bearing.

It was found that the level of water contamination in the lubricant significantly affected the mean value of the AE spectrum. The greater the level of contamination in the lubricant the greater the amplitude of the AE mean value for the frequency range 90 kHz-320 kHz.

The presence of water contaminant in the lubricant will affect its physical and chemical properties. This will include reducing its kinematic viscosity which will affect system stiffness, damping coefficient and friction coefficient which could affect the stability of the shaft movement. It will also affect the asperity contact area and numbers of asperities on opposing faces in contact with each other. Thus it would be expected that the introduction of water contaminant into the lubricant would increase the amplitude of the surface vibration and acoustic emission.

Further research should explore the specific effect of water contamination of the surface vibration and acoustic emission responses of a journal bearing with small water concentration in the lubricant.

6.4 Discussion of abnormal viscosity and water contaminated lubricant monitoring

The results obtained from monitoring water contaminated lubricant in a journal bearing through simultaneous surface vibration, airborne sound and acoustic emission measurement are:

6.4.1 Viscosity changing of lubricant

Time domain analysis of the surface vibration, airborne sound and acoustic emission are all unable to identify any changes of lubricant viscosity in the journal bearing.

The RMS values of the raw vibration signal of the surface vibration and airborne sound monitoring are also unable to identify changes in the viscosity of the lubricant. The RMS of the acoustic emission raw signal on the other hand was able to identify changes in the viscosity of lubricants in the journal bearings, but not consistently.

The kurtosis analysis used for the three monitoring techniques was unable to detect changes of lubricant viscosity in the journal bearing.

Spectrum analysis for surface vibration, airborne sound and acoustic emission shows the effect of changing the viscosity lubricant on bearing journal is not significant so that the spectrum analysis is also unable to detect any changes in viscosity. However the band pass spectra of the acoustic emission signal, at both lower and higher frequencies, are able to detect changes in the viscosity of lubricants in journal bearings.

The comparison of vibration spectrum between using ISO VG 32 to ISO VG 68 (Figure 6.43) shows that with higher viscosity generates smaller amplitude peaks in the spectrum. This is consistent with theory that by using a higher viscosity of lubricant the damping coefficient will increase and will reduce surface to surface contact, decrease the stiffness of the system and reduce the amplitude of the frequency response.

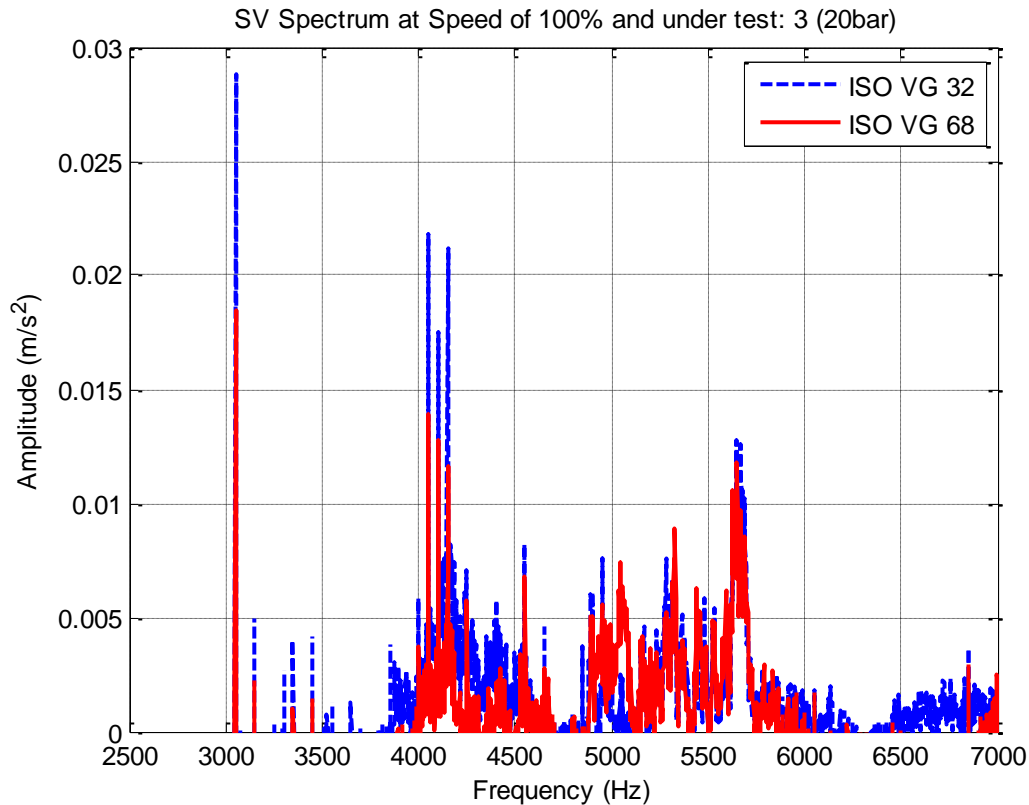


Figure 6. 43 SV spectrum under 20 bar, 100% and in different viscosity

The frequency analysis shows that the peak value appears at two frequencies 4.1 kHz and 5.6 kHz. The effect of lubricant viscosity changes appear significant at peak value that occur at 5.6kHz.

The mean value of the AE spectrum is capable of identifying the presence of lubricant viscosity change in the journal bearing.

6.4.2 Water contaminant in lubricant

The tests have shown that time domain analyses of surface vibration and airborne sound are unable to identify water contaminant in the lubricant.

Time domain analysis of the AE signal was able to identify the difference between water contaminated and non-contaminated lubricant in the journal bearing. The acoustic emission signal of water contaminated lubricant has more burst and hits than the non-water contaminated lubricant signal.

RMS value of raw signals for surface vibration and airborne sound were unable to detect the presence of water contaminant in the lubricant. However the RMS value for the raw AE signal was able to distinguish the influence of the concentration of water contaminant lubricant in the journal bearing.

Kurtosis analysis for the three techniques could not identify water contamination in the lubricant. The Kurtosis values for surface vibration and airborne sound were close to the value of 3.

Spectrum analysis for surface vibration, airborne sound and acoustic emission was not able to identify the presence of water contaminant in the lubricant.

Analysis of surface vibration and acoustic emission signals showed the mean value was able to identify a change in the concentration of water in the lubricant at all three loads used. The airborne sound mean value was not able to identify differences of concentration of water in the lubricant.

The surface vibration spectrum contained high amplitude peaks in the frequency ranges 3.9 kHz to 4.5 kHz and 5 kHz to 6 kHz. Individual peak amplitudes occurred at 3.1 kHz, 4.1 kHz and 5.7 kHz. The highest amplitude of the spectrum airborne sound arise at a frequency of 5.7 kHz.

The acoustic emission spectrum contains high amplitude peaks in the frequency ranges 3 kHz to 5.4 kHz and 12 kHz to 60 kHz. Peak values occurred at frequencies of 5.3 kHz and 36.5 kHz. However, specific frequency characteristics for water contaminant in the lubricant could not be identified clearly.

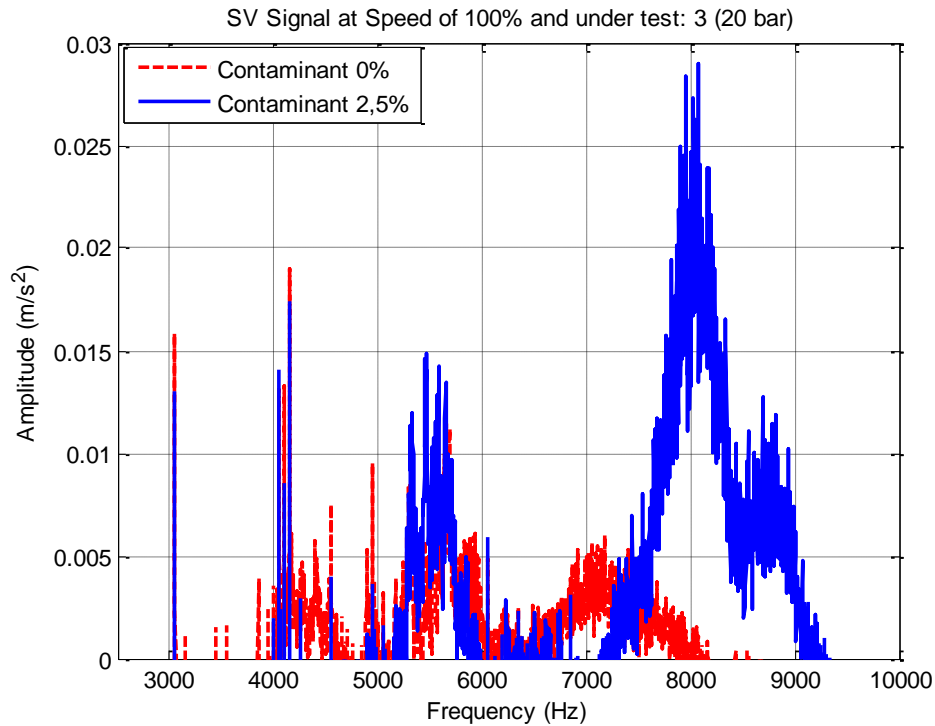


Figure 6. 44 Vibration spectrum under 20 bar, 100% and in different contaminant

The Figure 6.44 is a comparison of vibration spectra of a journal bearing using lubricant without contaminant and with 2.5% water contaminant in the lubricant. The spectra are significantly different. The water contaminated lubricants has a lower damping factor so the amplitude of the spectral peaks will increase. Also because lubricant contaminated with water has increases stiffness the frequency of the peaks will increase.

6.5 Summary of lubricant quality monitoring

Based on the lubricant quality monitoring experiment, analysis and discussion it can be summarized as:

6.5.1 The effect of changing viscosity on the surface vibration, airborne sound and acoustic emission responses.

The effect of changing viscosity on the surface vibration was as follows:

- In the viscosity variation also there is a positive correlation between speed and RMS value from the raw signal but effect of radial load variation is difficult to be determined.

-
- SV Kurtosis value was close to that of Gaussian the data distribution but was not influenced by change in viscosity.
 - High amplitudes also were dominant in the frequency range between 3 kHz and 6 kHz.
 - High amplitude peaks also occurred at 3.05 kHz, 4.1 kHz and 5.6 kHz. There is some influence in the SV spectrum with change in viscosity with higher viscosity generating lower amplitude vibrations.

Effect of viscosity variation of the airborne sound responses as follows:

- There is positive correlation of speed and RMS value until the speed reached 75% of maximum speed after which the RMS value decreased.
- The influence of viscosity and radial load on the RMS value of the raw signal is difficult to be distinguished.
- Kurtosis values due to speed variation are to Gaussian distribution but did not identify the influence of viscosity or change in radial load.
- High amplitude appear dominant in the frequency range from 4.25 kHz to 6 kHz.
- Highest amplitude peak lies at a frequency 5.4 kHz.
- The influence of viscosity and change in radial load on the mean value of the spectrum is difficult to distinguish

Effect of changing viscosity on acoustic emission response:

- There is a positive correlation between of speed and radial load and the RMS value from raw signal.
- The influence of change in viscosity on the RMS value of the raw signal is clear but less consistent.
- Kurtosis values do not match with Gaussian distribution data because of AE signal burst type.
- High amplitudes were dominant in the frequency range between 250 kHz and 425 kHz. Peak amplitudes occurred 366.2 kHz.
- The change to the spectrum mean value with change in viscosity was very clear and significant at frequencies 20kHz up to 90kHz and 90kHz up to 320kHz

6.5.2. The effect of water contaminant concentration in the lubricant on surface vibration, airborne sound and acoustic emission responses.

Influence of water contaminant concentration on surface vibration responses:

- The effect of speed variation on the RMS value from the raw signal was significant but the influence of radial load and water contaminant could not be distinguished.
- Kurtosis value cannot be used for identifying the water contaminant in lubricant
- High amplitudes appear in the frequency spectrum between 3 kHz to 6 kHz, but dominate in the frequency range between 4 kHz to 6 kHz.
- Highest peak amplitude was located at 5.6 kHz followed 3.2 kHz and 4.2 kHz
- Greater water concentration in the lubricant gave rise to higher amplitudes in the frequency spectrum of the vibration responses.

The effect of water contaminant concentration on the airborne sound response:

- Effect of radial load and water contaminant on the RMS value of the raw signal could not be distinguished but the influence of speed was clear, as described above.
- Kurtosis value showed a Gaussian distribution pattern but could not be used to determine the effects of radial load or water contaminant.
- High amplitudes dominate the frequency spectrum in the range between 4.8 kHz and 6.1 kHz. The highest peak amplitude is at 5.4 kHz.
- The effect of radial load and contaminant on the mean value of the spectrum at either low or high frequencies was not discernible.

Effect of water contaminant concentration on the acoustic emission:

- The effect of speed and radial load on the RMS value of raw signal was clear and significant.
- Effect of water contaminant on AE RMS value of the raw signal was clearly visible but less significant.
- High amplitudes dominate the spectrum in the frequency range between 250 kHz to 425 kHz and highest peak amplitude occur at 361.7 kHz .

-
- The effect speed, radial load and water contaminant on the spectrum mean value in both the low frequency and high frequency bands was clear and significant, although not large. Higher water contaminant in the lubricant generates a higher spectrum mean value response.
 - The effect of the water contaminant can be detected by surface vibration and acoustic emission monitoring technique.

CHAPTER SEVEN

SURFACE SCRATCH MONITORING

7.1 Introduction

There are many causes that lead to a bearing failure including poor journal surface finish due to such factors as inadequate lubrication with foreign solid particles embedded in the bearing surface. A consequence will be poor surface contacts or metal to metal contact which can generate large frictional forces resulting from resistance to shear of local contact points which oppose relative sliding motion. At these points rapid wear occurs and transfer of material to the counter surface which can result in deterioration of the bearing surface. Where hard particles of material contaminate the lubricant this can cause significant scratching which will affect the bearing journal's surface roughness, friction coefficient and stiffness. Scratches will influence surface vibration (SV), acoustic emission (AE) and airborne sound (AS) responses.

This chapter examines the characteristics of surface vibration, airborne sound and acoustic emission signals obtained when the surfaces of a self-aligning spherical journal are seeded with known scratches.

7.2 Test method

All the tests were carried out with the test rig arrangement and sensors described in Chapter 4.2. The bearing containing the seeded scratched surface was made in the NDE bearing; the healthy bearing was installed on the DE side. The radial loadings were 2 bar, 10 bar and 20 bar and the rotational speeds: 25%, 50%, 75% and 100% of maximum speed (1450 rpm). ISO VG 32 lubricant was used in both NDE and DE journal bearings. A description of the circumferential scratches seeded on the inner surface (0.05 mm deep and 0.1 mm wide) is given in Section 4.5 and Figure 4.9. As previously the temperature at which the tests were performed was 22.5 °C.

The analysis is done by comparing statistical parameters obtained from the time and frequency domains of the surface; vibration; airborne sound and AE signal spectra for the scratched bearing and reference bearing.

Surface vibration, airborne sound and AE characteristic for bearing reference has been obtained in previous experiments (see chapter five).

The results of the experiment are grouped into surface vibration, airborne and acoustic emission measurements.

7.3 Surface vibration analysis

7.3.1 Time domain analysis

Figure 7.1 shows SV signals in the time domain for the healthy or normal self-aligning journal bearing and scratched bearing for three radial loads at 100% of speed.

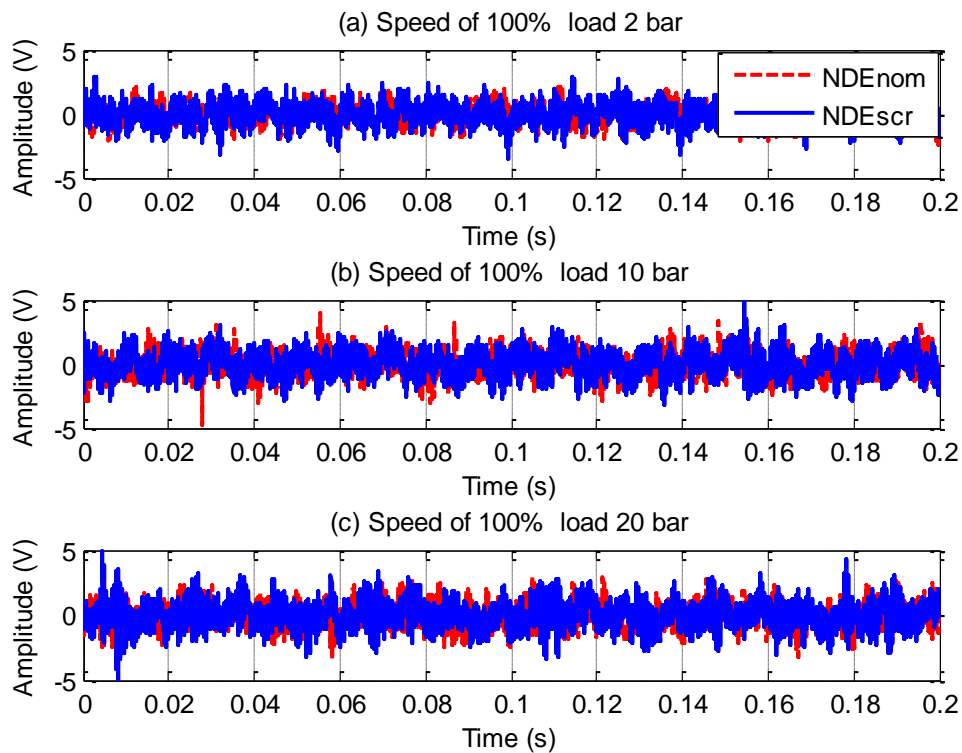


Figure 7. 1 SV signals for a normal bearing and a scratched bearing under different radial load at 100% speed.

The difference signals between the two bearings conditions are difficult to distinguish. The relationship between speed, radial load and bearing condition of the surface vibration RMS value from raw signal is presented in Figure 7.2.

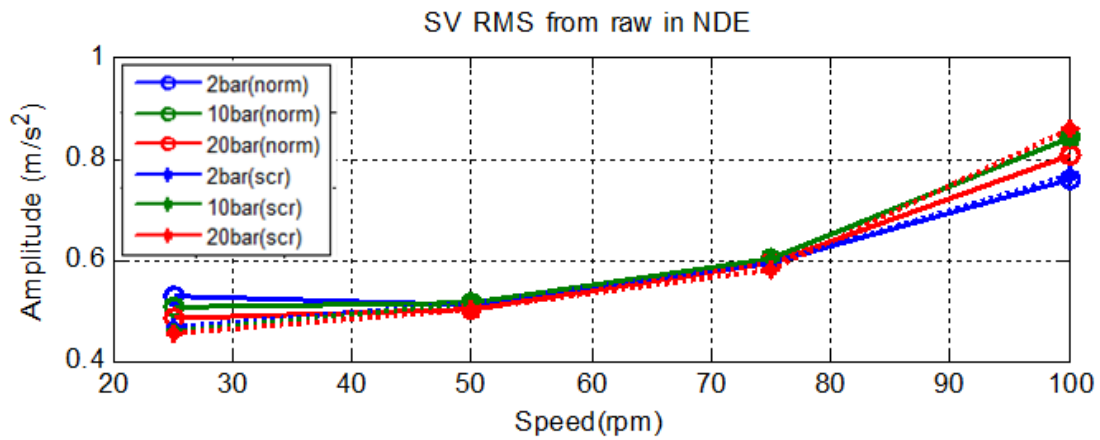


Figure 7. 2 RMS value from raw signal in different load, speed and bearing condition

Figure 7. 2 again show that the effects for speed and load on the RMS as previously noted. There is no clear difference in signals when the scratch is introduced.

Figure 7. 3 shows the Kurtosis values obtained from the raw time domain signals for different radial load and speeds for scratched and normal bearings. For the NDE bearing there is a significant difference between unscratched bearing and bearing with scratches seeded into it only at maximum speed.

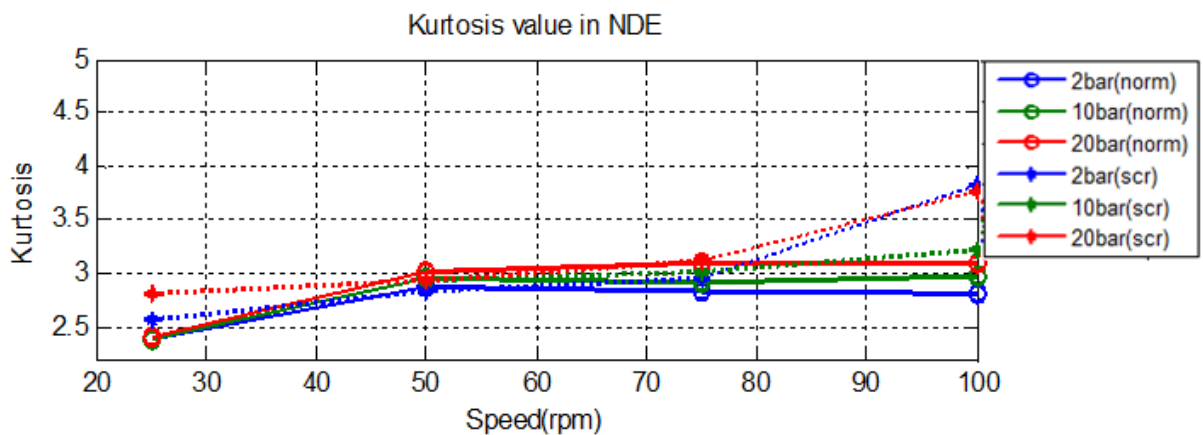


Figure 7. 3 Kurtosis value on bearing in different load, speed and bearing condition

The figure appears to show that generally the differences are not significant except at 100% full speed for loads 20 bar and 2 bar. Based on this analysis, Kurtosis analysis failed to identify clear differences between normal bearing and bearing with scratch fault.

The following analyses of the spectra are descriptive and comparative and include comparisons of mean amplitude for low and high frequency ranges.

7.3.2 Frequency domain analysis

SV response of the two bearings for three different radial loads at 100% speed is shown in Figure 7.4.

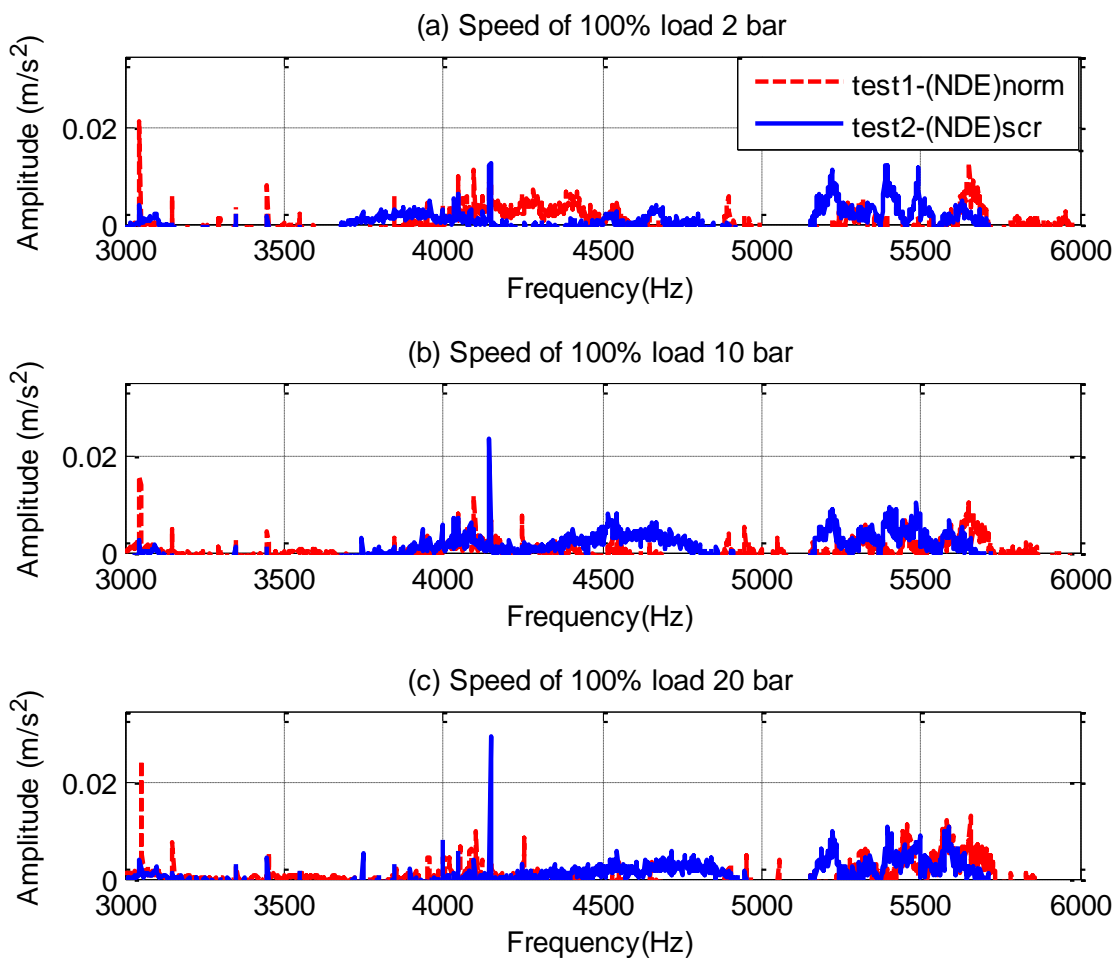


Figure 7. 4 SV spectrum under different load and condition at 100% of speed

The figure shows that there are differences in the spectra between the two bearings especially in the frequency range between 3.7 kHz to 4.8 kHz.

Increasing radial load increases the peak 4.2 kHz for the scratched bearing, this increase originates from scratching. However, spectrum analysis was also not able to discern clearly the influence of the scratches on the SV spectrum response. Further analyses of speed, radial load and bearing condition on the mean SV value for the NDE bearing in the low frequency range (2 kHz – 6 kHz) and high frequency range (6 kHz-40 kHz) are shown in Figures 7.5 and 7.6.

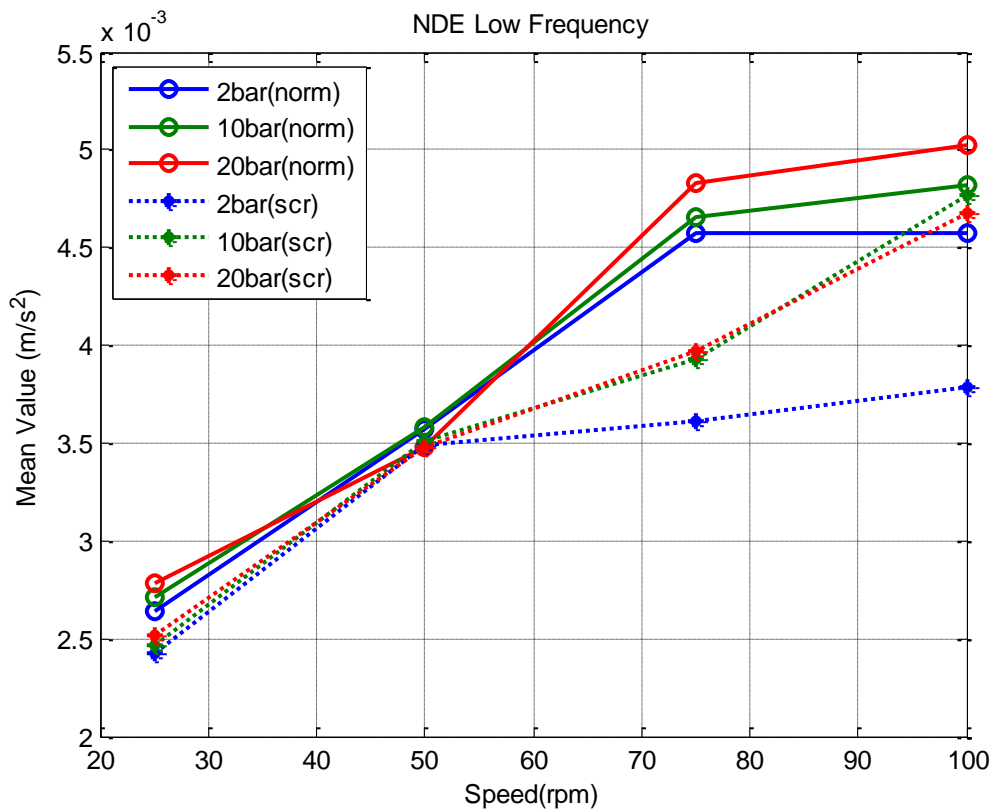


Figure 7. 5 SV mean value in bearing under different load, speed and bearing condition at low frequency range

Figure 7.5 shows the mean SV value for the low frequency band (2 kHz – 6 kHz) for normal and scratched bearings. The mean value for both bearings increases with speed. But SV mean value does not clearly and consistently distinguish between scratched and normal bearing. It is concluded that the mean SV value may not be appropriate to detect differences between normal and scratched bearings.

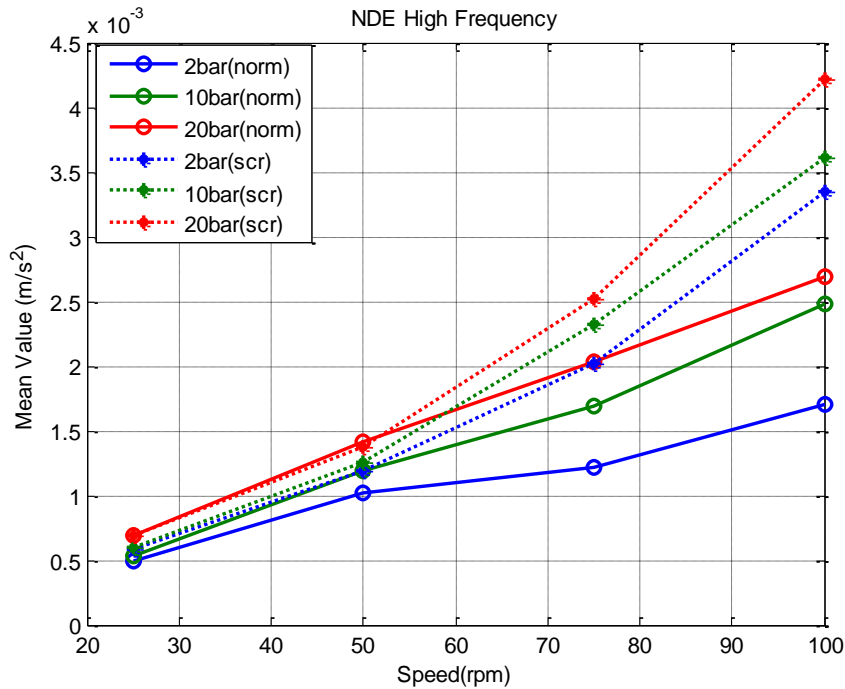


Figure 7. 6 SV mean value in bearing under different load, speed and bearing condition at high frequency range

The relationship between speed, radial load and bearing condition is presented in Figure 7.6 and shows that the mean value of the SV signal increases with radial load and with speed. Also a clear difference between the SV mean values for scratched and normal bearings can be seen. It is concluded that the mean value of the SV signal for the high frequency band (6 kHz-40 kHz) is a promising method of detecting scratched bearings. In this frequency range there is a significant different influence of scratching and normal bearing to the SV mean value. Vibration response due to scratching occurs at high frequency and randomly.

7.3 Airborne sound analysis

Monitoring airborne sound measurement for the normal and scratching bearing used time domain and frequency domain analyses, the results are presented below.

7.3.1 Time domain analysis

Figure 7.7 shows AS signal amplitude for the journal bearing when normal and scratched under three different radial loads for maximum speed. The figure does not show that any clear difference between the two bearings, thus the AS signals do not directly suitable to detect bearing failure due to surface scratches.

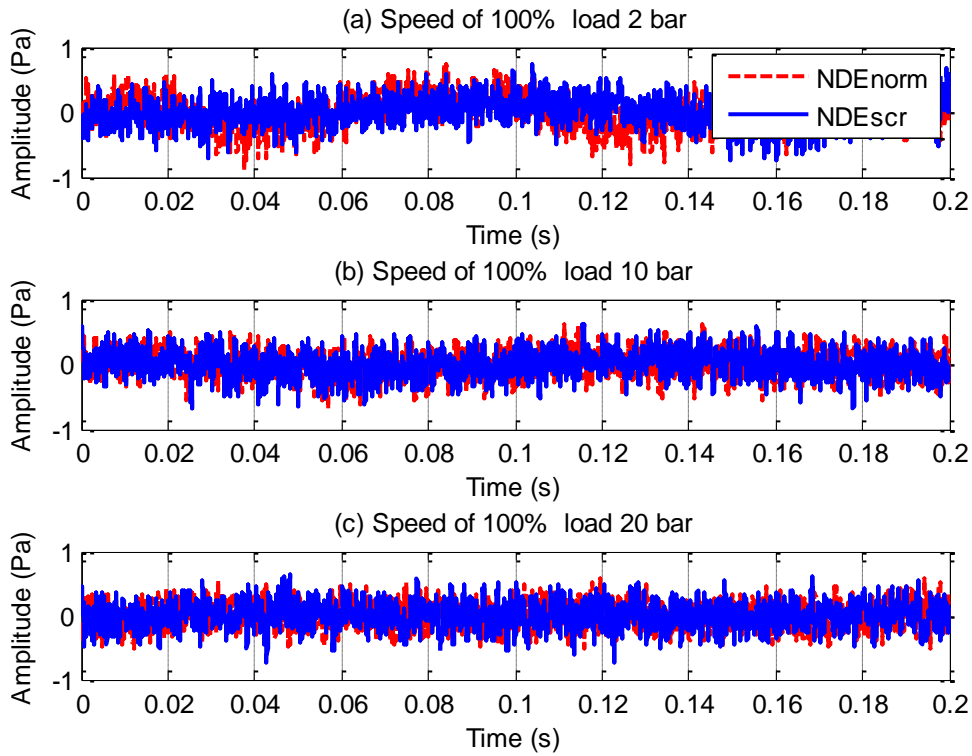


Figure 7. 7 AS signal different bearing condition and radial load at speed 100%

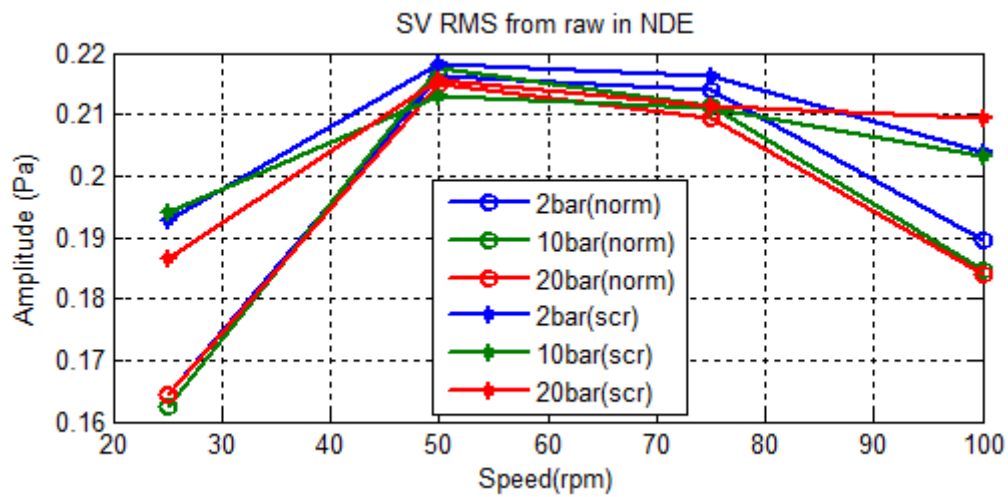


Figure 7. 8 AS RMS value from raw signal in bearing under different speed, radial load and bearing condition

Figure 7.8 shows the RMS value of the AS signal for three radial loads, a range of speeds for NDE bearing. The figure demonstrates that the RMS value of the AS signal cannot clearly and consistently differentiate the two bearings and so the AS time domain is deemed not suitable to detect bearing failure due to surface scratching.

Figure 7.9 shows the Kurtosis of the time domain of the RMS raw signal for both bearings with radial loading and speed.

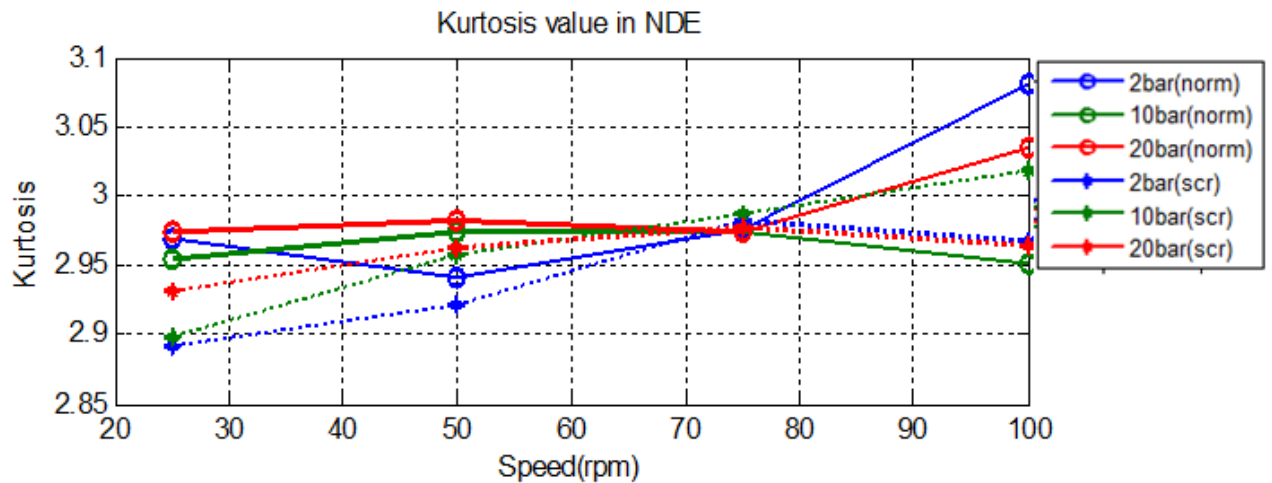


Figure 7. 9 Kurtosis value in bearing under different radial load, speed and bearing condition

Figure 7.9 shows that for NDE normal and scratched bearing cannot be distinguished clearly and consistently. Kurtosis values in NDE ranged from 2.9 to 3.1 which means the peaks in of the signal were close to a Gaussian distribution.

7.3.2 Frequency domain analysis

Figure 7.10 shows the AS spectra for scratched and normal bearings under different radial loads at 100% speed. It can be seen that the spectra for the raw AS signal cannot clearly differentiate between the healthy and scratched bearings over the range of speeds and loads tested. The highest amplitude in the spectra occurs in the frequency band between 4.75 kHz and 6.5 kHz.

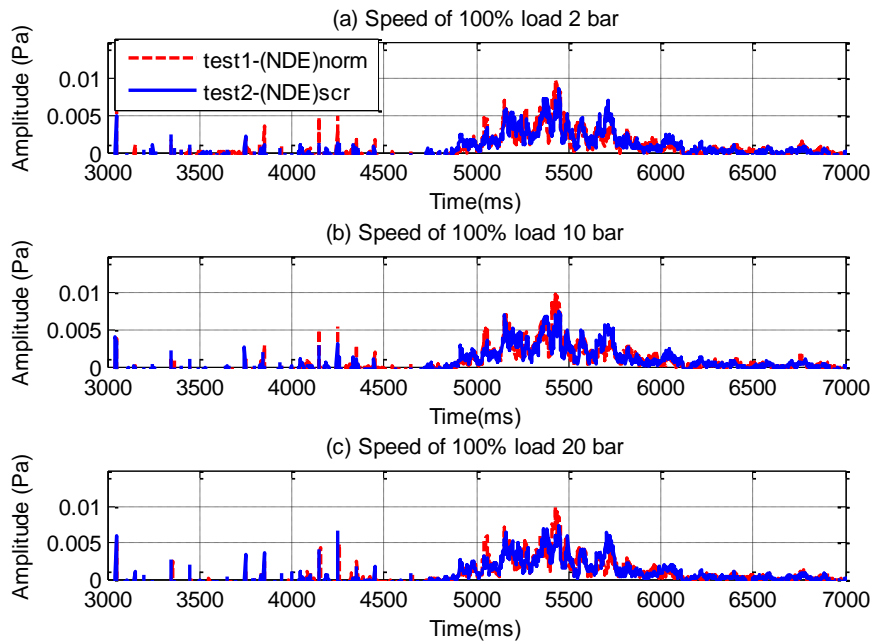


Figure 7. 10 AS spectrum in bearing under different radial load and different condition

Figure 7.11 shows the relationship between speed, radial load and bearing condition for the mean values of the raw AS signal. The figure shows that for the low frequency range (2 kHz-6 kHz) the AS mean value is unable to differentiate between the normal and scratched bearing.

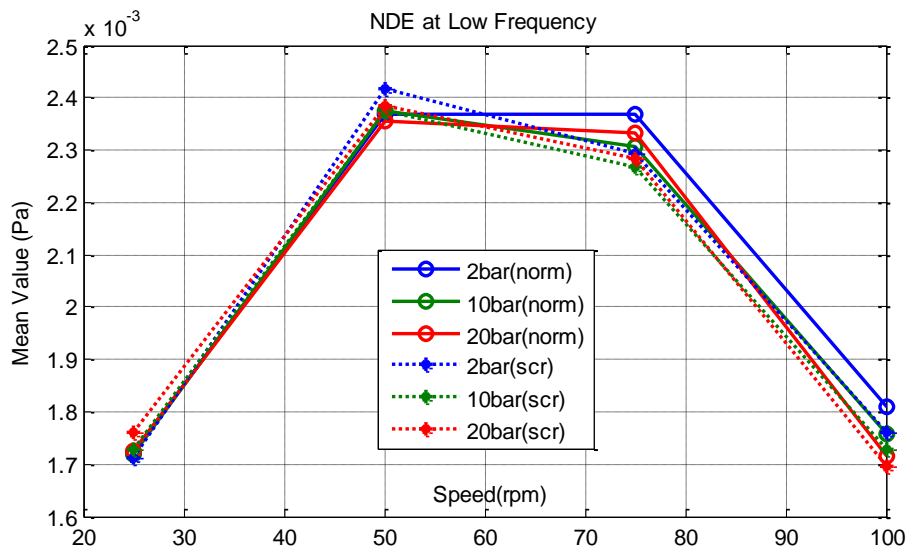


Figure 7. 11 AS mean value in bearing under different load and different condition at low frequency band

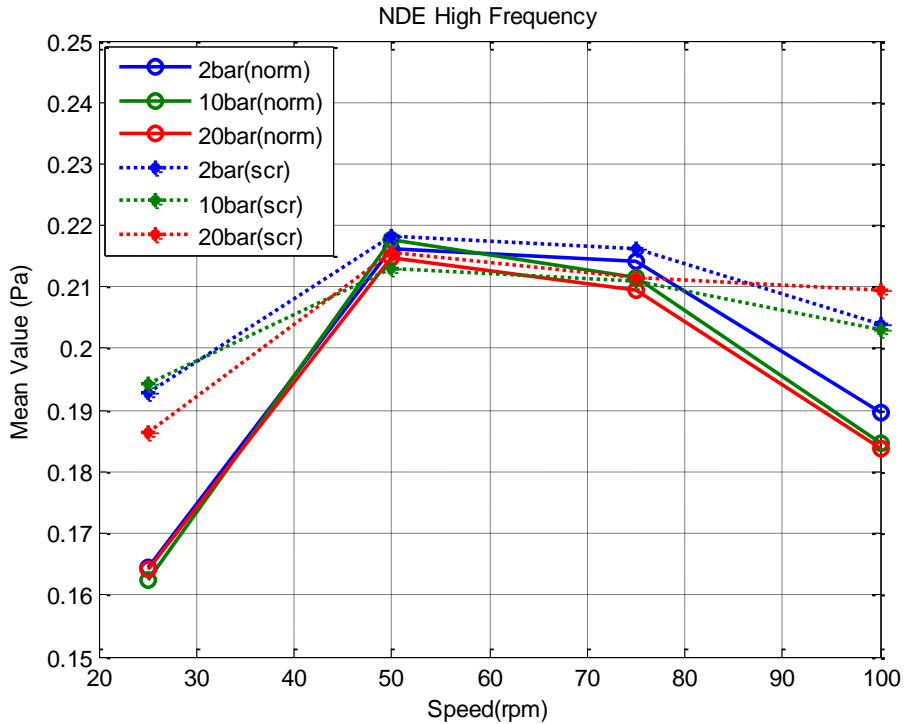


Figure 7. 12 AS mean value in bearing under different load and different condition at high frequency band

Figure 7.12 shows the relationship between speed, radial load and bearing condition for the mean values of the raw AS signal for the high frequency band (6 kHz - 40 kHz).

The figure also shows the effect of the scratch on the bearing can be distinguished at less than 50% of maximum speed. The effect then disappears but re-appears at after 75% of maximum speed. However it is concluded that the mean of the high frequency AS signal is not able to detect scratched bearings consistently.

7.4 Acoustic emission analysis

7.4.1 Time domain analysis

Figure 7.13 shows the time domain of the AE signals for scratched and normal bearings at maximum shaft speed for three different radial loads. As previously the figure indicates a clear and substantial difference between the AE signals at low radial load medium and high load.

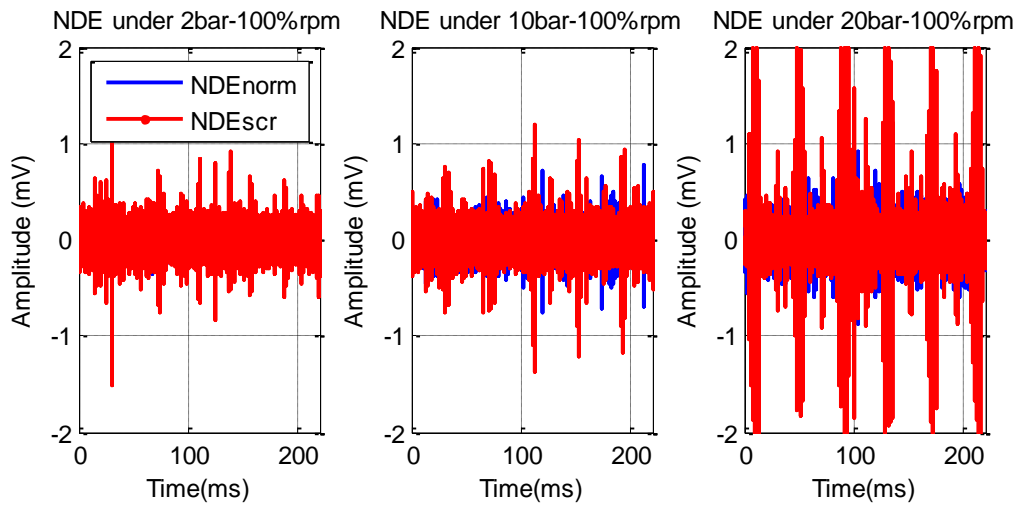


Figure 7.13 AE signal comparison for similar bearing condition under different load at 100% speed

Figure 7.13 shows there is significant differences between the two signals so the AE signal has the potential of demonstrating a clear and substantial difference between the normal and scratched bearings. It can be seen that the signal changes from a continuous to bursts type and this would be expected from insertion of scratches. An investigation of the influence of the level of scratch on the AE signal will be conduct in further experiments.

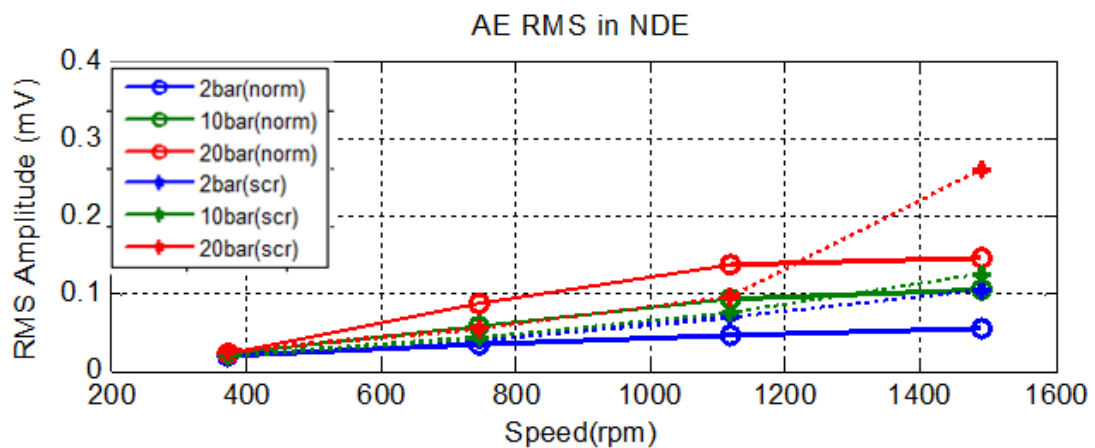


Figure 7.14 AE RMS value in bearing under different load and different condition

The influence of speed and radial load on the AE RMS amplitude of the two bearings is presented in Figure 7.14. It is clear that - as previously - the speed increased, the AE RMS amplitude also increases. The effect of increasing radial load is also significant. However, the effect of bearing condition on AE RMS amplitude had no significant. Thus the AE RMS value of the raw signal is not suitable for detecting scratched bearings. Frequency analysis of AE signal in descriptive and analytic terms is given below.

7.4.2 Frequency domain analysis

AE spectra of the normal bearing and bearing with scratches on the NDE side of the motor under three different loads at 100% speed are shown in Figure 7.15. It can be seen that responses between the normal and scratching NDE bearing are significant different. The influence of radial load in the spectrum responses is significant, for both bearing.

The high amplitude occurs at frequency range 3 kHz up to 100 kHz and dominant at 3 kHz until 40 kHz. The frequency at which the spectral peak occurred was about 30 kHz.

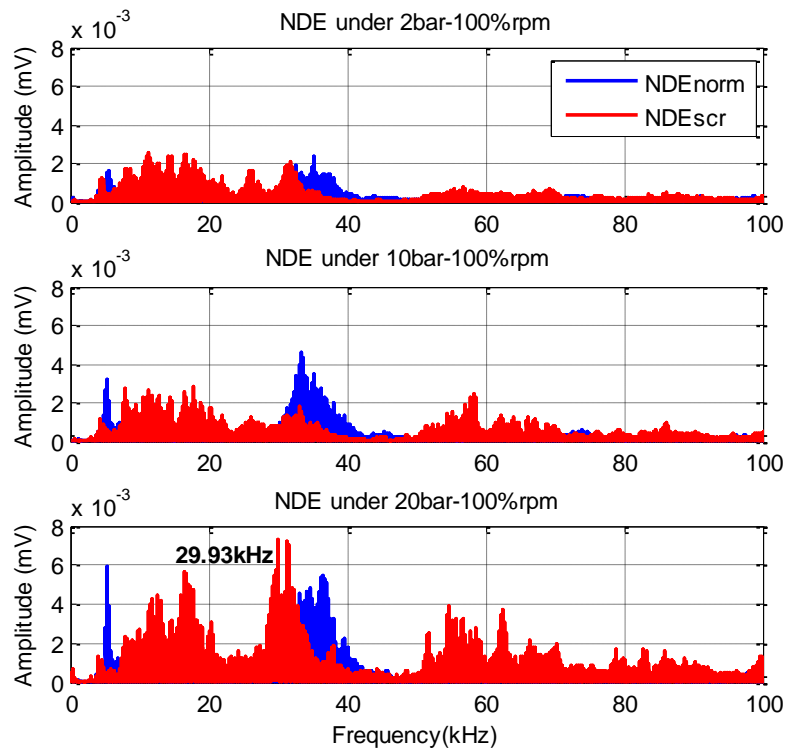


Figure 7. 15 AE spectrum in different bearing condition under different radial load at 100% speed

Figure 7.16 compares AE spectra for the normal bearing and bearing with scratch fault, substantial differences in amplitude and frequency can be seen immediately. At high load, the peak value of the scratched bearing is higher and the frequency of the maximum amplitude peak shifts 313.8 kHz. Thus AE frequency analysis can be used to distinguish normal bearings from scratched bearings.

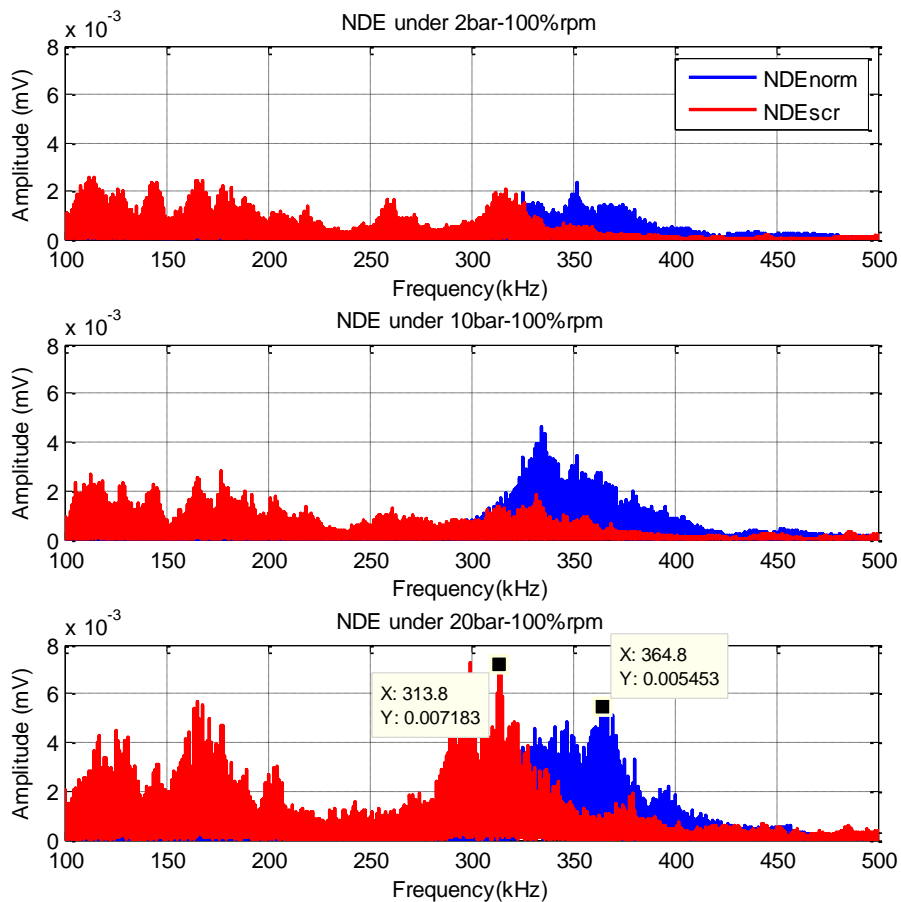


Figure 7. 16 AE spectrum in different bearing condition under different radial load at 100% speed

Figure 7.17 shows the relationship between speeds, radial load and mean value of the AE signal mean in the low frequency range (20 kHz – 90 kHz) for scratched and normal bearings. It is clear that there is no clear and consistent difference in the plots for normal and scratched bearings. Thus the AE mean value over the frequency range 20 kHz – 90 kHz is not suitable for the detection of bearing damage caused by scratching.

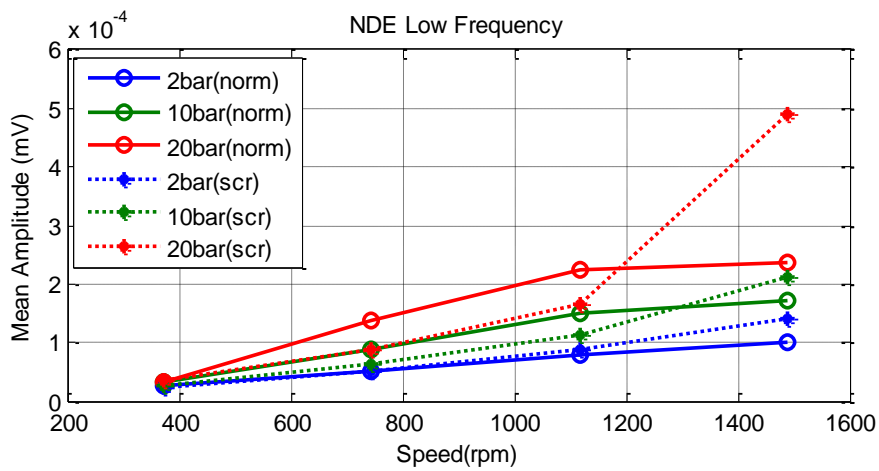


Figure 7.17 AE mean value in different bearing condition under different radial load and speed at low frequency

Figure 7.18 shows mean value for the AE signal for the high frequency range 90 kHz – 320 kHz for normal and scratched bearings under different radial loads and different shaft speeds.

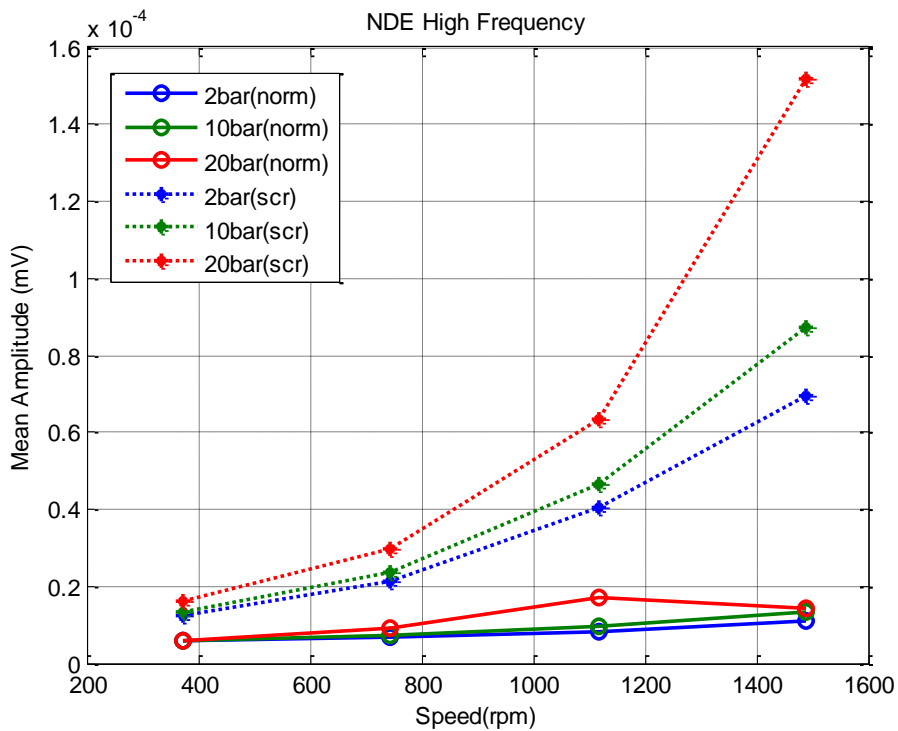


Figure 7.18 AE mean value in different bearing condition under different radial load and speed at high frequency

The figure indicate that there is a significant difference between the mean values for the normal and scratched bearing at all loads and at all speeds above the lowest speed (400 rpm). It is concluded that the AE mean value of the high frequency range could be useful for detecting the presence of scratched journal bearings. Generally the figure again shows positive correlations between speed and radial load and mean value of the AE signal

7.5 Discussion of monitoring of scratched surface

Discussion concerning the monitoring surface vibration, airborne sound and acoustic emission signals from normal and scratched self-aligning spherical journal bearings under different loads and speeds are as follows:

The surface vibration and airborne sound time domain analyses are unable to discern any differences between the normal and scratched bearing although RMS value analysis from raw signal can detect changes in speed and radial load.

In the time domain the AE signal clearly shows different responses for normal and scratched bearings. The amplitude of the AE time domain signal for a scratching bearing shows a significant higher amplitude when compared with a normal journal bearing and at high loads appears to be much more burst like in character.

The kurtosis analysis of the raw signal of surface vibration and airborne sound cannot distinguish between normal bearing and scratched bearing although the data of the signals are in Gaussian distribution.

The RMS values analyses of the raw signal obtained for surface vibration and airborne sound were unable identify the difference between normal and scratching bearings.

The high frequency spectrum mean value of the surface vibration is capable of distinguishing between normal and scratched bearings, but this is not the case for the airborne sound signal and it is concluded that the airborne sound spectrum analysis cannot detect the difference between normal and scratched bearings responses.

The acoustic emission spectrum analysis is able to differentiate the responses between the normal bearing and the scratched bearing very well.

Figure 7.20 is the vibration spectrum comparison between on normal journal bearing and scratching bearing under radial load of 20 bar at 100% speed. The figure shows that the vibration peak amplitude of the scratched journal bearing is higher than that of the normal bearing. Also the frequency at which the peak occurs is higher for the scratched bearing.

The scratched journal bearing has a lower damping coefficient if compared with the damping coefficient of normal bearing, therefore it will have a higher peak vibration amplitude. The scratched journal bearing also has a higher stiffness coefficient than a normal journal bearing which means the resonant frequencies will be higher.

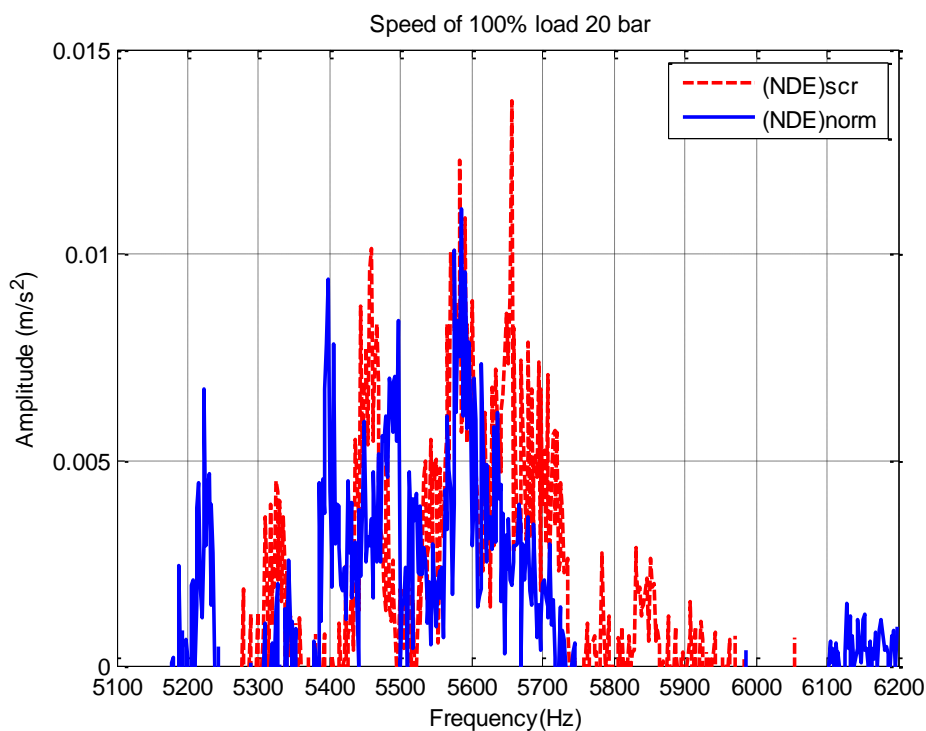


Figure 7. 19 Vibration spectrum under 20 bar radial load and 100% speed for scratched and healthy bearings

The spectra of the surface vibration responses of the normal and scratched bearings show that the highest peak of the amplitude occurs at 5.58 kHz for the normal bearing but at 5.66 for the scratched bearing see Figure 7.20.

The AE spectrum analysis can identify the difference between the normal and scratched bearings which occurs at a frequency of about 38 kHz for the normal bearing and 34.7 kHz for the scratched bearing.

In addition, the time domain analysis, spectrum analysis and AE mean value analysis (high frequency) are appropriate to be used to monitor and detect the appearance of scratches in journal bearings.

7.6 Summary of surface scratched bearing monitoring

The effect of scratching on bearing to the surface vibration, airborne sound and acoustic emission responses can be summarized as follows:

Influence of bearing scratch on vibration response:

- The effect of speed variation to the RMS value from the raw signal significant but the influence of radial load and scratching to the RMS value from the raw signal is not significant and cannot be identified.
- Kurtosis value close to normal distribution but could not be used to detect the presence of scratches in a journal bearing.
- High amplitude appears in frequency between 3 kHz to 5.7 kHz and frequency range between 5.2 kHz to 6 kHz.
- The highest amplitude peak for the scratched bearing was at 5.66 kHz.
- There are significant differences in mean values at high frequencies between normal and scratching bearings for low, medium and high radial loads.
- The presence of the scratch generated higher amplitude vibration responses.

Influence of bearing scratch on airborne sound responses as follows:

- The effects of speed variation and load on the RMS value of the raw signal were as obtained previously.
- The presence of the scratch could not be identified from the RMS of the raw signal.
- Kurtosis value was close to that for normal distribution but could not be used to detecting the presence of a scratch in the journal bearing.
- High amplitudes dominate the spectrum in the frequency range between 4.75 kHz and 6.5 kHz.
- Highest peak amplitude different between normal and scratching bearing located at 5.4 kHz.

-
- The effect of radial load and presence of a scratch on the mean value of the spectrum at both low and high frequencies was not significant.

Influence of scratching on bearing of the acoustic emission as follows:

- There is significant difference of AE signal between normal and scratching journal bearings.
- There is significant difference of AE spectrum between normal and scratching bearings.
- High amplitudes dominate the spectrum in the frequency range between 250 kHz and 350 kHz.
- Highest and big peak amplitude difference between normal and scratching bearing occur at 313.8 kHz.
- The effect speed, radial load and presence of a scratch on the spectrum mean value was clear and significant at high frequencies but less so for low frequencies.

CHAPTER EIGHT

CONCLUSIONS AND SUGGESTIONS FOR FURTHER WORK

8.1 Conclusions

The symptoms of failure should be detected as early as possible and surface vibration, airborne sound and acoustic emission monitoring techniques are suitable for this purpose for a self-aligning spherical journal bearing. Based on experiments and analysis of the Surface vibration, airborne sound and acoustic emission characteristics of the self-aligning spherical journal bearing the following conclusions can be made.

8.1.1 Conclusion of the repeatability experiments

Conclusion one: The overall repeatability of the measurements is acceptable, although not 100% for surface vibration, airborne sound and acoustic emission responses; the time and frequency domains including RMS value, Kurtosis and mean value analysis. It is suggested that the imperfection in repeatability is due mainly to radial load leakage in the hydraulic system because of the lack of sensitivity of the pressure transducer.

Conclusion two: The AE response shows the best repeatability, followed by surface vibration and then the airborne sound measurement.

8.1.2 Conclusion of radial load and speed variation responses.

Conclusion three: There is a positive correlation between the speed of shaft and the RMS value of the surface vibration in the raw signal but the influence of the radial load on the RMS value from the raw signal cannot be detected.

Conclusion four: High amplitude of surface vibration responses dominate at frequencies from 250 kHz up to 425 kHz and high amplitude peaks occur at frequencies 365.5 kHz.

Conclusion five: There is a positive correlation between speed and radial load variation on the spectrum means value of surface vibration responses and it appears clear and significant.

Conclusion six: There is a positive correlation between speed and the RMS value of the airborne sound raw signal but the influence of radial load on the RMS value cannot be detected.

Conclusion seven: High amplitude peaks of airborne sound spectrum dominate at frequency from 4.75 kHz to 6.5 kHz and the highest amplitude peak occur at 5.4 kHz.

Conclusion eight: There is a positive correlation between speed and spectrum mean value of airborne sound response but after the speed reached 75% of the maximum, the spectrum mean value slightly decrease but the effect of radial load is difficult to be distinguished.

Conclusion nine: There is a positive correlation between speed and radial load on acoustic emission RMS value from the raw signal and significant differences between in various loads.

Conclusion ten: High amplitudes of acoustic emission concentrated at frequency range between 250 kHz to 425 kHz and the highest amplitude peaks value occurred at 365.5 kHz.

Conclusion eleven: There is a positive correlation between speed and radial load and acoustic emission spectrum mean value responses in the low and high frequency ranges.

8.1.3 Effect of viscosity changing

Conclusion twelve: There is a positive correlation between speed and RMS surface vibration value from the raw signal but the effect of viscosity variation is difficult to be identified. The high amplitudes also dominant at frequency range between 3 kHz and 6 kHz and the peaks value appears at 3.05 kHz, 4.1 kHz and 5.6 kHz.

Conclusion thirteen: There is positive correlation between speed and RMS value of airborne sound until the speed reached 75% of maximum speed and the influence of viscosity and radial load on the RMS value of the raw signal is difficult to be distinguished. However the high amplitude appear dominant in the frequency range from 4.25 kHz to 6 kHz. The highest amplitude peak lies at a frequency 5.4 kHz.

Conclusion fourteen: There is a positive correlation between speed and radial load and the RMS acoustic emission value from raw signal but when use higher viscosity of lubricant generates the lower of RMS value of the raw signal.

Conclusion fifteen: When use higher viscosity of lubricant generate lower mean value of acoustic emission response at high frequency. High amplitudes dominant in the frequency range between 250 kHz and 425 kHz range and Peak amplitudes occurred 366.2 kHz.

8.1.4. Effect of water contaminant concentration in lubricant

Conclusion sixteen: The effect water contamination on the RMS of the surface vibration value from the raw signal is difficult to be identified. High amplitudes appear in the frequency spectrum between 3 kHz to 6 kHz, but dominate in the frequency range between 4 kHz to 6 kHz and the highest peak amplitude located at 5.6 kHz followed 3.2 kHz and 4.2 kHz

Conclusion seventeen: When use greater water concentration in the lubricant create higher mean value of surface vibration spectrum at higher frequency.

Conclusion eighteen: The effect of water contaminant concentration on the airborne sound response on the RMS and mean value airborne sound also difficult to be determined. However, high amplitudes dominate at frequency range between 4.8 kHz and 6.1 kHz. The highest peak amplitude is at 5.4 kHz.

Conclusion nineteen: The higher water contaminant concentration in the lubricant generates a higher RMS value and mean value of acoustic emission responses. High amplitudes dominate at frequency range between 250 kHz to 425 kHz. High peak amplitude occurs at 361.7 kHz.

8.1.5 Effect of scratched bearing

Conclusion twenty: The effect of scratching on surface bearing to the RMS surface vibration value from the raw signal is not significant and cannot be identified, but there are significant differences in mean values of surface vibration at high frequencies between normal and scratching bearings for low, medium and high radial loads. The presence of the scratching in the surface of journal bearing generates higher amplitude vibration responses on journal bearing.

Conclusion twenty one: High amplitude of surface vibration appears at frequency range between 3 kHz to 5.7 kHz and also frequency range between 5.2 kHz to 6 kHz and the highest amplitude peak for the scratched bearing was at 5.66 kHz.

Conclusion twenty two: Influence of bearing scratch on airborne sound responses as follows: The presence of the scratching in a journal bearing cannot be identified from the RMS airborne sound of the raw signal and from mean value of spectrum. High amplitudes dominate the spectrum in the frequency range between 4.75 kHz and 6.5 kHz and highest peak amplitude of normal and scratching bearing are located at 5.4 kHz.

Conclusion twenty three: There is significant different of acoustic emission signal and spectrum between normal and scratching journal bearings. The presence of a scratch on the journal bearing generates a higher spectrum mean value at higher frequencies.

Conclusion twenty five: High amplitudes of acoustic emission spectrum responses dominate at frequency range between 250 kHz and 350 kHz and the highest peak amplitude scratching bearing occur at 313.8 kHz and at 364.8 kHz for normal bearing.

Conclusion twenty six: Based on the investigation of surface vibration, airborne sound and acoustic emission characteristics at different speeds, radial loads, viscosities of the lubricant, and lubricant deterioration by water; and with the seeding of circumferential scratches it was observed that the most sensitive and best results were obtained from the acoustic emission signals followed by surface vibration and airborne sound. The mean value of AE spectrum and SV spectrum at high frequencies were better than RMS value analysis of the raw signals.

Conclusion twenty seven: Acoustic emission measurement and surface vibration measurement are effective and appropriate be used for condition monitoring for journal bearing of rotating machinery and equipment.

8.2 Review of Aims and Objectives

This section reviews the objectives and achievements of this research, by considering one by one the objectives of the project listed in Section 1.3.

Objective one: To design and test a self-aligning spherical journal bearing test rig.

Achievement one: The rig on which to test the self-aligning spherical journal bearing was successfully designed, built and used. The main part of the test rig consists of the drive and the radial load system for the bearing. The radial load on the bearing was applied by means of manual hydraulic equipment and torsion loading by a DC generator. Two hard rubber couplings (HRC) are used to carry the torsion load and connect the drive shaft supported by the two bearing being tested. Construction details and components are presented in Section 4.1 and Figures 4.1.

Objective two: To develop surface vibration, airborne sound signal generation sources for the self-aligning spherical journal bearing.

Achievement two: Surface vibration, airborne sound signals generated from the self-aligning spherical journal bearings are grouped into surface vibration, acoustic emission and airborne sound.

Vibration of journal bearings occurs over a wide frequency range. Vibrations at low frequencies are due to the test rig installation and include unbalance, misalignment and mis-assembly of components. The high frequency vibration is due to asperity contact between the shaft and bearings which may be described using a micro-spring damping model. Asperity contact also affects the friction and damping coefficients and frictional forces in the vibration system. The vibration system in the journal bearing is a forced multi degree of freedom system, requiring high order non-homogeneous differential equation, as described in detail in Section 3.2.

The source of airborne sound on a journal bearing is described Section 3.3. Airborne sound from journal bearings is due to electromagnetic and structural forces and changes in hydrodynamic pressure in the bearings, all of which propagate outwards through bearing and bearing housing. The fan on the drive motor and DC motor are also sources of airborne sound. This problem can be eliminated by filtering technique.

Acoustic emission is generated by the contact between bearing and shaft. The amount of energy released is strongly influenced by asperity contact and lubrication conditions. Acoustic emission in the journal bearing contact is explained in Section 3.4.

Objective three: To develop a monitoring measurement and diagnostic system for journal bearing condition monitoring.

Achievement three: A comprehensive system of machine surface vibration monitoring using accelerometers, airborne sound monitoring using a piezoelectric microphone and acoustic emission monitoring sensors were all used to detect and analyse the signals emitted by the bearing. These were able to detect the symptoms of bearing failure at low, middle and high frequencies by using vibration, acoustic and acoustic emission monitoring. Monitoring and analysis techniques are discussed in Sections 2.4, 3.2, 3.3 and 3.4.

Objective four: To study the characteristics of surface vibration, airborne sound and acoustic emission signal response of the self-aligning spherical journal bearing under the influence of radial load and speed variation.

Achievement four: The effects of radial load and speed variation on the surface vibration characteristics of the bearing were investigated simultaneously. The experiment for surface vibration, airborne sound and acoustic emission was performed at least three times to confirm the repeatability of data sets. Repeatability analysis for three kinds of experiments shows satisfactory results.

It was found that the surface vibration and acoustic emission RMS level increased when the radial load and speed was increased except for airborne sound. The radial load does not appear influence the airborne sound responses.

The repeatability analysis and effects change in radial load and speed on the vibration characteristics, airborne sound and acoustic emission of the journal bearings are described in Chapter 5.

Objective five: To investigate the characteristics of the surface vibration, airborne sound and acoustic emission response of the self-aligning spherical journal bearing under different oil viscosities.

Achievement five: The effects of lubricant viscosity on the surface vibration, airborne sound and acoustic emission characteristics of the bearing were investigated separately but under similar loading operation.

It was found that the influences of viscosity change may be clearly identified through surface vibration analysis and acoustic emission analysis, but airborne sound measurement failed to identify the influence of change in viscosity.

When using a more viscous lubricant the surface vibration and acoustic emission mean value amplitude decreased. The surface vibration, airborne sound and acoustic emission investigations of the journal bearing for different lubricant viscosities are presented in Chapter 6, Section 6.2.

Objective six: To investigate the characteristic of surface vibration, airborne sound and acoustic emission due to lubrication deterioration caused by water contaminant.

Achievement six: The effects of lubricant deterioration due to water contamination on the surface vibration and airborne sound characteristics of the bearing were investigated separately.

The presence of water contaminant in the lubricant was successfully detected using surface vibration and acoustic emission RMS spectra at high frequency. Airborne sound analysis failed to detect the presence of the water contaminant. Water contaminant in the lubricant created higher surface vibration and acoustic emission RMS mean values and the results are presented in Chapter 6, Sections 6.3.

Objective seven: To investigate the characteristic of surface vibration, airborne sound and AE due to the bearing surface deterioration caused by scratching.

Achievement seven: The changes in responses of SV, AS and AE signals when the journal bearing surface was scratched were very clear in both the time and frequency domains. The highest amplitude of the signal that occurs with each type of measurement is located at a different frequency.

The investigation of the influence seeded scratch faults on the Vibro-acoustic response of the journal bearing is described in Chapter 7.

Objective eight: To develop Matlab™ codes for processing and analysing the data outputs from the accelerometers, microphones and AE sensors in the time domain and frequency domains analysis.

Achievement eight: The experimental data is presented in a Matlab format. Processing and analysis was performed using Matlab programming including time domain, frequency domain and parameter statistical analysis. Matlab codes for processing and analysis of data for all the experiments are presented in ten data analysis programs includes repeatability and analysis program for surface vibration and airborne sound responses on journal bearing under radial load and speed variation; with different viscosity; with different concentration water contaminant in the journal bearing lubricant and with scratching bearing.

Acoustic emission analysis program also consist of repeatability and analysis of acoustic emission responses on the journal bearing under speed and radial load variation; viscosity variation; water concentration contaminant in the lubricant and with a scratched journal bearing.

Objective nine: To provide guidelines for further research and development of surface vibration, airborne sound and AE characteristic for self-aligning spherical journal bearing for early fault detection.

Achievement nine: Possible further research is presented in Section 8.4.

8.3 Contributions to knowledge

First contribution: The design and construction of journal bearing test rig with beam supporting loading system (described in Chapter 4) for Centre for Efficiency and Performance Engineering. This rig is able to investigate characteristic of normal bearings or bearings with seeded faults under different combinations of load (radial and torsion), shaft rotational speed, temperature etc., simultaneously. The test rig is equipped with all the basic sensors needed to investigate characteristic of bearings in a controlled manner using at least three different methods simultaneously such as surface vibration, airborne sound and acoustic emission.

Second contribution: Studies of the characteristics of the surface vibration, airborne sound and AE for a self-aligning spherical journal for change in radial load and speed have been done, see Chapter 5. This study provides basic information about surface vibration, airborne sound and AE for further research concerning the detection of early damage to the self-aligning spherical bearing journal using frequency discrimination (low and/or high frequencies).

This study will assist future researchers to determine the relative merits (strengths and weaknesses) of each system of measurement for any particular application to the monitoring of journal bearing

Third contribution: These studies report surface vibration, airborne sound analysis of the characteristics of the self-aligning spherical journal bearing due to abnormal lubricant and surface deterioration, particularly use of the high frequency response, see Chapters 6 and 7. Current surface vibration, airborne sound analyses focuses only on low frequencies.

8.4 Suggestion for future work

The first suggestion: To reduce the influence of surface roughness of shaft on the surface vibration, airborne sound and AE characteristics, the normal condition should use a standard shaft and bearing with a roughness standard of N5 or N6.

The second suggestion: To develop vibration numerical analysis on the self-aligning journal bearing at high frequency to get the natural frequency characteristic especially for fault or abnormal bearing.

The third suggestion: Conduct surface vibration, airborne sound and acoustic emission tests at high frequencies using the same data acquisition methods to perform integrative experiment for the self-aligning journal bearing for different levels of roughness or asperity.

The fourth suggestion:

Perform integrative testing with surface vibration, airborne sound and acoustic emission for self-aligning spherical journal bearings with different levels of surface scratching.

The fifth suggestion:

Perform integrative testing with surface vibration, airborne sound and acoustic emission for self-aligning spherical journal bearings with incremental surface wear.

The sixth suggestion:

Perform integrative testing with surface vibration, airborne sound and acoustic emission for self-aligning spherical journal bearings with lubricant deterioration and solid contaminants from very low concentration of contaminant.

The seventh suggestion:

Conduct integrative testing with surface vibration, airborne sound and AE for self-aligning spherical journal bearings with the surface deterioration using advanced analysis such as wavelet analysis.

8.5 List of Publications

The research so far has generated papers as follows:

1. P. Raharjo, J. Gu, Y. Fan, F. Gu and A. Ball, Early failure detection and diagnosis of a self-aligning journal bearing through surface vibration, airborne sound analysis, presented at CM - MFPT 2010, Proceedings: The Seventh International Conference on Condition Monitoring (CMM) and Machinery Failure Prevention Technologies (MFPT), 22-24 June 2010, M. Ahmed Stratford-Upon-Avon, UK
2. P. Raharjo, F. Al Thobiani, F. Gu, and A. Ball, Early failure detection and diagnosis of a self-aligning journal bearing, Proceeding of COMADEM 2010, June 28-July 2, 2010, 23rd International Congress on Condition Monitoring and Diagnostic Engineering, Nara, Japan.
3. P. Raharjo, S. Abdusslam, Tie Wang, F. Gu and A. D. Ball, An Investigation of Acoustic Emission Responses of a Self Aligning Spherical Journal Bearing, Proceeding: The

Eighth International Conference on Condition Monitoring (CMM) and Machinery Failure Prevention Technologies (MFPT), 20-22 June 2011, St. David's Hotel, Cardiff, Wales, United Kingdom

4. S. Abdussalam, P. Raharjo, F. Gu, A. D. Ball, Time Encoded Signal Processing and Recognition (TESPAR) Response to Different Bearing Faults, Proceeding of the 17th International Conference on Automation and Computing, University of Huddersfield, Huddersfield, UK, 10 September 2011.
5. P. Raharjo, S. Abdussalam, F. Gu and A. D. Ball, Surface Vibration, Airborne Sound Monitoring of a Self Aligning Spherical Journal Bearing due to Oversize Eccentric Bore Fault, Proceeding: The Ninth International Conference on Condition Monitoring (CMM) and Machinery Failure Prevention Technologies (MFPT), 12-14 June 2012, The Earl's Court Ibis Hotel, London, United Kingdom.
6. P. Raharjo, F. Gu, B. Tesfa and A. D. Ball, A Comparative Study of Monitoring a Self Aligning Spherical Journal using Surface Vibration, Airborne Sound and Acoustic Emission, COMADEM 2012, 25th International Congress on Condition Monitoring and Diagnostic Engineering, 18-20 June 2012, Huddersfield, England, UK, Journal of Physics, conference Series, IOP Conference Series, 364 (2012) 011001.
7. S. Abdussalam, P. Raharjo, F. Gu, and A. D. Ball, Bearing defect detection and diagnosis using a time encoded signal processing and pattern recognition method, COMADEM 2012, 25th International Congress on Condition Monitoring and Diagnostic Engineering, 18-20 June 2012, Huddersfield, England, UK, Journal of Physics, Conference Series, IOP Conference Series, 364 (2012) 011001.

REFERENCES

- Abdullah, M, Al-Ghamd, Mba D A, (2006), *Comparative experimental study on the use of acoustic emission and vibration analysis for bearing defect identification and estimation of defect size*, Mechanical Systems and Signal Processing, Elsevier, 20, pp. 1537-1571.
- Adam, M, (2001), *Rotating Machinery Vibration, From Analysis to Troubleshooting*, Marcel Dekker Inc, New York.
- Ahmad, H, Mollazade K, (2009), *Bearing Fault Diagnosis of a Mine Stone Crasher by Vibration Condition Monitoring Technique*, Research Journal of Applied Science, Engineering and Technology 1(3), pp. 112-115, ISSN: 2040-7467
- Ahmadi, H, Mollazade K, (2009), *Bearing Fault Diagnosis of a Mine Stone Crusher by Vibration Condition Monitoring Technique*, Research Journal of Applied Sciences, Engineering and Technology, Volume 1, Issue 3, pp. 112-115.
- Akay, A, (2002), *Acoustics of friction*, Journal of Acoustic Society of America,. Volume 111, Issue 4, pp. 1525-1548.
- Akintunde, D, (2008), *Spectrometric Oil Analysis, an Untapped Resource for Condition Monitoring*, AU JT 12(2), p. 107-114, October.
- Almeida, R, (2003), *Lubricant Condition Monitoring*, 5th Gear and Transmission Workshop, Paper XI, Portugal.
- Arvis, (2009), *Arvis Bearing Catalogue*, Criptic Arvis Ltd, Croft Grange Works, 16 Bridge Park Road, Thurmaston, LE4 8BL, Leicester, UK.
- Aurora, (2010) , *Flanged Bushing*, On-line Catalogue, Aurora Bearing, 90, Aucutt Rd., Montgomery, IL 60538, USA
- Babcock, W, Beilot B, (2003), *Understanding and reducing the effect of contamination on hydraulic fluids and systems. Material Ease*, The AMPTIAC Quarterly, Volume 7, Number, p. 11-15.
- Beijing Acoustic Sensing Technology, (2007) ,*ICP Microphone Preamplifier*, BAST YG 201, Unit 1, 26 Fairholme Rd, Manchester, M20 4NT, UK.
- Ben Abdelounis, H, Zahouani H, Le Bot A, Perret Liaudet J, Ben Tkaya M, (2011), *Numerical simulation of friction noise*, Wear, Elsevier, 271, pp. 621-624.

Berry, J, (2005), *Oil whirl and whip instabilities within journal bearings*, Machinery Lubrication, Noria Publication. No.754.

Bloch, H, (2005), *Oil Rings vs. Flinger Discs*, Reliability Advantage, Volume 2, Issue 1, AESEAL Inc.

Bonnes, R and McBride S, (1991), *Adhesive and abrasive wear studies using acoustic emission techniques*, Abrasive wear , Volume 149, Issues 1-2, pp. 41-53.

Cantley, R E,(1977), *The Effect of Water in Lubricating Oil on Bearing Fatigue Life*, ASLE Transactions, American Society of Lubrication Engineers, Volume 20, No. 3, p. 244-248, Philadelphia, Penn.

Choudhury, A and Tandon N, (2000), *Application of acoustic technique for detection of defect in rolling element bearing*, Tribology International 33, pp.39-45.

Choy, F, Zhou J, Braun M, (2005), *Vibration Monitoring and Damage Quantification of Faulty Ball Bearing*, Journal of Tribology, Volume 127, Issue 4, pp. 776-784, October.

Clevite, (2002), *Engine Bearing Failure, Analysis Guide*, A guide to analysis and correction of premature engine bearing failure, Clevite 77, Issue, Form CL77-3-402)

Cludema, K, (1996), *Friction abrasive wear , Lubrication, A Textbook in Tribology*, CRC Press , Florida, USA.

Commtest Ltd, (2006),*Beginner's Guide to Machine Vibration*, Commtest Instruments Ltd, New Zealand.

De Botton, G, Ari B, Sher E, (2000), *Vibration monitoring as a predictive maintenance tool for reciprocating Engine*, Proceedings of the Institution of Mechanical Engineer D, Volume 214, Issue 8, pp. 895, SAGE Publications.

De Camillo, S, He M, Cloud C, Byrne J, (2008), *Journal Bearing Vibration and SSV Hash*, Proceeding of the Thirty Seventh Turbo machinery Symposium, pp. 11-23.

De Courcey, W, (2003), *Statistic and Probability for engineering applications, with Microsoft@Excel*, Newnes, Elsevier Science,USA.

Dennis, J, Smith S, (1994), *An Introductory Guide to Industrial Tribology*, Ed. Baker, R. Mechanical Engineering Publication Limited, London.

Dickerhof , M, Albers A, Burger, W and Sovino R, (2006), *Monitoring Lubrication Regimes in Sliding Bearings – Using Acoustic Emission Analysis*, Practicing Oil Analysis, May, Noria Publication.

Emira, N A, Mohammad H T and Tahat M S, (2011), Stick slip detection through measurement of near field noise, *Journal of Mechanical Engineering Research*, Vol 3(3), pp 96-102, March.

Fan, Y, Gu F and Ball A, (2009), *Modelling acoustic emission generated by sliding friction*, *Abrasive wear* , Volume 268, Issue 5-6, pp. 811-815, Elsevier.

Finley, W, Hodowanec M, (2001), *Sleeve vs. anti friction bearings: Selection of the Optimal Bearing for Induction Motors*, IEEE

Flood, S, (2007), *Mechanical Seal Reliability, What realistically can be Achieved*, IMechE, London, April.

Ford, I, (1993), *Roughness effect on friction for multi-asperity contact between surface*, *Journal Physic, Applied Physic*, No. 26, pp. 2219-2225.

Genesca, M, Romeu J, Pamies T, Sanchez A, (2010), *Aircraft Noise Monitoring with Linear Microphone Arrays*, *IEEE Aerospace and Electronic Systems Magazine*, Volume 25, Issue 1, pp.14-18.

Gerges, N Y S, Schradt G A, Parthey W, (2013), *Noise Sources*, Occupational exposure to noise: evaluation, prevention and control, edited by: Berenice Goelzer, Colin H, Hansen and Gustav A. Sehmdt, World Health Organisation.

Girdhar, P and Scheffer C, (2004), *Practical Machinery Vibration Analysis and Predictive Maintenance*, Oxford, Newnes.

Glaeser, A, Ericson R, Dufrane K, (1992), *Tribology, the science of combating abrasive wear*, *Lubrication Engineering*, *Journal of the Society of Tribologists and Lubrication Engineers*.

Global Sensor Technology, (2010) *Dynamic data acquisition systems for use with a pre-amplifier YE6230B*, Unit 1, 26 Fairholme Rd, Manchester, M20 4NT, UK.

Global Sensor Technology, (2010) *General purpose piezotronics YD-5 4251*, Unit 1, 26 Fairholme Rd, Manchester, M20 4NT, UK.

Global Sensor Technology, (2010), *Weigh Transducer*, Catalogue, Unit 1, 26 Fairholme Rd, Manchester, M20 4NT, UK.

Gophinath, K and Mayuram M M, (no date), *Machine Design II*, Modul 5, Sliding Contact Bearing, Indian Institute of Technology Madras.

Gribble J, (2006), *Acoustic analysis for the rest of us*, Machinery Lubrication, Noria Publication, No. 839, January.

Hamernick, I, (2006), *Vibration Analysis for condition Monitoring, Maintenance Minders*, Pump and Systems, pp. 62-63.

Hamrock, B, (2006), *Mechanical Engineers' Handbook: Materials and Mechanical Design*, Volume 1, Third Edition. Ed. by Kutz, M. John Wiley & Sons, Inc. Columbus, Ohio.

Hengstler, (2008), *Incremental Shaft Encoders*, Type RI 32, Rotary Encoder Solution Limited.

Higgs, P, Parkin R, Jackson M, Al-Habaibeh A, Zorriassatine F, Coy J, (2004), *A survey of condition monitoring systems in industry*, Proc. ESDA, 7th Bienial ASME Conference Engineering System Design and Analysis, July 19-22, Manchester, UK.

Hori Y, (2006), *Hydrodynamics lubrication*. Springer Verlag, Tokyo, Japan.

Hydra Product, (2003), *Hand Pump Tank*, HP issue 2, TI-030-01,UK.

Hydra Product, (2003), *Hand Pump-Flange Mounted Single Acting*, HP issue B, TI-030-02,UK

Jayaswal, P, Wadhvani A K and Mulchandani K B, (2008), *Machine Fault Signature Analysis*, Review Article, International Journal of rotating machinery, Volume 2008, Article ID 583982, 10 pages, Hindawi Publishing Corporation.

Jiang, A, Gu F, Gennish R, Moore J, Harris G, Ball A, (2008), *Monitoring of Diesel Engine Combustions Based on the Acoustic Source Characterisation of the Exhaust System*, Mechanical Systems and Signal Processing, 22 (6). pp. 1465-1480. ISSN 08883270

Johnson, M, (2008), *Lubricant Selection: Bearing, gear drives and hydraulics*, Tribology and Lubrication Technology

Johnson, M, (2001), *Sleeve bearing lubrication*, Machinery Lubrication, Noria Publication, No. 242.

Joyce, D, (1995), *Lubrication, Tribological Design Data*, The Tribology Group, Institute of Mechanical Engineer.

Khurmi, R, Gupta J, (2005), *A text book of machine design*, Reprint Edition, S. Chand & Co Ltd, India.

Kim,, Y, Tan A, Yang B-S and Kosse V, (2007), *Experimental study on condition monitoring of low speed bearings*, time-domain analysis, 5th Australasian Congress on Applied Mechanics, ACAM 2007, Brisbane, Australia.

Kingsbury, Inc, (2010), *A General Guide to The principles Operation and Troubleshooting of Hydrodynamic Bearings*, Publication HB, Printed in USA 8/10.

Klebanov, B, Barlam D, Nystrom F, (2008), *Machine Elements Life and Design*, CRC Press, Taylor & Francis Group, USA.

Kolubaev, E, Kolubaev A and Sizova O, (2010), *Analysis of Acoustic Emission during Sliding Friction of Manganese Steel*, Technical Physics Letters, No. 8, pp. 762-765, Pleiades Publishing Ltd. ISSN 1063-7850.

Kreith, F, (1998), *The CRC Handbook of Mechanical Engineering*, CRC Press Inc, USA.

Le Bot, A, Bou Chakra, (2010), Measurement of friction noise versus contact area of rough surface weakly loaded, *Tribology Letter*, 37, pp 273-281.

Marques, de Sa J P, (2007), *Applied Statistic Using SPSS, STATISTICA, MATLAB and R*, Second Edition, Springer, Portugal.

Maryland Metrics, (2008), *HRC Coupling*, PO Box 261, Owing Mills, MD 21117, USA.

Mba, D, (2003), *Acoustic Emission and Monitoring bearing health*, *Tribology Transaction*, 46 (3), pp. 447-451.

Mechefske, K, Sun G and Sheasby J, (2002), *Using Acoustic emission to monitor sliding abrasive wear*, *Insight*, Volume IV, No. 8, August.

Mendenhall, W and Sincich T, (2007), *Statistic for Engineering and the Science*, 5th Edition, Pearson Prentice Hall, Upper Saddle River, New Jersey, USA.

Miller, R and McIntire K, (1987), *Non Destructive Testing Hand Book, Volume 5, Acoustic Emission Testing*, *American Society for Non destructive Testing*, p. 603, ISBN 0-931403-0202.

Mobley, R K, (2002), *An Introduction to Predictive Maintenance*, Second Edition, Butterworth Heinemann, Elsevier Science, USA

Mobley, R, (2004), *Maintenance Fundamental*, Plant Engineering Maintenance Series, Second Edition, Butterworth Heineman, Elsevier

Monavar, M, Ahmadi H, Mohtasebi S, Hassani S, (2008), *Vibration Monitoring Techniques for Fault Diagnosis of Electromotor with 1.5kW Power*, Journal of Applied Sciences, Volume 8, Issue 7, pp. 1268-1273.

Neale, M, (2001), *Lubrication and Reliability Handbook*, Butterworth Heinemann.

Neale, M, (2008), *Plain Bearing Failure*, Neale Consulting Engineers Limited, Highfield, Pilcot Hill, Dogmersfield, nr. Fleet, Hants, RG27 8SX, United Kingdom.

Nisbett, B, (2008), *Shigley's Mechanical Design*, Eight Edition, McGraw Hill Primis Companies

Noria Corporation, (2001), *Water in Oil Contamination*, Practicing Oil Analysis, July.

Noria Corporation, (2003), *On Line Sensor Measures Dissolved Water in Lubricating Oils and Hydraulic Fluids*, Practicing Oil Analysis.

Noria, (2004), *Failure analysis for plain bearings*, Machinery Lubrication. , No. 638

Norton, M and Karczub D, (2003), *Fundamentals of Noise and Vibration Analysis for Engineers*, 2nd Edition, Cambridge University Press.

Ohtsu, M, (2000), *Moment tensor analysis of AE and sigma code, Acoustic Emission Beyond Millennium*, Elsevier, Tokyo, Japan

Pandey, S, Nakra B, (2011), *Vibration Monitoring of a Rotor System using RMS Acceleration*, Journal of Engineering Science and Technology, Volume 3, Issue 4, pp. 2559-2572.

Physical Acoustic Corporation, (2010), *AE Sensor Calibration Certificate*, Mistras Holding Company

Physical Acoustic Corporation, (2010), *Differential Acoustic Emission*, Matras Group, 195 Clarksville Road, Princeton Jct, NJ 08550, USA.

Poley, J, (2007), *The History of Oil Analysis*, Machinery Lubrication, Noria Publication. No. 1113.

Price, E, Lees A, Friswell M and Roylance B, (2003), *Online detection of subsurface distress by acoustic emission*, Key Engineering Materials, Vol. 245-246, pp. 451-460, 2003, Trans Tech Publications, Switzerland.

Rao, S, (2004), *Mechanical Vibration*, International Edition, 4th Edition, Pearson Education International, Prentice Hall, USA.

Rho, B-H, Kim D-G and Kim K-W, (2003), *Noise analysis of oil lubricated journal bearings*, Mechanical Engineering Science, Proceeding Institution Mechanical Engineer, Vol 217, Part C, p.365-371.

Royersford Foundry and Machine Co. Inc, (2001), Po Box 190, Royersford, PA 19468-0194.

Roylance, B, (2003), *Machine failure and its avoidance-what is tribology's contribution to effective maintenance of critical machinery?* ,Proc. IMechE, Volume 217, Part J, Engineering Tribology, J05302.

RS, (no date), *GP Pressure Transducer, 0-40bar 0-100mV*

Saravanan, N, Cholairajan S, Ramachandran K,(2009), *Vibration based fault diagnosis of spur bevel gear box using fuzzy technique*, Expert Systems with Applications, Volume 36, pp. 3119-3135.

Scoot, R, (2005), *Journal Bearing and Their Lubrication*, Machinery Lubrication

Scott, R, (2008), *Basic abrasive wear modes in lubricated systems*, Machinery Lubrication, Noria Publication, No. 1375.

Shiroishi, J, Liang S, Danyluk, Kurfess T, (1999), *Vibration Analysis for Bearing Outer Race Condition Diagnostics*, Journal Brazil, Society Mechanical Science, Vol. 21, No. 3, Sept.

Shreeve, D, (1995), *Signal processing for effective vibration analysis*. IRD Mechanical, Inc, Columbus, Ohio.

Shreve, D, (2003), *Integrated condition monitoring technologies*. IRD Balancing LLC.

Sin, M, Soong W, Ertugrul N, (2003), *Induction machine on-line condition monitoring and fault diagnosis, a survey*, University of Adelaide.

Singh, H, (2001), *Lubricants Technology, An Overview*, Science in Africa, Science Magazine for Africa.

Stachowiak, G and Bachelor A, (2001), *Engineering Tribology*, Second Edition, Butterworth Heinemann, 2001, USA.

Steerforth, (2011), *Hydraulic Components*, Ramparts, UK

Stolarski, T, (1990), *Tribology in Machine Design*, Heinemann Newnes, UK.

TC, (2009) *Temperature Sensors, Miniature Thermocouples, Miniature 0.5mm Dia Mineral Insulated Thermocouple with Miniature Flat Pin Plug*, TC Direct, PO BOX 130, Uxbridge UB8 2YS, United Kingdom.

Tepler, D, Baldor L, (1996), *Sikorsky says of crash was subcontractor's bearing*, Connecticut Post, Vol. 5, No. 179, pp. 1 Ed.

APPENDIX

Appendix 1. Journal bearing capacity

The total load of journal bearing will support may be expressed by (Stachowiak, 2001)

$$W = \frac{U\eta\varepsilon L^3 \pi}{c^2(1-\varepsilon^2)^2} 4 \sqrt{\left(\left(\frac{16}{\pi} - 1\right)\varepsilon^2 + 1\right)}$$

Where:

W : Journal bearing capacity (N)

U : Linear speed of shaft (m/s)

d: Shaft diameter (m)

n: Shaft speed (rpm)

L: Length of bearing (m)

η : Absolute viscosity (Pas)

ε : Eccentricity ratio

c: Clearance (m)

Data of calculations:

Diameter of shaft $d = 35 \text{ mm} = 0.035 \text{ m}$

Length of bearing $L = 76 \text{ mm} = 0.076 \text{ m}$

Viscosity of lubricant: 46 cSt

Clearance $c = 250 * 1e-6 \text{ m}$

Eccentricity ratio $\varepsilon = 0.7$ (optimum)

Shaft speed variation $n = 1450 * [0.2 \ 0.4 \ 0.6 \ 0.8 \ 1]$ (rpm)

Conversion of kinematic viscosity to absolute viscosity:

$$\nu = \frac{\eta}{\rho}$$

$$\eta = \nu \rho$$

Where:

ν : Kinematic viscosity (cSt)

ρ : Lubricant density (kg/m³)

η : Absolute viscosity (Pas)

Numerical data:

Kinematic viscosity = 46 (cSt)=46 mm²/s=46 10⁻⁶ m²/s

Lubricant density = 850 (kg/m³)

1cP=10⁻³Pas

Absolute viscosity:

$$\eta = \nu\rho$$

$$\eta = 46 \cdot 10^{-6} \cdot 850$$

$$\eta = 0.0391 \text{ Pas}$$

$$\eta = 0.04 \text{ Pas}$$

$$\eta = 40 \text{ cP}$$

The journal bearing capacity in different eccentricity ratio is shown in Figure (A.1)

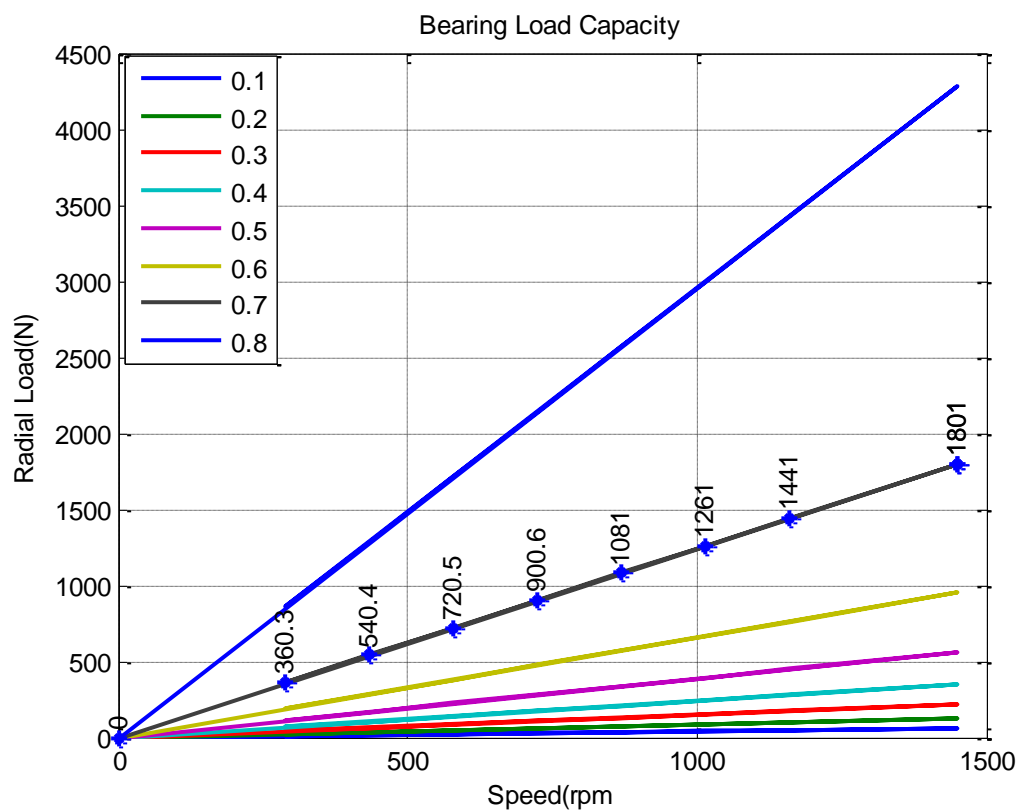


Figure A.1, Journal bearing capacity

List of journal bearing regarding to speed variation is shown in table A.1

Table A.1, Bearing load capacity

No	Operation (%)	Journal bearing capacity (N)
1	20	360.3
2	30	540.4
3	40	720.5
4	50	900.6
5	60	1081
6	70	1261
7	80	1441
8	100	1801

Appendix 2, Load cell calibration

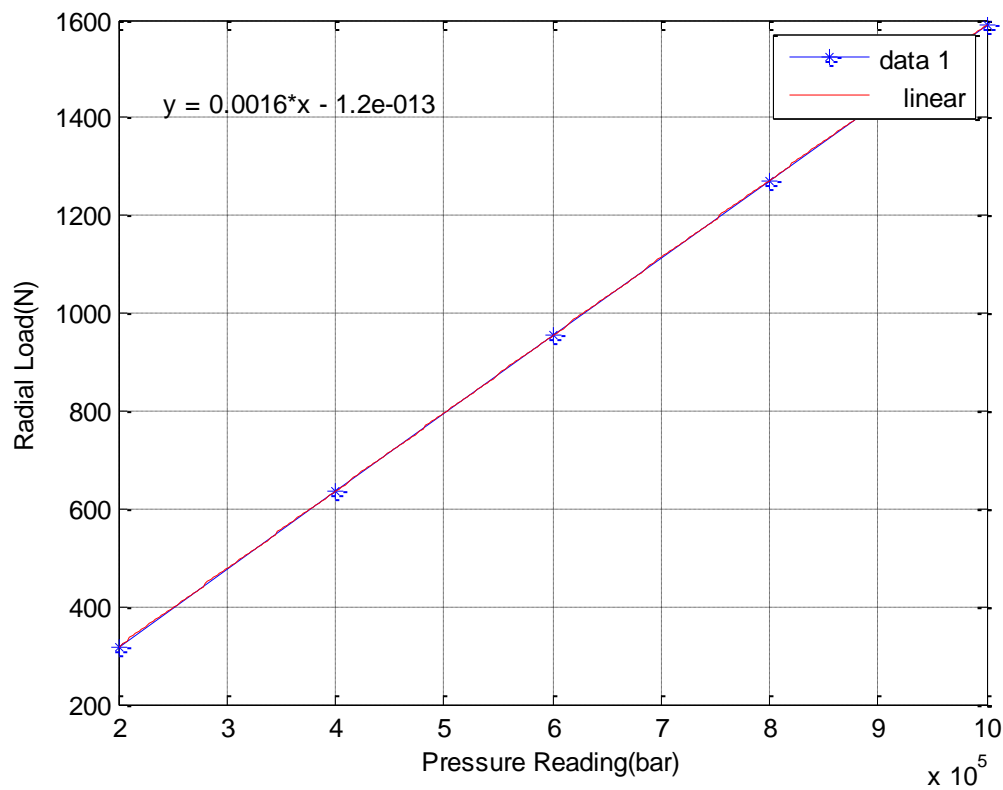


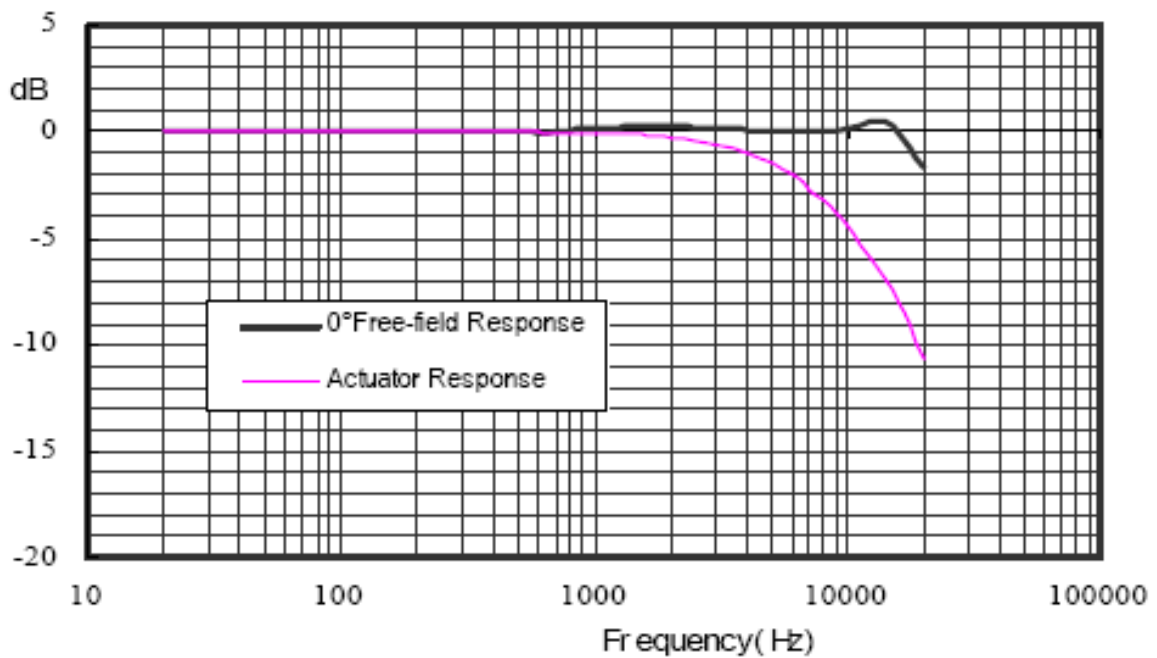
Figure A.2, Journal bearing capacity

Table A.2, Load cell calibration

No	Operation (bar)	Radial load (N)
1	0	45.3
2	2	277.0
3	4	445.8
4	6	676.8
5	8	843.2
6	10	904.1

Appendix 3, Microphone

Figure A.3, Microphone Calibration certificate



PHYSICAL ACOUSTICS CORPORATION
A MISTRAS Holdings Company

AE SENSOR CALIBRATION CERTIFICATE

Sensor Name: WD Max. Value (dB): -64.50 Test Date: 12/2/2010
Sensor S/N: FO35 Peak Freq.(kHz): 263.67 Tested By: N.M.
Comment: 1 METER CABLE

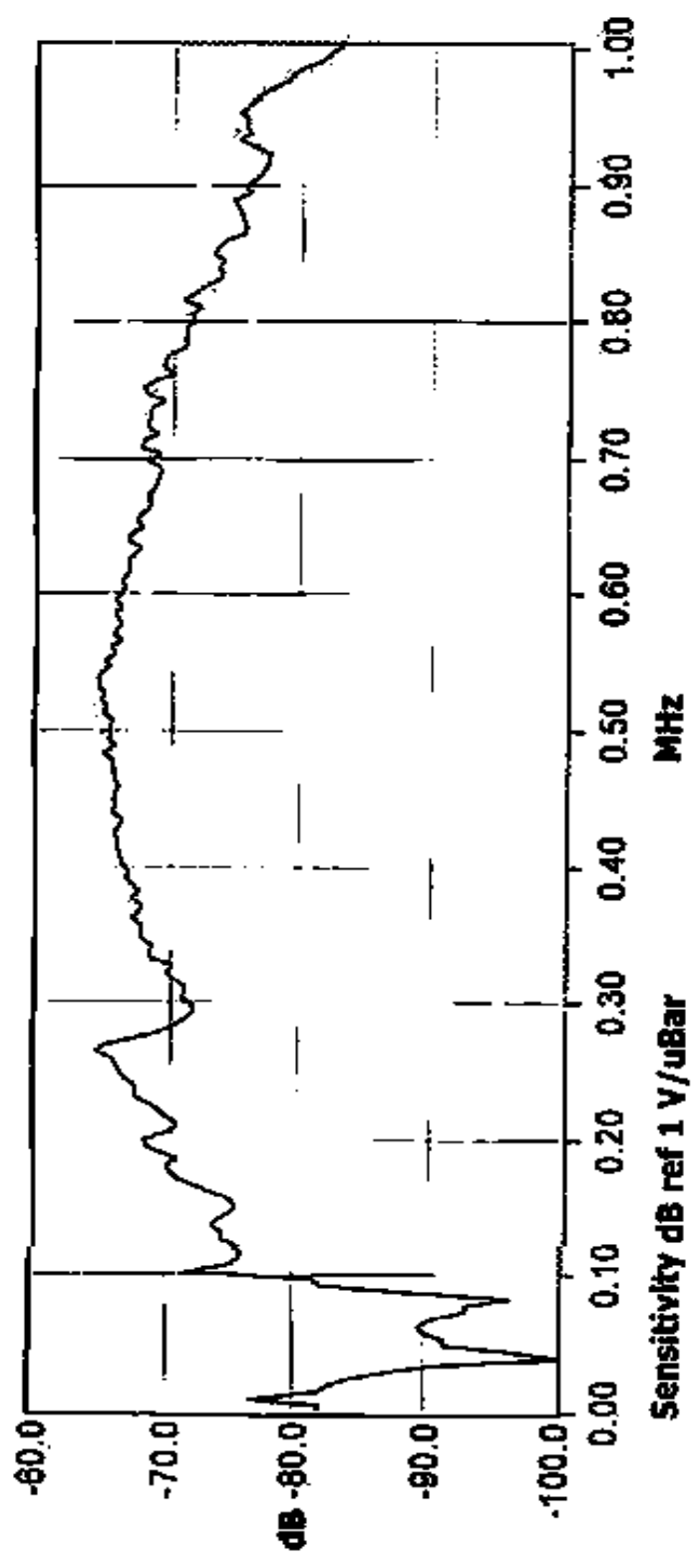


Figure A.4, AE Calibration certificate

Appendix 5, Accelerometer

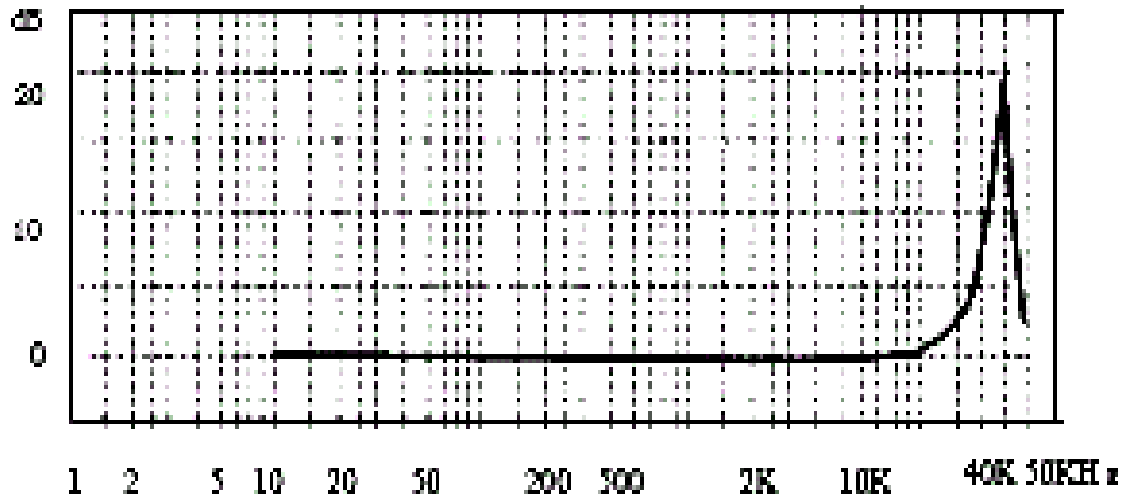


Figure A.5, Accelerometer Calibration certificate